UNIVERSITY OF SOUTHAMPTON
FACULTY OF ENGINEERING, SCIENCE & MATHEMATICS
SCHOOL OF ENGINEERING SCIENCES

Development and Assessment of Embedded Acoustic Emission Technology for Non-Destructive Assessment of Cemented Hip Replacement Constructs

By

Mark Noel Mavrogordato

Thesis for the degree of Engineering Doctorate

January 2010

UNIVERSITY OF SOUTHAMPTON

ABSTRACT

FACULTY OF ENGINEERING, SCIENCE & MATHEMATICS
SCHOOL OF ENGINEERING SCIENCES

ENGINEERING DOCTORATE

DEVELOPMENT AND ASSESSMENT OF EMBEDDED ACOUSTIC EMISSION TECHNOLOGY FOR NON-DESTRUCTIVE ASSESSMENT OF CEMENTED HIP REPLACEMENT CONSTRUCTS CORROBORATED WITH MICRO-COMPUTED TOMOGRAPHY IMAGE ANALYSIS

by Mark Noel Mavrogordato

The Acoustic Emission (AE) technique has been described as possessing 'many of the qualities of an ideal damage-monitoring technique', and has been used to aid understanding of failure mechanisms and damage accumulation in the component parts of a cemented stem construct. However, most of these investigations were restricted to *in-vitro* testing using surface mounted sensors since direct access to the bone cement layer/femoral stem is not readily available, and the bone surface is often the only practical option for sensor positioning. Acoustic signals are attenuated as they travel through a material and across interfaces and so it is arguable that mounting the sensors on the bone surface to investigate damage mechanisms occurring within the bone cement layer is not ideal. This project has investigated the potential for directly embedding AE sensors within the femoral stem itself; enabling a permanent bond between the sensor and structure of interest, allowing closer proximity of the sensor to the region of interest, and eliminating potential complications and variability associated with fixing the sensor to the sample. In-house AE sensors have been developed with similar response characteristics to commercial sensors and adapted for direct embedment into metallic structures. Data was collected during *in-vitro* testing of nominal implanted constructs, and information from both embedded and externally mounted AE sensors were compared and corroborated by micro-Computed Tomography (μ-CT) images taken both before and after testing. The present work has demonstrated that it is feasible to employ directly embedded AE sensors to enable *in-vitro* AE testing of cemented femoral stem constructs to be conducted without the need to consider sensor retrieval, clamping or modification of the simulated construct to accommodate sensors. Signal attenuation is reduced since the sensors are no longer positioned on the external surface of the bone, and the excellent temporal resolution allows a test to be interrupted immediately after the detection of significant damage. Furthermore, the system may be considered as the first step towards an *in-vivo*, cost effective, user friendly, non-destructive system capable of continuously monitoring the implanted construct and locating the earliest incidences of damage initiation.

LIST OF CONTENTS

LIST OF ILLUSTRATIONS

LIST OF TABLES

AUTHOR'S DECLARATION

I, Mark Noel Mavrogordato

Declare the this thesis entitled
'Development and Assessment of Embedded Acoustic Emission Technology for Non-Destructive Assessment of Cemented Hip Replacement Constructs Corroborated with micro-Computed Tomography Image Analysis'
and the work presented in the thesis are both my own, and have been generated by me as the result of my own original research. I confirm that:

- this work was done wholly or mainly in candidature for a research degree at this University
- where any part of this thesis has previously been submitted for a degree or any other qualification at this University or any other institution, this has been clearly stated;
- where I have consulted the published work of others, this is always clearly attributed;
- where I have quoted from the work of others, the source is always given. With the exception of such quotations, this thesis is entirely my own work;
- I have acknowledged all main sources of help;
- where the thesis is based on work done by myself jointly with others, I have made clear exactly what was done by others and what I have contributed myself;
- parts of this work have been published as: 'Acoustic Emission Monitoring and 3D Visualization of Polymerization-Induced Damage of Acrylic Polymer Materials' in Journal of Biomedical Materials Research Part B: Applied Biomaterials. Volume 90B, Issue 1, Pages 223-228. December 2008.

Signed: .....
Date:.....

ACKNOWLEDGEMENTS

The transposition of a thesis from the mind to paper is often deemed a solitary experience... Those who hold this view are blind - No words can portray the deep gratitude that I will always hold for all those who have supported me over the past few years and I'd like the reader to know that the words written on these pages can only begin to portray my recognition to the fact that I was never alone.

This is without doubt the toughest challenge I have ever tackled, although I may refer to the challenge as a figurative mountain, to me this mountain is definitely real and one so perilous that it does not rightfully belong on this Earth! I would not have even attempted to consider climbing such a beast without the reassuring support, encouragement and guidance of my supervisors; Professor Mark Taylor who has unprecedented patience and quietly exudes confidence - although it has to be said that we have shared a few nervous episodes: in the few moments before I was about to stand up and give my first ever conference presentation I explained that I was nervous because my presentation was a little "different" to everyone else's... but I couldn't explain why it was different and had to leave him hanging on the thought that he would find out what I meant shortly. It was the only time I have ever witnessed his otherwise unwavering and reassuring smile transform into a look of horror, and I would like to apologise now for putting him through that particular moment - That aside, I would also like to take this opportunity to thank him for his continued encouragement, clear foresight and for giving me a good old prod in the right direction when needed. Dr. Andrew Taylor's enthusiasm and energy is remarkable, I sometimes wonder whether he has in fact discovered the elixir of life, and I would very much like to thank him for creating some time to spend discussing this and other projects with me. Finally, I had to give up trying to find the words to express the depth of my heartfelt gratitude and respect that I have for Dr. Martin Browne. I would like to thank him for his tireless efforts to help me along the way, both academically and emotionally. He has selflessly thrown me a number of lifelines, whilst simultaneously bringing the world into perspective with his undeniably sharp wit and cracking comments. Without him this would not exist... It is as simple as that.

One of the key attributes of anyone who has written a thesis is that they have had a true period of time where they are able to reflect and assess who they are and where their true

interests lie. The fact that this project revolved around experimental testing that required a high degree of bespoke component manufacture ultimately led to the birth of Mavro Engineering and is one of my proudest achievements to date. Again, there is no way that I could have achieved the level of competency in the workshop or the trust in the experimental jigs (and hence results) without the companionship and guidance of a few people whose job is more than a job, and who gain true satisfaction from helping others succeed in their research. I'd like to give something back to these guys and ask everyone who reads this to know that none of the results of these experiments would be here without Chris Williams, Robert Barnes, Dave the welder, or indeed any of the other technicians who have helped me along the way.

As with any challenge, love and support from family can mean the difference between success and failure. It would be impossible to convey the emotional rainbow that I have gone through whilst writing this thesis to anyone who has not written one, but here is an extract from an e-mail that I wrote to my girlfriend, Anna, when I felt so near and yet so far from the end: *"Have you ever stood at the bottom of a mountain and thought it looked easy to climb, only to find that the top is surrounded by a fortress of sheer cliff faces, loose boulders and deep crevasses that would require equipment that you don't have to get over? Well, I'm kind of at that point now... what I thought was fairly straightforward is in fact becoming increasingly complicated and I'm not sure if I have all the equipment I need to go on. I certainly don't have time to go back down the mountain and get it so I guess I'll just have to struggle on with what I've got. The temptation to turn around and look at the view as opposed to what I need to do is enormous but I know that is not going to get me anywhere and as the sun goes down I will rapidly suffer from exposure and ultimately perish. I'm running out of energy as it is, and every step is increasingly difficult. On my journey thus far I have on occasion stumbled and twisted my ankle and grazed my palm; these little injuries that seem so insignificant on their own are slowing me down even more now. I wish I had chosen another route, but I can't change what I have done. One saving grace is preventing me from giving up completely, and that is that you know where I am and you may just be able to offer me a critical leg up to help me scramble over some of these boulders. Even something as simple as a hug gives me a brief feeling of security and shelters me from the elements."* It is moments like this that I really appreciate how lucky I am to have such a supportive family, and I'd like them all to know that I really do appreciate them... This thesis symbolises the patriotic flag now proudly flying at the peak

of this figurative mountain. I would like all of those mentioned here to regard the flag with pride and reside in the knowledge that their support is very much appreciated by the author and shall not be forgotten.

Finally I would like to thank the University of Southampton, Finsbury Development and the Engineering and Physical Sciences Research Council for their financial support during this project.

Thank you.

DEFINITIONS & ABBREVIATIONS

Acoustic Emission	AE	Elastic stress wave emitted due to the rapid release of stored energy from a localized source within a material
Acetabulum		Socket cavity allowing juncture between the femur and pelvis
Arthrography		An X-ray imaging technique used to assess the structure of a joint following injection of a radiopaque substance
Arthroplasty		Surgical replacement of a joint
Aseptic loosening		Loosening by means other than infection
Bone adaptation		The remodelling of bone to for structural optimization in accordance with changes to the loading environment
Bone cement	PMMA	A polymer (Polymethyl-methacrylate) used to position and fix prosthetic components in position
Bone Mineral Density	BMD	A representation of bone strength, and an indicative measure of bone degradation and osteoporosis
Carcinogenesis		The promotion or initiation of cancer cells
Curie Temperature		Temperature at which a piezoelectric material loses its piezoelectric properties
d_{33} coefficient		A measure of the charge density developed per given stress in the z direction of a piezoelectric material. Essentially this provides a measure of piezoelectric sensitivity.
Dislocation		Displacement and separation of a joint
Dispersion		The separation of a wave according to a specific characteristic such as frequency
Dual Energy X-ray Absorptiometry	DEXA	A radiographic technique used to measure bone density
Endoprosthesis		A prosthesis housed entirely within the body
Fatigue		Repeated loading and unloading leading to subsequent failure at a stress below the ultimate failure stress of a material
Femoral Head		Ball shaped region of the femur allowing articulation with the acetabulum
Femur		The bone which links the pelvis to the knee
Fracture		A break, or crack within bone
Hydroxyapatite	HA	A mineral coating designed to promote bone growth
In silico		Computer based modeling approach
In-vitro testing		An experiment conducted in an environment other than within a living body
In-vivo testing		Experiments carried out within a living body, such as a clinical trial

Laser interferometer		A device for measuring small distances and thicknesses based upon the interference of two laser beams - one reference and one experimental
Magnetostriction		The deformation of a ferromagnetic substance under magnetization
Micro-Computer Tomography	μ-CT	A high-resolution 3D volume reconstruction of multiple X-ray images taken at incremental angles around an object.
Osteoarthritis		A painful condition resulting from degradation of a joint
Osteolysis		Active resorption of bone
Osteonecrosis		Bone death
Pencil lead break test	Plb test	Introduction of an acoustic signal into a material using a Hsu-Neilson source (snapping a pencil lead).
Phonograph		A device which produces a voltage output from surface features
Piezoelectricity		The generation of voltage in response to a mechanical stimulus
Prosthesis		An artificial body part
Pulse Calibration Method		Using a transducer to send an acoustic pulse into a structure for known source detection and calibration of AE location
Quality Adjusted Life year	QALY	An adjustment factor for determining the value of life for one year. A year spent in perfect health has a value of 1, and this value reduces depending on the influence of a medical condition.
Rheumatoid arthritis		A systemic condition whereby the body's own immune system attacks the joints
Roentgen Stereophotogram -metric Analysis	RSA	A technique used to calculate the 3D position of markers from stereo images
Scintigraphy		Monitoring of radioactivity following administration of a radionuclide
Stress shielding		Local stress bypass due to the presence of a favorable load path which may lead to bone loss within the area of reduced stress
Sub-chondral bone plate		Bone which provides support for articulating cartilage
Wolff's Law		The adaptation of bone to minimize stresses imposed upon it such that areas of high stress will see osteogenesis, and areas of low stress will see bone degeneration. As such the skeleton is an adaptive and self-optimizing system.

CHAPTER 1 - INTRODUCTION AND AIMS

The aim of this project is to develop an embedded condition monitoring system, primarily for the assessment of aseptic loosening of femoral total hip replacement components. However, before launching into this specific application, this more general introduction has been written with the intention of providing the reader with a brief insight into some of the engineering considerations of total hip replacement design and development. As the reader will hopefully appreciate, the basic principle of the total hip replacement is actually a simple ball and socket bearing joint. However, because it must operate within a unique biological environment the performance of these joints becomes unpredictable and rather varied. As a result, many different designs exist on the market today, each one a compromise between the multitudes of factors that have been identified through the literature. However, the techniques used to assess implant performance in service have not developed significantly beyond patient pain scores, low-resolution radiographic imaging and statistical analysis of joint registry data. Consequently, much of the developments that have been seen within this field are simply the result of trial and error[1], and following decades of development and marketing of devices that ultimately failed to out-perform the original Charnley prosthesis, there was scepticism as to whether the push for new and radical designs were in the best interests of the patient[2]. Academics and surgeons have continuously pushed for improved pre-clinical testing standards of total hip replacement designs[1], and yet we still find that pre-clinical predictions fall short of clinical performance[3]. The inability to accurately represent the clinical environment in the laboratory has resulted in numerous and unexpected *in-vivo* complications[3-5] that may not come to light until a particular design has been implanted for many years with hundreds or thousands of patients potentially affected as a result[6]. It is argued that there is a need to develop more sophisticated monitoring techniques, both *in-vitro* and *in-vivo*, in order to push forward total hip replacement development, and this project was conceived in an attempt to address this issue. But before we go into too much detail, let us first appreciate why a patient may need a hip replacement operation in the first place.

A painful joint can have a huge impact on a person's quality of life, and a painful hip joint can be debilitating. The hip joint itself – shown in Figure 1 - consists of a ball and socket that act to form an articulating bearing surface. The natural joint is made up from a

cartilage lined acetabular cup (socket), and a cartilage covered femoral head (ball). The whole joint is enclosed within a fibrous capsule and is lubricated with synovial fluid. The combination of cartilage and synovial fluid results in a bearing surface with a coefficient of friction of 0.0075-0.04[7], which is less than virtually all manmade bearing surfaces. The proximal end of the femur consists of the head, neck and shaft. Bone, which allows the whole structure to bear load, is composed of a matrix of collagen fibres impregnated with calcium carbonate and calcium phosphate. Compact cortical bone forms a thin outer shell, covering the spongy or cancellous bone that contains the marrow. Bone is an adaptive material and responds to stress in accordance with Wolff's law of bone adaptation.

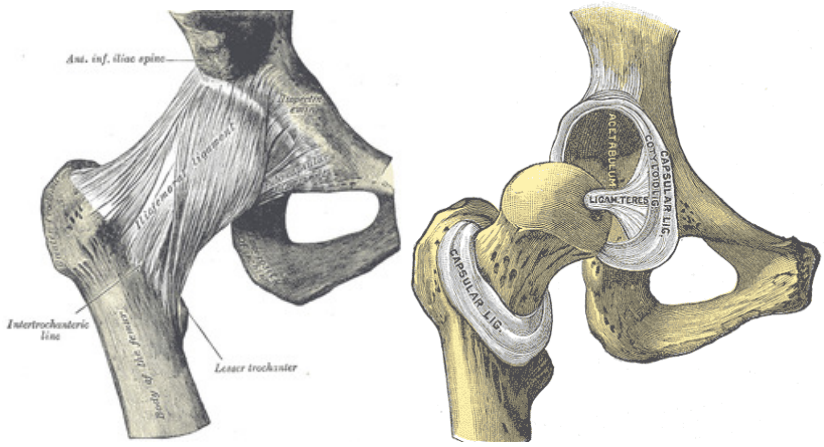

Figure 1 – Anatomy of a healthy hip joint. Source: www.bartelby.net/107/92.html

Despite the low friction articulating surface, there are circumstances where this joint becomes damaged, painful and unable to function normally. By far the most common cause of this is osteoarthritis which accounted for 94% of primary hip replacement procedures carried out in England and Wales during 2007[8]. An osteoarthritic joint loses its function due to a thinning of the cartilage layers and subsequent formation of extra bone known as osteophytes. This condition is particularly prevalent in the hip and knee due to the high loads that these joints must endure. Other conditions that lead to pain and possible joint replacement include rheumatoid arthritis which is a systemic condition that causes the body's own immune system to attack the joints, osteoporosis where the bone loses minerals such as calcium, and becomes porous and brittle and avascular necrosis where the femoral head loses part of its blood supply and dies.

To alleviate pain and restore function, surgeons developed a procedure to replace the worn or damaged components of the hip with artificial components. The first hip replacement

operation was performed in the 1890's when Gluck[9] used Ivory as a substitute for the natural femoral head. This proved unsuccessful, and was followed by a string of other unsuccessful concepts[10] until the 1960's when Sir John Charnley developed a low friction metal on polyethylene total hip replacement system that revolutionised the field of hip arthroplasty. Since then, there have been a multitude of design options that were developed for the method of fixation to the bone, geometrical considerations, and choice of materials.

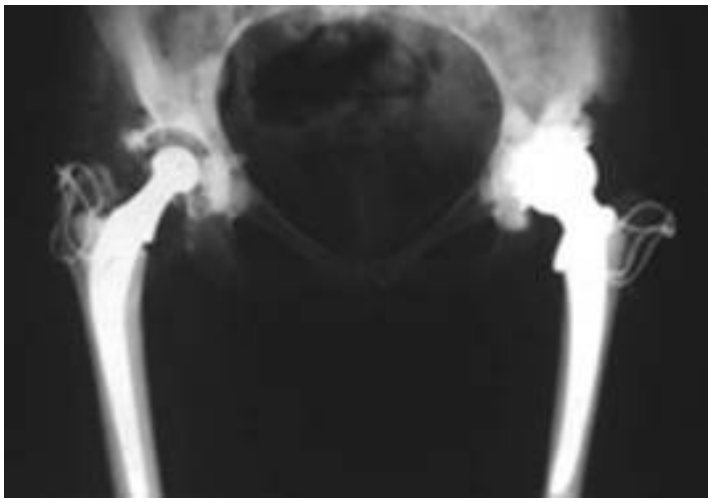

Figure 2 – X-ray image showing a patient with two designs of THR. The patient's right joint has been replaced with a Charnley Metal on Polyethylene design, and the left joint has been replaced with a McKee-Farrar Metal on Metal design. Source: www.jri-oh.com/hipsurgery/Surface.asp

Unfortunately, the need for such a variety of different designs has arisen from the small proportion, but large numbers of total hip replacements that fail. During 2007 England and Wales saw a total of 68,950 hip replacement operations. 9.7% of which were revision operations equating to 6,697 procedures from failed systems[8].

A total joint replacement may fail in a number of ways: There is always the possibility of infection with any surgery. An infection may be superficial – within the wound itself caused by the surgery, or a deep infection of the tissues surrounding the implant. Despite improvements in antibiotics, infection still accounted for 11% of revision operations carried out in England and Wales during 2007[8]. Fracture of either the prosthetic stem or surrounding bone can occur due to the prosthesis design, type of fixation, positioning during surgery, and high mechanical loads imposed on the implant. As well as gravitational and external forces, the muscles surrounding the joint also produce significant

forces that act on the joint surface. Forces of up to nine times body weight have been measured during stumbling[11]. However, fracture of modern implants is rarely seen and accounted for just 3% of revision operations seen by England and Wales in 2007[8]. Dislocation can occur and is related to the direction of surgical approach (the direction of dislocation is generally in the direction of the surgical opening) and the design of the implant – in particular the femoral head size. Other factors attributed to dislocation include poor positioning of the prosthesis during surgery (in particular if the angle of the acetabular cup is too steep) poor muscle strength or imbalance, and acetabular wear. Again the incidence of dislocation is relatively small, accounting for 13% of revision operations seen by England and Wales in 2007[8]. Aseptic loosening is by far the most common reason for revision surgery accounting for 55% of revision operations in England and Wales during 2007[8], and there is an increased risk of loosening among younger, more active, or overweight patients due to the increase in mechanical loading. It is generally agreed that aseptic loosening can occur through four main processes[12]: mechanical failure of the endoprosthesis components, physical motion at interfaces, stress shielding (The presence of a stiff prosthetic stem alters the loading path and stress distribution through the bone and leads to proximal bone degeneration due to bone adaptation), or the presence of wear debris along the interface leading to osteolysis (resorbtion of bone into soft tissue), resulting in a weakening of the bone structure surrounding the implant. However, the exact trigger and mechanisms for aseptic loosening remains an area of debate[13] and this is discussed further in the literature review.

As already mentioned, there are many different designs of total joint replacement systems available on the market today. Each design attempts to eliminate what could be some of the more important factors that lead to failure – predominantly aseptic loosening. The following paragraphs illustrate factors related to implant design and their influences on the overall system. In doing so, the complexities arising from integrating an artificial system into a biological, adaptive environment are illustrated. In every instance some factors are compromised over others, and the optimal design is largely patient specific.

Stem length: It has been shown that a shorter stem length significantly reduces the interfacial shear stresses in the bone[12] and encourages a more physiological stress distribution. However, it has also been shown that a longer stem provides greater initial stability and is more resistant to rotation than a short stem. The appropriate stem length is

therefore somewhat patient specific. It is generally agreed that a revision prosthesis should prioritise on fixation and longer stem lengths are therefore necessary[14].

Surface roughness: Prior to the 1980's most cemented stem designs focussed on achieving an inseparable bond between the stem and the surrounding cement. As a result, there are many cemented implant designs that feature textured surfaces, some even with a thin (0.1mm) pre-coated layer of polymethylmetacrylate (PMMA). Stone et al[15] experimentally tested the shear strengths of different materials, surface finishes, and pre-coated stems: they concluded that pre-coating the stem showed significant increases in shear strength of the stem-cement interface for all materials and surface finishes – although others raised concerns about the transposition of this technique into a clinical setting since Stone et al[15] had used a bonding agent not permitted in clinical practice and that there is a substantial decrease in bond strength when contaminated with saline solution[5]. However, during the 1970's and 80's a sequence of events led to the development of the Exeter stem. This stem had no collar, it had a highly polished surface finish to meet regulatory requirements of the material that was used to manufacture the stem, and it had a double tapered stem geometry to aid pressurisation of cement into bone during insertion. These design features enabled the stem to subside within the surrounding cement layer and although there were initial concerns over the relative migration of the stem within the mantle, this did not appear to affect the stems stability and was, in fact shown to maintain stability even after plastic deformation of the cement had occurred[16]. However, the stem's strength was inadequate and following a series of stem fractures the grade of stainless steel was changed to increase strength and allow for a rough surface finish to be applied to the implant. This alteration led to an unforeseen consequence *in-vivo* and it was found that the rough stem had a greater tendency to loosen than the previous polished stem version[17]. It was then realised that rough stems may produce larger volumes of cement wear debris resulting from micro-motion of the stem, and that although bone cement is bioinert in bulk form, particulates of the same material can trigger a macrophage response that could lead to bone resorption[18]. So another edition of the Exeter stem was released using the stronger material but retaining the original polished surface and has since shown considerable clinical success; According the 2007 Swedish hip arthroplasty register[19], the Exeter polished stem appears 2nd in the list of the top 15 most common stem components used during the last ten years. Other groups began to avoid the use of cement all together and develop cementless designs.

Stiffness: Stem stiffness in an area that has drawn a lot of interest. It has been shown that the bone resorption phenomenon associated with stress shielding is affected by the modulus of the stem. In theory bone resorption should decrease as the modulus of the stem becomes matched to that of the surrounding bone and several groups attempted to produce low modulus implants for this reason[20]. However, it has been demonstrated that an increase in flexibility of the stem also increases the proximal interface stresses that could lead to interfacial debonding, micro-motion, osteolysis, losening, and stem fracture[20-22]. Cementless stems tend to be stiffer than cemented stems due to their geometry, although some of the problems associated with the use of bone cement are avoided, stiff stems reduce the amount of proximal load transfer and thus increase proximal bone loss due to stress shielding and stress bypass[1].

One area of interest is the use of implants with tailored structural properties through the use of composite materials. In theory, these composite structures could be tailored to have a strong core, with a reduction in stiffness towards the exterior surfaces such that the strength of comparable metal components is maintained whilst increasing proximal load transfer without inducing excessive interfacial stresses. Evans and Gregson[23] have written a comprehensive account of the relative merits and areas of concern associated with composite components, and the reader is referred to this work for more information.

Collars: The use of a collar was intended to achieve a more physiological loading of the proximal femur, reducing stress shielding and bone resorption[24]. Although it has been shown that micromotion of the stem is reduced with a well seated collar, this also means that restabilisation in the event of interfacial debonding can not occur[15]. On the other hand, it has been shown *in-vitro* that a collared, well rounded design is an optimal design for the discouragement of interface gaps and cement cracks[24]. However, it is also reported that initial collar-calcar contact is difficult to achieve in practice and even then is lost with minimal bone resorption[25]. Once again the debate as to whether or not a collar is appropriate is a matter of prioritisation. It may be that patients with good bone stock could benefit from a collarless implant with the ability to subside and restabilise in the event of interfacial weakening whilst those patients with poor bone stock may benefit from a well seated collared implant since the hoop stresses in the weakened bone are reduced, but in general, collars have been found to cause problems, and have not shown much success at reducing proximal bone loss[5].

Head size: The size of the femoral head has a profound effect on the performance of the total hip replacement (THR). Sir John Charnley spent some time considering what size head would be appropriate to minimise the production of wear particles (small) whilst resisting undue penetration rates of the head through the socket (large). Charnley concluded that the optimally sized head should be half the external diameter of the socket[26]. However, later concerns over the osteolytic effects of polyethylene wear particles lead to a resurgence of metal on metal bearings, and the development of highly cross linked polyethylenes and ceramics[27]. Ultimately, the reduction in wear rates of these new materials and improvements to manufacturing technologies enabled larger head sizes to be used – increasing the possible range of motion to the patient[28] and encouraging the introduction of fluid film lubrication to the joint[29]. These advances have enabled a resurgence of resurfacing replacements - despite the historically poor performance of initial "surface replacements" produced during the late 1970's and early 80's[4] (thought to have been associated with the use of an equatorial as opposed to a polar bearing, and inadequate polyethylene thickness[30]) - allowing young patients with good quality bone stock to return to more active lifestyles[31].

Method of fixation: An implant may be fixed using either a cemented, cementless or hybrid configuration. A cemented implant uses polymethyl-methacrylate to form a grout that is pressurised into the cancellous bone on insertion of the implant. This technique was pioneered by Sir John Charnley[32] and has been proven as a viable means of fixing implants with more than 50 years of clinical experience. Cementless stems were widely introduced to prevent loosening from "cement disease"[33] where it was thought that a pathological reaction to particles of polymethylmethacrylate meant that no form of cemented prosthesis could ever be expected to last long enough to be implanted into young patients with 30+ years of life expectancy without revision. A cementless implant is located using an interference fit with the surrounding bone, uncoated cementless stems have been shown to increase stresses in the proximal region of the femur[34] theoretically reducing stress shielding. However, many of these stems were found to subside and jam distally due to difficulties in obtaining an accurate fit between the prosthesis and bone[1]. Various forms of coating subsequently became available to encourage the implant to remain in position. These coatings consisted of porous, hydroxyapatite, and hybrid coatings. A porous coating allows the surrounding bone to grow into the implant. If successful, the implant is capable

of transferring load in compression, shear, torsion, and tension. However, if micromotion above a certain threshold between the bone and implant is able to occur, bone ingrowth is prevented and subsequently the mechanical interlock will never form[35,36]. Hydroxyapatite coatings are osseoconductive, but there are concerns over the resorption of hydroxyapatite coatings and the production of third body wear particles if the coating fails, leading to loosening[37]. Ultimately, there is little evidence to suggest that cementless stems out perform their cemented counterparts or are less prone to aseptic loosening. The initial theory of cement disease has been the subject of some debate, and Huiskes[1] argued that the pathological reaction was more likely to have occurred as a result of polyethylene wear particles generated at the bearing surface rather than from the cement. Improvements to cement formulations and application methods have led to improvements in the performance of the femoral components[38], and cemented stems are still the most popular choice of orthopaedic surgeons today[19]. Therefore the science of bone cement, its application and monitoring is still a very relevant topic indeed.

Coating length (cementless stems): The coating length has an effect on the amount of distal load transfer and interface shear stresses. A longer coating increases the probability of sufficient bone ingrowth, but reduces proximal load transfer[1] – hence, encouraging bone loss (Wolff's law). However, limiting the coating to the proximal region reduces stress shielding but leads to higher interfacial stresses and subsequent failure. Huiskes[1] argues that the uncoated distal part of the stem is useful for initial stabilisation, but that it subsequently becomes redundant and more likely to cause problems.

Ultimately, each individual surgeon has his own personal preferences concerning the design and approach used in a total joint replacement operation. There is significant potential for variation in the success of the operation depending on the positioning of the implant, balancing of muscles, and mixing of the bone cement (if used). All of these factors depend on the individual surgeon and surgical technique used to perform the operation. Attempts are being made to reduce inter surgeon variability with the introduction of computer navigated surgery. However, this concept brings in an entirely new debate in itself.

The quality and state of the bone prior to surgery is largely patient specific and this brings in the third major area of factors that add to the uncertainty surrounding the performance of total joint replacement systems:

Age and activity level: A younger, more active patient is more likely to suffer osteolysis due to the increased wear volumes caused by the increased number of cycles experienced by the implant. A greater activity level also corresponds to greater mechanical stresses – hence greater potential for loosening, fracture and dislocation. This is confirmed by the national arthroplasty survey of Sweden[19], which shows that younger more active patients are at greater risk of revision whilst elderly patients, if fitted with an implant of proven design, and modern cementing technique are less likely to outlive their implant.

Weight: An obese patient increases the mechanical forces experienced by an implant, increasing the susceptibility to fatigue failure of the cement[19]. However, these patients also tend to be less active and several studies have found it difficult to provide a link between obesity and increased risk of loosening[19,39,40].

Genetic differences: Some people's bodies react differently to certain situations, and this is largely down to genetics. For example some people have a strong osteolytic reaction to polyethylene wear debris, where as others hardly show any reaction at all[41].

Summary

To summarise, it seems that at best a total hip replacement system may be a solution of best compromise from all of the interrelated factors mentioned above and considered for each individual patient. Finite element models, *in-vitro* testing and registry information all contribute to the body of knowledge and understanding that enable surgeons to make informed decisions and attempt to maximise implant longevity. However, despite all the pre-clinical testing and methods that are available, there is still an undeniable question mark as to how any new design of implant will actually behave in the body. The feedback from clinical trials remains inherently slow and is limited by the lack of detailed information obtainable through current monitoring methods. The above information sets the scene for the purpose of this investigation. The reader is reminded that this introduction was merely intended to provide a brief overview of the development of total joint replacements and hopefully provide some appreciation of the complexities of

integrating an engineered component into a self optimising biological system. It is important to realise that the small percentage of failures equate to large numbers in absolute terms, these failures are complex and most changes to implant design aimed at relieving a particular issue often has adverse effects that lead to other complications which may only present themselves after several years in service. Aseptic loosening has been identified as the major cause of total hip replacement failure and it has been stated that the various condition-monitoring methods have seen little progression beyond the rudimentary techniques used since the introduction of Sir John Charnley's first successful total hip joint replacement. The success of bone cement as a short term implant fixation method has been identified, and despite concerns related to bone cement disease and the development of cementless stems, it continues to be one of the most successful and certainly most popular methods of femoral fixation used to date. Now that the reader has an appreciation of the overall situation, the specific aims of this particular thesis will be established before proceeding into a honed review of the literature.

1.1 AIMS

As stated earlier, the overall aim of this project is to develop an embedded monitoring system for the assessment of total hip replacement devices. Ultimately, this may lead to a data rich and high temporal resolution *in-vitro* testing platform that permits test interruption when damage occurs rather than at set intervals, and is capable of observing sub-surface damage accumulation without the need for serial sectioning or even test interruption. This could be introduced as an *in-vivo* system capable of continuous self monitoring that could aid surgical decisions related to revision operations, or patient lifestyle activities and provide design engineers with progressive information from real-case situations without the need for post-mortem examinations, registry data, or ionising radiation. However, in order to realise this objective, there are several issues that need to be addressed, hypotheses that need to be tested and questions that need to be answered:

1) What monitoring techniques are currently used, what is available, and what would be suitable as a potential technique that could be integrated within an implant.
2) Is it possible to embed AE sensors directly into a femoral stem and do they show an improvement compared to surface mounted sensors?
3) The sensors have detected something – how confident can we be that this is actual damage, and can we assess the likely type and location of damage.
4) Corroborating AE information to actual damage is historically challenging. It is hypothesised that μ-CT may be used to visualise damage unobtrusively during testing such that a visual link may be established between the AE recordings and actual damage events. More importantly, the pre-loading state of the specimen under test may be visualised to ensure that existing damage is not confused with load induced damage. It is further hypothesised that resonant frequency analysis (RFA) may offer further corroborative evidence to verify whether or not the AE activity was able to detect real damage.

These questions are addressed throughout this thesis. Suitable monitoring techniques are discussed within the literature review, and it is hypothesised that the acoustic emission technique may be suitable for this application – both *in-vitro* and *in-vivo*. The second question is addressed in several parts: Integrating a commercially available sensor into a femoral stem is one solution. However, despite the initial convenience, there are significant restrictions associated with size, cost, fixation, cable connections etc. and it

quickly became apparent that the required flexibility from the sensors themselves could not be met by commercial products. CHAPTER 3 describes how in house sensors were developed, including an almost step-by-step approach of the manufacturing procedure such that others may follow on from this work. These sensors were designed such that they could easily be adapted for direct placement within a femoral stem and the reasons for choosing bulk PZT over thick film screen printing are discussed. CHAPTER 4 describes the development of a simplified stem construct to facilitate the incorporation of these sensors, and encourage failure within the cement mantle. The remaining questions are addressed in the experimental testing chapters that build up slowly from the initial polymerisation reaction and the potential for pre-load damage as discussed in CHAPTER 5 through to the static loading situation described in CHAPTER 6 , and finally using fatigue loading as described in CHAPTER 7 . Various practical concerns are raised as a result of this testing; μ-CT offered significant advantages over traditional serial sectioning techniques, although it was found that stem removal and the introduction of a radiopaque dye penetrant was necessary to observe cement damage. However, RFA was unable to be used reliably for these particular tests due to the polished surface of the femoral stem and the subsequent stick-slip behaviour during loading that enabled the system to appear acoustically stable even in the presence of substantial damage. In terms of the AE results themselves, the testing indicates that the response of embedded sensors compared to surface mounted sensors are more reliable and do include the theoretical advantages associated with mounting the sensor closer to the particular region of interest. However, distinguishing different types of failure mechanism and ensuring that the detected AE is related to damage as opposed to external sources is an area that remains questionable to an extent.

The following section presents a review of the literature, delving deeper into the specific areas that are deemed directly relevant to this project. The review shall focus on these areas and identify why aseptic loosening occurs and how attempts have been made to reduce its prevalence. The review will also discuss condition monitoring methods, their development, and why they are so important to the progressive development and success of total hip replacement technology.

CHAPTER 2 - LITERATURE REVIEW

Total hip replacements have transformed the lives of many people, alleviating pain and restoring function, often with little restrictions on normal day to day activities. However, despite vast improvements in general understanding, component design, and surgical technique, the complexities associated with the individualistic nature and the adaptive biological environment result in a small percentage but large number of devices that unfortunately fail. Statistically, aseptic loosening has been identified as the most significant failure mechanism, and there have been many different theories as to the initiating factors[1]. The first part of this literature review will aim to provide the reader with an appreciation of this condition, whilst not forgetting that the focus of this thesis is to assess and develop a technique that may have the potential to provide clinicians, research engineers, and patients with real time monitoring capabilities that may enhance understanding, development, and performance of hip replacement technology both in the laboratory and in the body. To develop and apply such a technique to all of the various forms of currently available implant designs would be impractical at this stage. Bone cement has historically been the subject of a number of concerns (cement disease[33], thermal osteonecrosis[42], and fracture[43]) and yet remains the most commonly used and successful form of femoral fixation method today[19], so focussing attention on the ability to monitor the performance of this particular material seems like a logical first step for the development of a clinically relevant condition monitoring system. The literature review will therefore pay particular attention to some of the issues associated with this material and its role in loosening. Having established that bone cement does fail, it is important to understand whether or not early detection of this failure is actually beneficial. The second part of the review shall therefore look at why condition monitoring is necessary and assess the techniques that are currently used. The third section of the review will go on to explain why certain condition monitoring techniques may be considered more suitable for incorporation into an implantable device than others and look at some of the work that has been done using these identified techniques. After a general review of possible monitoring methods, a more detailed review of two particular methods, Acoustic Emission and Resonant Frequency Analysis techniques are given. Both of these techniques are identified as possessing desirable qualities in that they are non-destructive, do not use any form of ionising radiation, are low cost and could potentially identify loosening at an earlier stage than current techniques.

Finally, it should be remembered that the ultimate objective of this project is to take the first step towards an intelligent *in-vivo* implant with condition monitoring capabilities. The concept of using implants with embedded instrumentation is not new, and some of the most recognised pieces of work in this field have used instrumented implants to collect *in-vivo* force[44], pressure[45] and temperature[46] measurements. Although an *in-vivo* device is beyond the scope of this project, it is felt that an appreciation of some of the challenges involved in fitting electronics within an implant is important, and hence these developments are discussed in the fourth section of the review.

2.1 ASEPTIC LOOSENING AND BONE CEMENT

As stated previously, aseptic loosening is the prime reason for revision surgery. However, it should be appreciated that the term "aseptic loosening" covers a multitude of factors that eventually result in pain and loss of function of the joint. Sundfelt et al[41] have written a review of some of the prominent theories behind the causes of aseptic loosening, and the reader is advised to consult this reference for further information on all of the different loosening mechanisms. Many of the theories behind aseptic loosening featured in the literature are concerned with the reaction of bone resorption to the presence of particles, be they cementf, metal or polyethylene[1] and the fact that the generation of these particles is thought to trigger osteolysis. Osteolysis by definition is an inflammatory response that results in a net resorption of bone[47]. It is important to understand that bone resorption is a normal occurrence in healthy bone, however, the resorption process is normally balanced by new bone formation (remodelling), and it is this balance that is upset in osteolysis around prosthetic artroplasty systems. Normal bone remodelling occurs at a rate whereby the entire adult skeleton is remodelled every 10 years[48], and it is beneficial adjustments to the remodelling process that enables the skeleton to continuously repair micro damage and heal complete bone fractures[49]. The detail of the precise biological processes that occur during bone remodelling would detract from the main focus of this thesis. In very simple terms, normal bone remodelling occurs by osteoclasts that remove bone through acidification and proteolytic digestion, followed by osteoblasts that form new bone through the secretion of osteoid which then mineralises into new bone[48]. The development of osteoblasts and osteoclasts is dependent on a number of growth factors and cytokines, and the suppression of some of these cells in the presence of foreign particles/mechanical processes is why osteolysis is thought to occur around prosthetic components.

Alternatively, the mechanism of loosening may be from mechanical processes such as interfacial de-bonding, bone cement fracture, high fluid pressure[50], or some combination of mechanical and biological processes such as high fluid pressures that force wear particles down into the bone-implant interface and once again trigger an osteolytic response. Again, an in depth analysis of all of these processes would detract from the focus of this thesis, and so we will now concentrate solely on the material that is most commonly used for implant fixation and what failure mechanisms are currently thought to operate within this material.

The use of an acrylic, cold curing cement in humans was first reported as being used to fix metallic femoral THR components in place in 1953 by Haboush[51] and then in 1960 by Sir John Charnley[52] who used the material along the entire length of the prosthetic stem. Charnley identified that in order to form an adequate connection between prosthesis and bone, the load should be transmitted over a wide area, thus necessitating a material that could be cast in-situ to match the complex and unique internal geometries of each femur. The material that Charnley used was a two part system consisting of a powder polymer and liquid monomer mixed to form polymethylmethacrylate (PMMA) also known as "bone cement". The powder typically contains the PMMA beads, initiators, and radiopacifiers, but may also contain certain antibiotics for slow release into the patient. The liquid typically contains the monomer along with an accelerator and stabiliser. When cured, bone cement consists of a matrix of PMMA beads, radiopacifier particles, porosity, and other impurities such as dust. Furthermore, the cement contracts during the cure phase, inducing residual stresses that are thought to contribute to crack initiation and propagation, although the exact mechanism for crack initiation is poorly understood[53]. Charnley postulated that an amine-cured ethoxylene resin as used by Bloch[54] for healing of bone fractures may have been a better substance due to its adhesive and possible acceptance of bone ingrowth. However, this avenue was never pursued for THA applications due to the possible toxic effects of the hardeners resulting in fibrous tissue formation[55]. By 1964, Charnley[32] had performed and assessed over 450 THR operations using PMMA, and reported good results with just two femoral prostheses needing to be revised due to loosening; in fact one of the greatest problems encountered by Charnley was associated with the removal of the prostheses from the femur. Further studies reported 92% success at 10 years using this method of fixation in the hands of various surgeons[56] and the cemented femoral stem used in conjunction with Charnley's polyethylene cup became the gold standard for THA[57]. However, loosening rates increased substantially between 10-20 years post operatively[1] and several concerns arose over the long term use and performance of cement.

Bone cement disease

Charnley believed that any tissue reaction with the resin was unlikely since continually abraded acrylic Judet[58] prostheses had caused no mal-effects in the surrounding soft tissue after 7-12 years[32]. However, roentgenographic analysis revealed pathologic reactions to foreign material at the bone-cement interface believed to be a contributing factor to loosening. Jones & Hungerford[33] have conducted a comprehensive review of this

"condition", and the reader is directed to that reference for further information since similar reactions have since been observed in cementless systems and thus the entire concept of "bone cement disease" was based on an erroneous assumption[59]. It is now believed that it is simply the presence of small particles, be they cement, polyethylene, or metal that can trigger this pathological response[59].

Thermally induced osteonecrosis

Charnley[32] recognised the possible issue of thermal osteonecrosis caused by the exothermic polymerisation reaction of bone cement, however, he initially thought that the rise in temperature of a thin layer of bone cement was unlikely to be significant. It was later suggested as one of the possible contributing factors to early loosening[60,61] and has since attracted much attention in the literature, with attempts to reduce the peak temperature and improve performance through pre-cooling the unmixed cement[62] (although Li et al[63] reported that pre-cooling the bone cement constituents may lead to an overall reduction of the prosthesis longevity due to decreased mechanical properties and other studies express concern that this may increase levels of residual monomer and potential toxic effects[64]), cooling the prosthetic components[42] (although this may have adverse effects on porosity), and reducing the ambient operating temperatures[65]. However, the true influence of the exothermic reaction on osteonecrossis around the femoral stem is still debateable. Reckling et al[66] observed that although the temperature in the centre of the cement layer may exceed 56°C (the reported temperature that protein is denatured), the temperature at the cement interface did not reach this value and suggested that previous studies that reported high cure temperatures had measured the temperature in the bulk of the cement as opposed to the interface. A finite element modelling approach conducted by Li et al[63] demonstrated the negligible effect of pre-heating or cooling prosthetic components on the bone-cement interfacial temperatures and concluded that overall pre-heating of the femoral stem was likely to increase the longevity of the THA. Lidgren et al[62] reported that vacuum mixing had a greater influence on peak polymerisation temperature than chilling the cement components, but that chilling the cement prior to mixing did improve mechanical properties of the set material. Furthermore, Lidgren at al[62] reported that the peak exothermic temperature could be substantially reduced by using a fraction of optimally sized pre-polymerised PMMA beads. Overall, it appears that the heat generated during polymerisation is more of a consideration for the acetabular component and only has a minor influence on the long-term survivorship of the femoral prosthesis.

The reduction of polymerisation temperature is therefore not considered in any further detail in this thesis.

Interoperative hypotension and cardiac arrest

There have been numerous reports of interoperative hypotension and cardiac arrest – most of which occur during the application of bone cement[67] within patients with some sort of femoral fracture using long stemmed prostheses[68]. Due to the association of this condition with the cementing procedure, it has often been labelled "bone cement implantation syndrome"[69] and is still reported as being poorly understood[68]. Initial studies thought that residual monomer may be to blame, but it was later suggested that the intramedullary pressures may be sufficient to cause embolisation[70]. Donaldson et al[68] have conducted a comprehensive review on the subject and since this topic is not the main focus of this thesis, no further discussion will be given here. Suffice it to say that considerable reductions of risk are associated with the use of medullary lavage[71], reducing the length of the prostheses[72], venting[68] or applying a vacuum to the medullary canal during cementation[67], retrograde cement application using a cement gun[68], using a cementless prosthesis[68], and pre-operative assessment of individual patient risk factors[68].

Porosity and pre-load cracking

It is widely accepted that porosity present within the bone cement mantle of total hip arthroplasty devices can act as stress raisers and fatigue crack initiation sites which directly affect the mechanical performance and longevity of the construct[73]. For a long time the porosity observed within the cement mantle was attributed to factors such as volatility of the monomer from heat generated during polymerisation[74], or air entrapped during mixing, transfer, delivery or even upon insertion of the stem[75]. Vacuum mixing methods were developed to reduce porosity with subsequent improvements in fatigue life of up to ten times that of hand mixed cement[62] and yet the expected clinical improvement associated with the reduction in porosity was not necessarily realised and there is evidence to suggest that vacuum mixing can result in an increased risk of early loosening[76,77].

It is only in recent years that the importance of cement shrinkage and the potential implications of this phenomenon have been investigated. Volumetric shrinkage of bone cement during polymerisation may induce porosity, weaken the cement-stem and cement-bone interfaces and induce residual tensile stresses making the cement more susceptible to

fatigue initiation and propagation[78-82]. There are two main reasons why there is a net shrinkage associated with the cure phase of bone cement; Firstly, the polymerisation reaction is exothermic, resulting in a shrinkage effect during cooling[80]. Secondly, the conversion from monomer (ρ = 0.937g/mL) to polymer (ρ = 1.18g/mL) results in an intrinsic density increase of the bone cement and hence volumetric shrinkage[82]. The figures quoted in the literature for the magnitude of this volumetric shrinkage range from approximately 3% to 7%[77,79,82] depending on the mixing method and proportion of monomer used. Hand mixed cements have smaller measured values of shrinkage due to the presence of pre-disposed pores. These pores are thought to expand during polymerisation and hence reduce the net shrinkage effect at the interfaces[83].

Studies that have attempted to measure cement shrinkage have tended to use water displacement methods[77,79,82], diametral methods[83] or theoretical calculation[82,83]. Although these methods have limitations associated with them[82], there is now strong evidence that cement shrinkage coupled with geometric constraints do influence the amount of porosity within the cement mantle and around cement interfaces. However, due to the difficulties in assessing the state of a cement mantle during or immediately post cure, there is less understanding of the extent to which pre-cracking may exist within the cement mantle prior to any load bearing activity.

Most inspection techniques rely heavily on serial sectioning which cannot give real time information during the cure phase of cement, are time consuming and cannot monitor the entire volume of cement. Race et al[84] have demonstrated that pre-cracking may exist *in-vivo* based on serial sectioning of cadaver samples, but the amount of information and hence understanding of pre-load damage is capped by the limitations imposed by current assessment techniques. Lennon et al[81] developed a 2-D femoral model which allowed cracks induced through polymerisation to be viewed by manual inspection. Although this model was a simplified version of a section of a stem construct, the authors were able to visualise pre-cracks present in the cement mantle and were the first to demonstrate a distinct relationship between residual stresses induced through polymerisation and observed cracking. Roques et al[85] have investigated the stresses induced during polymerisation on idealised cemented stem sections and estimated residual stresses as high as 10MPa. Stresses of this magnitude would cause damage immediately post implantation[81,85] and when the stress around a pore is taken into consideration, stresses as

high as 24MPa have been predicted[81]. Roques et al[85] were also able to show signs of cracking and rubbing during polymerisation using the acoustic emission (AE) technique.

There is a need to develop more sophisticated techniques to assess and visualise the pre-load cracking within the cement mantle. It is hypothesised that the condition of a cement mantle during polymerisation may be monitored accurately and easily through the use of multiple AE sensors. However, in order to quantify the accuracy of the information provided from the AE data, simultaneous assessment techniques must be employed that can give visual representations of any damage present within the mantle.

Fatigue Life

The fatigue life of bone cement is ultimately the limiting factor for this material and why all cemented type femoral prostheses will eventually fail no matter how secure their initial fixation. Topoleski et al[86] were the first to identify that fatigue was the primary *in-vivo* failure mechanism of bone cement. Their fractographic analysis showed that fatigue crack growth is preceded either by a damage zone of connected fibrils or by a "microcraze shower damage zone". The distinction as to which mechanism exists was shown to be dependent on the molecular weight of the polymer, with high molecular weight polymers exhibiting fibril formation, and lower molecular weight polymers exhibiting the microcraze shower zone. The crack growth in either scenario may be discontinuous with groups of fibrils breaking under sufficient stress, or microcraze coalescence determining crack growth.

The exact role of cement fatigue in the overall loosening process is somewhat uncertain since the chronology of events leading to loosening from deterioration of the cement mantle is debatable. Some studies report evidence to suggest that fatigue of the cement itself is an initiating factor[87], whilst others suggest that debonding of the cement-prosthesis interface occurs prior to fatigue damage[88]. Jasty et al[88] identify that the main reason for these discrepancies is that clinical radiographs are inadequate to identify the very early stages of failure and by the time that the implant is revised, the initial information has been lost. Nonetheless, bone cement does suffer from fatigue damage, and the fact that bone cement contains multiple constituents, all of which may play a role in determining the fatigue life of a particular cement, has lead to extensive research which has attempted to understand and improve its fatigue performance. Ageing of bone cement has been shown

to affect its material properties with a consequent reduction in strength and toughness[78] especially in a saline environment[62]. Lewis[89] reported that increasing the molecular weight of the polymer increases the fatigue life of the cured cement. Davies et al[90] investigated the effects of incorporating antibiotics into the cement formulation and found no significant effect whilst others report a decrease in mechanical properties and found that the addition of antibiotics made the initial mixing of cement more difficult[91]. The addition of radiopacifying agents, namely barium sulphate or an iodine containing copolymer has been shown to significantly increase the fatigue life of cements[89] and improvements of up to seven fold have been reported[92]. Molino and Topoleski[93] reported that this improvement was associated with crack path deflection as a result of the presence of radiopacifying particles. However, the positive effect of these radiopacifyers is the subject of some debate, with some researchers reporting that the addition of barium sulphate reduces fatigue life[94,95]. Both fibre and particle reinforcement techniques have shown significant improvements in the fatigue performance of cement formulations. These are thought to act in much the same way as the barium sulphate particles mentioned above in that the crack propagation is hindered and diverted thus requiring more energy to reach critical crack lengths. However, the bone cement constituent that has received the most attention, and proven to be the most controversial in terms of its effect on fatigue performance is porosity:

The influence of the size, geometry, distribution, and number of pores present in the cement has been the subject of much investigation. Some studies report a definite increase in fatigue life of cement associated with a reduction in porosity[62] or at least with a reduction in pore size[96]; others suggest that although this may be true of simple specimens used in laboratory tests, the same cannot be said in clinical practice[97-99]. Other researchers have identified the possibility that porosity may not be the principal stress concentration that initiates fatigue and so is perhaps less clinically relevant than previously thought[100]. The idea that the cement mantle may contain cracks prior to any active loading from the patient simply due to the stresses induced during polymerisation[81,85,101] supports this theory. The controversy over the influence of porosity on fatigue life is further complicated by evidence that suggests that porosity can actually reduce crack growth rates[96,102] and hence prolong fatigue life. Ishihara et al[96] reported on the differences between the fatigue behaviour of CMW type 3 and Zimmer bone cements. By subjecting specimens to a 4-point cyclic loading regime they were able to show that the CMW cement exhibited better

fatigue characteristics under this loading configuration. They attributed this difference to the reduced number of large pores (>300μm) that were observed at the bone cement surface. During crack propagation, however, the crack was shown to be arrested by subsequent pores, so the role of porosity was shown to be two-fold: Large surface pores acting to initiate fatigue cracks, and smaller subsurface pores acting to retard crack growth. Final failure resulted from the amalgamation of several propagating cracks. Sinnett-Jones et al[103] were able to use both AE and ultrasonic imaging to identify very early fatigue damage initiation within un-notched tensile specimens. These areas were visualised using synchrotron radiation computed tomography to obtain high resolution (0.7μm) 3D images of fatigue crack formation. They observed that the crack initiated close to, but not at the pore surface and that its formation may have been due to the combined effects of a geometrical ridge on the pore surface resulting to the intrusion of multiple PMMA beads, as well as the presence of a cluster of $BaSO_4$ agglomerates. However, in a clinical situation, there are likely to be significant stress concentrations due to the trabecular geometry on one side of the mantle, the stem geometry on the other, and the presence of pre-load polymerisation cracking, and Evans[104] argues that it is the understanding of fatigue crack propagation rather that initiation that may be more significant.

As mentioned previously, the fatigue behaviour of bone cement is somewhat more complicated than that of metals. Crack propagation is not continuous, but instead develops in a start-stop fashion[105], loading frequency may significantly alter the fatigue life of the material[106] and significant effects have been observed when sudden overloads are incorporated into a fatigue testing regime[104]. In agreement with the earlier work of Topoleski et al[86], Döll & Könczöl[105] describe the fact that the brittle failure of thermoplastics is dependent on the presence of a "craze" ahead of the crack tip, and subsequent crack propagation is dependent on the breakdown of this craze. Döll & Könczöl[105] used optical interferometry to quantify the size of the craze ahead of a propagating crack and reported craze lengths of between 10-35μm in high molecular weight PMMA. Their investigations showed that the crazed region may increase in size under constant load despite the crack itself remaining stationary perpetuating the idea of crack/craze formation start-stop crack propagation, and that a longer craze region may be observed at lower loading frequencies owing to the effect of strain rate. Pulos & Knauss[106-108] dedicated a significant amount of effort into trying to understand fatigue crack growth behaviour in PMMA and developed a methodology such that they were able

to investigate crack propagation at the micron level within a time resolution of less than one cycle. During these investigations, they demonstrated that loading frequency may alter the entire crack fracture morphologies and that the load history has a significant effect on crack propagation[107]. Rough fracture surfaces were observed during loading at high stress intensity factors due to the coalescence of the multiple craze regions that were shown to exist ahead of the crack tip. Conversely, microscopically smooth fracture surfaces were observed during loading at lower stress intensity factors as the crack was shown to propagate through the centre of the crazed region. These different propagation mechanisms have implications in terms of the acoustic activity that one may expect to detect. Koenczoel et al[109] conducted some early experiments around the AE generated from the crazed region during slow crack growth in polystyrene and reported that that majority of AE was associated with the breakage of fibrils around the crack tip. Their research suggested that the cumulative energy, duration and number of hits produced from crack propagation is proportional to the newly formed fracture surface area, whilst their rates are related to the crack speed. Further investigations into the relationship between AE waveform parameters and different damage mechanisms in bone cement is given later on in the literature review when acoustic emissions from bone cement are described.

Historically there has been a tendency to simplify laboratory test situations in order to try and predict clinical failure. However, more recent investigations are beginning to show that these tests may have been oversimplified to the point where the main clinical factors are overlooked. Ishihara et al[96] and Johnson et al[110] both noted an association between fatigue life and loading frequency, with longer fatigue lives being accomplished at higher frequencies. This effect was attributed to the viscoelastic nature of bone cement and the subsequent increase in local stresses during longer duration load cycles. Most fatigue tests use constant amplitude loading, yet Evans[104] was able to demonstrate a clear influence of variable amplitude loading on fatigue life, and we know from the work of Bergmann et al[11] that the types of load seen *in-vivo* are far from constant and may be quite extreme in certain situations. Relating this to the test methodology conducted in this thesis, it is almost certain that we should be more concerned with fatigue crack propagation rather than initiation in otherwise perfect specimens. The simplified construct that is described in CHAPTER 4 was designed specifically to introduce stress concentrations along the corners of the stem, and the work conducted in CHAPTER 5 demonstrated that the polymerisation process alone was sufficient to induce crack formation within the Technovit layer. The fact

that this pre-load cracking has also been observed around genuine THR stems[84] suggests that monitoring the progression of damage in complete constructs with pre-existing damage *in-vitro* may be a more representative way of determining the true influence of factors such as porosity *in-vivo*, and this is in-line with the findings of Cristofolini et al who were able to show a correlation between *in-vitro* and ex-vivo fatigue performance of different femoral stem designs using clinically representative *in-vitro* testing[111] of THR constructs. Overall it seems that the factors that cause significant alterations to the crack path have the largest effects on the fatigue performance of bone cement. For example, porosity distribution was shown to have a greater effect on fatigue life than the total pore volume per se[112], levels of reinforcement, and molecular weight are other factors that have been consistently shown to significantly affect fatigue performance - all factors that cause fatigue crack diversion.

Ultimately, bone cement accumulates damage through fatigue loading, and it is believed that the ability to detect the onset of fatigue failure within bone cement during its initial stages, is something that could be used to differentiate between different stem designs, cement formulations and implantation techniques.

As stated earlier, Jasty et al[88] have identified that radiographic analysis is not capable of detecting the early stages of failure and Sundfelt et al[41] described the use of registry information and revision rates as "blunt instruments". Early detection of such loosening may prevent the patient from experiencing unnecessary pain and suffering through early intervention, which itself has a greater chance of success when performed early[6]. Conversely, any patient undergoing a surgical procedure has a reduced quality of life during recovery, and the benefits of early revision must be assessed on an individual basis. However, in order to make informed decisions clinicians must have the ability to accurately assess the state of an implant. Hence it is clear that in order to appreciate the mechanisms of aseptic loosening and cement fatigue, other monitoring techniques must be considered. Current monitoring and diagnostic methods are improving, although most are expensive, limited in terms of the information they can provide, or inaccurate and the next section will review the use of current monitoring techniques.

2.2 CURRENT MONITORING METHODS

There is a significant debate over the most appropriate approach to patient follow-up for those who have received a THR. The British Orthopaedic Association recommends a clinical and radiological follow-up involving at least two x-rays (one A.P. and one lateral) during the first post-operative year and at intervals of five years thereafter [113]. However, the actual follow-up received by a patient is largely dependent on the clinician. Most surgeons discharge patients within the first post-operative year, and few follow patients for more than five years[114]. The British Orthopaedic Association argues that because THRs fail after five years, that patients should be followed in the longer term. Furthermore, if massive bone destruction is allowed to occur prior to a revision operation, then that operation is less likely to succeed, and puts a larger demand on resources[6]. This situation is worsened by "silent" patients who suffer from aseptic loosening but do not complain until the pain associated with the loosening becomes severe. Therefore a regular follow-up is necessary to identify progressive failure and enable revision prior to the onset of massive bone destruction. Other reports suggest that regular radiographic reviews are ineffective and should be restricted to a 6-12 week review followed by discharge if no problems are detected[115]. Bhatia & Obadare[115] reported on 100 patients who were followed up for an average of 2.3 years. During the study 187 radiographs were taken, however only 8 of these radiographs showed signs of abnormality, and 70% of patients requiring intervention were referred by a GP or the accident and emergency department. Therefore the effectiveness of regular reviews is called into question and Bhatia & Obadare concluded that the cost of such reviews could not be justified[115].

Radiographs are a convenient monitoring method as X-ray imaging techniques are commonly used and the necessary machinery is available in all hospitals. Factors such as bone density, prosthesis location, dislocation, or catastrophic implant failure can all be observed using this technique. However, in all cases the accuracy of the information is poor, and largely dependant on the image quality and inherent observer error. X-ray imaging often does not capture the early signs of failure due to its low resolution, and as such a radiologically loose prosthesis may remain undetected until the latter stages of failure/loosening[116]. Other diagnostic methods are available; however, the expense associated with these techniques has limited their use to clinical trials where generic information is required for the development of prosthetic design. Examples are listed below:

RSA – (Roentgen Stereophotogrammetric Analysis) was developed in 1989 by Selvik[117] and allows the determination of three dimensional relative orientations between objects such as a prosthesis and bone. It has been used to accurately detect micromotion and migration of prostheses (0.05-0.5mm translation, and 0.15-1.15° rotation)[38]. The early migratory patterns of hip prostheses has been shown as a possible method for predicting implants likely to become loose[118,119]. Kärrholm et al[118] studied and performed RSA on a total of 84 hip arthroplasties[118]. Their results suggested that early subsidence associated with the stem was an indicator of impending failure. Indeed the probability of revision was found to be greater than 50% if the subsidence at two years post operatively was greater than 1.2mm. Hauptfleisch et al[119], however, concluded that subsidence was not such a good predictor of failure and could not be used to distinguish between failed and non-failed femoral stems[119]. Instead Hauptfleisch et al[119] proposed the use of posterior head migration as a predictor. The posterior head migration is associated with internal rotation, and Hauptfleisch et al[119] found a clear distinction between the failed and non-failed femoral stems based on this.

It would appear that RSA can detect migration and that the early behaviour of prosthetic stems can be used as a predictor of failure. However, the predictive powers of the technique may not be as straightforward as previously thought. The differing performance of various stem designs may require selective factors for assessment. For example, Kärrholm et al[118] concluded that subsidence can be used as a predictor of subsequent loosening based on their work on the cemented Lubinus SPI arthroplasty. However, Hauptfleisch et al[119] compared migrations of the textured Charnley Elite-Plus femoral component and the polished Exeter stem – concluding that posterior head migration is a better predictor of loosening and subsidence would have conflicted with clinical results. Further work needs to be done in this area to verify that one factor such as posterior head migration may be used for all types of stem design. This problem cannot be easily addressed using RSA as the technique cannot be used for retrospective data from patients without implanted markers. Walker et al[120] did develop a method for measuring axial and varus-valgus migration from retrospective radiographs. Again the authors concluded that stem migration could be used as a predictor of failure; however, their method cannot be used to measure axial rotation.

DEXA – (Dual Energy X-ray Absorptiometry) allows bone mineral density (BMD) to be measured by using X-rays from two different sources that are directed through the bone at a certain frequency. The greater the bone mineral density, the larger the signal picked up by a photon counter. Using two different X-ray sources offers greatly improved accuracy over the more traditional radiography methods[37]. The technique has been used to demonstrate that bone loss does occur around endoprosthetic components and is most significant within the first six months post operatively[121]. It has also been shown that subjects with a low pre-operative BMD are likely to suffer more severe bone loss following surgery. However, little work was able to relate changes in BMD to aseptic loosening. Wilkinson et al[122] addressed this issue and reported that loosening was related to region-specific decreases in proximal BMD. However, they were unable to say the same for the acetabular component. Furthermore, it was not discernible as to whether the decrease in BMD caused loosening or vice versa. In summary the technique has identified a weak correlation between BMD and loosening, however, the technique requires specialist equipment and exposes the patient to relatively high doses of X-ray radiation and therefore is not ideal as an alternative loosening detection method compared to standard radiographs.

Post mortem examination - Inspection of endoprosthetic devices following autopsy provides valuable information regarding the *in-vivo* state of an implant. Once again the value of radiological examinations and the way in which they are interpreted was called into question based on histological evidence. Kwong et al[123] conducted a study comparing the radiographic evidence of loosening with retrieved specimens. Despite radiolucent lines being observed in 14 out of 15 samples, only one sample was physically loose – suggesting that the radiolucent lines that had previously been associated with a fibrous tissue at the interface may not be indicative of loosening at all. Unfortunately the inaccessibility to specimens and practical difficulties in assessing particular variables limit the use of such studies[41].

Other methods such as Arthrography – whereby a radiogram is made following an injection of a radiopaque substance[116], and Scintigraphy – whereby the radioactivity is recorded following the administration of a radionuclide are also used, but have been reported to have low sensitivity[116,124].

Summary

This section of the review has focussed on the fact that the principle cause for revision operations of total hip arthroplasty is aseptic loosening, and the techniques are currently used to assess this problem. Despite all the advances in diagnostic methods, one of the most reliable indicators that an implant is loose continues to be the patient. The review has considered other techniques that are not widely used, but that have demonstrated promising results in the literature. RSA was shown by several authors as a possible predictor of implant loosening. However it is time consuming, expensive, and must be planned in advance of any study[120]. DEXA has been shown as a useful tool to monitor BMD, which again may be associated with aseptic loosening, although there is a level of uncertainty associated with this hypothesis.

As Browne et al[116] point out; there are currently a significant number of loosened prostheses that are undetected. Current techniques are not capable of detecting the early events associated with failure and we do not have a clear understanding as to the chronology of events. This information is vital for the advancement of prosthesis design[125]. Furthermore since none of the techniques used thus far are capable of continuous monitoring, the accuracy of information is very much dependent on the frequency of review. There are, however, a number of techniques that are used in other industries that have successfully been used to monitor the condition of engineering structures non-destructively. The acoustic emission technique, resonant frequency analysis and ultrasonic imaging are all techniques that may be applicable for the detection of loosening implants if a system could be created that would allow the integration of these techniques into an implant. The next section of this review considers these techniques in some detail and explains the principles behind each technique, where these techniques are currently used and the foreseen merits and issues associated with incorporating these technologies into an instrumented prosthesis.

2.3 TECHNIQUES TO CONSIDER

This section of the literature review highlights techniques that have the potential to address some or all of the shortcomings associated with the current monitoring methods identified in the previous section. The main focus here is to propose a technique capable of detecting loosening at its earliest stages. Simplicity, accuracy and cost are major factors to be taken into consideration. This review will consider three techniques that have shown potential in this area, although none of them are currently the preferred method for identifying loosening of total joint replacements. These methods are resonant frequency analysis, ultrasonic imaging and acoustic emissions.

2.3.1 RESONANT FREQUENCY ANALYSIS (RFA)

RFA is a technique that has already been used successfully in bioengineering to assess the fixation of dental implants. Since the technique is already proven for such a similar application, it is only logical that it be considered to assess the fixation of hip prostheses. The concept of resonant frequency analysis (RFA), also known as vibration analysis, is very simple; the object of interest, namely a hip prosthesis is vibrated over a range of frequencies. By analyzing the response of the system, the resonant frequency may be determined. If the fixation degrades, the resonant frequency of the system will be affected. Thus it should be possible to use vibration analysis to identify early failure mechanisms and hence predict failure within an implant. This review will consider studies that have used the technique to assess total hip replacement stability. However, references are made to work done in related areas such as dentistry where the technique is established and used successfully.

DENTAL APPLICATIONS

Research aimed at developing instrumentation based on RFA for the assessment of dental implant stability has seen clinical success. The problems associated with identifying loosened implants through insensitive radiographic analysis were shared between dentistry and total hip replacement surgery and as such the reasoning behind work looking at alternative diagnostic methods was largely the same. Although a few preliminary studies have indicated the potential of RFA to assess the stability of total hip replacement constructs, the technique has been taken much further within the field of dentistry and several commercially available products have been successfully marketed. An explanation for the different rates at which this technique has been employed between dentistry and

total hip replacements is the accessibility to the implant: In dentistry, the practitioner has direct access to the implant and can attach the transducer directly to it – negating any transmission losses through interfaces and soft tissue. In the mid 1980s Kaneko et al[126] used an Acoustoelectric technique to monitor changes in frequency and amplitudes of response signals to a pulse input in order to assess the difference in fixation between non-bioactive and bioactive dental implants in animal trials. It was found that secure implants gave lower amplitude, higher frequency responses and the technique was more sensitive to the interfacial state than radiographic methods. In later work, Kaneko[127] considered the effect of excitation direction on response and concluded that in order to distinguish between a rigidly bonded bone-implant interface, and an implant merely in contact with the bone, the load should induce a shearing force at the interface.

Further encouraging results were presented by Meredith et al[128] who modelled the effects of changes to surrounding bone stiffness by measuring the resonant frequency response during the curing process of polymethylmethacrylate. The authors developed a device that measured the resonant frequency of a transducer that was attached to an implant. This device enabled changes in the implant-tissue interface and surrounding bone to be monitored. The transducer consisted of a small beam with 2 piezoelectric elements attached to it. By exciting one of the piezoelectric elements with a sinusoidal signal, and measuring the response of the other, the resonant frequency of the system could be determined.

The resonant frequency of a cantilever beam, supported at one end can be calculated from the formula:

$$R_f = \frac{1}{2\pi}\sqrt{\frac{3EI}{l^3 m}} \qquad \textbf{Equation 1}$$

Where:

R_f = Resonant frequency (Hz)
l = Effective beam length
m = mass of beam
E = Youngs modulus (GNm^{-2})
I = moment of inertia

From this expression, it is clear that the resonant frequency of the system will vary with length and stiffness. Experimental work carried out by Meredith et al[128] confirmed this and showed the tests to be representative and repeatable. It was found that the resonant frequency increased significantly with increasing stiffness. Meredith et al also performed *in-vivo* measurements, and found the results correlated well with their *in-vitro* model[128].

A later study conducted by Glauser et al[129] showed that failing implants were subject to a sustained decrease in stability and the resonant frequency was substantially lower than that noted for secure implants during the first few months post operatively. The findings from the RFA technique were verified from clinical observation. It should be noted that the clinician was not aware of any measured RFA values and as such could not bias his opinion. It was demonstrated that RFA can be used to diagnose failing implants prior to any clinical manifestations indicative of failure and since this study, the RFA technique has been made commercially available (OSSTELL, Integration Diagnostics, Savedalen, Sweden), and the Periotest® - developed by Siemens AG.

APPLICATION OF RFA IN SUBCUTANEOUS ORTHOPAEDIC APPLICATIONS

Similar to RFA used in dentistry, the technique was first used in the late 1980's to assess hip implant loosening. However, unlike in dentistry, the technique has not been so widely accepted and the following review attempts to provide an understanding as to why this is the case.

Rosenstein et al[130] performed a study whereby they were able to discriminate between secure and loose femoral components both *in-vitro* and in a pilot clinical study. The *in-vitro* study used cadaver femurs from post-mortem operations. The constructs were excited using a shaker coupled to the lateral femoral condyle and the output recorded from a piezoelectric accelerometer mounted on the greater trochanter. Loosened implants were simulated by allowing bone cement to cure around the femoral stem prior to implantation or by deliberate loosening of a well fixed implant through removal of proximal bone cement and separation of the stem-cement interface. It was found that well-fixed components gave a regular sinusoidal output with no significant harmonics. Loosened implants, however, produced superimposed waveforms with a large increase in the number of harmonics. In their pilot clinical study, Rosenstein et al performed tests on seven

patients with symptomatic signs of loosening, and a further four patients with recently implanted prostheses assumed to be well fixed. Again, the system was excited using a shaker over the lateral femoral condyle, and the response obtained from an accelerometer held over the greater trochanter, although the excitation and measured response had to pass through the skin. Of the seven patients admitted for a revision operation, five were found to have loosened implants, the remaining two were found to be securely fixed. The results from the operational observations agreed with Rosenstein et al's diagnosis using RFA. Four of the patients also underwent a preoperative arthrography procedure, which was found to give false results in two cases. The authors conclude that although further work is necessary, their early findings show that RFA could be used as a non-invasive technique for early identification of implant loosening.

Collier at al[131] uses what they describe as a "phase delay" technique. The authors argue that resonant frequencies *in-vivo* are hard to measure due to the damping effects of the surrounding soft tissues and the influence of other factors unrelated to the state of the bone itself. The authors studied the effects of fracture healing on the time taken for an induced vibration to travel through a known length of bone. By expressing this time delay as a fraction of one complete cycle (one cycle was defined as a completion of a loop between the shaker and the accelerometer), the authors were able to measure the "phase delay" by adjusting the frequency of the shaker until the inverse corresponded to the time to complete one loop. The presence of a fracture was shown to reduce the velocity in the affected region and hence induce a longer phase delay. The authors took measurements at various positions along the tibia of a "normal" leg, and a fractured leg both before and after the fracture had unified (determined through manual manipulation) and the authors were able to demonstrate a large variation in phase delay between points measured around the fracture site. It was shown that healthy subjects would enable frequencies of over 100Hz to be recorded, whereas fractured subjects produced much lower frequencies. However, the number of subjects used in this trial is not stated, and therefore the statistical relevance of these findings is not identified. Collier et al also reported work conducted in a very similar manner to the work of Rosenstein et al[130] where the degree of fixation was identified by the effect on harmonics. This work added credit to the work of Rosenstein et al in that their findings also showed that this method could be used to assess implant loosening. However, Collier et al were only able to justify their findings based on the fact

that most patients studied underwent revision surgery. No reference as to whether the method accurately diagnosed loose prostheses was given.

A later study conducted by Puers et al[132] attempted to avoid some of the problems associated with attenuation through soft tissue by placing an accelerometer inside the head of the prosthesis itself. Although this method enabled the acquisition of "better" measurements, the authors were confronted by other restrictions such as power consumption and physical dimensions of the device. In their study, Puers et al excited the system in a similar fashion to other studies by using a shaker held over the lateral femoral condyle. Loosening was detected through the amount of distortion imposed on the detected sinusoidal waveform. It was found that an excitation frequency of 150Hz gave good results showing a clear distortion in loosened prostheses compared to a clean sinusoidal waveform for well fixed prostheses. However, despite the positive results obtained through cadaver experiments, results from clinical trials were never published.

The vibration technique is looked at in detail by Georgiou and Cunningham[133] who also used a similar method to Rosenstein et al[130]. Georgiou and Cunningham's study compared results from their vibration measurements with radiographic analyses and found the vibration technique to be 20% more sensitive and able to definitively diagnose more patients than radiographic methods. Limitations of the technique were realised, and it was found that the vibration technique could not give a definitive diagnosis in 8% of patients[133]. The authors concluded that improvements in the vibration testing technique could enable it to be used as the preferred method of diagnosing implant loosening over currently used radiographic methods. In their study, Georgiou and Cunningham studied a frequency range between 0 and 1000Hz. 23 patients took part in the study with both clinical and radiographic signs of loosening along with 10 control patients who had recently undergone surgery. The true stability of the implant was assessed during the revision operation. During vibration analysis, loosening was identified by both the presence of harmonics, and the number of resonant peaks. One of the key differences with this study compared to others is that the vibration data was interpreted by "blind" assessors who had no prior knowledge of the technique, and were simply given a set of guidelines in order to classify the subjects into categories of secure or loose prostheses. It should be noted however, that certain patients were unable to proceed with the vibration analysis due to discomfort induced by the vibrator, or an inability to manoeuvre into the required

position – thus highlighting a limitation of the technique. Furthermore, Georgiou and Cunningham were the first to assess loosening of the acetabular component as well as the femoral component using the vibration technique, and found that it was only capable of accurately diagnosing 50% of loose acetabular components, which is similar to that identified for both arthrography and radiographic methods. However, the authors argue that for a technique in such an early stage of development these results remain promising.

More recently, Pastrav et al[134] hypothesised that a more sensitive measure of prosthesis fixation could be obtained using the vibration technique if the vibration modes of the prosthesis itself could be shown to be more affected by the degree of loosening than the modes of the femur. The authors looked at the frequency response functions for prostheses with varying degrees of induced loosening. By exciting and measuring on the prosthesis itself, a clear distinction between the various loosened states could be established. It was also shown that the vibration analysis technique was more sensitive to loosening among the higher order mode shapes and the differences in sensitivity between the lower and higher order modes were significant. As such it was reported that resonant frequencies below 500Hz were relatively insensitive to the quality of fixation, whereas peaks above 1500Hz show a distinct shift for various degrees of fixation. However, the authors found difficulty interpreting resonant peaks above 7000Hz. The main drive of their work was to develop a method for monitoring fixation during stem insertion, that is, to identify a point during stem insertion at which it may be said to be secure. Although this is not strictly the same as diagnosing implant loosening, their work is of particular interest to this project since an important aim is to develop an implanted system that would rely on the stimulation and response of the prosthesis as opposed to the femur. Furthermore, it seems that by stimulating the prosthesis, the authors were able to obtain a greater distinction between the various degrees of loosening than previous studies had been able to achieve. Subsequent work by Pastrav et al[134] identified a distinct endpoint for stem insertion when the R value correlation (this is a measure of how strongly pairs of variables are related) between frequency response functions from successive hammer blows tended to 1 over the frequency range of 200-7000Hz. The authors also suggested that the technique could be applied to prosthesis loosening.

Summary

Vibration analysis has been used as a successful tool within dentistry to distinguish between a stable and a loose implant. Commercial products have been developed based on this technique. It should be noted that dentistry permits direct access to the implant itself, and as such there are no complications concerning signal attenuation as it passes through skin etc.

Attempts have been made to use this technology to detect loosening in total hip replacements; however, attempts to create an instrumented hip without affecting the fundamental design of the prosthesis have so far been inadequate and required an external excitation from a vibrator placed above one of the condyles of the knee. This immediately decreases sensitivity due to the attenuating nature of the skin, and the fact that the measured frequency response is that of the femur as opposed to the prosthesis.

2.3.2 ULTRASOUND

One of the first forms of ultrasonic imaging was developed in the 1940's when Dr. Karl Dussik produced a form of ultrasonic brain scan based on the attenuation of the signal as it passed through the skull. The strength of the signal was measured by recording the brightness of a light bulb linked to the receiving transducer[135]. Since then, significant developments have occurred and ultrasonic imaging has established itself as one of the main techniques of imaging soft tissue and sub-surface features.

Medical applications are one of the fastest growing areas of ultrasonic applications. Ultrasound is already used for foetal imaging and other areas including cardiology, urology and ophthalmology[136]. Its appeal to the medical industry is based on two significant advantages:

Speed: The information is displayed in real time

Penetration: Ultrasonic waves propagate through opaque materials – enabling a cost effective and reliable method to build an image of any interior features of an opaque object.

ULTRASONIC IMAGING IN THR

Any diagnostic technique aimed at detecting aseptic loosening must be capable of distinguishing between bonded and de-bonded stem-cement and bone-cement interfaces. Davies et al[137] demonstrated that a mechanical bond does indeed exist between the metal-cement interface although clinical experience shows that this bond is susceptible to failure. As stated earlier, current radiographic techniques are simply not sensitive enough to detect this de-bonding, and it is often only detected following sectioning and microscopic analysis post mortem. Davies et al[137] attempted to investigate the possibility of using ultrasound to detect de-bonding without the need for such sectioning. Initially, the authors concentrated on simple methods to indicate the potential of the technique. The authors used flat slabs of bone cement and cobalt alloy bonded using cyanoacrylate at one end, hence simulating both bonded and un-bonded regions within the same specimen. Further samples were prepared by bonding the cement directly onto the cobalt alloy plates and inducing a de-bonded region by forcing separation using a knife blade. By clamping the

de-bonded surfaces together, the authors were able to determine the necessary pressure at which the ultrasound technique could no longer distinguish between a bonded surface and a de-bonded surface forced into contact. The experiments were developed to include simulated stem constructs using both fibreglass and cadaver femurs. To ensure that the ultrasonic wave arrived normally to the stem surface, slots were milled into both the medial and lateral sides of the bone such that the bone cement in the region of interest was machined flat and parallel to the stem surface. It was found that the technique could detect interfacial de-bonding due to the total reflection of the ultrasonic wave on meeting a surface adjacent to air. Thus a de-bonded interface would reflect the signal having passed through the bone cement alone and arrive at the transducer out of phase with the original signal. A bonded interface would allow propagation into the metal stem, and reflections could be seen from both the stem-cement interface on both sides of the stem. It is recognised, however, that the stresses present in cemented hip arthroplasties could be capable of mechanically closing a de-bonded region such that it would appear bonded to the ultrasound technique. Furthermore, the presence of a fluid filling the de-bonded space enabled transmission across the interface and therefore de-bonding could no longer be accurately determined. It is therefore concluded that the technique may be useful for identification of interfacial de-bonding *in-vitro*, however there are several factors that limit the technique's ability to be used *in-vivo*.

Gibbon et al[138] identify a plethora of other issues that limit the use of ultrasonic imaging for *in-vivo* prosthesis evaluation. First and foremost is that bone has a similar reflectivity to metal, and although distinctions can be made between the two and indeed de-bonding identified in certain joint arthroplasties, the same may not be true for THR where the object of interest is largely encapsulated in a long bone. Furthermore, for assessment of deep structures, a lower frequency transducer must be used to achieve the required penetration, and this sacrifices resolution[138,139]. Despite this, images relating to infected total hip arthroplasty are presented and indicators of infection may be seen from the scanned images, although identification of such indicators would not be apparent to the untrained eye, which in itself poses further limitations of the technique. It was recognised in their paper that the technique is useful for identifying infection and soft tissue reactions to wear debris. Whilst this was useful for the distinction between aseptic and septic loosening, the initial identification of loosening was most likely to come from radiographic analysis.

Ostlere and Soin[140] reiterate many of the points made previously in their review of imaging techniques for prosthetic joints. However, unlike many authors, they suggest that standard radiographs coupled with clinical symptoms are sufficient to diagnose most cases of aseptic loosening. However, in this example, the importance for early revision for subsequent success is not strongly argued. Furthermore, the authors highlight a difficulty in the differentiation between aseptic loosening and infection, and point out that detection of loosening in revised prostheses is even more challenging from standard radiographs due to the residual radiolucent lines present after surgery. The authors again state that the use of ultrasound is limited to the observation of soft tissue regions surrounding the hip and for the identification of infection.

Summary

Ultrasonic imaging is a useful technique for sub surface identification of defects. The technique has been successfully used *in-vitro* and is particularly suited to the identification of the early stages of interfacial de-bonding. Browne et al[141] used the technique to locate initial de-bonding of the cement-metal interface. The authors correlate their findings to the acoustic emission technique, and a more in depth review of this article is presented in the next section. However, ultrasound as a diagnostic method for determining prosthesis loosening has severe limitations *in-vivo* due to the inherent physical separation from the object of interest, the possible presence of fluid within de-bonded regions, and difficulties in acoustic resolution of an object encased within the long femoral bone. Hence, as Davies et al[137] recognise, the technique is more appropriate for *in-vitro* assessment where it could be used to compliment and aid verification of other techniques.

2.3.3 ACOUSTIC EMISSIONS (AE)

An acoustic emission is the term commonly used to describe the transient elastic wave resulting from a rapid release of energy from a localised source within a material. This technique is described in some detail since it is the main focus of the research presented in this thesis. The concept of using acoustic wave characterisation as a means to assess structural integrity and predict failure is so well established within nature, it is perhaps surprising that the technique has seen such a slow integration into failure prediction of orthopaedic joint replacements. The ability to interpret acoustic waves is critical to the survival of many living species. Without it, the ability to sense and avoid predators or respond to danger would simply be insufficient. Beattie[142] uses the example of breaking wood as an illustration of this.

The ability to "hear" the elastic waves produced from microscopic changes to a material structure is largely dependent on converting physical displacement into a voltage-time trace. There are various methods of doing this: Phonograph pick-ups, magnetostrictive devices, laser interferometers, and piezoelectric devices are just some examples. However, to fully understand how these devices can be used to detect changes to a material structure, an appreciation of how waves propagate through a material must be established.

An acoustic wave is induced when a material is subjected to an applied stress sufficient to cause dislocation movement. The subsequent change in the surrounding stress field releases energy that excites nearby atoms. The motions of neighbouring atoms are related allowing the transfer of kinetic energy to propagate away from the original disturbance as an acoustic wave.

An acoustic emission generates numerous forms of wave, all propagating in their own characteristic manner. The interaction of waves leads to complications arising from component geometry, material structure and interface effects that shall be discussed later in this report. Firstly, the main types of wave and their distinguishing features shall be identified.

Acoustic waves can be divided in to three main categories; Bulk Acoustic Waves (BAC), Surface Acoustic Waves (SAW), and Plate Waves.

The type of wave that may be expected within a structure depends on component geometry, and the material of that structure. An important consideration is the expected wavelength in relation to the physical dimensions of the structure. CHAPTER 4 describes the design of the simplified stem construct that is used for all experimental testing within this thesis. The Technovit layer has a minimum thickness of approximately 2mm along the corners of the stem and a maximum thickness of approximately 3.5mm perpendicular to the stem edges. The stem itself has a maximum diagonal dimension of approximately 22.5mm at the proximal end, and 12.8mm at the distal end. The expected frequency range associated with crack formation is in the region of 200-800KHz (frequencies outside of this range would not be picked up reliably by the sensors used in these experiments). The speed of sound was measured as approximately 150cm/ms within the Technovit, and 450cm/ms within the stem. We may therefore calculate the approximate acoustic wavelengths that would be expected to be travelling within the construct:

$$\lambda = v/f \qquad \textbf{Equation 2}$$

where:

λ = wavelength

v = speed of sound

f = frequency

The expected acoustic wavelengths are therefore expected to be in the region of 2 - 8mm within the Technovit layer, and 6 – 23mm within the stem. In both the Technovit layer and the stem, the physical dimensions of the components lie somewhere within the range of expected acoustic wavelengths. To understand how this information relates to the types of wave that may be expected to be generated from crack initiation and propagation, we need to appreciate some of the different types of waveform, that may exist.

BULK ACOUSTIC WAVES

Bulk acoustic waves occur in components whose dimensions are far greater than the acoustic wavelength. In fluids, the only type of bulk wave that can occur is via a compression (Longitudinal) wave in which the particle motion is parallel to the direction of motion[143]. The result is a pulsing motion similar to that seen on motorways when travellers experience periods of slow traffic followed by fast, free moving traffic with no apparent reason for the delay. This motion is illustrated in Figure 3.

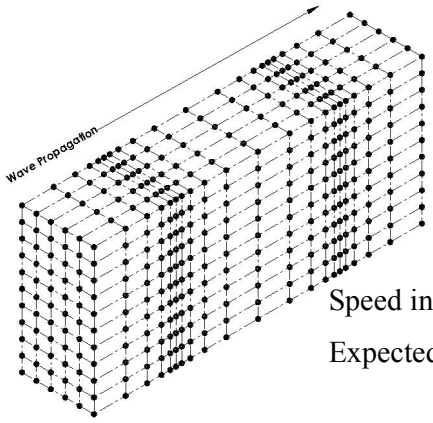

Speed in Technovit ~ 1500m/s

Expected wavelength ~ 2 – 8mm

Figure 3 – Diagram showing longitudinal wave motion

The stronger inter atomic bonds present in solids allow both longitudinal and shear motions to propagate through the material. Shear (Transverse) waves travel at approximately half the velocity of longitudinal waves[142,143] and thus in a perfect medium in which there is no attenuation or dispersion, and at some distance from the point of excitation, there would appear to be two distinct waves – one longitudinal, and one transverse. The motion of a transverse wave is illustrated in Figure 4.

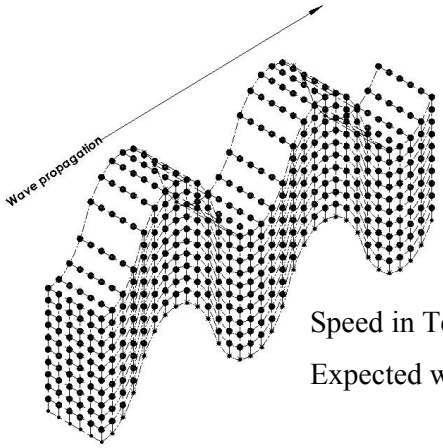

Speed in Technovit ~ 750m/s

Expected wavelength ~ 1 – 4mm

Figure 4 – Diagram showing transverse wave motion

SURFACE WAVES

Additional forms of wave are produced at the surface of a material due to the anisotropic nature of the atomic coupling forces[142]. Unlike bulk acoustic waves that are able to dissipate energy in three dimensions, surface acoustic waves are confined to a two dimensional plane and so attenuate less. There are two main types of surface wave; Rayleigh waves and Love waves, both of which are described below:

Rayleigh waves: A Rayleigh wave propagates along the surface of a material. It is characteristically defined in that the wave amplitude decays exponentially with respect to depth such that the region of displacement is confined to within a wavelength or so of a surface[143]. In contrast to bulk longitudinal and shear waves which travel at different velocities, the longitudinal and shear components of a Rayleigh wave are coupled together and travel with matching velocities, less than the shear wave velocity. The general form of Rayleigh wave propagation is shown in Figure 5 below:

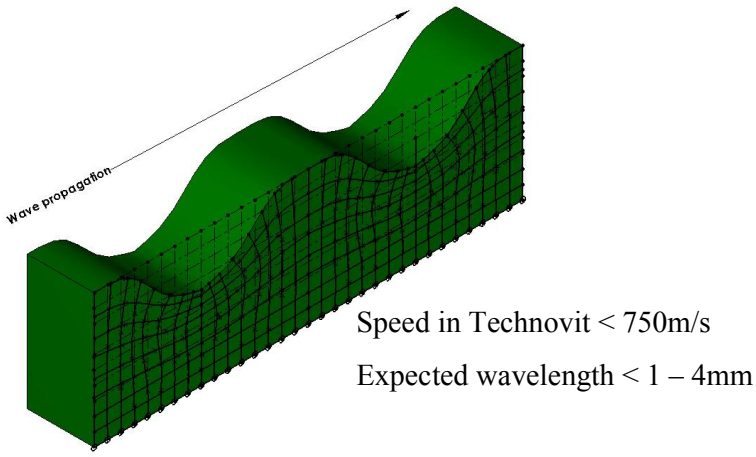

Figure 5 - Illustration of Rayleigh wave propagation

Love waves: A Love wave is a guided acoustic mode that propagates within a thin layer mounted on a substrate. Although still slower than the shear bulk acoustic wave, Love waves are the fastest form of surface wave and propagate with particular motion parallel to the surface and normal to the direction of propagation[144]. The Love wave motion is illustrated in Figure 6.

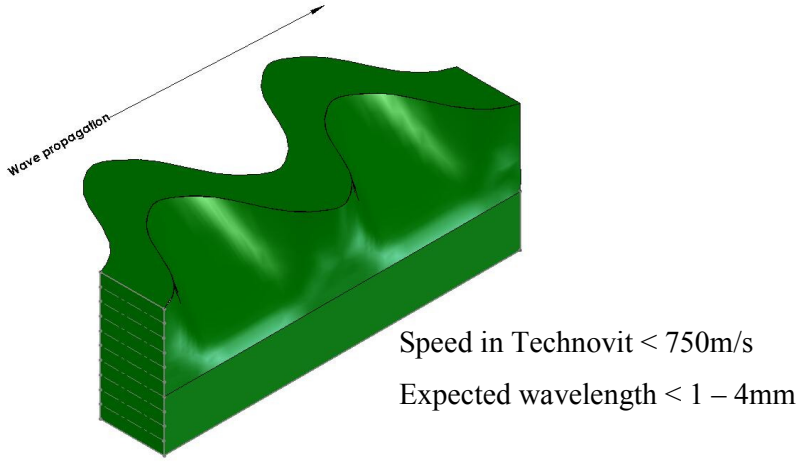

Figure 6 – Illustration of Love wave propagation

LAMB (OR PLATE) WAVES

Lamb waves are particularly important when using acoustic emissions for the condition monitoring of industrial machinery. Often the machines under investigation consist largely of plate like structures in which wave propagation is complicated by interactions with the two free surfaces[143]. Unlike the other forms of wave discussed thus far, the velocity of a Lamb wave is dependent on frequency as well as the plate thickness[136].

A Lamb wave may be considered as two Rayleigh waves travelling on each side of a plate with a thickness in the order of a few acoustic wavelengths[53]. Lamb waves may propagate as symmetrical and asymmetrical waves – as shown in Figure 7

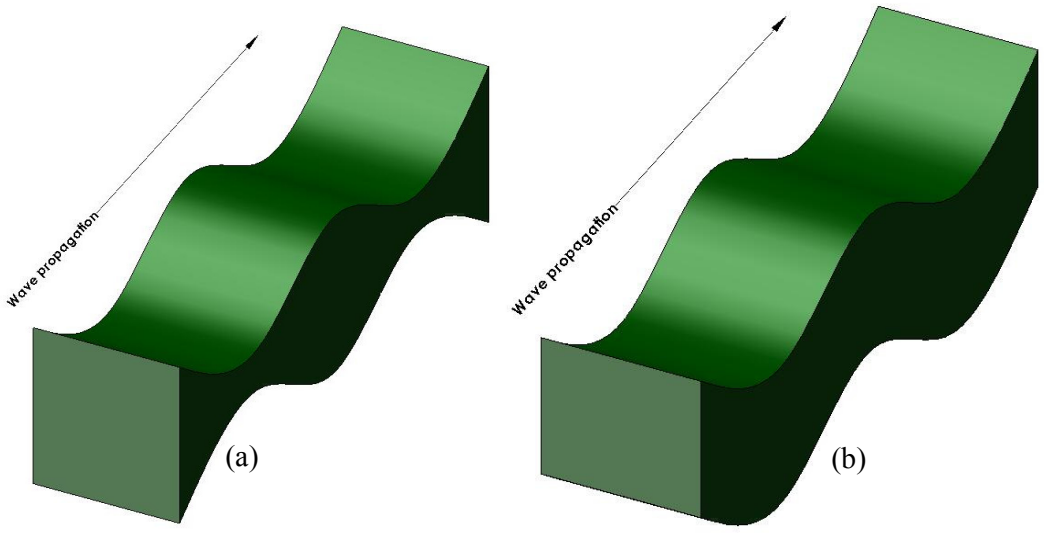

Figure 7 - Lamb wave in a) first symmetric mode and b) first asymmetric mode

INTERFACE EFFECTS

So far, only waves travelling in a single medium or at a surface have been addressed. However, waves travelling along or meeting an interface may produce other forms of wave, reflect or refract[142]. These forms of wave must also be considered since the simplified construct used in later experiments has several interfaces along which these waves may propagate.

Leaky Rayleigh Waves: Rayleigh waves, as discussed previously, are a form of surface wave. They are generally induced at the boundary between an elastic half-space and a vacuum or air[145]. However, waves resembling Rayleigh waves may also propagate along the interface between a solid and a fluid, radiating some energy into the fluid as it travels. These waves are known as leaky Rayleigh waves[136].

The radiation of energy into the fluid layer attenuates the wave rapidly. Cheeke[136] uses the example of a drop of water placed on a surface acoustic wave (SAW) delay line which kills the signal instantly, illustrating the significance of this attenuating effect.

Stoneley Waves: This type of wave travels along an interface, however, unlike the leaky Rayleigh waves, these are "true" interface waves and propagate without attenuation in a lossless media[136]. They occur at the interface between two elastic media and may therefore be present at the cement-stem interface.

PRACTICALITIES OF ACOUSTIC EMISSION MONITORING

If each of the above wave types is taken individually, then it would appear that the detection and analysis of an event resulting in an acoustic emission is relatively straightforward. However, the real situation is complex and a single event may trigger multiple types of wave. The complex structure of a THR consisting of various geometries and non-homogeneous materials, makes wave path prediction very complicated with multiple reflections and refractions being set up within the structure. The result is that the acoustic emission will consist of an initial shock wave followed by a series of chaotic echoes. This will have an effect on location accuracy of results and interpretation of what

is actually being detected, whether it be the initial high speed longitudinal wave, another waveform, or a reflection.

AE DETECTION

There are various methods for detecting the motions induced by the presence of an acoustic wave. In certain situations, it may be appropriate to induce an acoustic wave along the surface of a material such that the surface of the material itself can be used as a sensing device. This technique is used for Surface Acoustic Waves devices (SAW's) which have been in existence for the past 40-50 years. Their main use is within telecommunications as bandpass filters. Other applications include torque and tyre pressure sensors - within the automotive industry; chemical sensors – within the medical industry; as well as vapour, humidity, temperature and pressure sensors – for commercial applications[146].

Other techniques rely on a more passive approach and acoustic waves are induced by changes to the material structure. This is the technique that has been used in previous studies looking at acoustic emissions from bone cement[147,148], composite structures[149], as well as *in-vitro*[150,151] and *in-vivo* studies[152,153] of acoustic emissions from total hip replacement constructs. Since it is the state of structure itself, rather than the environment surrounding the structure that this study is investigating, this latter approach is the favoured technique for monitoring damage within a total hip joint replacement system.

Nearly all acoustic wave devices use the properties of piezoelectricity to generate/detect acoustic waves[136]. Therefore, to understand how these devices operate the concept of piezoelectricity must be appreciated.

WHAT IS PIEZOELECTRICITY?

Piezoelectricity was first discovered in the 1880's by Pierre Curie. The term piezoelectricity is named after the fundamental property of certain crystalline materials, such as Quartz and Lead Zirconate Titanate (PZT), which produce a voltage proportional to an applied pressure – hence the name piezoelectricity (pressure electricity).

The exact properties of a piezoelectric material are set up during the poling process. By applying a DC poling field, the mechanical and electrical axes of orientation can be set to the required direction. This process enables the designer to induce piezoelectric characteristics in a specific or multiple directions. Hence the piezoelectric material properties are anisotropic, and their properties are defined in each of the three axes denoted by numerals where 1 corresponds to the x-axis, 2 corresponds to the y axis and 3 corresponds to the z axis.

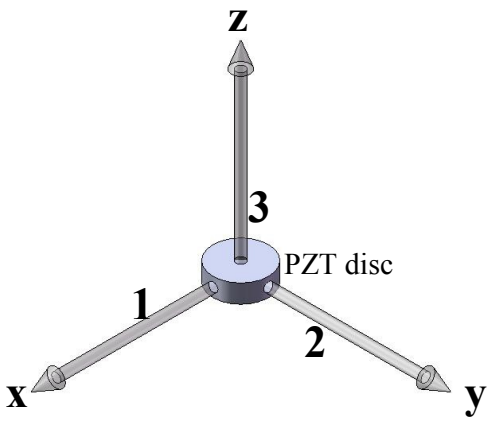

Figure 8 – Diagram to illustrate standard notation for the description of piezoelectric properties

Piezoelectric effects:

1) Actuation effects: Once the piezoelectric material has been poled, the dimensions of the material may be altered simply by applying a voltage to the material that is less than the poling voltage. Once the voltage is removed, the material returns to its original, poled, dimensions.

2) Voltage effects: Applying a voltage alters the dimensions of the material, the opposite effect also occurs in that an alteration to the dimensions of the material will induce a resultant voltage. By squashing the material in the same direction as the poling voltage,

the material will produce a voltage with the same polarity as the poling voltage. Conversely, stretching the material in the same direction as the poling voltage will induce a voltage with the opposite polarity to the poling voltage. A material's ability to exhibit a piezoelectric effect relies on the fact that its crystalline structure is noncentrosymmetric. The resultant effect is that its properties are anisotropic, and that the nature of the noncentrosymmetric crystalline structure produces net electric dipoles. Any regions consisting of dipoles aligned in the same direction are known as Weiss domains. Piezoelectric ceramic materials are only noncentrosymmetric below a certain temperature known as the Curie temperature. Above the Curie temperature, the material becomes centrosymmetric, and it loses its piezoelectric capabilities.

When a piezoelectric crystal is subject to a dynamic situation such as a vibrating beam, the response is maximised when the piezoelectric is operating around its resonant frequency. In general, piezoelectric devices may be classed into two broad categories, resonant and non-resonant. As the term implies, resonant devices operate at their mechanical resonance or within one octave of that resonant frequency. Non-resonant devices are designed to operate well below the resonant frequency, or over a large frequency range.

Limitations:

Temperature – A piezoelectric material has a temperature limit, depending on its chemical composition. Exceeding this limit can cause the material to de-polarize, thus lose its piezoelectric capability. Complete loss of piezoelectric properties occurs if the temperature is allowed to exceed the Curie temperature[92]. Piezoelectric ceramic materials are also subject to an ageing effect such that their piezoelectric properties diminish with age and operation.

Voltage limitations – A piezoelectric ceramic may become de-polarised if subjected to a strong electric field of opposing polarity to the material's poling voltage.

Mechanical stress – Subjecting the material to high mechanical stress loading may depolarize or even fracture the material.

CHARACTERISATION AND ANALYSIS OF ACOUSTIC EMISSIONS.

Acoustic emissions tend to be analysed statistically due to the multitude of factors that can influence the waveform, and it is extremely unlikely that two signals would ever be identical[142]. There are two basic methods for AE analysis that have been adopted in the literature: analysis of AE feature data, and analysis of the frequency response of the signal. Figure 9 shows two AE response curves, the first shows an AE response as a voltage-time curve, and the second shows the frequency response from the same signal.

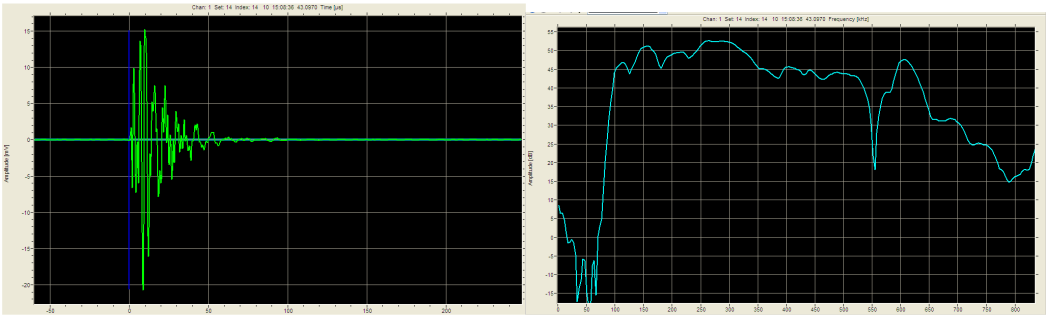

Figure 9 – Graphic representation of an AE response, as a voltage-time trace and a frequency response curve.

There are two basic forms of an acoustic emission response, continuous and transient as shown in Figure 10.

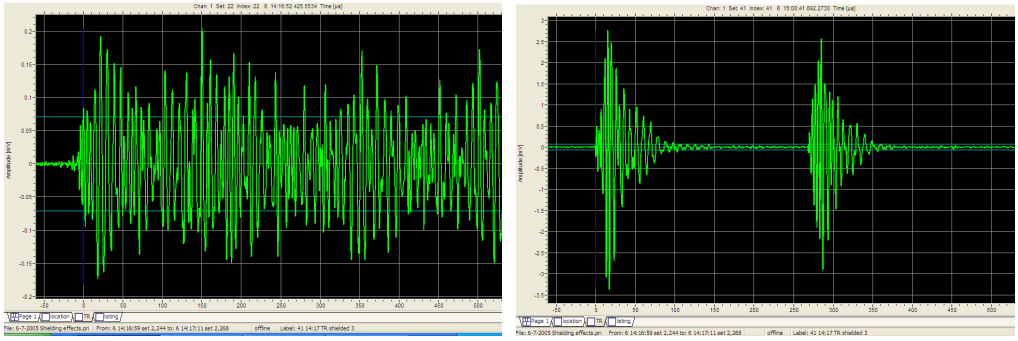

Figure 10 – Typical AE responses for: (a) a continuous emission and (b) a transient emission

Within a continuous response there are amplitude and frequency variations, but the signal never ends – a large part of the signal is formed from noise, and it is difficult to extract any meaningful data from the signal. This type of AE is thought to be caused by internal friction processes within a material[154]

A transient response has clearly defined start and end points of the signal that are distinguishable from background noise. This type of AE is thought to be produced from events such as crack initiation and propagation[154]. There are several features of a transient signal that can be used to characterize the particular signal. These are illustrated in Figure 11 and listed below:

Threshold levels – these are values set by the user to distinguish a desired signal from background noise. For analysis purposes, only sections of the signal greater than these threshold values are considered. The chosen threshold level could be so high that important events related to damage rather than background noise are ignored and Funk et al[155] suggested that another method of crack detection should be used with any given experimental set up to determine these threshold levels. This in itself brings inherent problems as other suitable and accurate damage detection methods must be employed and may not detect the damage as accurately as the acoustic emission technique. Furthermore, acoustic emissions from events such as crack propagation have such distinct signals from the background noise that threshold levels may be set with experience of similar experimental set-ups.

Arrival time - The arrival time is determined as the first point in either a positive or negative direction in which the signal crosses the threshold. Knowledge of the speed of sound within a particular structure, and the use of multiple sensors enables the source location to be determined using differences in arrival times at the various sensors.

Peak amplitude – the maximum value of the signal. Funk et al[155] claimed that this is the most important parameter for dynamic testing as it "is a measure of the strength of the acoustic emission". However, due to the uncertainty associated with the wave path from the source location to the sensor, the peak amplitude from one signal should not be used in this sense. The peak amplitude may appear large and hence correspond to a strong signal, however, it may also be the result of a superposition of waves that are in phase and present a large peak amplitude at the sensor[142]. Furthermore, peak amplitude is expected to attenuate with distance from the source, and unless this distance is taken into consideration, peak amplitude as a measure of strength could again be misleading[142]. However, when data from a large number of signals is collected and averaged, peak amplitude does indeed prove a useful parameter for the assessment of AE signals, and

Funk et al[155] were able to show that higher amplitude events were detected in injured human lower legs compared to legs without injury. Peak amplitude has been used by other researchers to significant effect. In Kohn's review of acoustic emissions in biomaterials[152], it was demonstrated that different failure modes within carbon fibre reinforced materials can be identified using peak amplitude. High amplitude events corresponding to fibre fracture, medium amplitude events to matrix deformation, and low amplitude events to interfacial failure.

Rise time – This is the time difference between the arrival time and the peak amplitude. Schwalbe et al[154] demonstrates that a short rise time followed by an exponential decay is indicative of bone cracking, whereas long rise times and non-exponential decays were associated with wear and friction of human joints. Schwalbe et al's study is of particular interest as they were able to relate the onset of burst type acoustic emissions to crack initiation using fluorescence microscopy.

Duration – The time between the first and last threshold crossing

Counts – The number of threshold crossings. Count rate is a particularly useful parameter and forms the basis for both the Kaiser effect[156] and the Felicity effect . Both of which refer to the acoustic emissions produced from a material that is re-loaded beyond its previously loaded limit. The Kaiser effect was developed from the work of Joseph Kaiser in the 1950's and describes the fact that a material exhibits little or no acoustic emissions until its previously experienced maximum stress is reached. Using this principle, Kaiser was able to analyse components that had been stressed in service, and determine the maximum stress to which they had been subjected[156]. The Felicity effect applies to materials with inherent damage, such as fibre fracture in composites. In this case, acoustic emissions occur prior to reaching the previously applied stress and the fraction of the applied load at which the onset of AE occurs is referred to as the felicity ratio[157]. The two effects complement each other and allow assessment of damage in materials that are able to exhibit the Felicity effect.

Energy - The integral of the squared amplitude over the signal time:

$$E = \frac{1}{R}\int_0^T \bar{v}_{RMS}^{\,2}(t)dt - \frac{1}{R}\bar{v}_n^{\,2}T \qquad \textbf{Equation 3}$$

Where:

E = Signal energy - measured in computer energy units (eu)

R = Resistance

$\bar{v}_{RMS}$ = average signal $_{RMS}$ value

$\bar{v}_n$ = average noise voltage

T = duration of complete signal

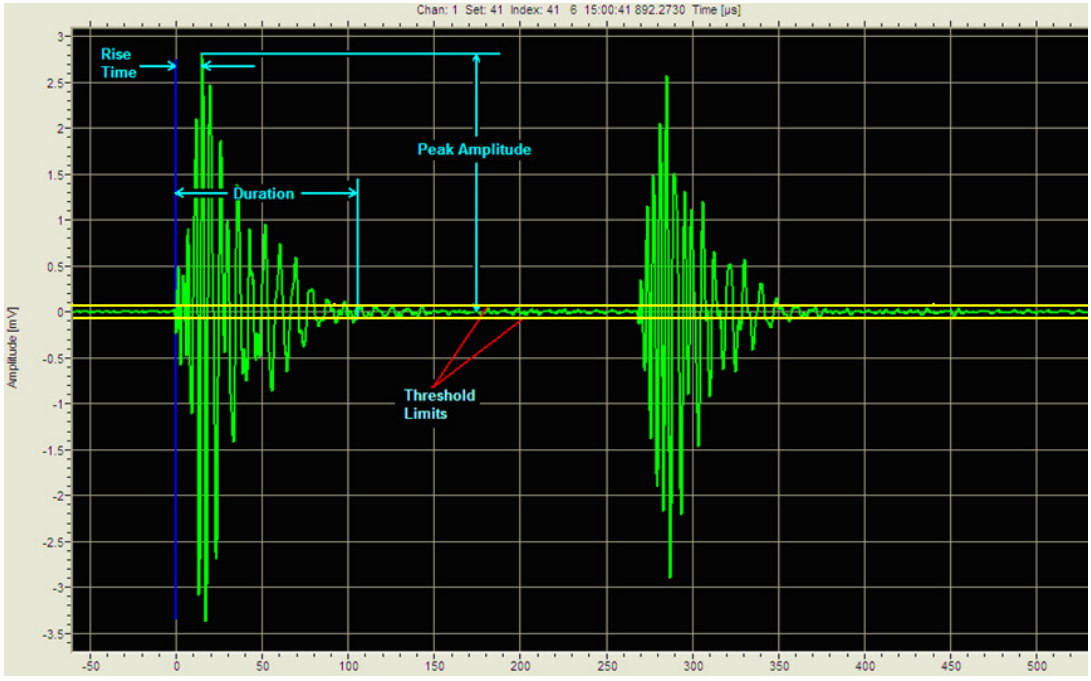

Figure 11 – Typical AE response illustrating various signal parameters

Location – The ability of the acoustic emission technique to locate events adds significantly to its attractiveness as a non destructive testing method. The technique is capable of locating events by using the difference in arrival times of emissions originating from the same source. If it is assumed that the wave propagation is of constant velocity in all directions surrounding the source, then knowledge of the velocity of sound for specific materials should enable the source location to be identified. This principle is illustrated below:

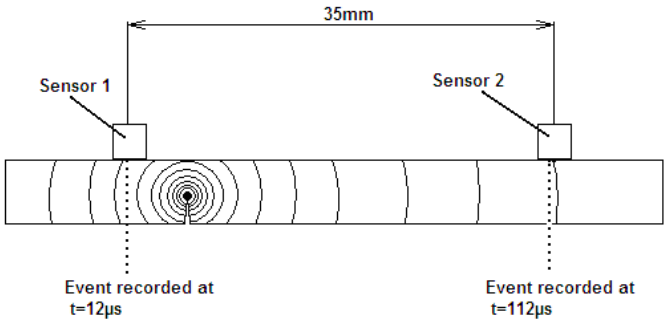

Figure 12 – Diagram showing an AE detected at differing times from two sensors

In the case of Figure 12, if we assume that it has been shown that acoustic waves travel through the material at $300ms^{-1}$, then the distance from sensor 1 to the source can be calculated as 300*0.000012 = 3.6mm, and the distance from sensor 2 to the source can be calculated as 300*0.000112 = 33.6mm. Since there are only two sensors present, it is only possible to locate along a line between the two sensors. There is an inherent error by the fact the source is located some distance below this line, and hence the total distance travelled by the wave is greater than the distance between sensor centres.

To correctly identify source location, there must be a sufficient number of AE sensors that all detect the same event. For example, to detect an event along one axis requires two sensors, to locate an event in a 2D plane, at least 3 sensors are required, and a minimum of 4 sensors are required for 3D location within a structure. The time of arrival method for source location is generally the method adopted by commercial software packages and used in most studies within the literature. However, the technique is only really applicable for structures with a simple geometry, consisting of a single material or materials with similar acoustic velocities. Several studies have looked at addressing these limitations and providing alternative methods of source location for use in more complicated structures. Holford et al[158] present a method of source location by a single sensor using the frequency dependent velocity of Lamb wave components, Li et al[159] used a variable wave velocity model, and Baxter et al[160] used a more empirical approach using the difference in arrival times of known events between sensor pairs to build a map of known event locations on a structure of interest from which subsequent source locations may be determined.

2.3.4 THE USE OF AE IN BIOMEDICAL ENGINEERING

Since the work of Kaiser that established the use of the acoustic emission technique in the 1950s, various studies have looked at applying the technique within the field of biomedical engineering. Two comprehensive review papers[116,152] are cited here and are recommended reading for anyone considering using this technique on biomaterials. Kohn[152] assesses the techniques used for monitoring damage in a variety of materials, including bone, and concludes that the acoustic emission technique "possesses many of the qualities of an ideal damage-monitoring technique" due to its high sensitivity and ability to detect sub-surface, multiple damage sites in real time. Kohn was also able to relate the onset of AE to visual crack formation in Ti-6Al-4V. In his work, he used a closed circuit television system with 125x microscopic zoom lens. It was found that AE was always generated prior to the visual detection of fatigue crack growth which was only capable of observing surface crack greater than 10μm[152]. However, in another statement, Kohn identifies a study on titanium alloys where the first acoustic emission is correlated to an optically observed crack of 30μm – suggesting that the crack had initiated prior to the detection of acoustic events. This irregularity may be explained if the crack existed prior to testing, however, this is not made clear in his report. Kohn made other significant observations such as a rapid increase in the AE event rate corresponds to an increase in the rate of optically observed crack propagation. Kohn was also able to detect both crack growth and friction emissions caused by the rubbing of existing crack surfaces. Kohn attributed three forms of failure mechanisms to AE event amplitudes and accumulation rates. It was found that events produced during low stress loading cycles were caused by crack surfaces rubbing against each other, whereas events produced at intermediate stress levels were indicative of plastic yielding, and events produced at peak stresses corresponded to crack propagation. Evidence is presented for the ability of the AE technique to detect and identify damage in a number of different materials. Following Kohn's review on the technique applied to monitoring of bone deformation, it is concluded that damaged bone produces greater amounts of AE than healthy bone and it is argued that the AE technique is a suitable method for assessing the state of bone[152].

More recently, Browne et al[116] reviewed work involving AE as a potential monitoring tool for use in orthopaedics. Despite the passing of almost a decade since the publishing of Kohn's review article, Browne et al re-identify the problem that current diagnostic methods used in orthopaedics are not sensitive enough to detect early signs of loosening,

and that the AE technique has the potential to overcome these problems. More importantly, Browne et al recognise that the technique has the potential to be incorporated into "smart" implants, allowing continuous monitoring, informed surgical decisions and a greater success rate of revision operations.

The slow integration of the AE technique into standard monitoring methods for total hip replacements begs the question: why has it been so slow? Perhaps the answer lies in the significant work necessary to correlate acoustic emission signals to different failure mechanisms in different materials. This review will therefore focus on how work in the literature has attempted to make this correlation and identify why authors have struggled to convincingly link acoustic emission events to failure mechanisms. Of particular interest is the characteristic behaviour of acoustic emissions within bone cement and at the bone cement - prosthesis interface as these are considered weak areas in terms of long term survival of cemented prostheses.

ACOUSTIC EMISSIONS FROM BONE CEMENT

Crack propagation in polymethylmethacrylate (PMMA) or bone cement has been thoroughly investigated in the literature. Matsushige et al[161] conducted a very thorough study in 1984 investigating secondary crack formation in PMMA. A combination of AE, high speed shadow-optical techniques, X-ray element analysis and scanning electron microscopic observations were all used to investigate the origins and behaviour of secondary cracks. These secondary cracks were believed to initiate in a crazed region ahead of the primary crack front. The fracture surface of a PMMA specimen has typical parabolic markings associated with the fracture surface. Matsushige et al[161] studied a range of crack velocities and investigated the focus region of each parabolic marking. The equipment used had a resolution of 20nm and could detect impurities of 10^{-17}g in weight. Elements associated with catalysts and accelerators were generally not present in these regions, however, silicon, which is associated with dust particles and impurities, was present. The use of shadow graphs displayed the acoustic wave front in real time, and it was possible to see the acoustic wave emitted from the crack tip hitting the AE transducer, and the corresponding acoustic signal produced from the AE transducer displayed on an oscilloscope. The authors linked increasing crack velocity to the clarity of stress waves emitted, intensity of AE signals, and parabolic marking density. It was noted that as the

velocity and stress intensity of the main crack increased, so too did the amplitude of the AE signal. Therefore, the amplitude of AE signals was considered an important parameter for the analysis of acoustic emissions within PMMA. It was also stated that the acoustic emissions from the main crack tip could have a considerable effect on the initiation of secondary cracks. Further evidence of this was presented in Boudet and Cilberto's study[162], and it was concluded that although the sound energy was just 5% of the surface energy in PMMA, it caused significant modifications to the crack dynamics.

Attenuation is an important factor in any study of acoustic behaviour. The signal attenuates as it spreads out through the media in which it is travelling. The amount of spreading may be affected by the geometry of the sample and the presence of interfaces. Qi[163] investigated this with respect to waves travelling in a bulk media and across interfaces and concluded that the signal attenuated in a linear relationship with distance travelled though the media (although this may have been influenced by the geometry of the specimens that he used – 15x5mm rectangular cross section bars 120mm long – such that the wave was actually guided along the sample rather than being able to spread), and that acoustic energy was more sensitive to attenuation than signal amplitude. Qi[163] used pencil lead brake tests at various distances along the specimen from the sensor. He found that the signal had lost 60% of its energy and 15% of its amplitude just 90mm away from the source within a bone cement specimen. It was recognised that signal energy conveyed more information about the whole signal than peak amplitude, and a greater attenuation of energy is expected since it is the summation of the square of each datum. Qi[163] also concluded that the presence of a couplant had a major impact on the attenuation across an interface. Qi[163] uses what he describes as a discrete wavelet-based signal processing technique. This technique decomposes the signal into various frequency ranges and then analyses the components present in each frequency range in more detail. Qi[163] studied the attenuation of the signal using three sensors mounted at different distances from the source (Hsu-Neilson). Individual sensor sensitivity calibrations were not given and therefore the attenuation measured by Qi's experiments could have been influenced by individual sensor response variations. Nonetheless, the importance of measuring signal energy was highlighted.

In a later study conducted by Roques et al[148] acoustic emissions from damage occurring in a bone cement sample under four point bend loading conditions were analysed in terms of peak amplitude, duration, rise time, number of counts and energy. It was shown that

acoustic activity was dependent on the applied load level, and that the environmental conditions surrounding the sample had an effect on the acoustic response. The authors state that all tests gave similar ranges of peak amplitude (44-76dB) and that if used alone, this parameter could not be used to characterise signals. Both rise time and duration of signals were dependent on load level to some degree, with longer rise times and durations occurring at lower stress levels (durations of low stress specimens (tested at 18MPa) were mainly less than 200μs compared to mainly less than 120μs for higher stress specimens (tested at 35MPa), and rise times were mainly less than 20μs for lower stress and less than 25μs for higher stress specimens). The authors concluded that the onset of failure could be predicted by the appearance of high energy events with durations longer than 200μs.

The acoustic emission technique has also been shown to be a valuable tool for the validation of finite element (FE) damage prediction models[164,165]. It is probably the most readily available and useful technique for detecting and locating subsurface damage accumulation in real time, and thus permitting chronological corroboration with predicted models. Jeffers et al[165] used AE to study fatigue characteristics of dog-bone shaped bone-cement samples under uni-axial fatigue loading and found that porosity was an important factor in the determination of fatigue life. Results from their AE data showed that damage accumulation within bone cement was a non-linear, discontinuous process and the authors were able to use this information to assess the accuracy of their FE damage accumulation models. Coultrup et al[164] used a similar experimental set-up configuration using data from micro computed tomography to incorporate the samples actual pore distribution into the model. The authors found that pores were responsible for a diffuse damage accumulation process, but unlike previous studies[89,92,93], Coultrup et al[164] concluded that barium sulphate particles did not significantly affect fatigue performance. Furthermore the predicted and observed site of final fracture did not always coincide, although the predicted failure location did coincide with sites that had produced acoustic activity throughout the test; failure was rapid and always produced high-energy events.

AE AND THR CONSTRUCTS

All of the aforementioned studies relate to work using very simple geometry specimens of bone cement. However, the differences in geometry alone between such specimens and a more realistic stem construct are sufficient to cause considerable complications in terms of AE investigation (Figure 13).

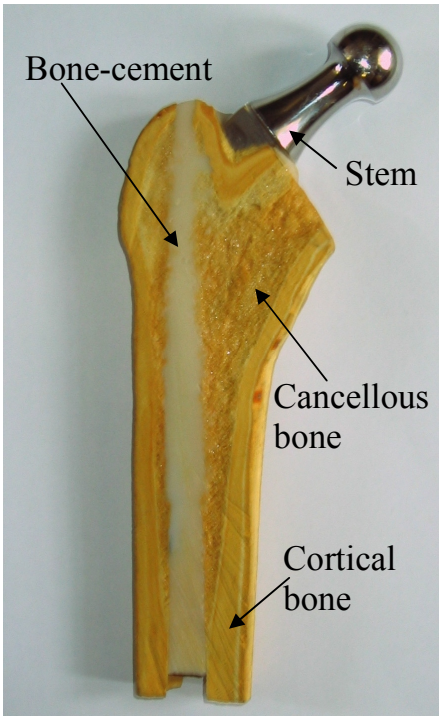

Figure 13 – Photograph showing cross-section through a model of a cemented femoral construct.

Qi et al were the first to extended the technique from the identification of failure locations in simple notched bone-cement specimens[166] to more complicated femoral stem construct configurations[150]. The authors attempted to monitor the formation of cement micro-cracks under fatigue loading conditions. Eight AE sensors were mounted on the external surface of the composite femur and the authors determined that the majority of located micro-cracks occurred within the proximal third of the stem and that the rate of micro-crack formation decreased with increasing numbers of loading cycles. The stem used for these experiments was a pre-coated design supplied by Zimmer, Inc. Warsaw, IN. It has been reported that pre-coated stems have shown an increased risk of early failure[167] and it is not known whether the detection of located events in Qi's study is indeed related to micro-crack formation or something more superficial such as stem migration, interfacial de-bonding or noise originating from the mechanical loading configuration. The authors state

that in comparison to the pencil lead break tests performed to calibrate the location response of the system, the amplitude of signals generated from "micro-crack" formation varied considerably. Both the results of this and previous studies have shown that cement cracking is linked to high energy, short rise-time events. The generation of a range of signal parameters is an indication of multiple failure mechanisms. Qi et al, fail to acknowledge the fact that not all of the detected AE signals may have originated from micro-crack formation and do not corroborate the AE results to any visual analysis of micro-crack formation. The ability of the AE technique to locate and quantify specific failure patterns is therefore not addressed sufficiently in Qi et al's study and questions remain as to what failure mechanisms were actually detected. However, the work conducted by Qi et al[150] was the first time the technique had been used to assess an entire stem construct in an attempt to locate micro-damage from within the cement layer during fatigue loading. The complicated structure in terms of varying geometry, the presence of multiple interfaces and the substantial variations in speed of sound between the different construct materials meant that the ability of the AE technique to accurately locate damage was significantly reduced. Li et al[159] later developed a location algorithm such that variations in the speed of sound throughout the structure were taken into consideration and using the same experimental set up as Qi et al[150], the authors were able to demonstrate a significant improvement in location accuracy. Li et al, sectioned the samples at six locations along the longitudinal axis of the femur and scanning electron microscopy was used in an attempt to visually corroborate the findings from AE. They were only able to find micro-cracks present on the section corresponding to the most AE activity, which, whilst encouraging, is only based on one stem construct and so the repeatability of these results are unknown.

The problem associated with correlating acoustic emissions to actual failure is the need for an equally sensitive technique capable of visually linking the acoustic emission to a physical occurrence. As already discussed, Kohn[152] linked AE events to optically observed crack growth in a titanium alloy. However, the optical equipment used was less sensitive than the AE technique and was only capable of showing crack propagation along the surface. Thus acoustic emissions were detected that could not be linked to any observed change.

The work of Gao et al[153] indicates that the acoustic emission technique is more sensitive than X-ray observations for assessing the fixation of artificial joints. The authors mounted AE sensors on the surface of a patient's skin over the lateral femoral condyle and the posterior-superior iliac spine. Patients ranging from 4 months to 10 years post operatively were monitored during a range of activities and their movements together with emitted acoustic emissions were recorded using a video camera. These results were then compared to plain radiographs and clinical inspection. Despite analysing a complicated structure and measuring through a highly attenuating media, the authors demonstrated a link between frequency composition of the detected waveforms and state of the implant. The authors identified three main states: state 1 related to the main frequency component below 50Hz. This was found to correspond to a loose femoral component. State 2 where the main frequency component was between 200-350Hz implied a well-fixed implant, and state 3 where the main frequency component was above 500Hz corresponded to a femoral stem that had entered cortical bone. This study was published in 1990 and since then, there have only been a few *in-vivo* studies considering the acoustic emission technique as a clinical tool for implant assessment[152,154]. Schwalbe et al[154] looked at the acoustic response from joint friction and were able to link their data to known cartilage defects, and Kohn et al refers to work done on total knee replacements where the amplitude and number of acoustic events showed a marked increase for radiographically loose implants.

Other authors have used ultrasound, together with radiographic analysis, dye penetrant techniques and serial sectioning as an attempt to link sub-surface damage to acoustic emissions. Davies et al[151] investigated the de-bonding of the cement-metal interface since this has been observed in retrieval studies; however its role in initiating loosening remains uncertain due to the inability of current diagnostic techniques to identify initiation and progression of de-bonding in real time. Davies et al's *in-vitro* study concluded that de-bonding could indeed be a major influence with regard to prosthesis loosening. The two techniques of AE and ultrasound were complimentary, and the authors used AE to determine when failure occurred, and then ultrasound to identify what mechanism of failure had occurred, be it de-bonding or cement cracking. Unfortunately, the ultrasonic technique requires signals to be sent through the cement mantle, and modifications to the femoral construct were necessary to ensure the signal arrived normal to the metal surface. However, due to some of the geometries associated with the stems, ultrasonic testing was not possible over the entire length of the stem. The authors also used vegetable dye along

the region of ultrasonic evaluation to visually inspect for cement cracks, as well as radiographically inspecting the specimens and then sectioning and polishing the samples for further verification of de-bonding. This study made substantial efforts to link AE events to physical phenomena. The techniques used to verify the AE were all in themselves accepted techniques. The work of Davies et al therefore went some way in providing evidence for the ability of the AE technique to identify real failure mechanisms in the cemented stem construct. However, the authors were not able to identify from the AE data alone what type of failure mechanism had occurred, and it was only through the use of other failure detection systems that this information could be extracted. It is clear, therefore that in order for the technique to be accepted as a true diagnostic tool, greater information should be extracted from the acoustic waveforms to identify failure mechanisms.

Summary

This section of the review has looked at the principles behind the acoustic emission technique and highlighted some of the complexities that have slowed the acceptance of the technique in orthopaedics. The amount of research and positive conclusions drawn from acoustic emission testing indicate that the technique could indeed be used as an alternative clinical assessment tool for total hip replacement devices. However, a major factor in establishing the AE technique as a tool for the assessment of total joint replacements is the ability to correlate the parameters of an AE signal to real damage mechanisms. This has so far proved difficult due to the complexities and sensitivity of the technique, and very little work exists where there is an unquestionable correlation between acoustic emissions and physical phenomena. Despite this there is an ever-increasing body of evidence to suggest that the technique could be used to assess orthopaedic implants and the few *in-vivo* studies aimed at demonstrating this have shown promising results.

Studies that have applied the technique to complete stem constructs *in-vitro* have so far applied sensors externally, usually on the bone surface, so that acoustic emissions generated within the bone cement must travel through a significant mass of material and across multiple interfaces before reaching the sensor. Since acoustic signals are attenuated as they travel through a material and across interfaces[163], it is arguable that mounting the sensors on an external surface to investigate damage mechanisms occurring within the

bone cement layer is not ideal. However, since direct access to the bone cement layer is not readily available, an exposed surface is often the only practical option for sensor positioning. It is hypothesised that this issue may be avoided completely by directly embedding AE sensors within the femoral stem itself and may permit a greater fidelity of relevant acoustic information to be gained and analysed. This would eliminate some of the interfaces between the sensor and structure of interest, allow closer proximity of the sensor to the region of interest, and eliminate potential complications and variability in the method used to clamp the sensor to the sample. However, it should be noted, that no study has yet been conducted in which the AE sensors are placed inside of a femoral stem component despite the theoretical advantages.

Projecting this idea to the successful development of a self-contained, *in-vivo*, condition-monitoring prosthesis using embedded AE sensors to routinely monitor the performance of total joint replacements could enable early failure diagnosis such that the prosthesis could be revised before significant damage had accumulated. It has been shown that early revision significantly reduces the risk of complications in surgery and careful monitoring is the only way to identify loosening before too much of the bone stock is destroyed[6]. Therefore a system that can detect early signs of loosening without necessitating ionising radiation or periodic review via hospital appointments would represent a step change in the information available to design engineers, clinicians, and patients alike.

However, this vision is reliant on the ability to incorporate these technologies successfully into an endoprothesis – and this is yet to be established. Therefore initial efforts should focus on an *in-vitro* device and it is envisaged that this product will show significant improvements to current experimental assessment in its own right. *In-vitro*, the AE technique could be used to monitor the progression of damage without the need to incorporate sensors directly into the prosthesis. The temporal resolution of the technique alone could guide other monitoring techniques to interrogate the specimen following the onset of damage, rather than after an arbitrary time period or number of loading cycles. However, the permanent fixation and placement of the sensors inside the prosthesis may allow for greater experimental repeatability without the need for external jigs, fixtures, or modifications to the surrounding environment – thus permitting more representative test scenarios whilst increasing the level of performance information in a time effective manner. The predicted performance of *in-vivo* endoprosthetic devices is established and

optimised using *in-vitro* and in silico methods. However, there are still occasions where implants fail unexpectedly with expensive consequences, so there is still a tremendous demand for registry information to feed into implant designs/materials/implantation techniques. Unfortunately, this information can only highlight poor performing implants/bone cement formulation/implantation techniques after multiple failures have been detected through the current monitoring techniques i.e. patient pain scores and standard radiographic imaging; methods that detect failure late or even after failure has occurred. This results in a delayed feedback situation during which time there may be many more poor implant designs implanted in to patients that will subsequently require revision.

Overall, the concept of an instrumented system shows many potential benefits, however, transposing the idea of an instrumented implant into reality is not simple and goes beyond the scope of this project. The next section of the review will look at some examples of instrumented prostheses that have been used successfully *in-vivo* – highlighting some of the issues that are married to this type of device.

2.4 *IN-VIVO* MEASUREMENTS IN TOTAL HIP REPLACEMENTS

It has often been said that there are limitations with studies that attempt to represent a living, adaptive system by either cadaveric specimens or mathematical simulations under simplified loading conditions[45,168-171]. Computer simulations are growing in popularity, however, as with any computer generated model, the outcome is very much dependent on the accuracy of information supplied. Both methods are essential for pre-clinical testing and screening of implants. However, clinical studies remain the only true method of obtaining unequivocal hard data. Unfortunately, the nature and location of the hip joint make data acquisition from clinical studies difficult. This has led to an engineering science based on assumptions; however, the volume of work in this field is slowly unlocking and revealing the complex processes that influence the performance of arthroplastic devices.

Prior to the work of Rydell in 1966[172], who pioneered an instrumented endoprosthesis for the measurement of *in-vivo* loading conditions, the magnitudes of forces acting at the hip joint were determined through calculation alone. Rydell's work[172] hinted at a discrepancy between predicted and actual hip loads, although his database of just two patients was not statistically significant enough to warrant major changes in the way that predicted hip loads were calculated.

Subsequently, other groups such as Carlson & Mann[173], English & Kilvington[174], Bergmann et al[175] developed and improved instrumented endoprosthetic devices, such that data could be collected over longer time periods and in a greater number of patients. The progression from the earliest instrumented hip endoprosthesis through to the latest devices is illustrated on the timeline below:

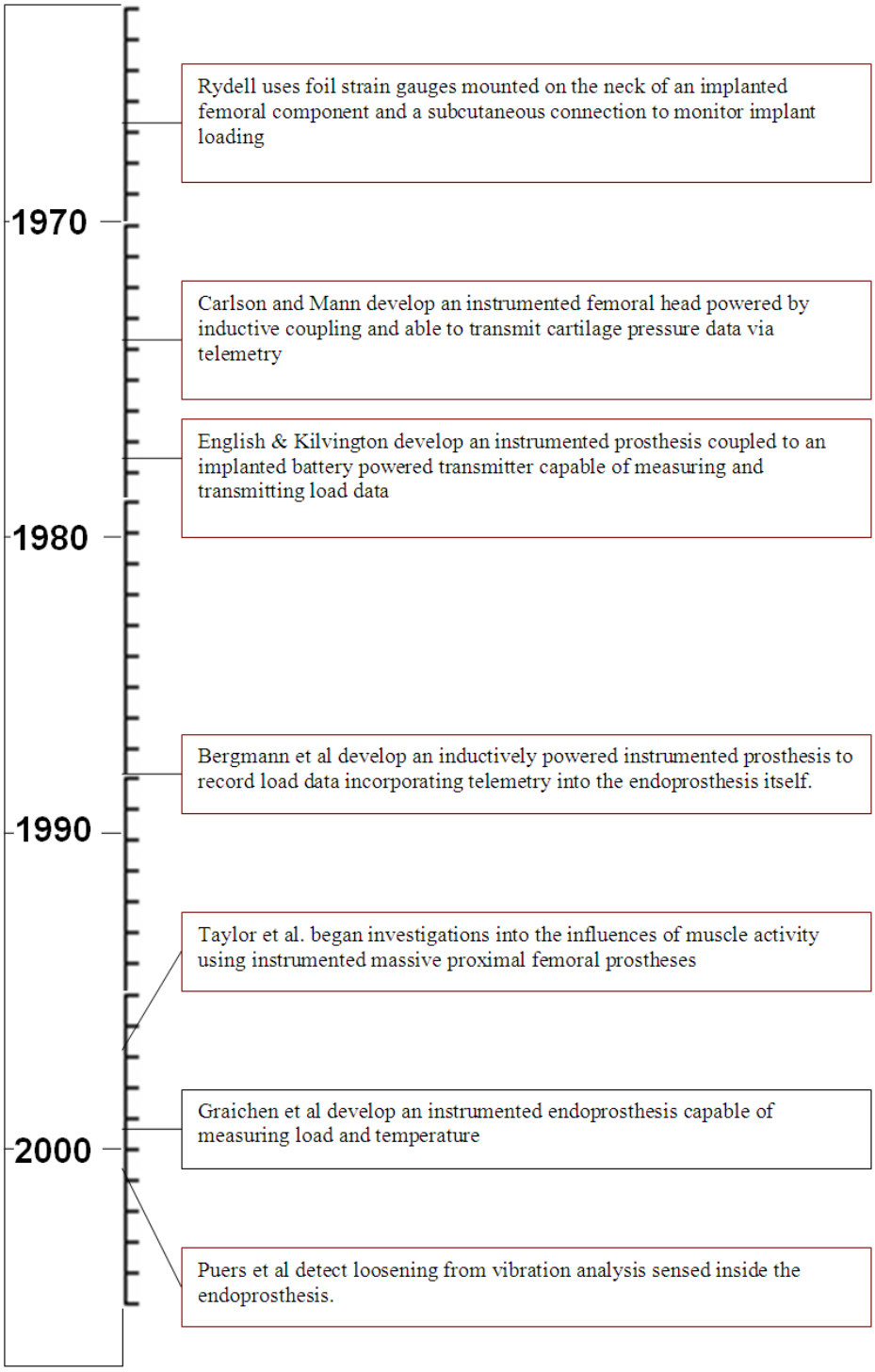

Figure 14 - Timeline showing major developments of instrumented endoprosthesis

In all cases some discrepancies between predicted and actual loads were observed, although most were unable to form a direct comparison between predicted and measured data from the same patient until Heller et al[176] and Stansfield et al[170] addressed this issue. In both cases the authors claimed a good correlation between the predicted and measured

data. Heller et al[176] demonstrated an average variation between the data of 12% for walking and 14% for stair climbing. Similarly, Stansfield et al[170] demonstrated average variations of 13.85% in one of his two subjects and 18.11% in the other. However, if the actual variations between the results are considered, then it becomes harder to state that the measured data agrees well with the predicted data. Heller et al[176], measured variations from as little as 0.3% in one patient, and up to 33% in another. Stansfield et al[170] also recorded large variations between the data of up to 38.78%. Accurate predictions remain elusive due to the complex loading conditions imposed by muscle contractions. Measuring muscle forces is difficult without interfering with the tissue itself, and musculoskeletal models tend to represent muscles as straight lines rather than the real curved pathways that are observed in the human body[176]. Heller et al[177] went on to develop a simplified version of his earlier model and was able to demonstrate similar results between the two models. Whilst the development of such models are essential for pre-clinical testing of prosthetic designs, and that simplification of such models is beneficial where possible, the large variations between measured and predicted data reflect the need for further *in-vivo* testing and general understanding of the forces imposed from the surrounding muscles.

Although this project is not concerned with measuring hip loads, the relevance lies in the fact that this has been the principle area of interest for most instrumented endoprostheses up until now. Hip load data also affects the way in which pre-clinical tests are performed, particularly when loads recommended by standards such as ISO 7206 are called into question[44]. Other factors have been measured *in-vivo* such as temperature due to frictional heating[178], contact pressure distributions[45] and some preliminary work with vibrational analysis[179]. In most cases, the *in-vivo* data has altered perceptions, allowed greater understanding, or even surprised researchers in this field. Load measurements have shown that mathematical models over-estimate hip loads and tend to respond to changes faster than predicted[44,170,176], pressure measurements have demonstrated rapidly varying pressure distributions and highlighted the role of surrounding muscles in stabilising the joint even prior to the application of an external load[45], and temperature measurements have shown that artificial bearing surfaces may reach temperatures sufficient to cause osteonecrosis[178]. *In-vivo* measurements have also informed clinicians as to how recovering patients should be treated. Bergmann et al[180] demonstrated that soft soled shoes do not ease joint loads and can actually have an adverse effect due to the increase in muscle activity necessary to stabilise the joint, Hodge et al[45] showed that the use of a cane as opposed to a crutch had

less of an effect on joint loads than previously anticipated, and the importance of accurate alignment during surgery has been underlined through Bergmann et al's[44] extensive work that shows the peak hip contact force direction relative to the femur is consistent for all types of activity. However, up until now the only instrumented hip endoprosthesis that is able to provide an indication as to the "health" of the joint is that of Puers et al using vibrational analysis[179].

Attempts have been made to develop a data set describing a "typical patient" such that realistic load data throughout the gait cycle may be used in computer simulations. The most complete work in this area was conducted by Bergmann et al[44] who successfully recorded gait patterns and loading conditions at the hip in four patients. However, with over 40,000 primary hip replacements being conducted annually in the UK alone[8], and with Bergmann's own comment that the average loads observed within the four patients "would change if more or other patients had been included in the study" indicates that there is still a great deal of work to be done before *in-vivo* conditions can be reconstructed accurately for use in pre-clinical testing.

Accurate loading conditions are important for the *in-vitro* or in silico assessment of early loosening mechanisms. The relative magnitudes of axial loads compared to torsional loads, which were found to exceed the experimentally determined torsional strength of implant fixations[169], as well as force directions and cyclic loading patterns may influence the manner in which loosening is induced. Furthermore, the constraints imposed by surrounding soft tissues may influence conditions and behaviour of the hip replacement construct that have not been considered in the past. The significant influence of the complicated geometry and soft tissue was highlighted by Hodge et al[45] in their work on cartilage pressures. They found that previous *in-vitro* studies looking at the response of cartilage tissue to an applied load did not reflect the true *in-vivo* behaviour. The use of cartilage samples allowing radial or unconstrained expansion coupled with the axial flow of lubricating fluid as used in other studies was a misrepresentation of the situation within the human body[45].

However, there are unavoidable problems associated with *in-vivo* testing that need to be recognised. Difficulties associated with ethics committees, finding willing patients, working with strict requirements such as hermetic sealing and biocompatibility issues, the

long time delay associated with obtaining real data, and the cost associated with the development of an implantable system have made *in-vitro* testing and computer analysis attractive alternatives, despite the assumptive nature of these techniques. Using the example of Bergmann et al's efforts to obtain clinical data illustrates the time-scale involved in the development of a clinical device. Bergmann's earliest work in this field (1980) reports the use of an endoprosthesis instrumented with strain gauges arranged inside the neck of the femoral component to record the directions and magnitudes of hip joint forces in sheep. The first clinical trials in humans were reported nine years after the first animal trials of the instrumented endoprosthesis[181]. This does not include the time taken before animal trials to develop the concept, initial designs and *in-vitro* testing of the instrumented prosthesis.

Summary

This section of the literature review has focussed upon the development of instrumented hip prosthetics. In doing so, the reasons why computer simulations and *in-vitro* and *in-vivo* testing procedures are essential have been highlighted, together with their respective shortcomings. The review has demonstrated that *in-vivo* data has repeatedly altered perceptions as to the way the human system operates and as such a true understanding of the early loosening mechanisms may only be achievable through *in-vivo* analysis. However, it is perceived that such data will not be realised for some time due to the lack of work in this area.

At present, there is no condition monitoring system that can detect the earliest stages of loosening of an implant *in-vivo*. Telemetric force data has demonstrated that this may be possible, but the force data itself gives no indication of failure. The forces imposed across a loosening implant will remain the same until the patient experiences such pain that they avoid movement and loading of the joint. It is hoped that the reader now has an appreciation of the unique benefits of *in-vivo* monitoring using instrumented prostheses. The main hypothesis of this study is that this technology may be extended from simple joint contact force, pressure and temperature analysis to condition monitoring of the hip joint incorporating wireless technology such that evaluation of new of modified implant designs may be evaluated easily, giving early indications of failure before the onset of excessive trauma.

2.5 SIGNIFICANT FINDINGS FROM THE LITERATURE

It has been stated that much of the historical development of total hip replacement designs have resulted from trial and error, leading to unfortunate and unforeseen failures in vivo. The review focused primarily on aseptic loosening and bone cement interfacial failure since these have been noted as being most associated with failure of total hip replacement devices to date. In an attempt to improve the quality of information available prior to the release of such devices, the review has considered several techniques that may be able to offer significant gains over the currently used condition monitoring techniques. It was identified that aseptic loosening may be caused by a number of factors that ultimately influence the balance of natural bone remodelling, and that although bone cement was initially held responsible for triggering an osteolytic reaction, it was since determined that this response occurs from a variety of otherwise bioinert material particulates. The inability of cementless stems to outperform their cemented counterparts, has sustained bone cement as the primary method of femoral stem fixation. Therefore, in order to assess a potentially new condition monitoring technique; cement failure and aseptic loosening were identified as relevant processes to investigate.

The review has looked at the composition of bone cement and identified that certain particulates such as Barium Sulphate – used to enhance radiopacity - may improve fatigue life[89] (although this is the subject of some debate), whilst pores - or more significantly - the distribution of pores have been shown to decrease the fatigue life of the cement mantle significantly. A significant amount of work has focused on the exothermic reaction during polymerization and its potential contribution to thermal necrosis[32,60-62], however, the true influence of this effect is debatable and it could be argued that necrosis would occur anyway due to the reaming procedures used to prepare the medullary canal for the prosthesis[182]. Various authors have concluded that cracks may form from the residual shrinkage stresses prior to any applied loading[81,85,101], and that the shrinkage is more severe in bone cement prepared by vacuum mixing[83]. However, despite this, the increased risk of early failure[99], and questions being raised as to whether the technique does actually reduce porosity in a clinical setting[76], vacuum mixing remains the favoured method of bone cement preparation and it does appear to have better long term results[99]. Roques et al[85] demonstrated that the AE technique could be used to detect damage associated with the

shrinkage phenomena non-destructively, and this capability is investigated further in Chapter 5 of this thesis. If pre-load cracking is a substantial factor in determining whether these vacuum mixed devices fail early or not, then the information provided from this monitoring could prove to be a significant contribution to the field. If successful, the method could be applied to assess a number of different cement formulations and stem designs such that pre-loading cement damage can be minimized in service and hopefully reduce the figures associated with the risk of early loosening in vacuum mixed devices.

The review also set out to answer the question as to whether condition monitoring and the ability to detect loosening at an early stage would actually be worthwhile. The review indicates that this is in fact essential and some of the clinical failures could have been avoided through the use of better *in-vitro* testing. Furthermore, earlier detection of failure *in-vivo* is not only beneficial for timely revisions, but if poor implant designs can be better identified at the design stage *in-vitro* then large numbers of prospective implant failures may be prevented from being implanted before failure is recognized. Unfortunately, current follow up procedures are not sufficient to detect failure during its earliest stages and in fact the number of radiographs that are performed compared to those that show signs of failure before the patient experiences pain are very small. In most cases the onset of failure is identified through an admission to A&E or GP referral[115], and it could be argued that patients are being exposed to unnecessary levels of radiation and that the resources of the national health service are not being used effectively. There are of course other, more sensitive monitoring techniques that have been used. The review discussed techniques such as DEXA and RSA, however, once again there is considerable cost associated with these techniques and their use has largely been restricted to smaller scale clinical studies. Either way, the effectiveness of any of these techniques is dependent upon the frequency of review and therefore a method of continually monitoring implant fixation and integrity could be beneficial.

The review considered several potential techniques that may be able to offer improved detection of loosening, and it was concluded that ultrasound, RSA and AE showed promising characteristics. However, the AE technique is the only one able to offer continuous passive monitoring capabilities. The review therefore has considered the science and development of this particular technique in some detail. The technique may be affected by noise and attenuation, it has proven difficult to link detected AE to specific

failure mechanisms, and although the technique has been used very successfully on simple coupon specimens, attempts to scale up to more complicated/realistic stem geometries have experienced difficulty in locating events. Up until now external sensors have been used to monitor different test specimens – however, it is argued that for this particular application, the ability to directly embed sensors within the femoral stem may offer significant advantages both *in-vitro* and *in-vivo* and would: 1) Enable a permanent bond between the sensor and the structure, reducing potential complications of poor sensor fixation and eliminating test-to-test variations in sensor fixation. 2) Allow a closer proximity of the sensor to the region of interest, directly reducing the attenuation of the signal before reaching the sensor and reducing interface effects. The signal received by an embedded sensor only has to cross the interface between the cement and the stem before reaching the sensor - as opposed to the traditional path of the signal received *in-vitro* by external sensors that require the signal to cross the cement-bone interface, then travel through the bone itself which has varying density and acoustic transmission characteristics, before finally crossing the interface between the bone and the sensor case. This situation is worsened *in-vivo* where the signal must also travel through flesh and skin – effectively limiting the signal information to the low frequency range and therefore dramatically limiting the amount of information available 3) Permit greater experimental flexibility as the test does not have to be designed to enable recovery of the sensors following testing, and 4) permit a more realistic test environment since the test chamber/bone specimen does not have to be altered in order to accept the sensors. These advantages are all hypotheses at this stage, however the experiments reported in Chapters 5, 6 and 7 of this thesis aim to assess and answer them. However, before these questions can be answered, there are several steps that must first be completed; namely the development of embedded AE sensors and a system that can be used as a test platform for all of the subsequent experiments. These steps are described in the following chapters (4&5).

Finally, the review considered previous studies that have used instrumented implants for *in-vivo* data collection. Although a complete *in-vivo* system goes beyond the scope of this particular thesis, it was felt necessary to have an awareness of these systems since an *in-vivo* system may well form part of the future work that builds on this thesis.

CHAPTER 3 - AE SENSOR DEVELOPMENT

3.1 OVERVIEW

From the technologies considered in the literature review, acoustic emissions stood out as a technique that could offer many benefits to this application. The ability to determine the chronology of events and to be able to detect them in real time as they occur and at the earliest stages of occurrence are all considered advantageous for the progression of total hip replacement development. Unfortunately, there is a slight drawback with the commercial products as they currently stand: Cost. A typical AE system comprises of sensors, preamplifiers and an analyser. The commercial systems are designed to operate on a range of structures and the whole system is moved from one test specimen to the next. However, this project is aimed at creating an integrated condition monitoring system into the femoral stem of a total hip prosthesis. This is not an application where the system may simply be dismantled after each test and then installed again for the next test. Any components that are placed inside the prosthesis will have to be hermetically sealed within it and left there for the entire life of the prosthesis. It may be possible to justify a substantial increase in cost to a clinical *in-vivo* system that is able to offer significant advantages over the current monitoring methods; however, if this system is to be used routinely in the laboratory, as a research tool, it must be affordable. Most of the system (pre-amplifiers and analyser) can remain separated from the object of interest and be used for all tests, so commercial products shall be retained for these components, however, the sensors themselves will be placed inside the prosthesis and will not be recoverable. At the time of writing, a commercial sensor of suitable size and specification for this application costs £400, and if location capabilities are desired, then two sensors are required and this would put the cost of each test prosthesis at £800 for the sensors alone without considering the labour charges and machining costs of modifying the prosthesis to accept these sensors. Thus, in house sensors were developed at a fraction of the cost, which enabled this project to be considered viable for laboratory experiments. This section of the report describes how these sensors were developed and compares their response to the equivalent commercial sensors.

3.2 SENSOR SELECTION

There are very few commercially available sensors that are small enough to be implanted and sealed within a prosthetic hip replacement. The Bioengineering research group (University of Southampton) has traditionally used Pico-Z type acoustic emission sensors manufactured by Pancom. The sensors are cylindrical with dimensions 4.7mm in diameter and 5.8mm high. At the time of writing, these sensors cost £400 each. AE sensors use the principles of piezoelectricity to generate voltage signals from structural energy wave propagation as described in the literature review. In essence the sensor comprises of a shielded PZT crystal sandwiched between two electrodes. By manufacturing the sensors in-house, the total cost of the project was reduced substantially and enabled the PZT to be directly embedded into the femoral stem of a THR. PZT ceramics are available in a range of shapes, sizes and forms - all at considerably lower cost than a commercial AE sensor. Commercial sensors use PZT in its bulk form, but of particular interest to this project is whether thick film processes could be used to apply the active sensing material directly to the prosthesis. This section of the thesis will therefore consider the use of both bulk PZT and thick-film technology for the manufacture of such devices and then describe the manufacturing process used to create the low cost "in house" sensor. For evaluative purposes, the Pico-Z sensor is treated as a benchmark to which all other forms of sensor are compared.

3.3 THICK FILM TECHNOLOGY

Thick film technology is very attractive due to its process economics, and miniaturised circuitry capabilities. Complicated patterns may be easily produced using a screen-printing process. Essentially, the desired substance composition is made up as a paste and forced through openings in a screen such that the required pattern is reproduced on an underlying substrate – usually alumina. The pattern is then dried and fired using a pre-determined time-temperature profile with peak temperatures typically in the region of 600-1000°C[183]. The technique can be used to create multi-layer circuits where films of dielectric separate the active circuitry with through holes to enable connections between the layers. This presents the potential of creating a thick film AE sensor with an integrated preamplifier.

To investigate the feasibility of using thick film devices, comparisons were drawn between the commercially available Pico-Z type sensor, and a thick film sensor obtained from the School of Electronic and Computer Science (ECS), University of Southampton[ii]. Aspects such as cost, sensitivity, ease of manufacture, size, and attainability were considered important factors.

Cost of production is extremely low compared to the commercially available Pico-Z type sensors. The thick film manufacturing process was really intended as a fast bulk manufacturing method and as such there is significant cost savings associated with volume production. The main costs associated with the process are involved in the initial set up and screen manufacture. As a rough guide, and in consultation with Professor Neil White, to produce 1000 sensors would typically cost £2000 broken down as follows:

Screens	= £100
Gold	= £700
Labour	= £500
Substrates	= £700
Total	= £2000
	= £2 ea.

[ii] I am indebted to Professor N. White for his generosity is supplying samples of these sensors for evaluation and testing purposes.

The gold is required to make the bottom electrode. The use of a gold bottom electrode as opposed to a silver/palladium electrode was shown to dramatically increase the d_{33} coefficient by allowing a greater electric field to be applied during the poling process[184]. Torah et al[184] conducted significant work on the optimisation of the d_{33} coefficient of a thick film PZT device. The d_{33} coefficient refers to the charge density developed per given stress. The subscript $_{33}$ simply refers to the direction of excitation and response. In the case of '33' this refers to excitation and response measured in the z direction. Note that the above breakdown of costs does not include the PZT material itself, or other constituents such as the vehicle, binder or top electrode which would preferably be a silver polymer as this was also shown by Torah et al to allow greater d_{33} coefficient[184]. A vehicle allows the functional constituents to be 'carried' in a suitable form for screen-printing. They typically consist of a volatile solvent and a non-volatile resin. During the firing process the volatile portion of the vehicle evaporates and combustion of the non-volatile resin occurs – leaving the desired constituents on the substrate together with an appropriate binder. A binder (usually glass) reacts to some degree with the substrate and affects the sintering process of the functional constituents. The binder literally holds the composite structure together. Torah et al[184] found that through careful selection of powder preparation, and poling parameters, they could increase the d_{33} coefficient of the thick film devices from 52pC/N to a maximum of 131pC/N. However, this remains considerably lower than that of the bulk PZT-5H quoted as having a d_{33} coefficient of 593pC/N[185].

Another factor to consider is size; the Pico-Z sensors are fixed cylinders of 4.7mm diameter and 5.8mm in height. Thick-film technology enables any planar shape or size so long as it can be screen-printed. However, size has implications regarding piezoelectric sensitivity and although thick film offers far superior properties in terms of cost and size, the sensitivity of the device must be sufficient for the application. The next section will describe the experimental testing that was performed to assess the performance of the thick film samples as compared to the Pico-Z sensor. It was determined that the type of coupling between the sensor and structure of interest has a significant effect on the response of these thick film sensors, and again the methodology and findings from these experiments are described.

METHODS

All testing was performed on samples of vacuum mixed CMW1 type bone cement with dimensions 90x20x8mm. The thick film sensors were obtained from the ECS department (University of Southampton) and soldered to a coaxial cable with a BNC connector to fit into the acoustic emission signal conditioning hardware. Two conventional AE sensors (type PICO-Z) were fixed to the sample such that the centres of the sensors were positioned half way across the width and 10mm from the ends of the sample. Thus the sensors were positioned such that their centres were positioned 60mm apart, equidistant from the centre of the sample. Two thick film AE sensors were then attached directly opposite the Pico-Z sensors.

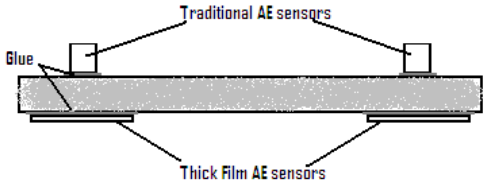

Figure 15 – Diagram showing bone cement sample with Pico-Z sensors mounted on one side and thick-film sensor mounted on the opposite side

The sensors were connected to an AMSY4 four-channel PC based data acquisition using visual AE software (Vallen Systeme GmbH, Munich). The preamplifiers used were fixed 40dB gain and had 100kHz-1MHz filters. The sample was held securely in a vice, with rubber-padded jaws to damp acoustic transmission to the vice. A pencil lead break was used to induce a sudden release of stress on the surface of the specimen at the point of contact between the pencil lead and the specimen. This source of acoustic wave is also known as a Hsu-Neilson source. According to ASTM E976-05 the lead should be of 0.3-0.5mm diameter, with consistency regarding the length of lead that is broken as well as the angle and direction of the lead. In this experiment 0.35mm leads were broken using a "shoe" supplied by Vallen System GmbH to ensure consistency with ASTM E976 in the centre of the specimen and repeated a total of 6 times to allow sufficient data to be analysed such that any impact of the investigator on the experimental results could be minimised.

RESULTS:

PICO-Z response

Thick Film response

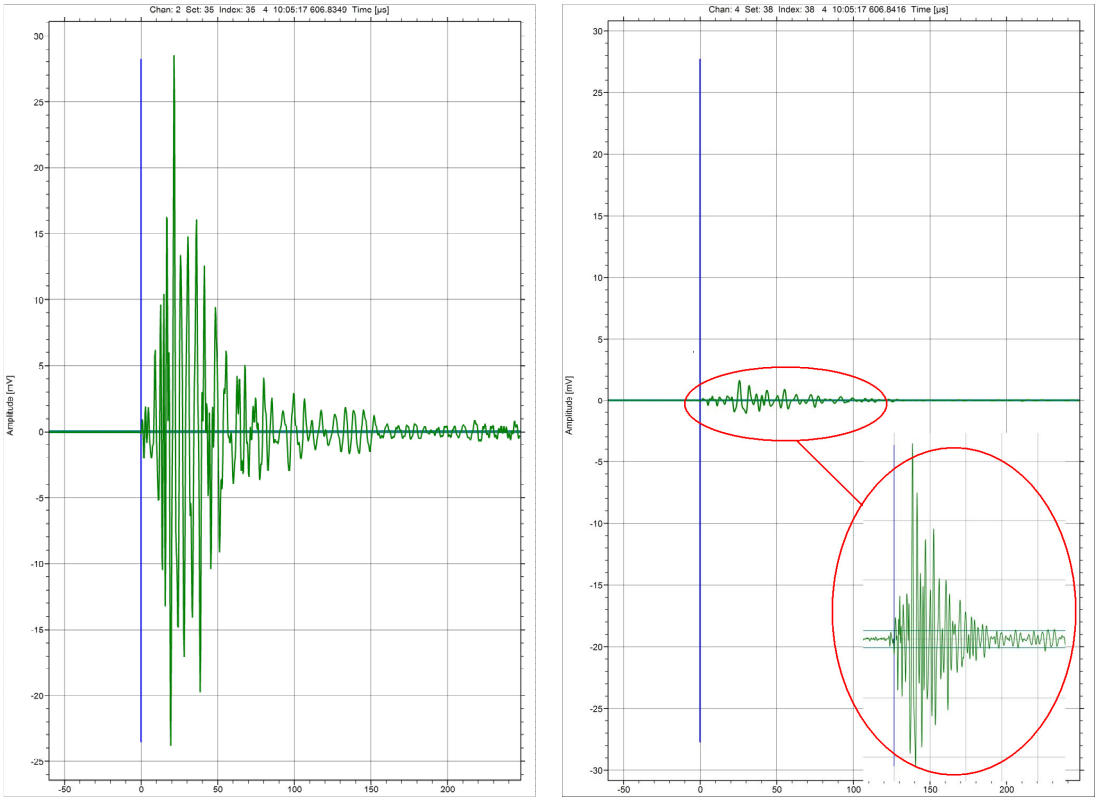

Figure 16 – Graphs showing comparisons between Pico-Z (Left) and Thick-film (Right) type AE sensors. The plots are on the same scale and the Thick film trace has been scaled vertically to show that the trace contains the similar information to the Pico-Z sensor

Parameter	Pico-z	Thick Film
Amplitude (dB)	86.1	58.7
Rise time (µs)	21.7	25.0
Duration (µs)	375.2	161.3
Counts	71.3	22.3
Energy (Eu)	395.0	25.7

Table 1 – Side by side comparison of average response characteristics from the 6 pencil lead break (plb) tests

Figure 16 shows the contrast in sensitivity between the two types of sensor. The thick film sensor is much less sensitive to the Hsu-Neilson source than the Pico–Z type sensors.

Assuming peak amplitude as a measure of sensitivity, the thick film sensors gave an average response of 27.4dB less than the Pico-Z sensors. Despite the low amplitude signal, the thick film response still contains detailed information as can be seen from the scaled up inlay. It should be noted that under quiet laboratory conditions, the low amplitude signals detected by the thick film sensors are not a problem. However, these signals were easily lost when placed near to a source of electromagnetic radiation such as a computer monitor. This loss in sensitivity may be due to several influential factors. The first relates back to the work of Torah et al[184] in that the d_{33} coefficient of the optimal thick film devices was only 22% of the bulk material. The second relates to the resonant frequency of the device and is discussed below:

The Pico-Z type sensors contain a bulk PZT disc 3mm in diameter and 1mm thick. The resonant frequencies in both the thickness and radial directions may be calculated from the equations and data given in Morgan Matroc Ltd's piezoelectric ceramics data book[185].

For a disc, the resonant frequency in the thickness direction is given as:

$$f_r = \frac{N_{33}}{thk} = \frac{2000}{1x10^{-3}} = 2 \text{ MHz}$$

In the radial direction, the resonant frequency is given as:

$$f_r = \frac{N_p}{OD} = \frac{1965}{3x10^{-3}} = 655 \text{ KHz}$$

If we now assume that a thick film sensor can be treated as a plate, and this should be possible since the equations are valid when the length and width are both much greater than the thickness then:

In the thickness direction:

$$f_r = \frac{N_{33}}{thk} = \frac{2000}{1x10^{-4}} = 20 \text{ MHz}$$

In the transverse direction:

$$f_r = \frac{N_1}{L} = \frac{1420}{10x10^{-3}} = 14.2 \text{ KHz}$$

The majority of acoustic emissions are expected to occur in the range 25 kHz – 1MHz[143]. Although the Pico-Z sensor is designed to be a broadband sensor, the fact that its resonant

frequencies lie closer to the range of interest and in terms of radial resonance actually within the range of interest, the signal amplitudes are likely to be greater.

Indeed, as seen from Table 1, the thick film sensors, using the same equipment as the Pico-Z sensors, show significant attenuation (an average of 27.4dB) less than the Pico-Z sensors. Duration, rise time, and counts are similar, which is a reflection on the amount of information contained within the signal. The energy is much less and this is expected since the waveform is essentially a scaled down version of the Pico-Z response and hence the area under the signal curve will be less. As identified in section **2.3.3** the energy associated with an acoustic emission signal is given as the integral of the voltage over the signal time. However, it should be noted that the Vallen Systeme equipment used in testing approximates the true energy by the signal strength. The signal strength is obtained by integrating the absolute value of the signal:

$$\text{True energy} = \frac{1}{R}\int_0^T u^2 dt$$

$$\text{Signal strength} = \frac{1}{R}\int_0^T |u| du$$

Where u is the voltage of the signal at the sensor output.

A correction factor of 1.11 is then applied to the signal strength to give an approximation to the true energy. This correction factor is based on the ratio difference between the true energy and signal strength associated with a sine wave. The Vallen Systeme software also ignores the constant resistance value R and gives the energy in "energy units". If true energy is used, then one energy unit is defined as 1eu = $10^{-14}V^2s$ (equivalent to 10^{-14}Ws or 10,000aJ since $W=V^2/R$ but the resistance term is constant), however, the AMSY5 system used in all the experiments in this thesis only calculates the approximated "energy" signal strength, and since the absolute voltage is used instead of the squared voltage, so one energy unit equates to 1nVs[186].

The choice of couplant was not ideal for this experiment. The sensors were bonded to the sample using a thermoplastic adhesive, and it was noted that the thickness of the bonding agent was far greater for the thick film sensors than the Pico-Z sensors due to the relatively large surface area. Sufficient pressure to provide a thin layer of thermoplastic adhesive,

similar to the thickness used for the Pico-Z was not achieved. There were concerns that the attenuating nature of the thermoplastic adhesive may distort the sensitivity of the signal, and tests were therefore conducted using a range of different couplant materials. Indeed, different couplant materials affected the response significantly, and although tests were limited to adhesives that allowed removal and reattachment of the sensors, increases of 9.5dB were observed in the peak amplitude measurements using silicone rubber compound. Practically speaking, the silicone rubber compound is easy to apply, and poses no difficulties in adhering to steel (a complication with regard to using a thermoplastic adhesive). The only slight disadvantage of the silicone rubber is that it has a longer curing time and thus the sensors remain moveable for up to 30 minutes following fixation. Even greater increases in amplitude were observed when the sensors were held onto the sample using a mechanical clamping arrangement, as shown in Figure 17.

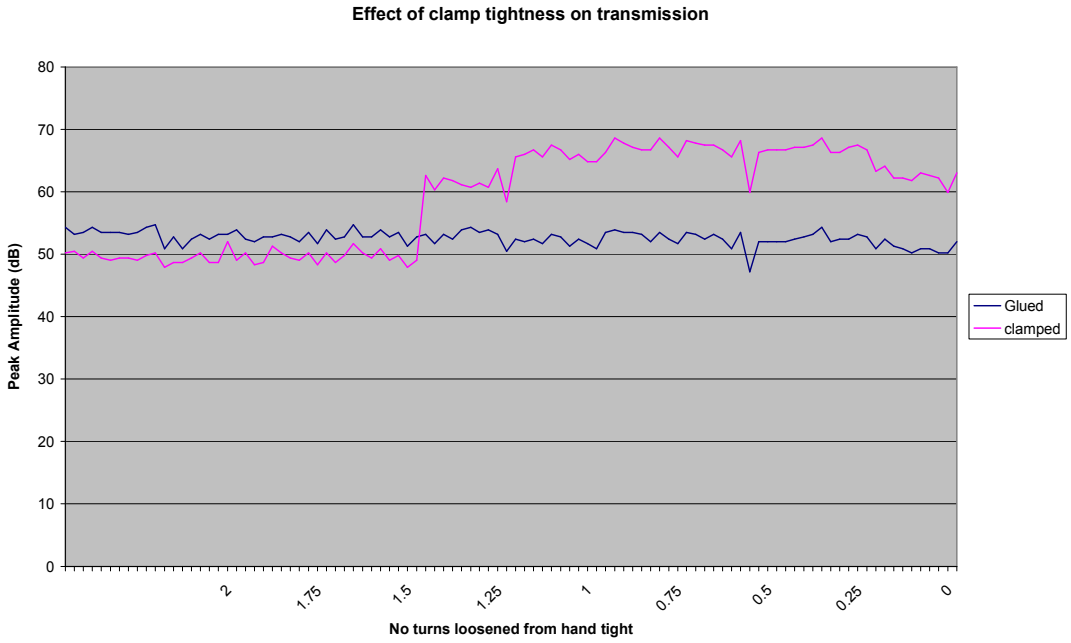

Figure 17 – Graphs showing distinct change in signal amplitude following the application of a mechanical clamp to a thick film sensor

There was a clear correlation between clamping pressure and peak amplitude. The graphs show the control sensor giving almost constant response amplitude – hence the pencil lead break tests were performed consistently. However, for the same set of tests, the clamped sensor shows slight attenuation compared to the glued sensor until we reach 1.5 turns from hand tight on the clamped sensor. This initial stage is believed to be when the clamp was in fact loose on the sensor, so the sensor itself was only being held onto the specimen by

the weight of the clamp. After 1.5 turns from hand tight, the response of the clamped sensor jumps up approximately 12dB. This is the point where the clamp begins to act as a clamp and force the sensor harder onto the sample.

Following this initial pinching, the response continues to rise to a maximum (and an increase of 13.9dB over the maximum amplitude of the control (bonded thick-film sensor using silicone rubber compound), before dropping off again as the clamp tightens even more. It is believed that this drop off in response as the clamp is tightened fully, may be due to the clamp itself bending around the sensor – thus the effective clamping area decreases, and provides a less efficient contact between the sensor and the sample. Amplitude only gives an indication of sensor performance; however, by considering the transient response of the clamped sensor against the control sensor as shown in Figure 18, the clamped arrangement gives a clearer response with a definite peak and exponential decay.

Clamped Control

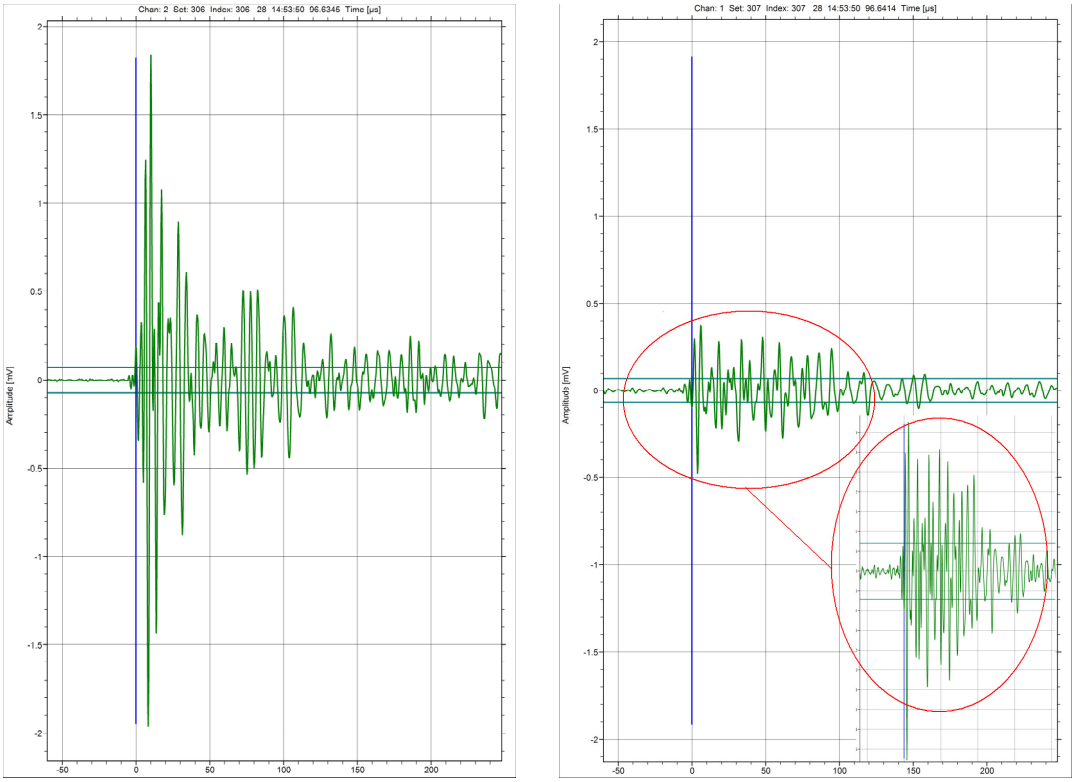

Figure 18 - Graphs showing comparisons between a mechanically clamped thick film sensor (Left) and a control thick film sensor using silicone rubber compound as a bonding agent (Right). The plots are on the same scale and the control trace as been scaled vertically to show differences in clarity of the response.

DISCUSSION

These investigations into the use of thick film sensors have shown that the cost of sensors used in the final instrumented prosthesis may be producible at approximately 0.5% of the price of a Pico-Z sensor. Improvements in sensitivity may result from the use of multi-layered devices such that the thickness is increased, the d_{33} coefficient is improved, and the resonant frequencies move closer to the range of interest. The influence of multi-layered thick film devices is illustrated by Harris et al[187] who showed a increase in d_{33} coefficient from 81pC/N in a single layered device to 323pC/N in a three layered device. Harris et al[187] also demonstrated that thick film devices were twice as efficient at converting electrical energy into acoustic energy than equivalent bulk PZT devices.

It is hypothesised that with the increases in sensitivity apparent from optimisation of the manufacturing and poling process[184], together with the use of multi-layered devices[187], and efficient coupling to the subject of interest – or even direct firing of the active constituents onto a stainless steel stem could render the use of thick film devices as the favoured choice of sensor technology for this application.

However, initial tests must first prove the concept that acoustic events may be detected and analysed from within the prosthesis, and the initial expenditure and time required to set up the production of a batch of thick film devices is questionable. Furthermore, only a limited number of sensors are required for initial testing. It was therefore proposed that the use of bulk PZT should be considered as a possible method for achieving good sensitivity, but at a fraction of the cost of the Pico-Z type sensor. At the same time, thick film technology should be investigated further for final volume production of instrumented prosthetic devices.

Summary:

Thick film sensors are relatively low cost if produced in large numbers and their design flexibility in terms of size, shape and incorporation into miniature circuits make them an attractive option for use in instrumented prostheses. However, the thick film sensors used in this study suffered a greatly reduced sensitivity compared to the PICO-Z, and whilst this was not an issue under quiet laboratory conditions, signals may be lost in noisy environments such as may be encountered in the replaced hip. This response was improved through an investigation into various bonding agents, and it was observed that the largest responses were obtained when the sensor was mechanically clamped to the sample. However, the response remained significantly attenuated compared to that of a Pico-Z sensor.

3.4 BULK PZT

Bulk PZT is readily available in a large range of shapes and sizes. The samples used for testing were manufactured by Morgan Electro Ceramics and are supplied with fired on silver electrodes. The price of each PZT sample depends on the order quantity. At the time of purchase, an individual sample PZT-5H disc 3mm diameter and 1mm thick cost £27.04, however this reduced to £12.93 if more than 25 samples were ordered. Hence, the potential cost implications of individual Pico-Z sensors and initial set up costs for thick film devices could potentially be avoided through the direct use of bulk PZT ceramic devices.

Bulk PZT is used in the Pico-Z sensors. However, these sensors are not only expensive but they have been found to be very delicate and easily damaged. They use an extremely thin coaxial cable to link the sensor to the preamplifier. Whilst this enables minimal strain to be imposed on the sensor whilst mounted to a specimen, the cable is easily damaged. Furthermore, the PZT crystal is housed within a thin stainless steel case. Silver loaded epoxy is used to bond the PZT crystal and the shielding of coaxial cable to the case, the core of the coaxial cable to the upper electrode, and a small piece of steel studding which provides an access path for the coaxial cable to the crystal. The case itself has a very thin cap, which seals the whole unit. This is easily popped off and difficult to reattach whilst maintaining a watertight seal. The PZT crystal itself can also come de-bonded from the case from rough handling such as forced removal from a sample. It is thought that a slight deflection of the case is enough to weaken this bond and decrease the sensors performance. The inner detail of the sensor can be seen in Figure 19.

The piezoelectric material chosen for this study was PZT-5H due to its relatively high d_{33} charge constant of 593pC/N. The Curie temperature of the material is ~195°C which is sufficient for this application. Efforts were concentrated on creating a case design that would reduce the delicate nature of the Pico-Z type sensors. The use of silver loaded epoxy was seen as a weak structural link and the sensor design was developed such that any electrical connections made were mechanically reinforced.

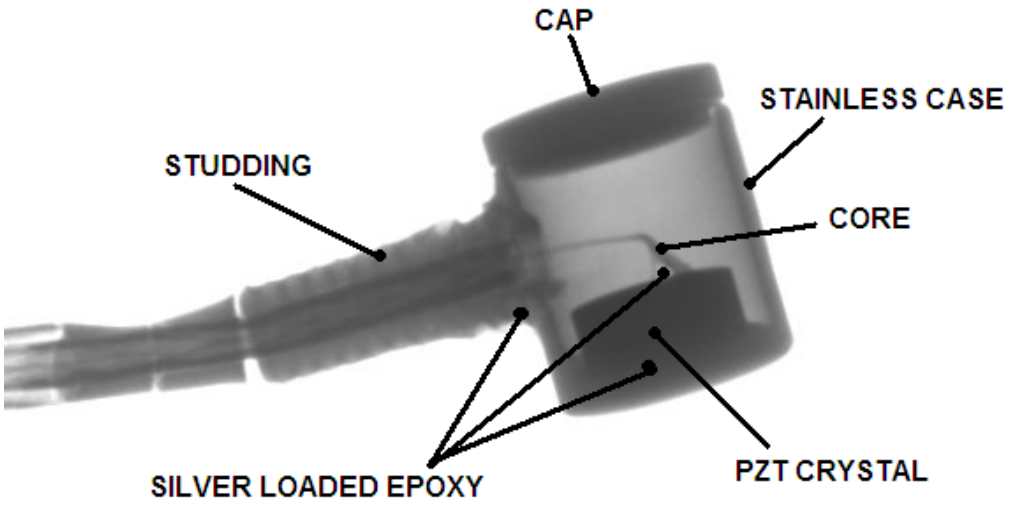

Figure 19 – X-ray image of a commercial sensor showing inner construction and key features of the design.

DESIGN IMPROVEMENTS

It was hypothesised that the PZT crystal could be held firmly in position with the use of a dielectric screw. The screw would enable a variable amount of pressure to be exerted on the crystal and take advantage of the efficient mechanical clamping arrangement demonstrated in section 3.3. The screw was also used to reinforce the contact between the core of the coaxial cable and the top electrode of the PZT crystal.

The development of a sensor with comparable reliability and performance to a Pico-Z sensor involved several iterations, however, only the final design and manufacturing process is described here. Three models of sensor were produced as a result of this study (Figure 20); one with a side mounted fixed coaxial cable similar to the PICO-Z, one with a top mounted detachable co-axial cable, and finally using the same construction methods it was possible to embed the PZT crystal directly within a metallic structure (this is discussed in detail in Chapter 4), and these in house sensors were used for all remaining testing.

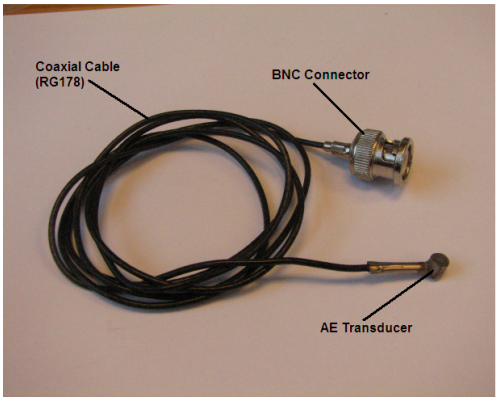

(a)

(b)

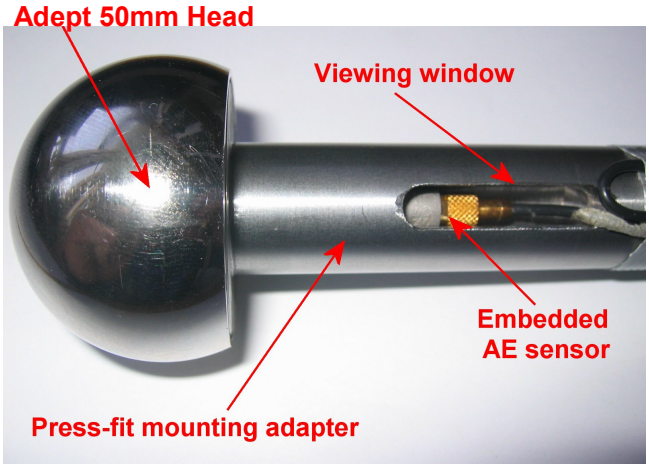

(c)

Figure 20 – Photographs showing various models of in-house AE sensors; (a) shows the side mounted, fixed cable sensor, (b) shows the top mounted removable cable sensor, and (c) shows an embedded sensor mounted within an Adept 50mm head.

MANUFACTURING PROCESS

The process described here is that used to manufacture a top mounted microdot type sensor and the internal components of one of these sensors are illustrated in Figure 21. Similar methods of construction are used for the embedded and side mounted models.

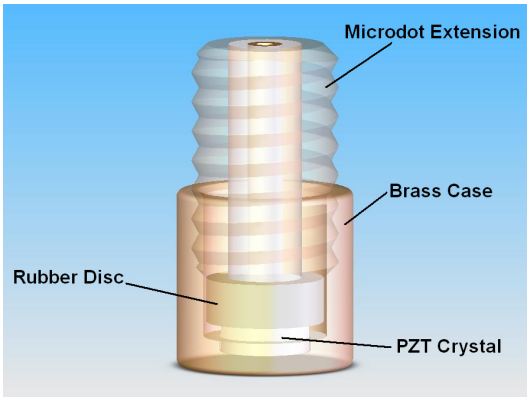

Figure 21 - Image showing internal component assembly of a top mounted removable cable type in house AE sensor.

1) Machining the case.

The casing for these sensors was machined from 6mm diameter brass rod. The internal bore was machined to include an M5 thread and flat bottomed using a 2 flute over-centre slot drill. It was essential to ensure that the PZT could rest on a flat surface and that the machining process did not leave a centre "pip".

Figure 22 - Machined brass sensor cases

2) Preparation of the PZT crystal

The PZT crystal was prepared in a specifically designed jig that held the crystal to enable both electrodes to be cleaned gently using a glass brush. The entire jig was heated to around 60°C which was found to encourage good adhesion of the silver loaded epoxy and

make soldering easier if applicable (soldering to the crystal is only necessary in the side mounted and embedded sensor configurations). Prior to insertion into the case, the crystal was encased with a 1mm length of heat shrink such that the crystal would be positioned centrally within the case and so that the top electrode did not create a short circuit with the case.

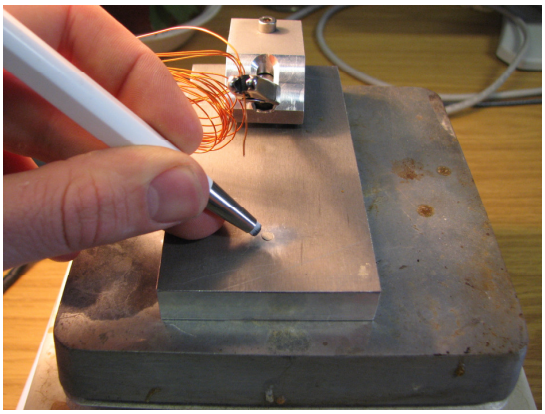

Figure 23 - Preparing the PZT crystal

3) Preparation of the rubber disc

Another specifically designed jig was manufactured to create the rubber discs. This jig was capable of punching out 5mm diameter discs of 1mm thick rubber whilst simultaneously creating a 1mm hole in the centre of each disc.

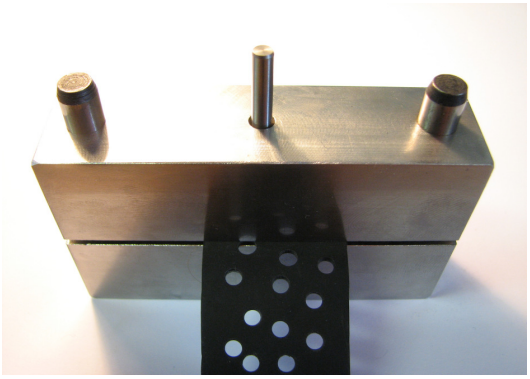

Figure 24 - Jig used to punch out 5mm discs with 1mm centred hole

4) Assembly of the rubber disc and microdot extension

The microdot extension was held in a vice with a small amount of flux placed into the centre conductor. A small amount of solder was then applied to the centre conductor. In the case of top mounted microdot sensors a 10mm length of RG178 coaxial cable was cut and stripped to the inner insulation, a further 2mm of insulation was stripped off one end and the 7 core wires tinned with solder. The tinned wires were then soldered to the centre

conductor of the microdot extension and the remainder of the insulation removed. The 7core wires were then fed through the rubber disc and separated into a star pattern on the exposed side of the disc. Any excess wire was carefully trimmed.

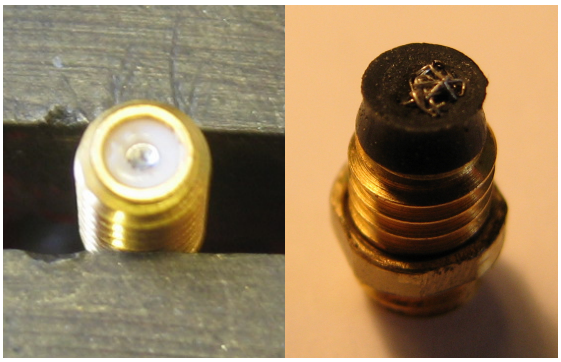

Figure 25 - Microdot extension (a) soldered and (b) with rubber disc and wire in place ready for final assembly

5) Mounting the crystal inside the case.

The case was thoroughly cleaned using acetone and left to dry before attempting to mount the crystal inside it. The case was heated to 60°C prior to insertion of the crystal to provide good adhesion of the silver loaded epoxy. One side of the PZT crystal was coated with silver loaded epoxy (Circuit Works CW2400 conductive epoxy) and placed inside the case using a specifically designed insertion tool. The assembly was removed from the heat source and clamped together gently before being left to cure for 12 hours.

6) Bonding the microdot extension and rubber assembly to the case

A small amount of silver loaded epoxy was applied to the threads of the microdot extension as well as to the star patterned wires on the underside of the rubber disc. The microdot extension was immediately screwed into the case until slight resistance was felt from the contact between the rubber disc and PZT crystal. A 1mm thick brass nut was then screwed on top of the extension to prevent any accidental movement of the extension within the case. After a further 12hrs, the sensor was ready to be tested and used.

7) Side mount and embedded sensors:

The basic manufacturing process of side mount and embedded sensors is largely the same as described for the top mount microdot sensors. However, the core connector wire is soldered directly to the PZT crystal rather than using silver loaded epoxy. Low temperature solder (containing a high silver content) together with a temperature controlled

soldering iron heated to 250°C was used to form these joints. The soldering iron was held in contact with the crystal for as short a period of time as possible to avoid heating the PZT in excess of its curie temperature.

RESPONSE CHARACTERISTICS

Calibration curves were obtained using the Vallen Sensor Tester (VST) which controls a function generator to drive an emitter with a known frequency response. The function generator used in this series of tests was the Agilent 33220A 20MHz Function/Arbitrary Waveform Generator, and the emitter was the Panametrics-NDT™ V103 transducer (see appendix A for the calibration certificate. The calibration test setup is shown in Figure 26.

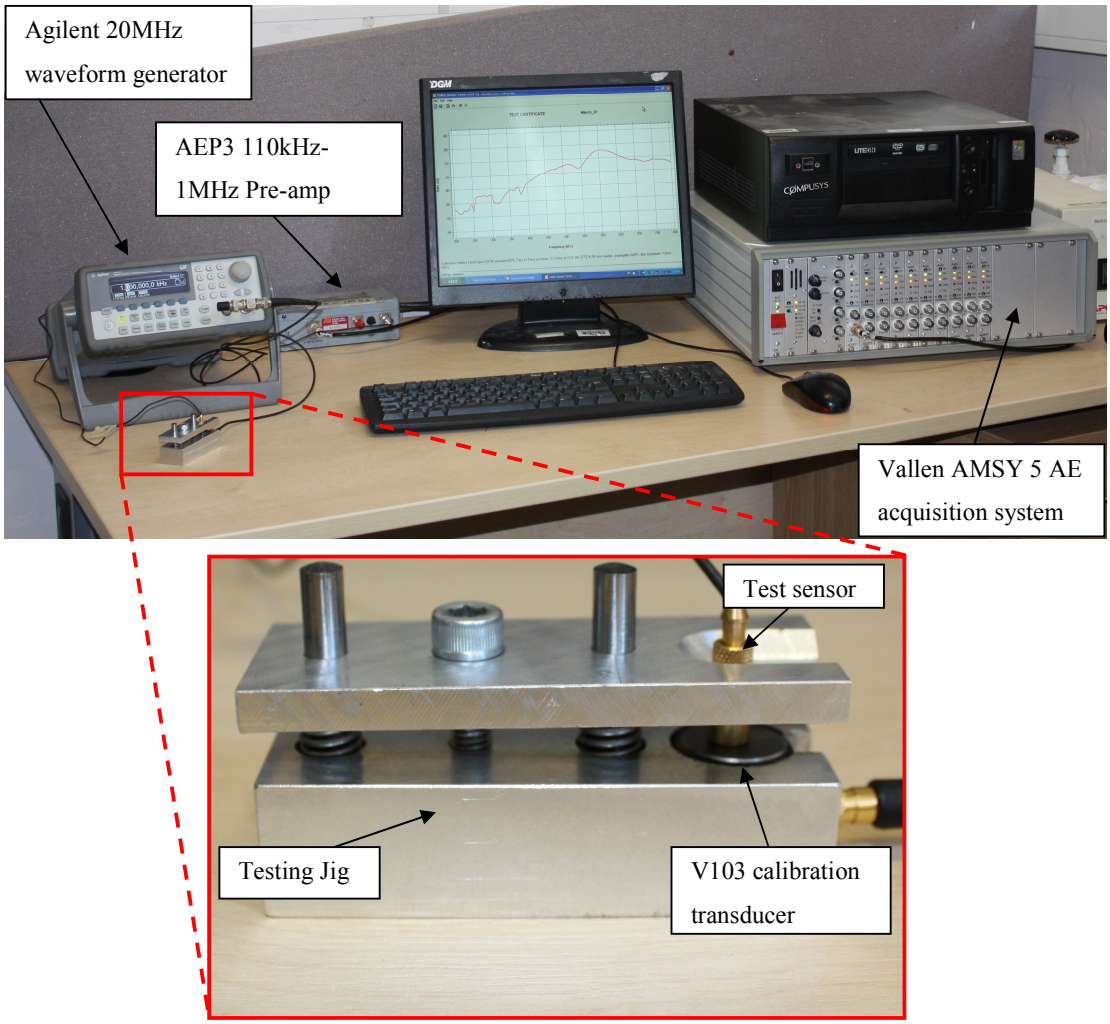

Figure 26 – Photographs showing AE sensor calibration test setup. The magnified image shows the face-to-face contact between the V103 transducer and the sensor under investigation.

All testing was performed using face-to-face excitation with the contact faces between the emitter and sensor under test being held in contact using a purpose built clamping jig. 3-in-1 oil was used to ensure good acoustic coupling between the emitter and sensor under test. The response function of the sensors was recorded over the range 200-800KHz and compared to that obtained from a commercial sensor of similar size. A typical response calibration curve is shown in Figure 27 and further calibration responses can be seen in Appendix B.

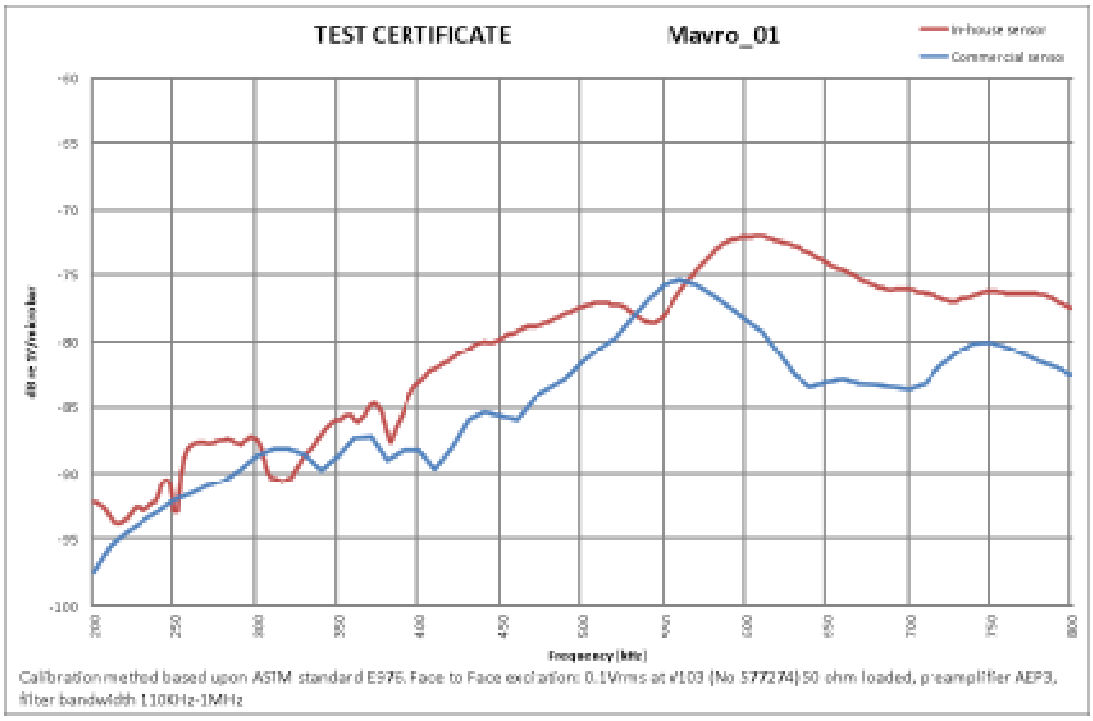

Figure 27 - Calibration response from an in-house sensor (red) compared to the calibration response of a commercial sensor (overlaid in blue).

DISCUSSION

This chapter has looked at various ways to obtain accurate AE data from in-house sensors and introduced ways of embedding sensors directly within devices. The development of thick film technology and the flexibility of this approach are promising for use in an *in-vivo* system especially if the PZT paste can be fired directly onto the component under investigation. However, the reduced sensitivity and high set up costs meant that bulk PZT and the development of bulk PZT sensors was a more practical approach for this project.

From this work, it has been possible to produce sensors that are lower cost and have a similar, if not slightly better, response than commercial sensors of a similar size. Figure 27 compares the frequency response of one in house sensor to that of a commercial sensor and depicts a greater amplitude response over almost the entire frequency range. The response of these sensors across the 200-800KHz range enables a wide range of damage mechanisms to be detected without bias at any one particular frequency. The sensors also have a slight increase in sensitivity in the higher frequencies, which is beneficial since higher frequency signals are subject to greater attenuation.

Based on the success of an earlier version of these in-house sensors, an attempt to licence these sensors was made. Links were established with Vallen, Physical Acoustics Corporation and Pancom, however, despite these companies agreeing that the sensors gave a good response coupled with their low size and cost, a successful licence agreement was not formed. For the reader's information, a breakdown of component costs in order to manufacture these sensors is given in Appendix C.

The ability to embed sensors directly within metallic structures has the potential to provide significant improvements into the flexibility of design for instrumented implantable devices. The reasonable cost enabled sensors to be incorporated into experimental procedures without the need for later retrieval and the removal of the outer casing also removed two interfaces between the subject of interest and the sensor itself - allowing less interference of the signal and better acoustic coupling. The permanent fixation of these sensors also removed variations in sensor fixations between experiments allowing greater repeatability of results.

Although the top mounted microdot sensors allow greater flexibility and easy replacement of coaxial cable if it becomes damaged, the joint between the top electrode and 7-core wire is delicate and care must be taken to ensure that these sensors are not mishandled particularly when replacing the coaxial cable. For this reason, side mounted and directly embedded type sensors should be used in preference where possible.

CHAPTER 4 - SIMPLIFIED STEM CONSTRUCT DEVELOPMENT

The literature review identified that the majority of work so far investigating the use of acoustic emissions within bone cement has been conducted on very simple geometry coupon specimens[141,148,164,165], and areas of concern have been highlighted regarding the work that has been conducted on representative stem constructs without clear corroborative evidence that the detected acoustic events were related to micro-damage[188]. Unfortunately, coupon specimens are gross simplifications of the *in-vivo* environment. Whilst they are useful for looking at generic fatigue propagation within bone cement, they do not allow for all the compounding factors present within the body. Conversely, realistic stem constructs using representative bone geometry, materials and loading conditions require assumptions to be made concerning the source of acoustic events. It was therefore determined that this gap in experimental work needed to be filled with a simplified geometry total stem construct that would encourage failure within the bone cement layer, minimising other potential noise sources, and hence increasing confidence that any acoustic activity was related to events within the bone cement layer. The complexity of the testing configurations could then be built up slowly to a representative *in-vivo* system. The next few chapters of this thesis aim to achieve this, starting by verifying the use of embedded AE sensors within a construct, then going onto look at the detection of damage during polymerisation of the cement layer, and finally building up loading sequences to the final cyclic fatigue situation. This chapter describes the development of the simplified construct with embedded AE sensors incorporated into the femoral stem. Since this is the first time that sensors have been embedded in this way, externally mounted sensors were also used for comparison against the embedded sensors. An assessment of the system's ability to detect and locate events is presented.

In order to simplify the construct, bone was represented by a Tufnol tube, which has similar mechanical properties to cortical bone (Table 2), but permitted the use of a simplified geometry and uniform properties throughout the thickness of the material.

	Cortical Bone	Tufnol (Whale Brand)
Young's Modulus (GPa)	4-25[189]	6.3
Relative Density	1.9[190]	1.36
Compressive Strength (MPa)	176-365[189]	310

Table 2 - Table comparing principle mechanical properties of cortical bone and Tufnol**. Data related to the mechanical properties of Tufnol were obtained from Tufnol Composites Ltd It should be noted that the properties of bone are dependent on a number of factors and experimental variations.**

Technovit 3040 (Technovit 3040 - Heraeus Kulzer GmbH) was chosen as a substitute material for bone cement because it is PMMA based and therefore has similar properties (Table 3) and behavioural characteristics at a fraction of the price of sterilized and packaged bone cement formulations.

Property	CMW1	PalacosR-40	Simplex P	Technovit 3040
Compressive strength (MPa)	114.7±9.75[191]	94.9±10.98[191]	102±7.99[191]	**110**[192]
Flexural Strength (MPa)	81.7±4.09[191]	51±3.72[191]	76.5±0.5[191]	**96**[192]
Modulus of Elasticity (GPa)	2.5[191]	1.4[191]	2.8[191]	**2-2.3**[192]
Shrinkage by volume %	5.2[79]	6.9[79]	5.8[79]	**5.7**[192]
Peak temp. during cure (ºC)	Large variation, up to 124ºC[193]		**110**[192]	

Table 3 – Table showing comparisons of material properties between three commercially available bone cement formulations and Technovit 3040

Initially, the femoral stem itself was based on the Freeman hip stem in terms of length, taper angle, and diameter. However, taking the round profile and extending it along the whole length of the stem simplified the stem. In order to provide representative axial and torsional loads together with appropriate bending moments, the design incorporated the ability of accepting an offset load. A total of five stems were produced: one was taken in its raw state to be tested and highlight any issues with the experiment itself. The remaining four received surface treatments. Two were highly polished to encourage cement-stem separation, and two were grit-blasted to encourage cement-stem macro-interlocking (Figure 28).

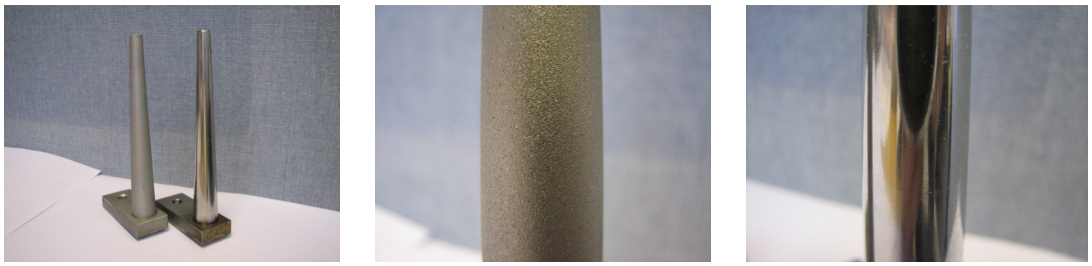

(a) (b) (c)

Figure 28 – Photographs showing simplified stem with contrasting surface finishes (a), with close up images of the grit blast surface finish (b) and the highly polished surface (c).

However, the round stem was abandoned in favour of a polished 2° tapered stainless steel 316 square section stem, 100mm in length and with a maximum transverse section of 16x16mm (Figure 29) as it was found that the polished round stem had a tendency to rotate within the cement mantle, and the grit blast surface finish meant that the stem could not be removed prior to CT scanning. Removal of the stem was necessary to obtain sufficient contrast to be able to assess the integrity of the cement mantle both before and after testing. Furthermore, the square section stem design introduced stress raisers that aided cement failure and thus accelerated testing.

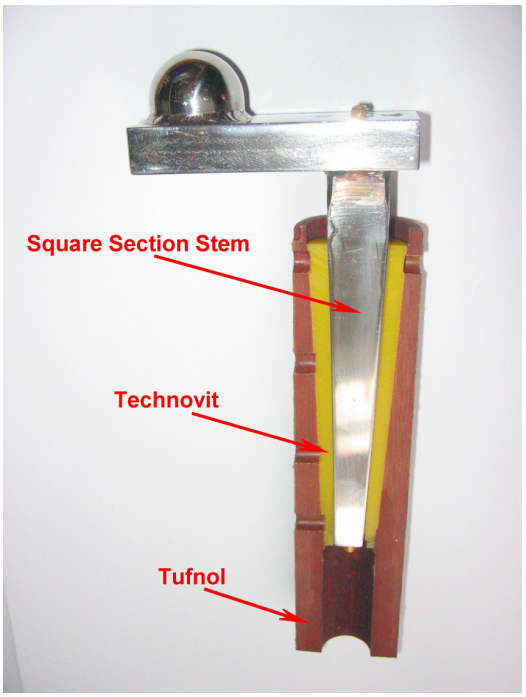

Figure 29 - Photograph showing the Final square section polished stem inserted into a cutaway model of Tufnol and Technovit.

4.1 ENSURING CENTRALISATION OF THE STEM WITHIN THE CONSTRUCT

For repeatability, it was important that as few variables were able to influence the results as possible. It has been reported in the literature that the thickness of the cement mantle can influence fatigue crack formation[194]. As such, variations in the cement mantle thickness were minimised through the development of a centralising jig. The jig consisted of a stainless steel base that was pressed into the distal end of the Tufnol tube. The base had a hole machined into it containing an O-ring seal that accepted a guide wire that in turn screwed into the distal end of the stem (Figure 30). Thus the distal end of the stem was constrained concentrically with the Tufnol tube, with a uniform gap of 2mm between the stem edges and the Tufnol tube. The proximal end of the stem was held in position using a separate component of the jig. An aluminium block was machined to clamp over the Tufnol tube with a square hole machined into its centre such that when the square stem was inserted, the longitudinal axes of both the stem and Tufnol tube would be forced into alignment (Figure 31).

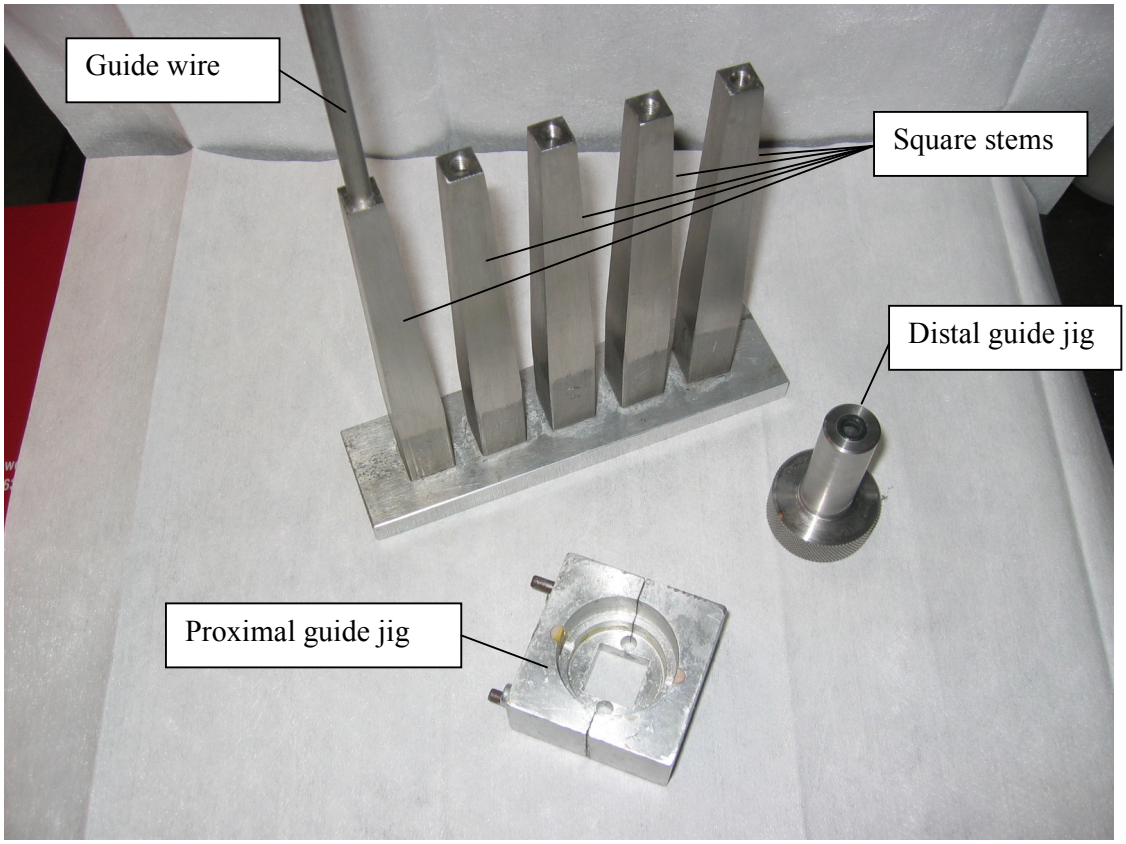

Figure 30 - Photograph showing square stems prior to insertion in Technovit together with components to make up the centralising jig

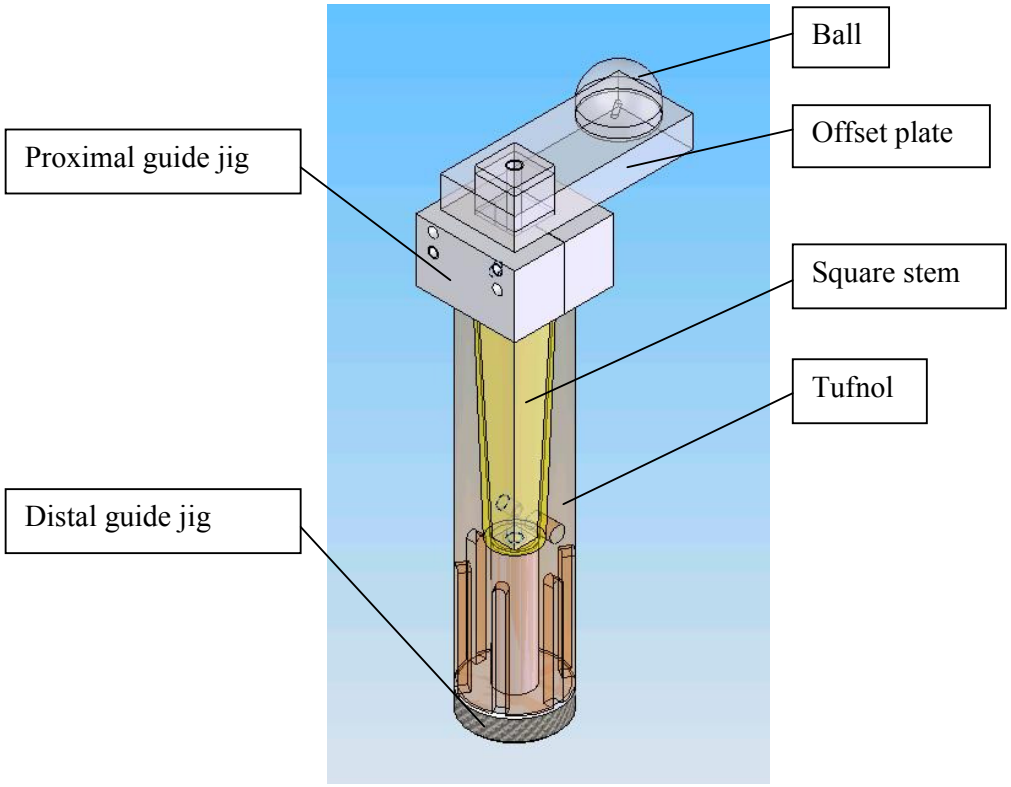

Figure 31 - Illustration showing construct assembly held within positioning jig to ensure concentricity between the stem and Tufnol tube

The system was designed such that it may be disassembled, leaving just the stem mounted in a uniform layer of bone cement and held in the Tufnol tube. The components of the jig itself could all be removed from the system once the bone-cement has cured.

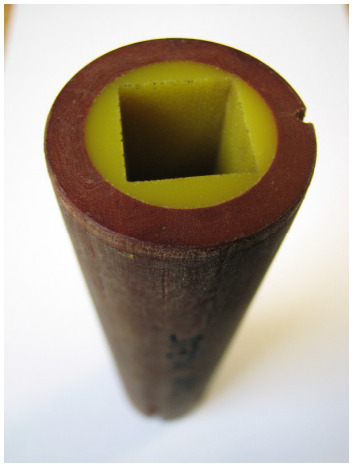

Figure 32 – Photograph showing uniform Technovit layer following removal of centralising jig and stem.

4.2 CEMENTING THE STEM INTO THE CONSTRUCT

The following methodology describes the process that was followed in order to cast the stem into the Technovit, resulting in the complete construct that was used for all subsequent testing described in this thesis. This process was performed under laboratory conditions at an ambient temperature of 20°C. During initial testing (Chapter 5) the femoral stem was inserted without any heat treatment. However, the literature review had identified that pre-heating the femoral stem affects the porosity distribution within the cement mantle with a propensity for pores to form at the cement-bone interface as opposed to the cement-stem interface. It was determined that a smooth stem-cement interface would be beneficial for the identification of cement cracks on the μ-CT scans (the justification for this decision is presented below) and so prior to mixing of the Technovit compound in all later experiments, the stem was pre-heated by immersion into a water bath at 80°C. The distal guide jig (Figure 31) was smeared with Vaseline and inserted into the pre-machined Tufnol tube. The guide wire was then partially inserted into the distal guide jig before clamping the assembly firmly in a floor standing pillar drill to act as a vertical press. The stem was then removed from the water bath and the distal end screwed onto the guide wire, the proximal end was then clamped firmly in the chuck of the pillar drill. A thermocouple was attached to the external surface of the stem such that the stem temperature could be monitored. The Proximal guide jig (Figure 31) was placed over the stem and left whilst the Technovit constituents were prepared. The Technovit constituents were measured by mass, and the appropriate volume and consistency of Technovit was found to be achieved using 20g of powdered polymer and 12g monomer. The measured constituents were mixed together when the temperature of the stem was recorded as 57°C and were mixed continuously by hand for approximately 60 seconds until the temperature of the stem was recorded as 51°C. The whole volume of the mixture was then poured carefully into the Tufnol tube and then the stem was gently lowered into the construct using the quill of the drill to control this action. When the distal end of the stem met the surface of the distal guide jig, the quill was clamped off and left for one hour to allow polymerisation to occur. The construct was then removed from the drill and the guide jigs removed from the construct. A simple jacking device was then used to gently remove the stem from the construct such that the proximal surface of the cured Technovit could be machined and prepared for μ-CT scanning. E-Appendix_01 contained on the electronic DVD version of this thesis shows a video of this casting process, removal of the stem, and

machining of the proximal surface of the Technovit. Once the construct had been scanned, holes were drilled through the Tufnol tube 10.0, 37.5, 65.0, and 92.5mm from the distal tip of the Technovit layer. The depth of these holes was such that the bottom of each hole just exposed the surface of the Technovit. This allowed the in house external AE sensors to be placed directly onto the Technovit layer using a petroleum jelly couplant and secured using a mechanical clamping arrangement (Figure 33).

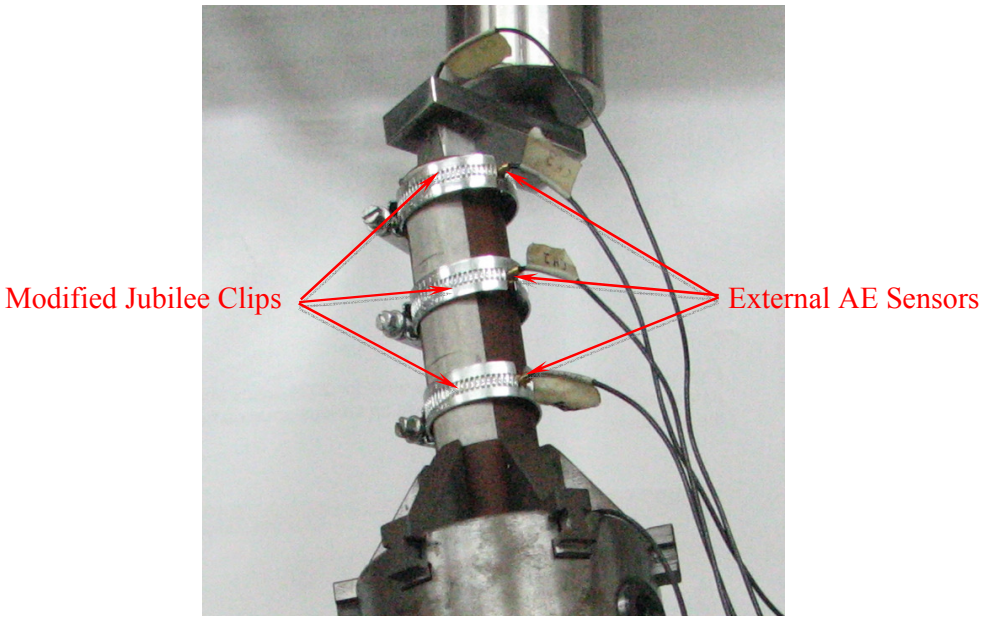

Figure 33 – Photograph showing modified Jubilee clips used to secure the external sensors to the construct.

During testing, the sensors were connected to preamplifiers with bandpass filters in the range 110KHz-1MHz and 40dB gain. The data was recorded and analysed using Vallen Systeme's GmbH AMSY-5 panel and visualisation software.

4.3 CT SCANNING THE CONSTRUCT

As mentioned previously, the stem was removed from the construct prior to scanning in order to achieve sufficient contrast within the bone cement layer to visualise defects. Although pores are clearly visible within the Technovit in its raw state, it was found that cement cracks were difficult to depict since they had a tendency to close upon removal of any load. This problem has been overcome by the composites community through the use of a solution of zinc iodide[195]. This solution acts as a radiopaque penetrant to successfully highlight cracks that may otherwise appear difficult to visualise. The solution used in these experiments consisted 60g 98+% pure zinc iodide powder, 8ml distilled water, 10ml isopropyl alcohol and 3ml Kodak photoflow. In order to ensure adequate penetration of the solution into cement defects, the construct was filled entirely with this solution and left for 20 minutes. The solution was then drained back into its container and the surfaces of the construct wiped thoroughly with a cloth in order to remove any excess solution. The pre-heated stem was shown to successfully shift the porosity distribution away from the stem-cement interface. It was found that a porous stem-cement interface resulted in a domination of zinc iodide solution highlighting pores, which subsequently made identification of cracks more difficult. Hence the pre-heated stem technique was used during casting of the cement layer.

All scans were conducted using an X-TEK Systems Ltd Benchtop CT 160Xi micro CT scanner at 35-39 micron resolution. Images were taken using 82KV and 100μA with an exposure of 2134ms and 1x digital gain. The images were reconstructed and segmented using VG Studio Max (Volume Graphics GmbH) and concatenated with ImageJ software (National Institutes of Health, USA) such that the damaged regions could be viewed easily in 3-D.

4.4 EMBEDDING AE SENSORS WITHIN THE STEM

Acoustic emissions have never before been measured from the inside of a femoral stem. The literature contains studies looking at acoustic emissions from *in-vivo* systems measured outside of the body, and *in-vitro* systems measuring emissions on the outside of artificial bone. However, since fatigue damage is often associated with cement mantle failure or de-bonding of the cement-stem interface, it seems logical to measure the acoustic emissions as close to the expected source as possible. The development of in-house sensors lead to knowledge of sensor construction and it was hypothesised that these same manufacturing techniques could be applied to effectively use the femoral stem as the sensor case. Thus the PZT crystal could be fixed directly within the stem simply by machining flat-bottomed holes at the required positions together with microdot extensions to allow the connection of coaxial cables to the stem (Figure 34). Design drawings of the stem and construct components are all presented in Appendix D.

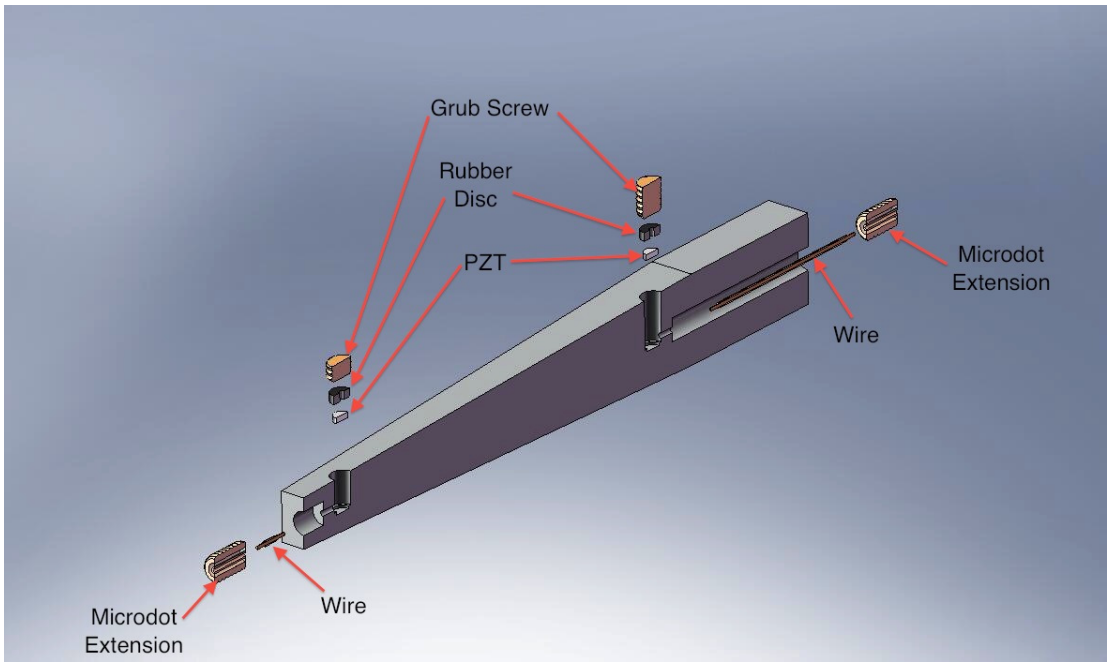

Figure 34 – Exploded section-view of an embedded stem assembly showing the main components and how they are positioned within the stem

Two PZT crystals were embedded into the stem to permit longitudinal event location. The sensors were positioned 10mm and 93mm from the distal end of the stem to allow a wide coverage of the cement mantle (events originating either proximally to the proximal sensor, or distally to the distal sensor would not be located). However, the ability of these

embedded sensors to detect acoustic activity accurately still needed to be verified. Verification was achieved using the calibration function built into the Vallen Systeme AMSY5 acquisition software. This procedure used one sensor as a transmitter to send a series of pulses. These pulses were received and recorded by the other sensor before switching to transmit to the next sensor and repeating the process. This enabled the relative sensitivities of each sensor to be obtained (Figure 35).

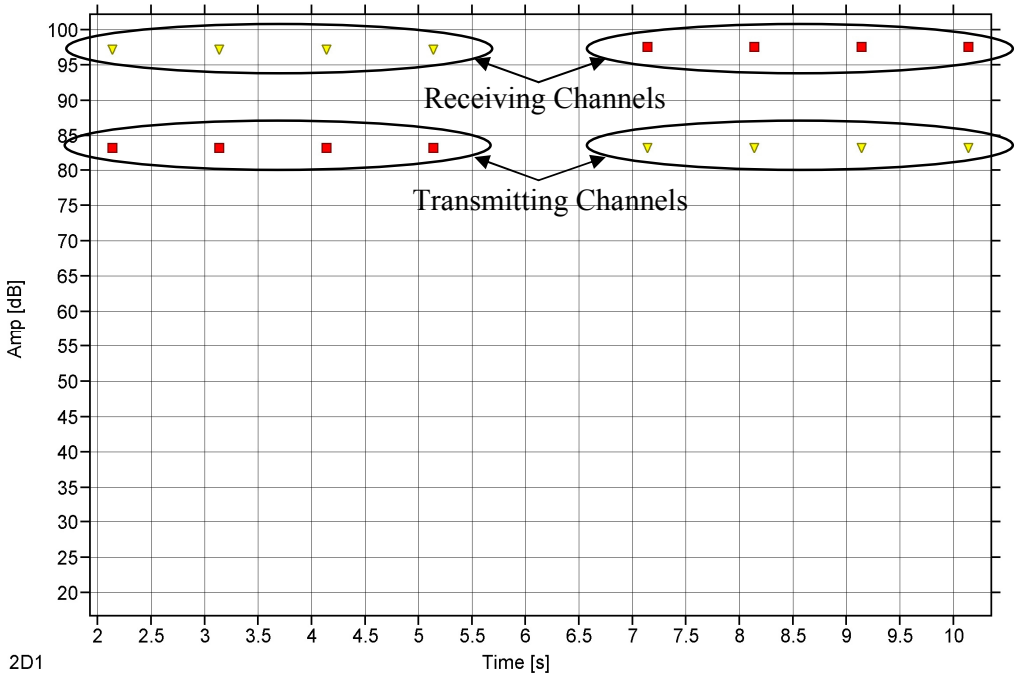

Figure 35 - plot showing amplitude responses of embedded sensors during automatic calibration. The red squares show the response of channel 1, and the yellow triangles represent channel 2. Initially channel 1 was pulsing and channel 2 was receiving. After 4 pulses, channel 2 becomes the transmitter, and channel 1 becomes the receiver.

Following this initial calibration, the speed of sound through the stem could be calculated based on the known distance between the sensors and the difference in arrival times of an individual event (Table 4).

Channel	*Time [ms.µs]*	*ΔT [ms]*	*Distance between sensors [mm]*	*Amplitude [dB]*	*Risetime [µs]*	*Duration [µs]*	*Counts*	*Energy [eu]*
Start Calibration								
2	640.4153		83	83.3	10.2	57.4	9	171
3	640.4337	0.0184	83	97.2	80.8	9446.4	2381	14500
2	640.8225		83	83.3	10.2	57.4	9	171
3	640.8408	0.0183	83	97.2	80.8	9446.4	2364	14500
2	641.2297		83	83.3	10.2	57.4	9	171
3	641.2481	0.0184	83	97.2	80.8	9446.4	2367	14500
End Calibration								

Table 4 - Waveform parameters recorded during automatic calibration process

So by taking the first recorded event (highlighted in Table 4), the difference in arrival times of the same recorded event by each sensor was (0.4337-0.4153) = 0.0184ms. The sensors are located 8.3cm apart, and therefore the speed of sound is calculated as 451cm/ms that are the units used by the Vallen software. By using this as the speed of sound for the location algorithm, the accuracy of the location prediction was tested. To induce a signal into the stem pulses were sent through a transmitter attached to the stem at known locations using cyanoacrylate adhesive. The transmitter was positioned at 1cm intervals along the stem and the calculated location is shown in Figure 36. A comparison was made between the actual location of the pulsing transducer and the average detected location – shown in Figure 37

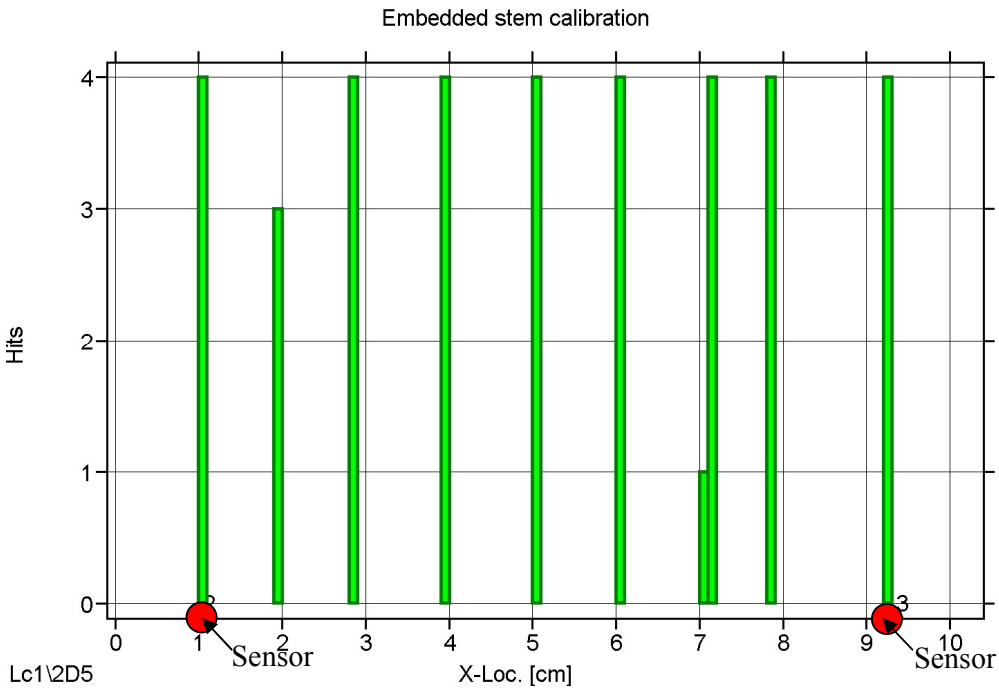

Figure 36 - Plot of located events during pulse location calibration of embedded sensors within a simplified femoral stem. The pulses were induced using another AE transducer that was glued onto the stem at 1cm intervals along its length.

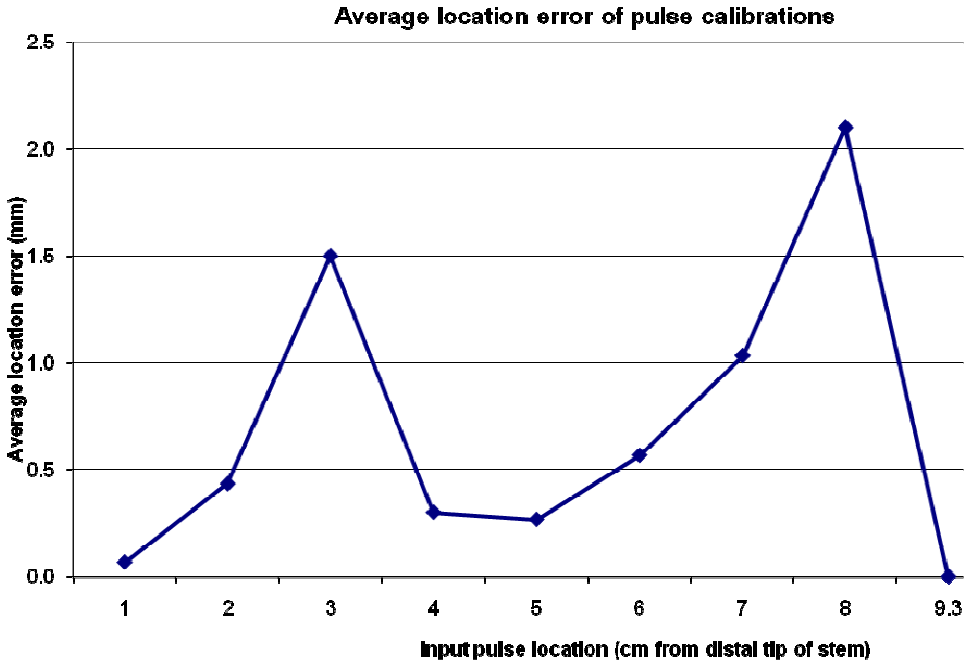

Figure 37 – Plot showing the average location error from calibration pulses sent into the stem at known locations.

From this information, the location accuracy of the embedded sensors was found to be within +/-2mm (within the location accuracy of the transmitter). However, the ability of the embedded sensors to detect events occurring within the metal stem itself is not the objective of this project. In order for the system to be worthwhile, it must be able to demonstrate the ability to detect and locate events occurring elsewhere within the construct – principally within the cement layer. As described in further detail in Chapters 6 & 7, the cement mantle of each construct was scanned using micro-Computed Tomography both before and after loading. In order to achieve enough contrast within the cement, it was necessary to remove the stem prior to scanning. It was found that the subsequent stem-cement interfacial conformity was affected upon reinsertion of the stem, requiring an initial "bedding in" period of loading in order to return the stem to its original cured position. During pencil lead break tests to check the operation of the sensors prior to loading, it was noticed that the embedded sensors failed to accurately locate the pencil lead break (plb) tests on the surface of the Tufnol tube, but that this inaccuracy diminished as the stem subsided with the application of load. The next section presents an investigation into this issue and assesses whether or not it is appropriate to use the speed of sound within the stem to locate events originating within the cement mantle.

4.4.1 Ability of embedded sensors to detect and locate events that do not originate in the stem

As mentioned previously, it was noticed that the ability of the embedded sensors to accurately locate pencil lead break tests performed on the surface of the Tufnol tube following re-insertion of the stem into the construct was noticed to be poor. This may have been due to the chosen speed of sound used to analyse the location of events. The measured speed of sound within the stainless steel stem and surrounding Technovit layer was ~460cm/ms and ~150cm/ms respectively. During calibration, pulses sent from one embedded sensor to the other were located to within +/-2mm (Figure 37). However, prior to loading, pulses sent directly into the Tufnol/technolvit were not located accurately by the sensors within the stainless stem and pulses sent from the stem were not accurately located by the external sensors. It was hypothesised that the inability of the sensors to accurately locate events originating in another material other than that in which the sensors themselves were located was due to a lack in conformity of the interfaces rather than the variations in acoustic velocity between the two materials, since the location accuracy seemed to improve with stem subsidence. However, these observations were noticed empirically, and so this section of the thesis is intended to present a more formal investigation into this observation. The initial error associated with events originating from one material but detected in another has implications for the accuracy of any attempt to corroborate AE location of damage to μ-CT imaging using embedded sensors. It is therefore important that this effect is quantified and taken into consideration when using embedded sensors to assess source location. An experiment was conducted to measure the variation in location error across materials with increasing interface conformity. It was hypothesised that the location error would decrease as the two materials form a conforming interface since the point of acoustic transfer from one material to another will become closer to that of the true origin (Figure 38).

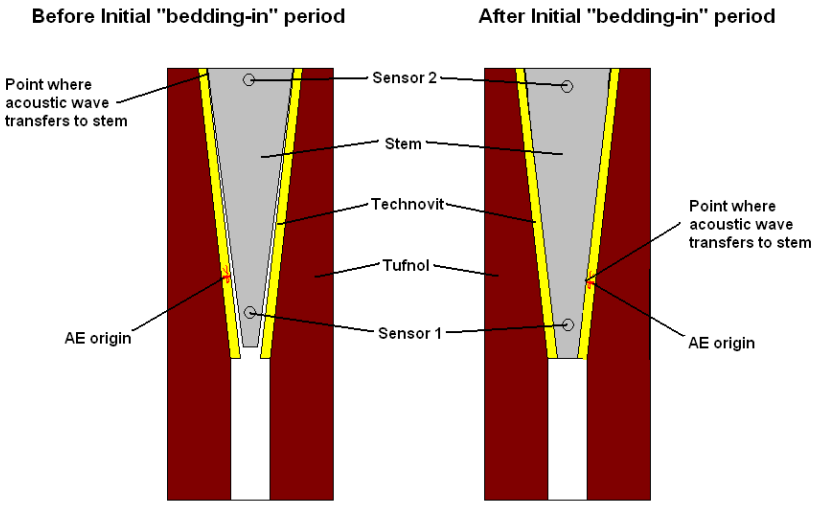

Figure 38 - Diagram showing predicted effect of interface conformity on location accuracy of events originating outside of the femoral stem.

The lack of initial conformity between the stem and the construct was caused by the removal of the stem prior to μ-CT scanning. The stem was re-inserted into the construct by gently pushing it in by hand, and there was often noticeable lateral movement of the distal tip of the stem. The lack of interfacial conformity could be observed when the construct is viewed from the distal end of the construct (Figure 39).

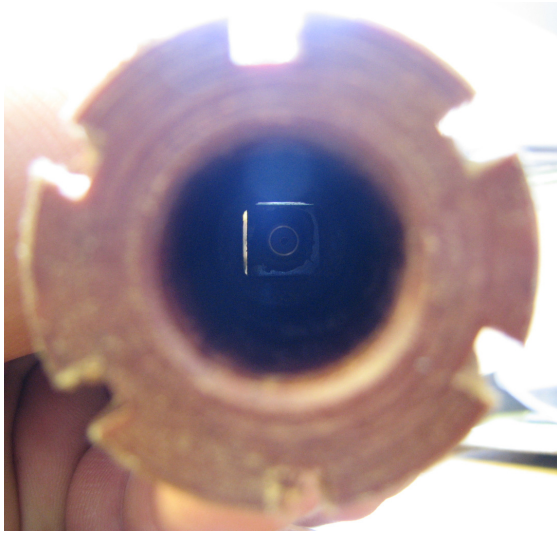

Figure 39 - Photograph looking up the distal end of a stem construct. The stem has been re-inserted by hand following removal prior to μ-CT scanning. Air gaps are visible indicative of poor interfacial conformity.

Furthermore, as the load increased the stem subsided within the construct; altering the relative positions of the sensors and thus inducing a progressive offset error as the stem subsided.

METHOD

The standard simplified stem construct configuration as described earlier was used for all testing. Four external sensors were mounted onto the external surface of the Tufnol tube at positions 52.5mm, 80.0mm, 107.5mm and 135.0mm from the distal end of the Tufnol tube. Initial speed of sound calibrations of the construct and the stem were performed using Vallen Systeme's auto calibration software. Axial compressive load was applied to the construct using an Instron servo hydraulic test machine. The relative positions of the embedded sensors to the Tufnol tube were recorded prior to the application of any load and the actuator position of the Instron machine was tracked during testing to measure stem subsidence. 0.1KN load increments were applied from 0kN up to 1kN and then 0.5kN load increments up to 10kN. The auto calibration software was used to send pulses through each external sensor in turn following each load increment. The calculated pulse locations were then adjusted to take account of stem subsidence, and the absolute location error recorded.

RESULTS

The sensor calibration gave the speed of sound in the stainless steel stem to be 461cm/ms, and 260cm/ms through the Tufnol/Technovit construct. At 0kN load, the embedded sensors were not able to locate any of the external sensor pulses, however, as the load was increased so too did the detection and location accuracy of the results. The pulses sent from the external sensors were located to within +/- 53mm at 0.1KN (4mm subsidence), but the proximal and distal external pulses were not located until the load reached 5kN. Decreasing the speed of sound used by the location algorithm would enable all four pulse locations to be identified on the location plot, but it was only after the load exceeded 5KN when all four pulse locations were identified using the speed of sound of the stem (this corresponded to a subsidence of 10.2mm). As a consequence, only the two centre pulse locations were used to illustrate the variation in location error with load and subsidence respectively.

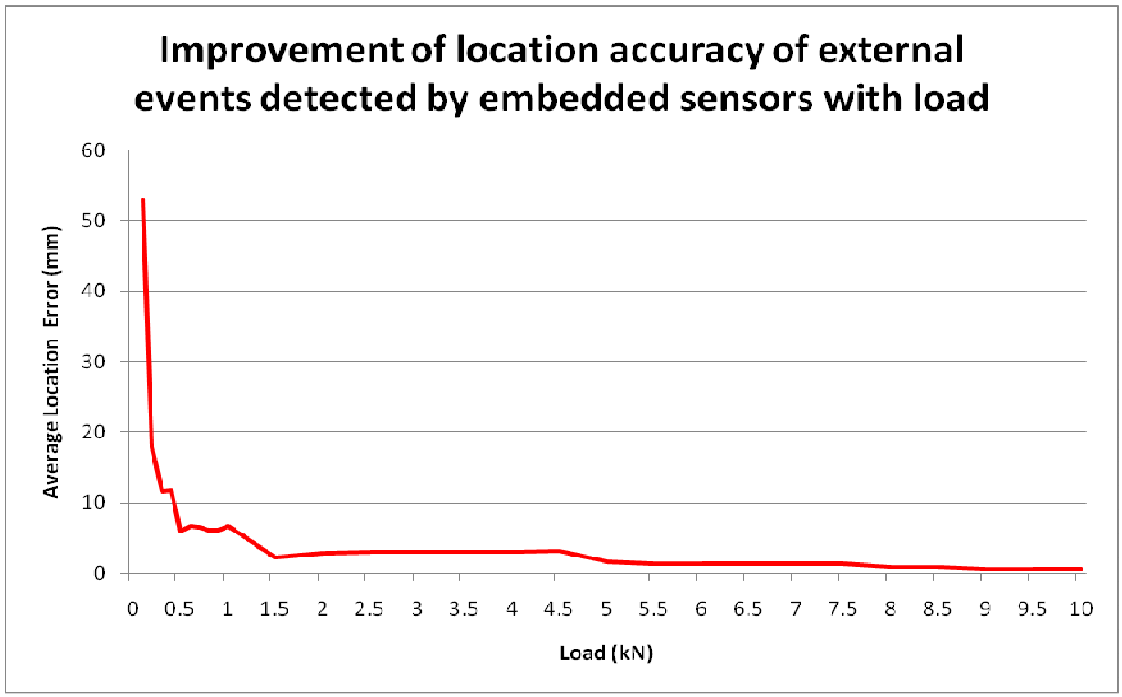

Figure 40 - Graph showing variation in measured location error with applied load from known external events detected by sensors embedded within the femoral stem.

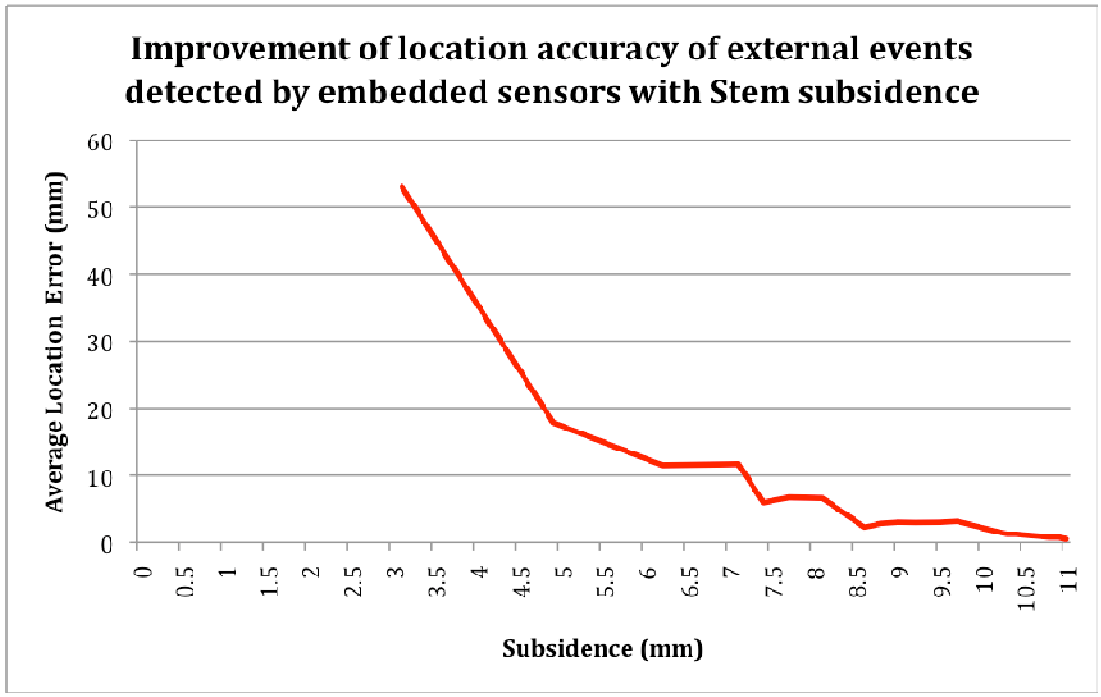

Figure 41 - Graph showing variation in measured location error with stem subsidence from known external events detected by sensors embedded within the femoral stem.

Analysis of the peak amplitude responses of the embedded sensors demonstrated a correlation between stem subsidence and signal attenuation. When under 0kN load the

pulse amplitude was recorded as 83.3dB, and the corresponding response at the receiving sensor was 96-96.4dB. At maximum load (10KN), the pulse amplitude remained at 83.3dB, however the corresponding response at the receiving sensor had decreased to 84dB (Figure 42). The subsidence of the stem follows the stick-slip type behaviour as identified by Verdonschot and Huiskes[196] and there are notable slips at 5KN and at 8KN (Figure 42). These movements in stem subsidence corresponded to a marked increase in attenuation of signals sent through the stem. This was particularly evident at 8KN and corresponded to a large burst in acoustic activity (Figure 43).

Further analysis of the signals identified the presence of a sudden burst of high amplitude (>65dB), high energy(>100Eu), short rise-time (<20µs) and long duration (>500µs) events that were not associated with any pulse calibrations on loading to 4.5KN (Figure 44). The values used to identify a threshold for each of these parameters were based on an elimination of the majority of events occurring at other load steps (Figure 43 & Figure 44). These events corresponded to a slight jolt in actuator position and tended to be located 11-12cm from the distal end of the Tufnol tube (Figure 45).

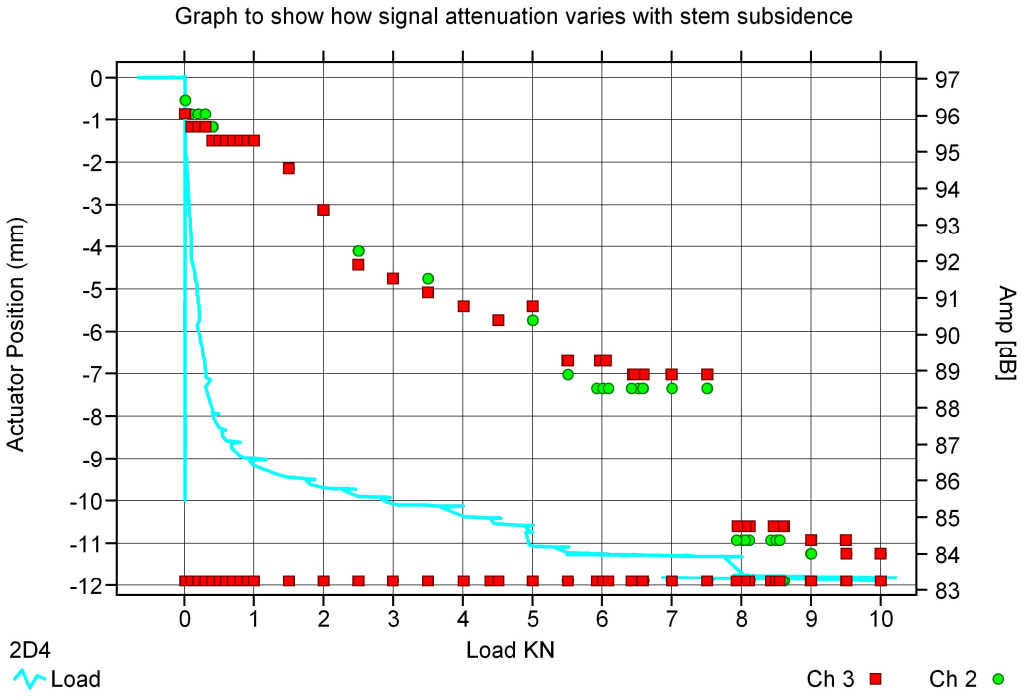

Figure 42 - Plot showing increase in signal attenuation from pulse events in relation to applied load and stem subsidence

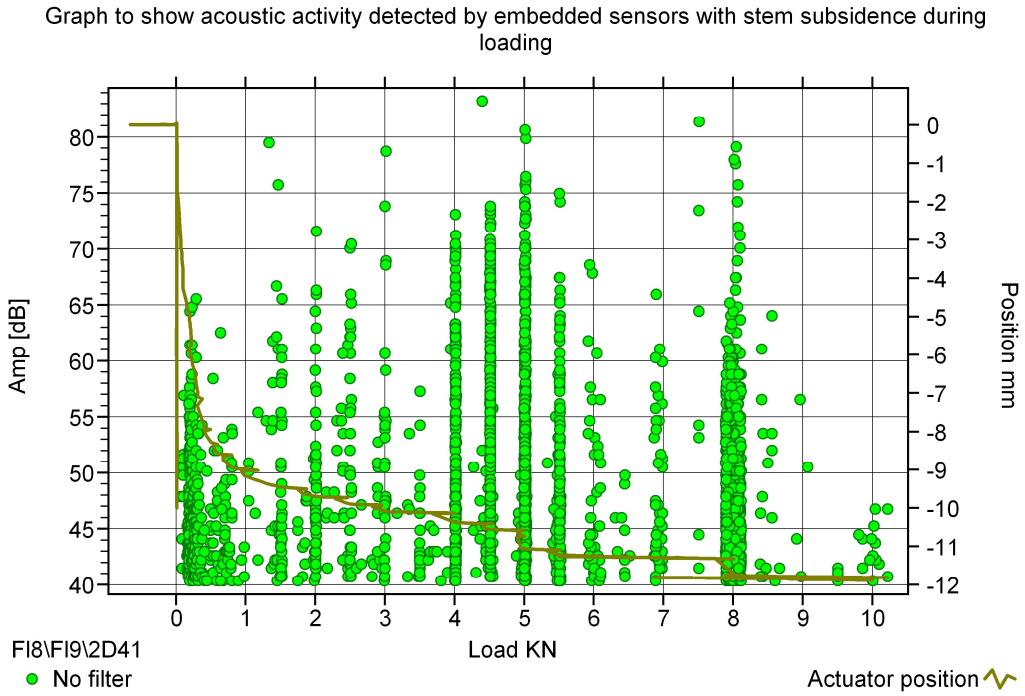

Figure 43 - Plot showing acoustic activity during loading as detected by the embedded sensors, excluding events recorded from the calibration pulses.

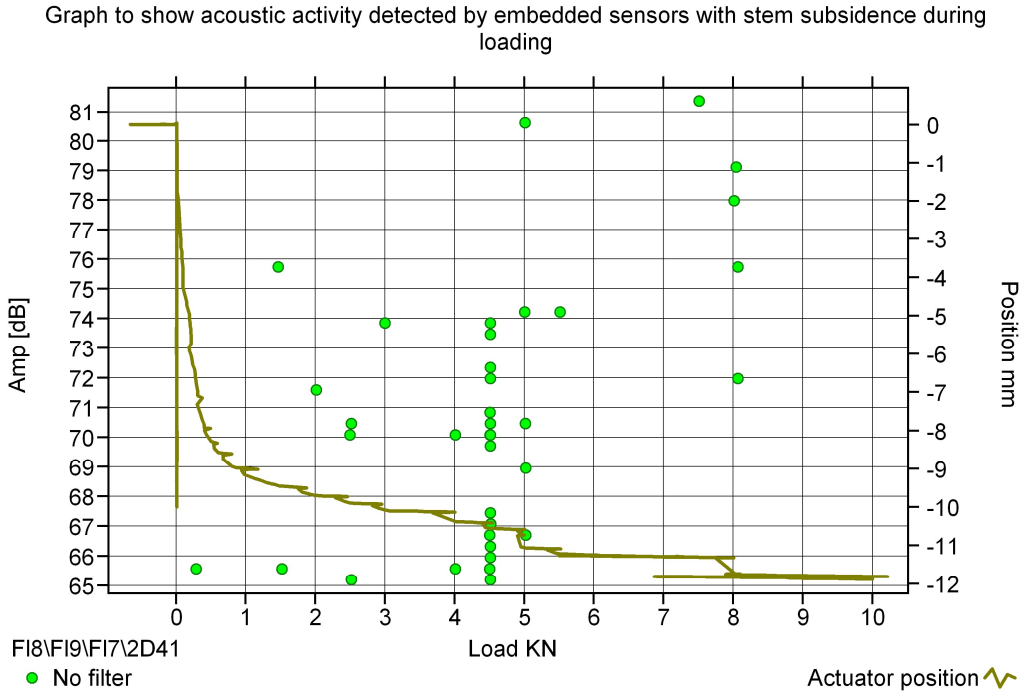

Figure 44- Plot showing high amplitude (>65dB), high energy(>100Eu), short rise-time (<20µs) and long duration (>500µs) acoustic events during loading as detected by the embedded sensors, excluding events recorded from the calibration pulses.

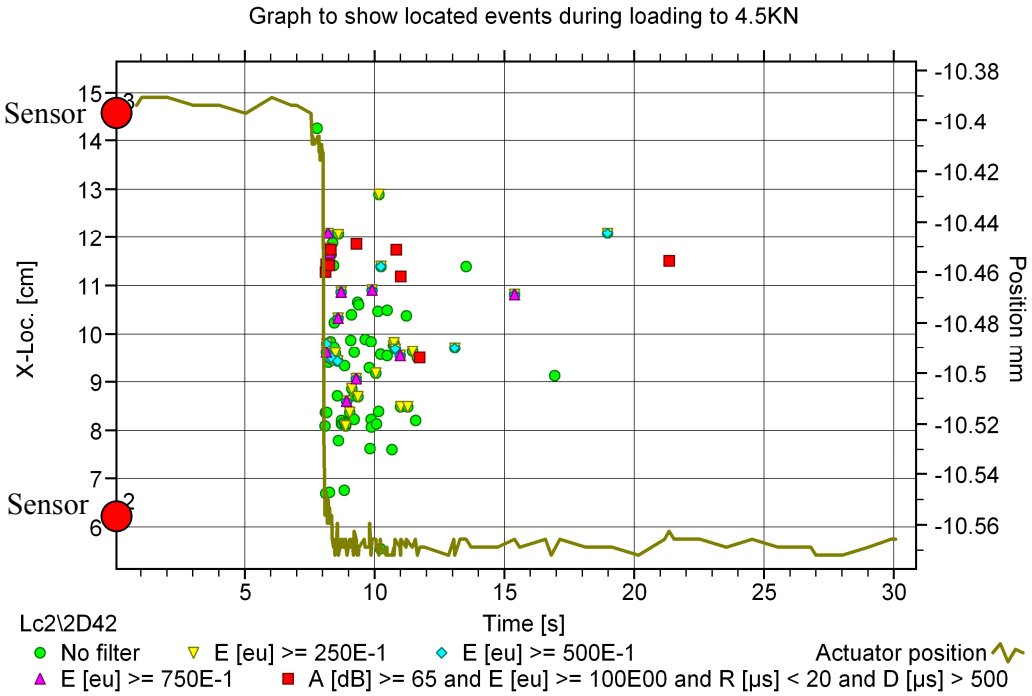

Figure 45 - Plot showing close-up of acoustic activity during loading to 4.5KN. Events of high amplitude (>65dB), short rise time (<20µs), long duration (>500µs) and high energy (>100Eu) are highlighted in red

DISCUSSION

Substantial location error was observed when using the embedded sensors to detect events within neighbouring materials when the stem was not sufficiently seated within the surrounding construct. Significant subsidence was necessary (>10mm) before the embedded sensors could locate events occurring in the surrounding construct to within +/- 2mm. At this point the two materials appear to be acoustically bonded. It should be noted that the subsidence necessary to reposition the stem into its original position during polymerisation of the surrounding Technovit was ~5-10mm, and so the 10mm necessary to achieve adequate interfacial conformity was perhaps not so surprising.

This study has demonstrated that once the stem is sufficiently embedded within the construct, the use of the speed of sound of the stem alone is justified for accurate location analysis of events occurring within the construct and care should be taken when using location analysis on a stem that has not been embedded properly. The loading regime used in this study was done incrementally, and it is hypothesised that a fatigue-loading regime would enable sufficient subsidence to embed the stem properly at lower loads. This variation in location accuracy has potential implications as an assessment tool - the accuracy of an external stimulus could be used to assess implant fixation. A polished stem would have to be properly embedded in order to accurately locate this stimulus. Conversely, textured surface cemented stems may well have a good location response from time of implantation, but it is also hypothesized that location accuracy would diminish in these stems in the event of interfacial de-bonding.

A further observation was the increasing attenuation through the femoral stem as it subsides within the construct. Although the reason for this is unknown, it is believed that greater conformity with the surrounding construct enables greater leakage of the acoustic wave away from the stem – effectively damping the signal. This effect could also be used to assess implant fixation.

It is difficult to categorically state whether the sudden slips at 5 & 8KN or the burst in high amplitude, high energy, high duration and short rise time events at 4.5KN correspond to a particular damage mechanism such as crack formation. Roques et al[148] have stated in earlier work that events generated from brittle failure tended to have durations up to 400μs

and rise times less than 25µs, whereas more 'plastic-type' events tended to have shorter durations and longer rise times. As stated in the results, on loading to 4.5KN events containing signals of short rise-times (<20µs), high amplitude (>65dB), high energy (>100Eu) and long durations (>500µs) were identified almost exclusively. Although the categorisation of what is meant by a long duration event is different from the work of Roques et al[148], the general waveform characteristics are in agreement with that expected if cracking was indeed present. The fact that the actuator position jolted during loading to 4.5KN (Figure 45) is further evidence that a sudden instability in the construct may have developed around this time. A similar jolt was observed during loading to 5KN when the actuator position recorded the stem to have subsided 0.18mm from its previous location, but suddenly subsided a further 0.34mm before coming to rest (Figure 46). This jolt was accompanied by a burst in acoustic activity, however the majority of these events were of low energy (<25Eu).

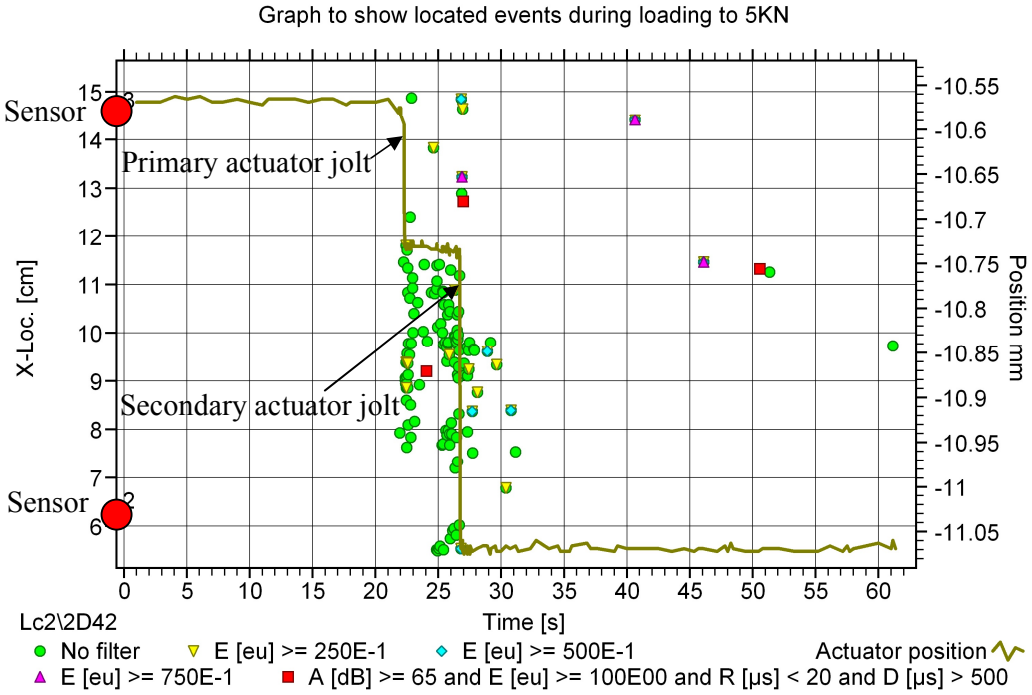

Figure 46 - Plot showing sudden jolt in actuator position during loading to 5KN with corresponding acoustic activity - indicative of cracking? Events of high amplitude (>65dB), short rise time (<20µs), long duration (>500µs) and high energy (>100Eu) are highlighted in red.

In contrast to this, no secondary jolt in actuator position was observed when loading the construct to 8KN (Figure 47) and indeed there are relatively few located events associated with the subsidence. This implies that the initial crack formation was more likely to have

occurred during loading to 4.5KN, and the subsequent slips at 5 & 8KN were more likely to indicate further crack opening rather than initiation.

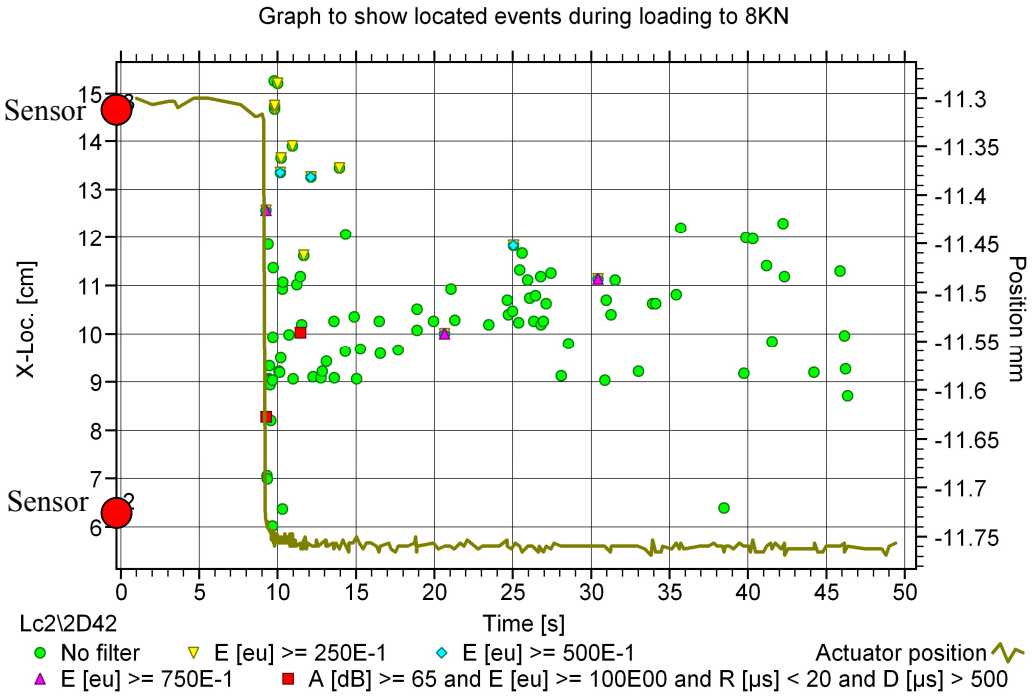

Figure 47 - Plot showing actuator position during loading to 8KN with corresponding acoustic activity.Events of high amplitude (>65dB), short rise time (<20µs), long duration (>500µs) and high energy (>100Eu) are highlighted in red.

SUMMARY

This chapter has described the development of a simplified stem construct to act as a test bed for the assessment of AE sensors embedded within a femoral stem. In essence, the final polished stem acts similarly to the Exeter stem described in the introduction to this thesis, in that it appears to subside further within the mantle to achieve greater fixation. This subsidence increased the acoustic conformity between the Technovit and stem which in turn had an effect on the location accuracy and attenuation of signals that were transmitted across the Technovit-Stem interface. This effect itself was investigated further to assess whether it was justified to use the initial calibrated speed of sound between embedded sensors to accurately locate events occurring within the other material constituents of the construct. Since the accuracy of events located on the external surface of the Tufnol tube increased with stem subsidence, it was concluded that the speed of sound through the stem could be used for event location provided that the stem is properly

seated within the construct. Furthermore it was proposed that the relationship between location accuracy of pulse events that were sent from one embedded sensor to the other may have greater implications as an assessment tool for stem fixation and loosening. This is not investigated further in this thesis, although it is something that should be investigated as part of any future work of this project.

Having established a method for embedding sensors within the stem and confirming that they operate satisfactorily under simple pulse testing, the question as to whether this could be transposed to more complicated and realistic testing applications needs to be addressed. The next few chapters use this embedded construct in a variety of test configurations to assess whether the embedded stem continues to operate satisfactorily, highlight any potential issues, and contribute to the understanding of cement damage formation. The complexity of test scenarios are built up stepwise – Chapter 5 monitors the construct during polymerisation of the surrounding cement layer. As identified in the literature review, several authors have alluded to the possibility of crack formation occurring within the cement mantle during polymerisation, and it is hypothesised that the embedded construct may be able to detect this damage as it occurs. It is acknowledged that polymerisation cracking in this construct does not necessarily mean that polymerisation cracking occurs in bone cement mantles around prosthetic stems used *in-vivo* – but if it can be shown that this system is capable of detecting such damage, then this is a potential future application for the system. Chapter 6 investigates a simple loading configuration intended to induce damage within the cement mantle, before extending the technique to a fatigue-loading scenario in Chapter 7 that is more representative of the type of loading seen by total hip replacements *in-vivo*.

CHAPTER 5 - ACOUSTIC EMISSION MONITORING AND 3D VISUALISATION OF POLYMERISATION INDUCED DAMAGE OF ACRYLIC POLYMER MATERIALS[III]

5.1 INTRODUCTION

The work presented so far has concentrated on the identification of suitable condition monitoring technologies, followed by the development of a simplified construct and a femoral stem containing embedded AE sensors. It was stated in the literature review that one of the shortcomings of the commonly used serial sectioning technique for assessing the integrity of the cement mantle retrospectively is that the technique does not account for any pre-existing damage prior to loading and that the specimen is destroyed in the process. The literature review also discussed several studies that had suggested that the stresses induced during the polymerisation of cement might be sufficient to cause crack formation prior to loading resulting from shrinkage or and the presence of pores[81,84,85]. In order to eliminate the possibility of confusing pre-load and loading damage in subsequent analysis, it was hypothesised that micro-Computed Tomography could be used to scan and assess the cement mantle integrity prior to loading. Unfortunately, the μ-CT technique can only show damage after the cement mantle has cured, however, based on the work of Roques et al[85] who used one AE sensor to monitor polymerisation of cement around a stainless steel tube, it was also hypothesised that multiple AE sensors could be used to detect, locate and determine when damage forms during polymerisation in the simplified construct. It was not possible to connect the embedded sensors for this particular study due to the design of the jig used to hold the stem in position during polymerisation. Therefore, all of the results presented in this chapter are from external sensors. However, it was felt that an assessment of the ability to corroborate initial damage detected using the AE technique to visual damage observed in pre-load μ-CT scans was an important step in order to lay the

[iii] The work presented in this chapter has been published: Mavrogordato M, Taylor M, Taylor A, Browne M. Acoustic Emission Monitoring and 3D Visualization of Polymerisation-Induced Damage of Acrylic Polymer Materials. Journal of Biomedical Materials Research Part B: Applied Biomaterials 2009; 90B(1):223-228.

foundations for subsequent data obtained from embedded sensors during loading. To put this work into the context of contributing to the field as a whole, the ability to monitor damage formation during polymerisation could be used to quickly assess the cure behaviour of different cement formulations, stem geometries etc. *In-vivo*, this information may give an early indication of individual total hip replacements that may be predisposed to fail as a result of poor initial cement integrity.

5.2 METHODS

Five stem constructs were prepared in accordance with the methodology described in Chapter 4 (The stems were not pre-heated for this particular experiment). Four sensors were attached to the external surface of the Tufnol Tube (it was not possible to mount the sensors directly onto the Technovit since it was polymerising) and acoustic activity was recorded for 60 minutes post-implantation as the Technovit polymerised.

In order to relate damage to the thermal effects of the exothermic reaction, a further sample was tested with thermocouples mounted within the cement mantle. The time from initial liquid powder contact to peak temperature was recorded and it was assumed that any evidence of cracking prior to peak temperature being attained was not related to any thermal contraction.

The constructs were prepared and μ-CT scanned in accordance with the methodology described in Chapter 4. Following reconstruction, the location results of the AE data were corroborated to these images.

5.3 RESULTS

In order to assist with the analysis of and correlation between CT and AE data, it was decided that the length of the stem should be divided into 3 zones; proximal (zone 1), middle (zone 2) and distal (zone 3) see Figure 48 & Figure 49. When discussing areas of damage these zones shall be used to identify its location.

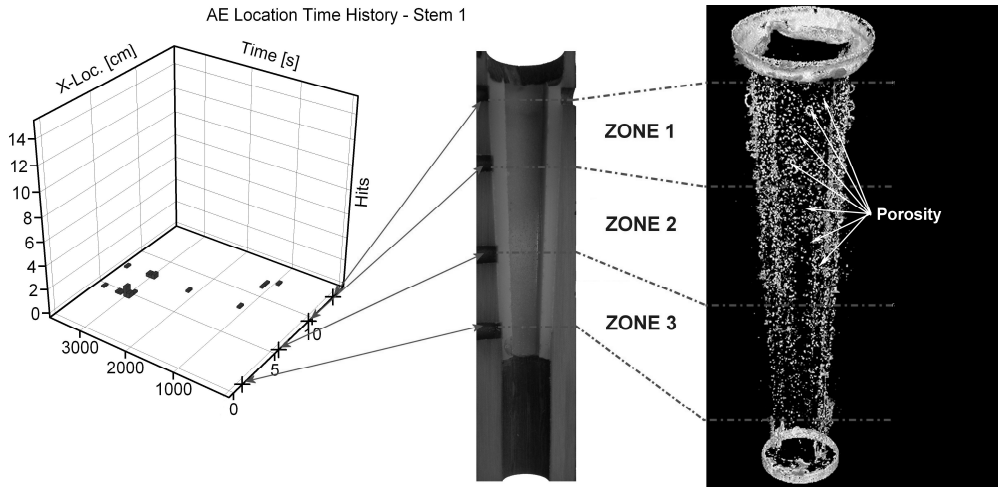

Figure 48 – AE plot showing time-progressive distribution of located events along the length of stem 1 and correlated to zonal locations shown on both a section photograph of the stem and reconstructed 3D CT image depicting damage highlighted by radiopaque Zinc Iodide solution.

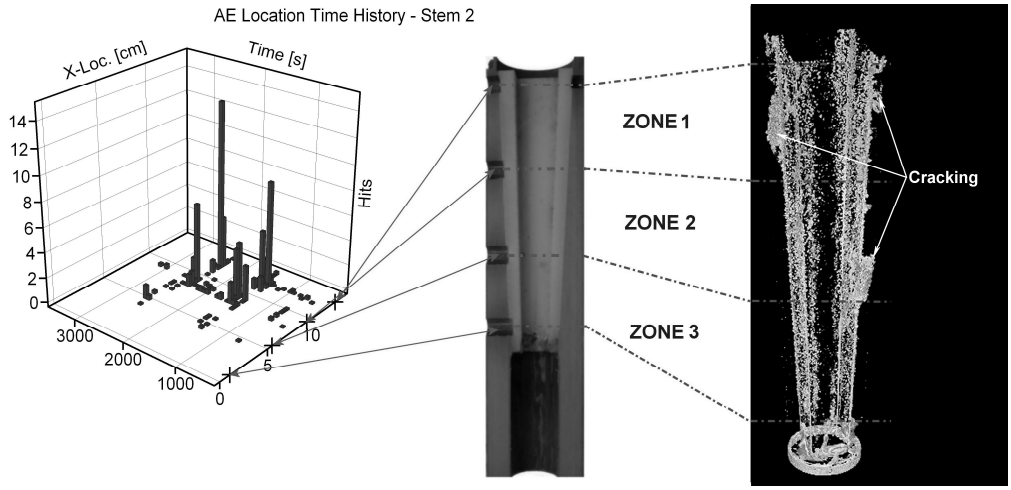

Figure 49 – AE plot showing time-progressive distribution of located events along the length of stem 2 and correlated to zonal locations shown on both a section photograph of the stem and reconstructed 3D CT image depicting damage highlighted by radiopaque Zinc Iodide solution.

Acoustic activity was observed in the form of bursts of high activity followed by periods of silence (Figure 50 & Figure 51). Using stem 2 as a typical example, the first burst of

located acoustic activity occurred between 600 and 700 seconds. However, significant bursts of activity were also observed at around 1300-1500 seconds and again at around 2250 seconds (Figure 51). This burst type activity was observed in all five specimens. It was observed that the first major burst of activity occurred around 651-820 seconds following first liquid/powder contact in all stems.

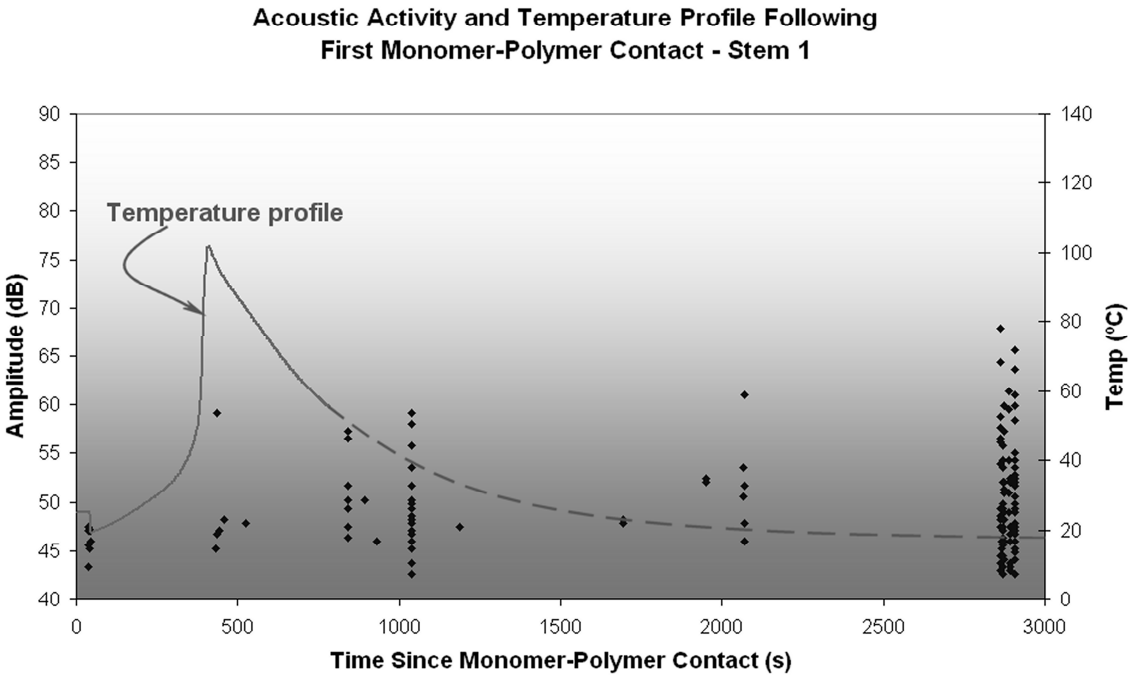

Figure 50 - Plot to show time-history of acoustic activity present in stem 1 highlighting bursts of acoustic activity plotted together with the temperature-time profile recorded during polymerization of Technovit.

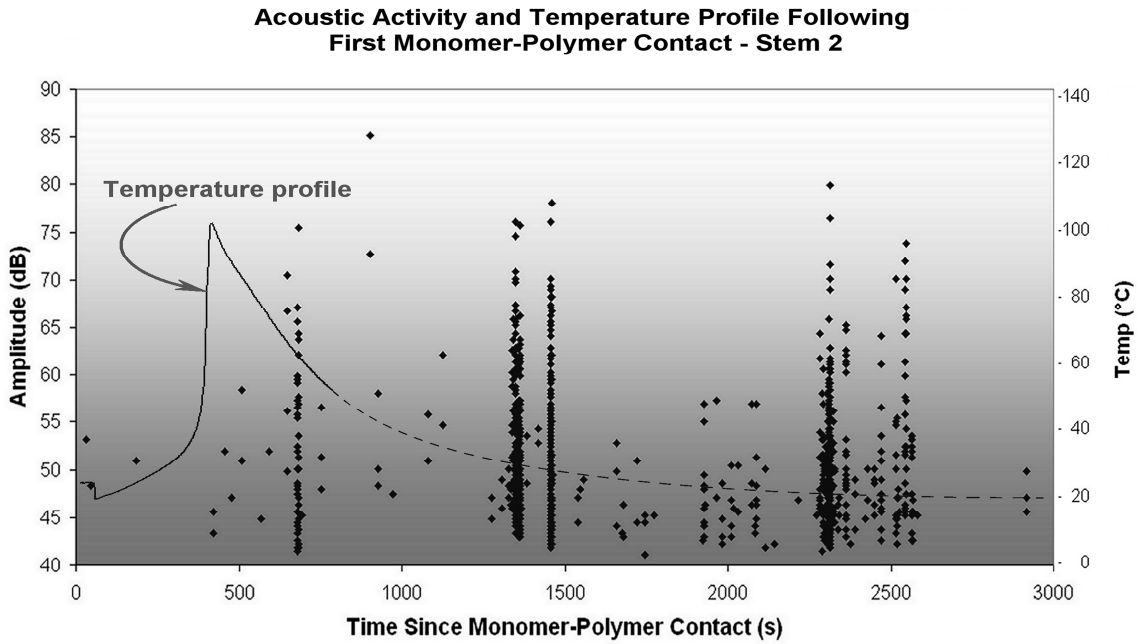

Figure 51 – Plot to show time-history of acoustic activity present in stem 2 highlighting bursts of acoustic activity plotted together with the temperature-time profile recorded during polymerization of Technovit.

The thermocouple data (Figure 50 & Figure 51) shows the time to peak temperature as being approximately 450 seconds after initial polymer-monomer contact. To equate these acoustic events to a location along the construct, the speed of sound through the construct was determined by dividing the distance between sensors 1 & 4 by the time taken for a signal induced using a Hsu-Neilson source (Pencil lead break)[16] at sensor 1 to reach sensor 4. In this way the speed of sound through the Tufnol was calculated to be 150cm/ms, and the calculated location of various pencil lead breaks along the length of the construct was shown to match the actual location to within 2mm. However, since Technovit was changing state during the experiment this speed of sound was only used as a first approximation during set up. Analysis of the data showed significant numbers of events occurring outside of the Technovit mantle using this figure. The speed of sound employed in calculations was therefore reduced until all of the events appeared to be constrained within the length of the Technovit, and a final figure of just 15cm/ms was used. It is recognised that this is not an accurate method for determining the speed of sound, however, since we were only interested in relative regions of damage and as a first stage in the monitoring of the cement mantle, it was deemed appropriate. Stem 1 showed very little

acoustic activity and the majority of activity that did occur was located towards the distal tip (Figure 48). By contrast, stems 2-5 showed a large amount of acoustic activity with a proximal dominance. Taking stem 2 as an example the majority of located events occurred within zone 1 and 2 with very little located activity in zone 3 (Figure 49).

The CT images highlighted areas of damage in all of the tested stems. In agreement with the AE data, stem 1 showed very little evidence of damage relative to stems 2-5 and any damage that was present seemed to be located in zone 3 towards the distal tip (Figure 48). Conversely, stems 2-5 showed more significant damage in the proximal section. Stem 2 was chosen as a representative sample from this group (Figure 49). From the CT images, damage can be seen in the form of cracks running along the corners of the stem and de-bonding between the Technovit/Tufnol interface. Indeed, in this example there is evidence of a crack forming in zone 1 that runs vertically along one of the corners of the stem along with another more substantial crack on the opposing corner. In zone 2, there was further evidence of substantial cracking, and at the zone 2/3 interface there was evidence of further cracking along the corner of the stem. Zone 3 presented little evidence of cracking although there was a marked region of porosity around the distal tip of the stem.

5.4 DISCUSSION AND CONCLUSIONS

This experiment was the first time that the in-house sensors had been used to actively monitor real-time processes occurring within the cement mantle. The data obtained from the results were in agreement with the study of Roques et al[85] who observed similar burst type activity during polymerisation of bone cement using a commercial AE sensor. In terms of a contribution to this thesis, this experiment has shown that the AE technique can be used to monitor internal defects forming within the Technovit layer, and that the zinc iodide solution used to prepare the sample for scanning was successful in highlighting defects – the penetrating capacity of the zinc iodide solution was sufficient to highlight cracking present within the Technovit mantle together with de-bonded regions at the Technovit-Tufnol interface, and surface porosity at both the Technovit-stem interface and around distal/proximal regions. However, it should be noted that the amount of damage shown in the reconstructed CT images is likely to be conservative since the zinc iodide solution can only penetrate into defects that are physically linked to the Technovit surface through open cracks or voids. It is also accepted that the removal of the stem may induce some damage within the mantle; however, removal was necessary to achieve sufficient contrast on the subsequently obtained radiographic images. The polished surface finish of the stem coupled with the use of a release agent ensured that the force needed to remove the stem was minimal and the jacking technique prevented shock loading of the mantle. E-Appendix_01 contained on the electronic DVD version of this thesis shows a video of the construct casting process and removal of the stem – it can be seen that the stem is removed smoothly using this technique and no shock loading is necessary.

The results of this study demonstrate that acoustic emission data can be used to provide a greater understanding of the time-history of polymerisation events. No acoustic activity was observed for an initial period following insertion of the stem whilst the consistency of the Technovit remained largely fluidic. The initial burst of acoustic activity occurred approximately 650-820 seconds after initial liquid-powder contact in all stems. This correlates well to the findings of Gilbert et al[82] who observed a rapid onset of shrinkage in bone cement between 400–600 seconds and Lennon et al[81] who used an adaptation of Baliga et al[197] and Starke et al's[198] mathematical model incorporated into their finite element model to predict the point of maximum temperature and time to complete polymerisation. They predicted a peak temperature in their samples to occur at 536

seconds and complete polymerisation after 697 seconds. Our results showed the peak temperature to occur at 451 seconds and it would not be unreasonable to assume complete polymerisation to have occurred after 600-700 seconds. The major burst of acoustic activity occurred approximately 3-6 minutes after the maximum temperature reached during exotherm, and hence it was assumed that the Technovit had polymerised by this stage; this suggested that the main source of pre-load damage can be attributed to thermal contraction effects rather than pure volumetric shrinkage.

In addition to revealing information about the chronology of events, AE data can be used to verify where the damage was located, and the type of damage that occurred. The location capabilities of the AE technique are well established, however, the location accuracy of these particular results is vague at best. The construct consists of multiple materials, and although the geometry is simplified compared to a clinical device, there are still geometrical effects that could affect the wave propagation. The acoustic wave will therefore spread, reflect and refract, and multiple wave modes are likely to be in existence at any one time. It is hypothesised that the speed of sound within the Technovit changed during polymerisation and that using the initial calibrated speed of sound through Tufnol did not give a representative distribution of events. The speed of sound used in calculations was therefore reduced significantly to ensure that all located events appeared within the sample. Whilst this process meant that no quantitative assessment of location accuracy could be drawn from the data, it still gave relative locations of damage – i.e. whether it was detected in the proximal/distal regions of the cement – and this was still more information than had been obtained previously. Located events were plotted against time (Figure 48 & Figure 49) to give a greater understanding of the processes occurring during polymerisation for each sample. Acoustic activity was observed in some areas from a very early stage. These regions saw a progressive accumulation of acoustic activity and were shown to correspond to damaged regions observed visually using μ-CT. The waveform characteristics showed evidence of crack type behaviour - events of high energy (greater than 10^3 EU) and long durations (greater than 3000μs) - together with events characteristic of rubbing (events with relatively long rise-times and durations) the classification of events in terms of cracking/rubbing is derived from the work of Roques et al[148] who used four point bend specimens of bone cement to locally assess the change in acoustic response with the onset of crack formation.

The AE technique was also shown to give a clear indication as to the extent of damage that occurred within the specimens with stem 1 producing significantly less acoustic activity that stems 2-5. It is not clear why stem 1 produced significantly less damage, and one potential reason was that stem 1 was not subject to the same constraints as subsequent stems due to insufficient filling of the mould cavity with Technovit. Gilbert et al[82] demonstrated this effect by comparing constrained and unconstrained samples of polymerising translucent bone cement at various time intervals following initial mixing. They observed pore development and growth in the constrained samples, but no such porosity was evident in the unconstrained samples. However, for cracking along the length of the stem, the most influencing factor is expected to be a constraint in the hoop direction rather than the longitudinal stress imposed by a proximal constraint. Furthermore, based on the work of Gilbert et al, one would expect significantly more porosity to develop within the constrained samples and whilst this is observed around the proximal and distal tip regions, there appears little difference in porosity along the medial sections. Other factors may therefore be influencing the level of damage present within the Technovit layer. It is well known that the temperature of the stem has an influence on the curing characteristics of the cement[199,200], although again this is thought to influence the level and distribution of porosity within the cement mantle rather than formation of physical cracks.

In conclusion, this study has demonstrated that AE can be used to monitor real time events occurring within the cement mantle of this simplified construct and that μ-CT can be used in conjunction with zinc iodide solution to visualise damage within the cement mantle without the need for serial sectioning. These concepts are taken forward and developed over the next couple of chapters. As already discussed, it was not possible to use the embedded sensors to monitor the polymerisation process due to the design of the jigs used to position the stem centrally within the mantle. Therefore, the next logical step is to perform a simple experiment that uses the embedded sensors to monitor active damage formation within the cement mantle and compare the information to that of external sensors and the visual information from CT scans. This process is described in the next chapter and is seen as an intermediate step before going onto look at the more complex cyclic fatigue-loading scenario presented in Chapter 7.

CHAPTER 6 - REAL TIME MONITORING OF PROGRESSIVE DAMAGE DURING LOADING OF A SIMPLIFIED TOTAL HIP STEM CONSTRUCT USING EMBEDDED ACOUSTIC EMISSION SENSORS

6.1 INTRODUCTION

The research presented in this chapter focussed on assessing the embedded sensors ability to monitor progressive failure within the cement mantle of the simplified construct and corroborate this information to data obtained from externally mounted sensors and μ-CT scans taken both before and after loading as well as periodic RFA assessments. *In-vivo*, the type of loading scenario applied to total hip joint replacements is typically cyclic, and as discussed in the literature review it is the fatigue performance of bone cement that is ultimately thought to limit the long-term survivorship of any cemented total hip replacement. However, it was felt that subjecting the construct to a fatigue cycle at this stage in the development process would introduce too many potential noise sources. The behaviour of this construct under load has not yet been established and acoustic signal characteristics of failure have thus far been limited to pre-load cracking during polymerisation. Therefore, an experiment was conducted that would enable the construct to experience loading to failure of the cement mantle in a controlled manner. As discussed in the literature review, the AE technique can be used to determine the maximum stress experienced in service by a material, known as the Kaiser effect whereby a specimen is gradually loaded and the onset of acoustic events indicates the maximum previously experienced stress level of the specimen[156]. This effect holds true unless irreversible damage is present within the sample, in which case acoustic events are observed before the previously attained stress limit, known as the Felicity effect[201]. It is hypothesised in this chapter that these effects could be applied to monitor the integrity of this simplified construct during an incrementally increasing static loading regime. This is the first time that the original hypothesis of the thesis concerning the use and potential advantages of directly embedded AE sensors into a femoral stem in order to monitor the integrity of the cement layer is tested.

To remind the reader, it was hypothesised that directly embedding the sensors within the femoral stem would:

1) Enable a permanent bond between the sensor and the structure, reducing potential complications of poor sensor fixation and eliminating test-to-test variations in sensor fixation;

2) allow a closer proximity of the sensor to the region of interest, directly reducing the attenuation of the signal before reaching the sensor and reducing interface effects. The signal received by an embedded sensor only has to cross the interface between the cement and the stem before reaching the sensor - as opposed to the traditional path of the signal received by external sensors that require the signal to cross the cement-bone interface, then travel through the bone itself which has varying density and acoustic transmission characteristics, before finally crossing the interface between the bone and the sensor case;

3) permit greater experimental flexibility as the test does not have to be designed to enable recovery of the sensors following testing, and

4) permit a more realistic test environment since the test chamber/bone specimen does not have to be altered in order to accept the sensors.

6.2 METHODS

Nine simplified stem constructs were manufactured in accordance with the methodology presented in Chapter 4. The first five constructs were those used in the previous study looking at damage accumulation during polymerisation and these did not receive any pre-heating of the stem. However, in order to try and improve visualisation of cement cracking as opposed to porosity at the stem-cement interface, the subsequent 4 stems were pre-heated in order to encourage polymerisation to initialise close to the stem, resulting in less porosity at this interface[199]. The change in porosity distribution is shown using axial slices of a μ-CT reconstructed image (Figure 52).

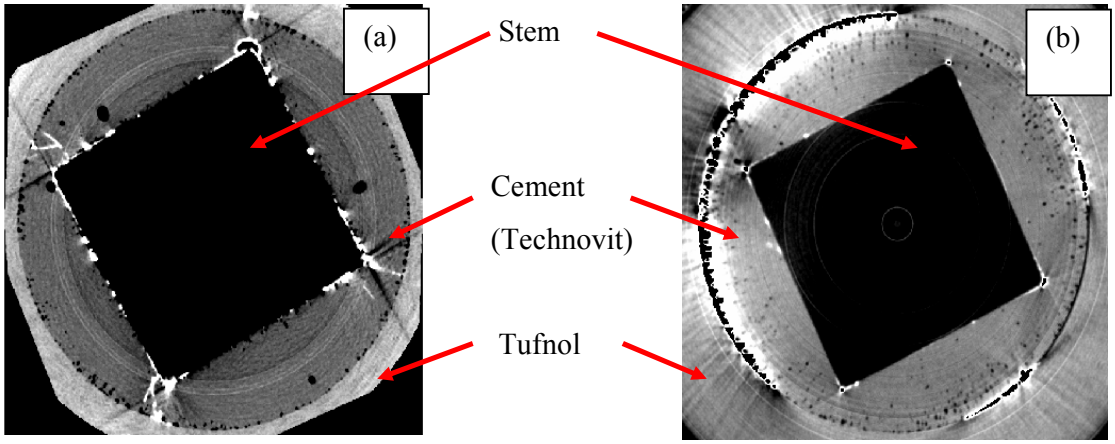

Figure 52 - Axial slice images of cement layer following insertion of stem at room temperature (a) and at 50°C (b). Image (a) shows porosity throughout the cement mantle, whereas image (b) shows negligible porosity around the stem-cement interface. Image (b) shows a significant increase in interfacial de-bonding and porosity at the Tufnol-cement interface.

Five of the stem constructs were instrumented with external AE sensors in accordance with the methodology described in Chapter 4. Three constructs were tested using both the external sensors and stems containing embedded sensors. The final construct was tested using embedded sensors only.

The experiment was set up in an Instron 8502 hydraulic testing machine with the construct held between two ball and socket joints to allow minimal constraints to be imposed on the construct under compression loading (Figure 53). ISO 7206-4 states that the implant should be inclined at 10° in adduction and 9° in flexion to induce torsion as well as bending and compression during loading. This configuration was followed for this experiment and the correct angles on inclination were achieved through the use of a

purpose built device consisting of an aluminium block faced off at the required angles and a surface mounted spirit level (Figure 54).

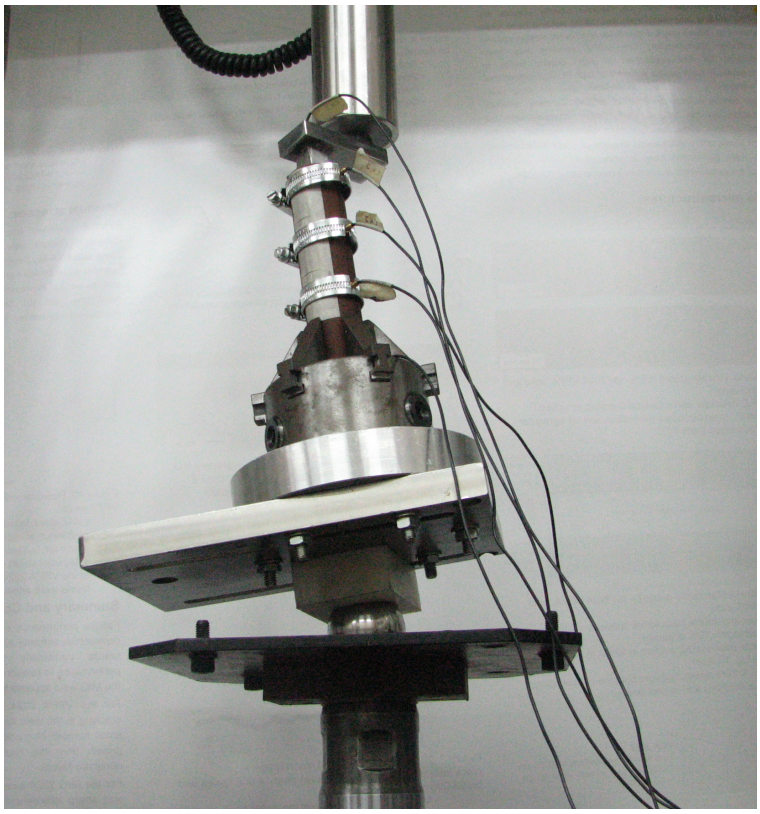

Figure 53 - Photograph showing stem construct mounted in an Instron 8502 hydraulic testing machine

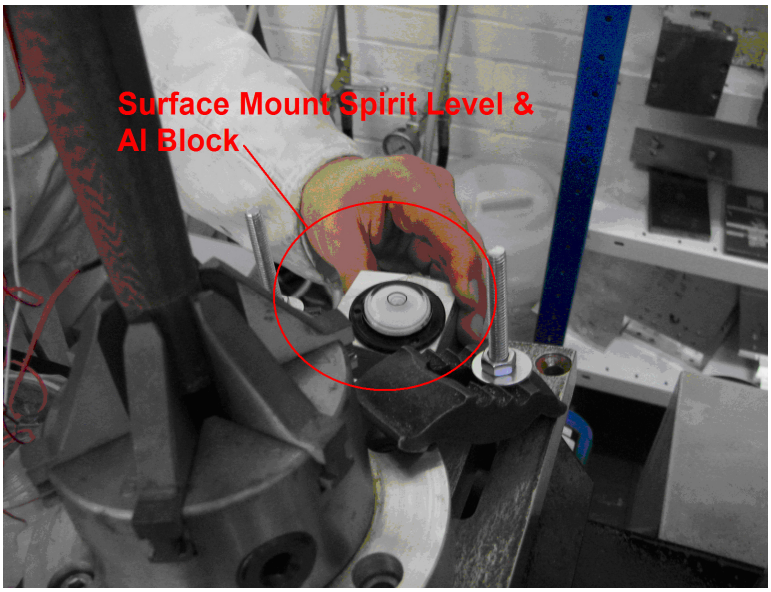

Figure 54 – Photographs showing faced off aluminium block and surface spirit level to ensure correct angles.

The samples were loaded to a pre-defined stress, unloaded, and then loaded again to a level exceeding the previously attained stress level by a pre-determined increment and repeating this whole process until substantial damage could be seen or the sample reached a set stress (Figure 55). This loading regime allowed the determination of the Felicity ratio[202] – as mentioned previously, the Felicity ratio is used to assess damage accumulation in composite materials and is defined as the ratio of the load at which AE is observed upon reloading to the maximum previous load.

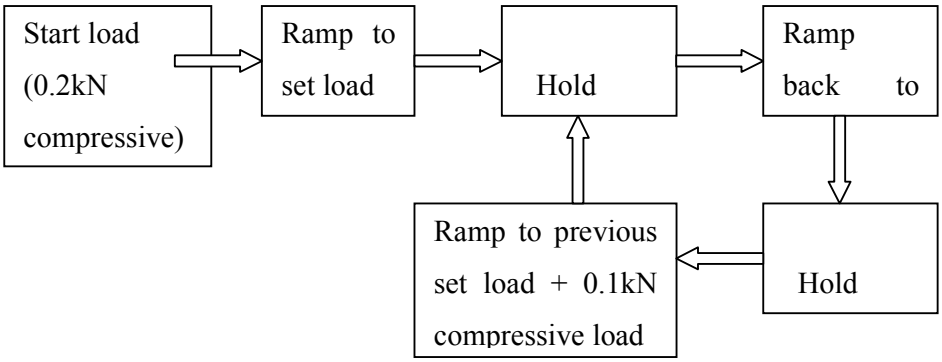

Figure 55 – Flow diagram showing Felicity loading sequence.

The AE data was recorded and analysed using a Vallen Systeme GmbH AMSY-5 panel and visualisation software. Data was recorded from the acoustic emission sensors together with parametric data corresponding to the applied load and position of the Instron machine. AE data was acquired continuously throughout the loading regime. To equate these acoustic events to a location along the construct, the speed of sound through the construct was determined by dividing the distance between sensors by the time taken for a signal induced using a Hsu-Neilson source (Pencil lead break)[16] at one sensor to reach another sensor. In this way the speed of sound through the construct was calculated to be 150cm/ms through the Tufnol/Technovit and 460cm/ms through the stem. Predicted locations of various pencil lead breaks along the length of the construct were observed to match the actual location to within +/-2mm.

μ-CT images were acquired both before and after loading, in accordance with the methodology described in Chapter 4, to allow a direct comparison between the load induced cracking identified by the μ-CT and the predicted regions of damage according to

the AE data. Quantitative comparisons were made between the damage detected using the external and embedded sensors' to the damage observed on the μCT by using image processing techniques such that the volume and surface area of the load induced cracks could be quantified: Image J (National Institutes of Health, USA) was used to subtract the before load scan volume from the after load scan volume. The result was that only cracks that formed during testing, as well as some residual zinc iodide on the surfaces of the Technovit layer remained visible (Figure 56c). The residual zinc iodide was removed using a simple macro (the code for this macro can be found in appendix F) that was written in order to extract the Technovit layer on its own (Figure 56d).

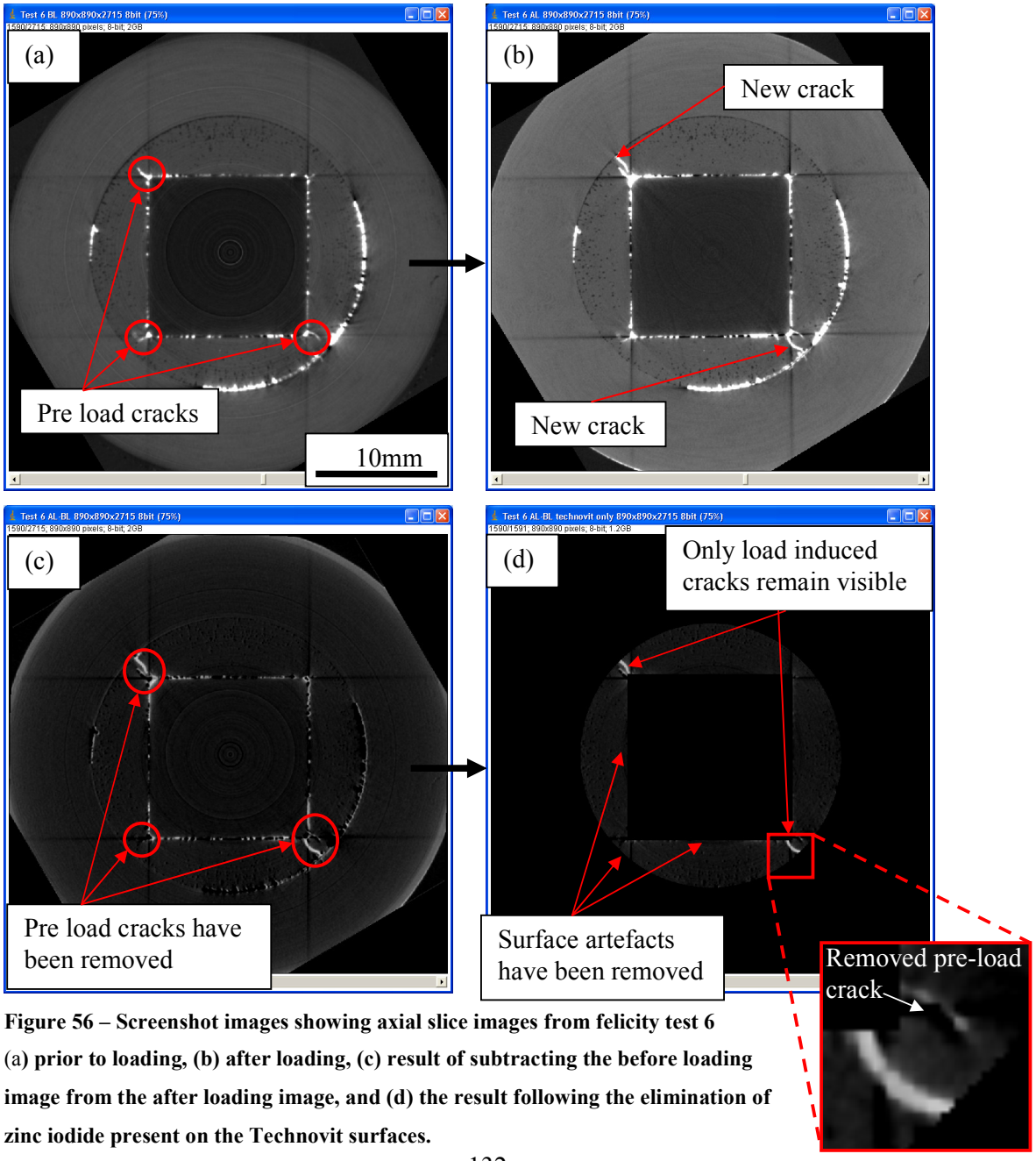

Figure 56 – Screenshot images showing axial slice images from felicity test 6 (a) prior to loading, (b) after loading, (c) result of subtracting the before loading image from the after loading image, and (d) the result following the elimination of zinc iodide present on the Technovit surfaces.

The modified volumes were then imported into VG Studio Max 2.0 (Volume Graphics GmbH) for 3D analysis. Regions of bright zinc iodide indicative of cracking were segmented as a separate volume using a static 3D seed point region growing algorithm. Extracting the resulting segmentation as a separate volume enabled the volume and surface area of the cracked regions to be measured (Figure 57). Further segmented volume images from other specimens are shown in appendix E.

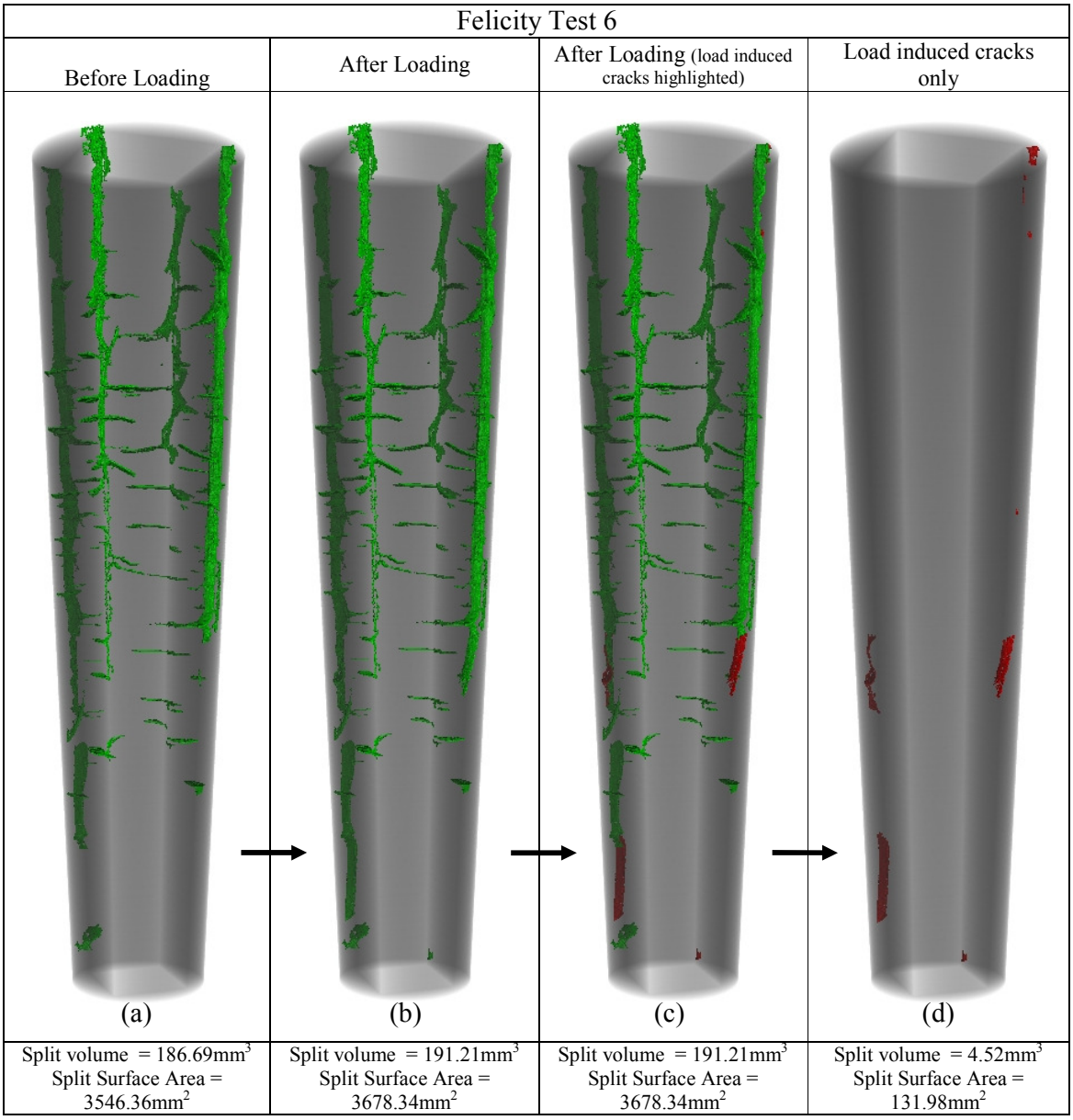

Figure 57 – 3D rendered volumes of Felicity loaded specimen from test 6. The Technovit layer is shown as a transparent solid to help the reader orientate themselves to the position of the splits. Image (a) and (b) show the state of the Technovit layer before and after loading respectively. Image (c) highlights areas of load induced damage in red, and image (d) shows only the load induced cracks following the pre-load crack removal methodology described above

It should be noted that the amount of pre load damage in this specimen (Figure 57) was considered to be extensive relative to the other specimens tested (see appendix E). In this example, the volume of the load induced splits was calculated to be 4.52mm^3, with a surface area of 131.98mm^2 – using the original scan resolution of 39μm.

In accordance with the findings of Koenczoel et al[109], cumulative energy was chosen as the relevant AE parameter in order to obtain a quantitative measure of the amount of load induced cracking detected using AE. This information was obtained for both the externally mounted and embedded sensors, as well as for unfiltered and high energy only located events.

RFA was conducted on the first 5 stems using an instrumented hammer and teardrop accelerometer linked to a spectrum analyser and SignalCalc analysis software (Data Physics Corporation). RFA data was recorded after each load increment.

6.3 RESULTS

General Observations

During Felicity loading, the stem constructs were shown to obey the Kaiser effect[156] (no acoustic activity was observed until the previous maximum stress experienced by the sample was exceeded) until such a point when bursts of acoustic activity were observed during reloading at less than the previously reached stress level (Figure 58). However, following a burst of high energy short rise time acoustic events, the constructs would often return to obey the Kaiser effect on subsequent load steps. This behaviour suggests that some initial damage may have occurred but then the stem re-stabilised.

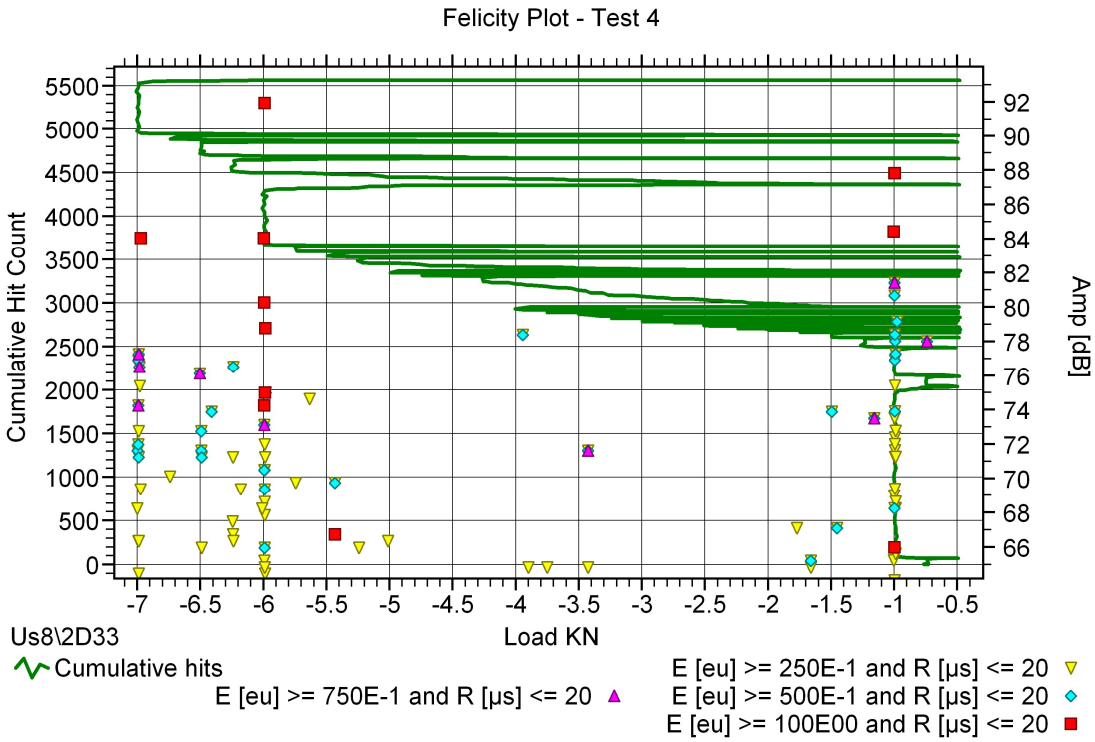

Figure 58 – Felicity plot from test 4 showing large amounts of acoustic activity occurring at 1kN, 6kN and 7kN. Only events with rise times < 20µs, and energy > 25Eu are highlighted.

RFA plots for each of the first five stems gave repeatable resonant peaks. It was noted that in cases where damage was evident from both AE and µ-CT imaging, that a shift in the RFA trace occurred corresponding to the load cycles with a sudden increases in acoustic activity. However, the RFA plot would revert back to its original shape following further loading, agreeing with the suggestion from the AE data that the construct had returned to a stable state (Figure 59).

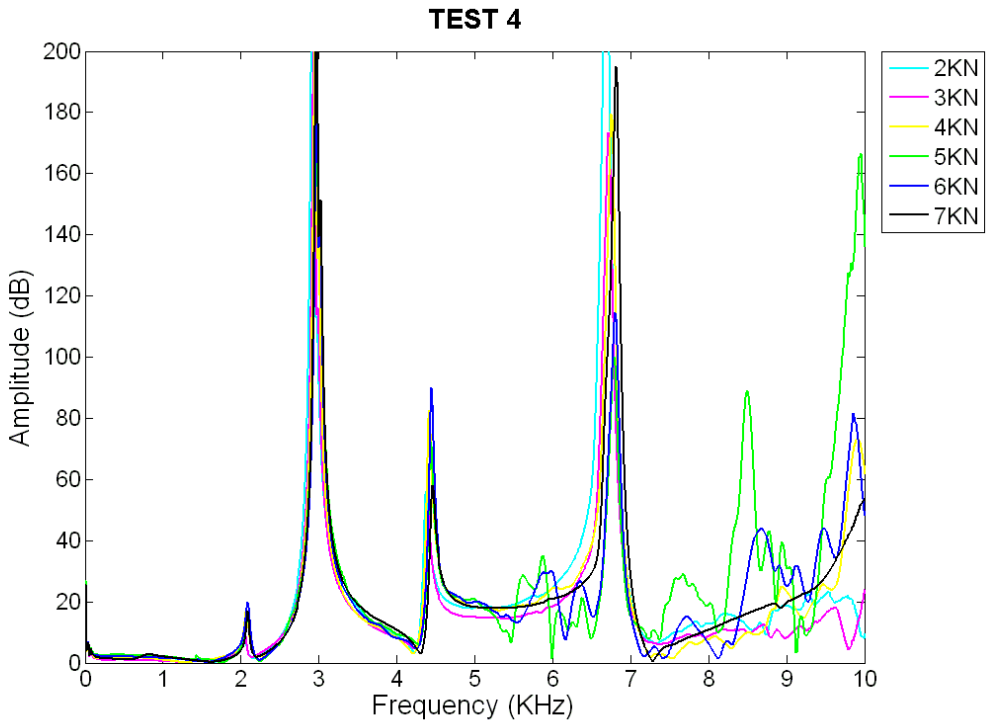

Figure 59 - RFA plots showing frequency response of construct with damage evident from AE and micro-CT imaging. The trace shows an unstable response after loading to 5 and 6KN, and returns to a stable response after further loading to 7KN

Tests 1-3 & 5 showed few signs of damage initiation using either AE or μ-CT imaging. The level of acoustic activity in these constructs was negligible compared to constructs that showed evidence of significant damage (Table 5). The external AE data indicated that most of the constructs suffered some form of distal damage (Figure 60) and this was corroborated by cement damage observed from the before and after loading μ-CT images (Figure 61) for tests 1-4.

Test	Surface-mount AE sensors	Embedded AE Sensors	Max load (KN)	Cumulative Hit count	μ-CT indicating Damage
1	•		-7	900	Cracks observed 0-3.3mm, and 8.2-9.9mm below proximal cement surface. Distal cement chipped
2	•		-7	800	Proximal crazing in cement layer, cracking observed in distal section. Distal perforation of Stem-Cement interface
3	•		-7	700	Proximal and distal corner cracks. Distal cement chipped.
4	•		-7	5500	Large crack extending 40mm vertically from proximal surface. 5.4mm distal corner crack.
5	•		-7	700	Crazed stem prior to loading. No significant load induced cracks observed.
6	•	•	-6	7100	Crazed stem prior to loading. Load induced cracking observed along length of stem.
7	•	•	-6	7500	Proximal cracking along corners of cement mantle.
8	•	•	-5	5600	Proximal cracking along corners of cement mantle.
9		•	-7	>7500	Crack running virtually entire length on stem along corner of cement & evidence of other minor cracks throughout cement mantle.

Table 5 - Comparison of assessment techniques showing levels of acoustic activity and observations made from μ-CT imaging

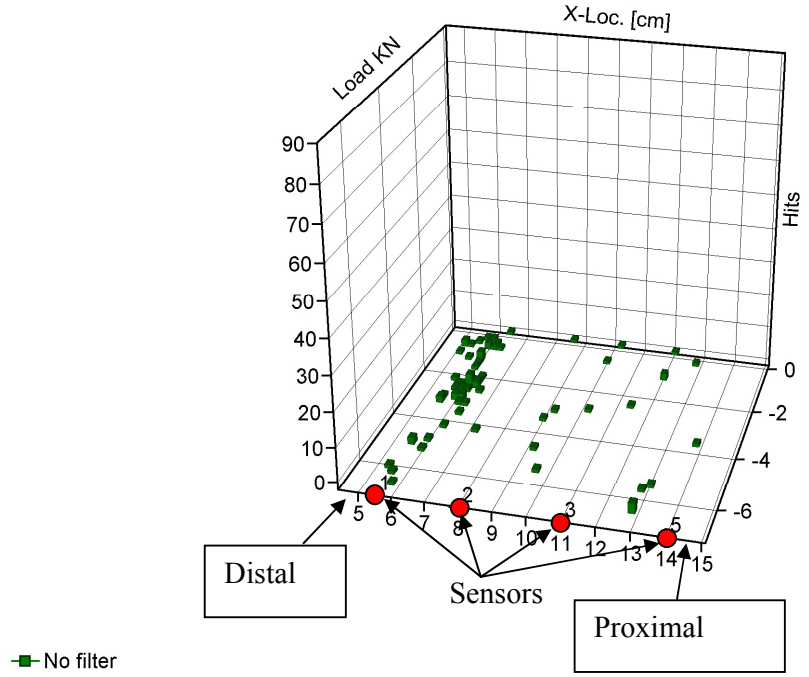

Figure 60 - Location plot of acoustic hits against load for test 2 showing slight distal activity, which may be indicative of damage.

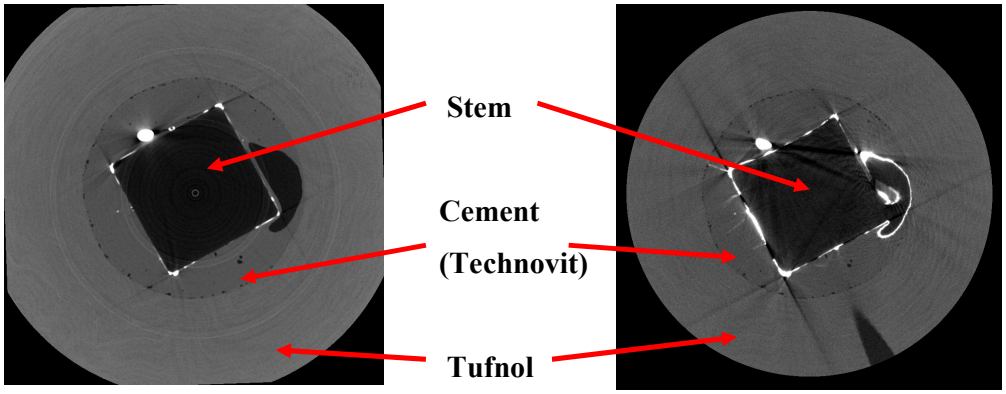

Figure 61 - Before loading (left) and after loading (right) distal slice images taken from test 2 showing a large pore present before loading. This pore is shown to have perforated the Stem-Cement interface during loading, resulting in cement cracking and AE generation.

AE on both constructs 1 and 2 indicated that there was some distal activity and μ-CT images demonstrated that damage had occurred in this region, however very few high energy (>100Eu) and short rise-time (<20μs) acoustic events were recorded which would be indicative of cracking. The only events that did meet the high energy and short rise

time criteria occurred when the construct was loaded to 1KN (Figure 62), suggesting that any brittle failure occurred very early on in the test.

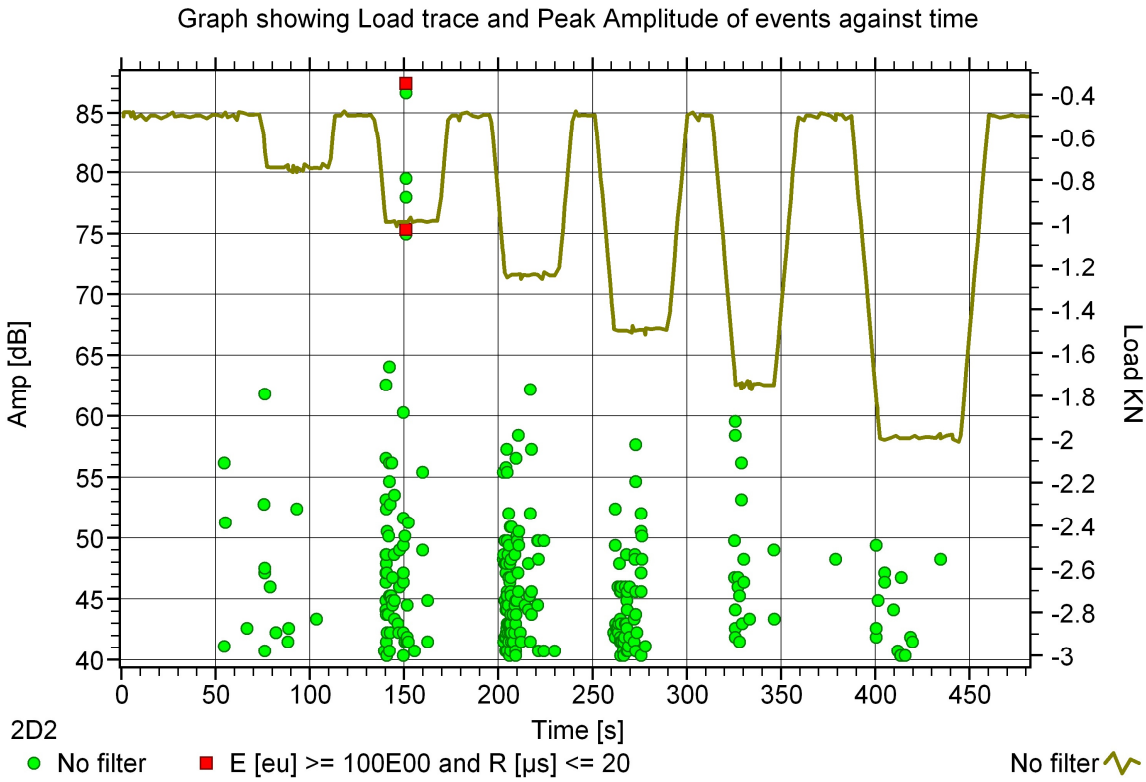

Figure 62 - Plot showing close up of load trace and amplitudes of acoustic events against time for Test 2. High energy (>100Eu) and short rise-time (<20µs) thought to be associated with cracking are highlighted in red.

Test 4 showed significant AE activity at 1kN and high energy, short rise time events were observed at this load level - indicative of cracking. Subsequent loading saw very little high energy, short rise time events until the construct reached 6kN when a burst of activity was observed. A further burst of high-energy events was observed at 7kN. Interestingly, there was an increase in acoustic activity during loading to 4.25kN, 5.25KN and 6.25KN, however the acoustic parameters associated with these events were of lower energy and longer rise times. Loading to 4.5KN occurred after the test was left to stand overnight at 0.5KN, and loading to 5.25KN and 6.25KN also followed periods of rest. It is hypothesised that stress relaxation occurred during these rest periods causing the stem to subside on subsequent loading without further damage to the Technovit layer. Hence the

events seen during these loading periods are more likely to be associated with the stem slipping rather than Technovit cracking.

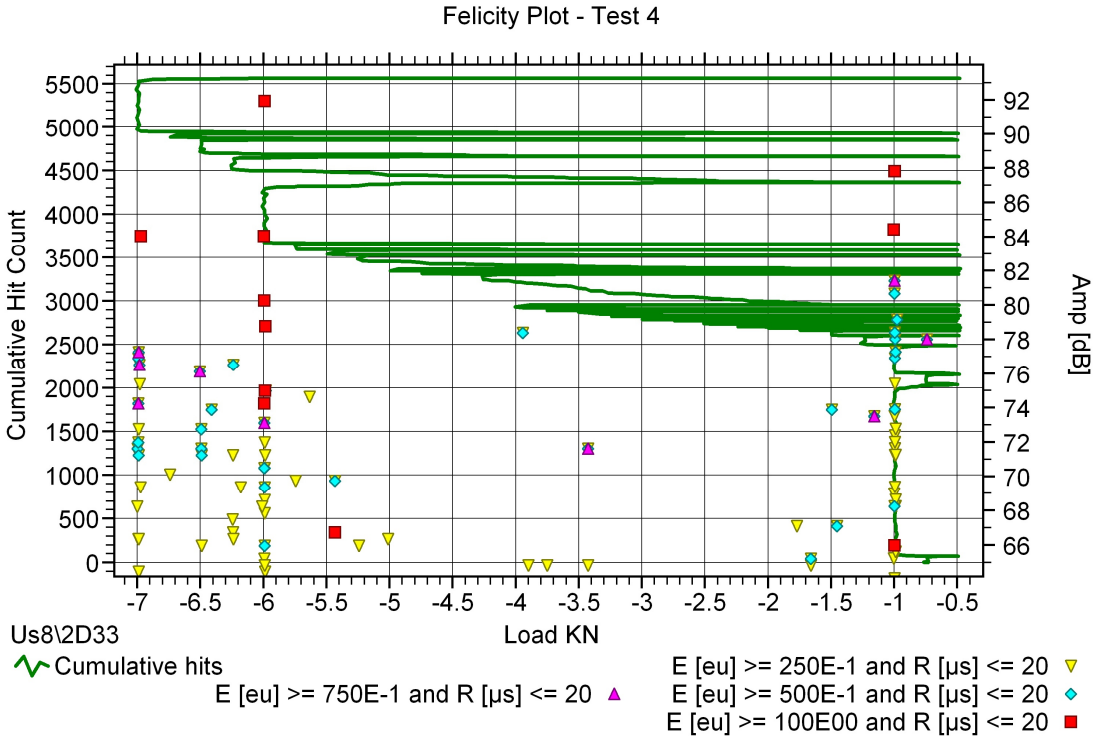

Figure 63 – Felicity plot from test 4 showing large amounts of acoustic activity occurring at 1kN, 6kN and 7kN. Only events with rise times < 20µs, and energy > 25Eu are highlighted.

Location analysis demonstrated that the initial burst of high energy, low rise time activity at 1KN was located at the very distal tip of the construct (Figure 64). However, subsequent bursts at 6KN and 7KN were located proximally and extended 40mm from the proximal end of the Technovit down to sensor 3. (Figure 65).

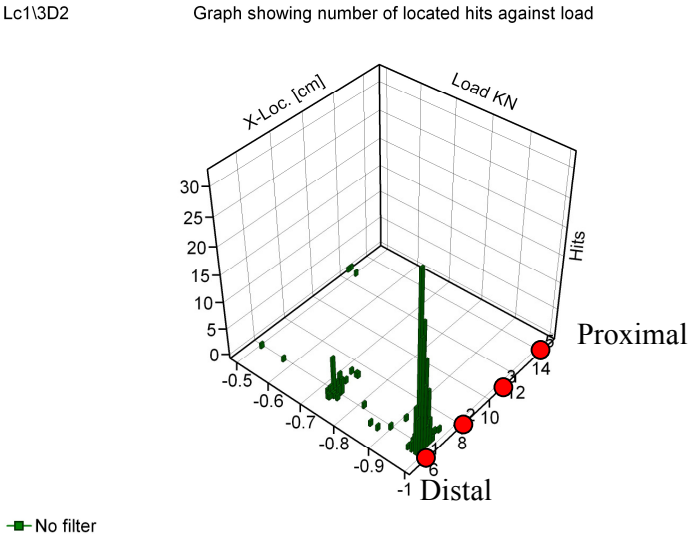

Figure 64 - Plot showing located events up to 1KN during test 4. A large concentration of events are seen at 1KN located around sensor 1 (The distal tip of the Technovit layer).

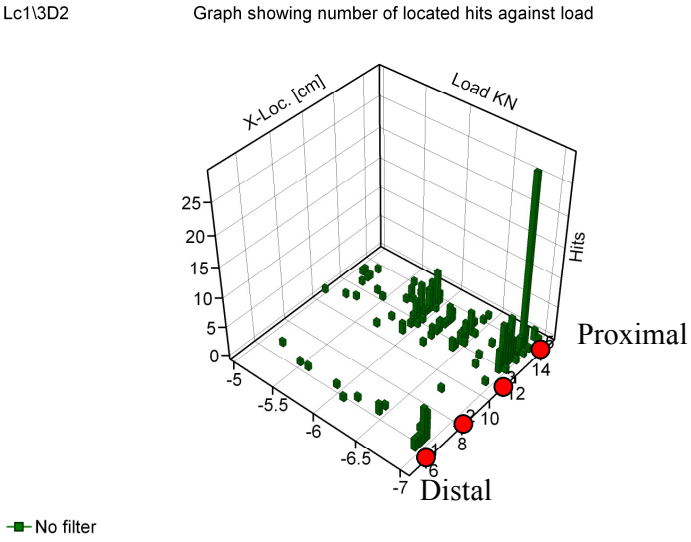

Figure 65 - Plot showing located events from 5KN up to 7KN during test 4. Concentrations of events are seen at 6KN and 7KN extending between sensors 5 & 3 (A region extending 40mm from the proximal end of the Technovit layer).

The corresponding μ-CT scan revealed the presence of a large crack within the Technovit layer running from the proximal surface of the Technovit down to 40mm below this surface (Figure 66).

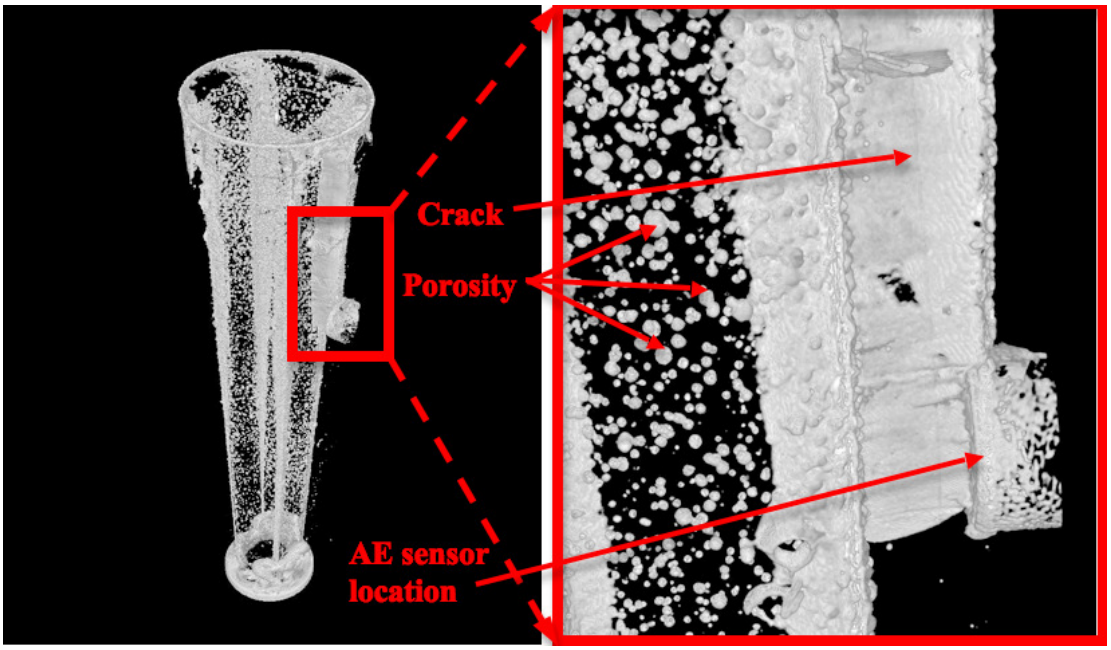

Figure 66 – CT Images showing Presence of cracking extending to a depth of 40mm below the proximal surface of the Technovit layer highlighted using a Zinc Iodide solution

Complimentary to this, the RFA showed a change to the structural integrity indicated by a sudden shift in the frequency response (Figure 67).

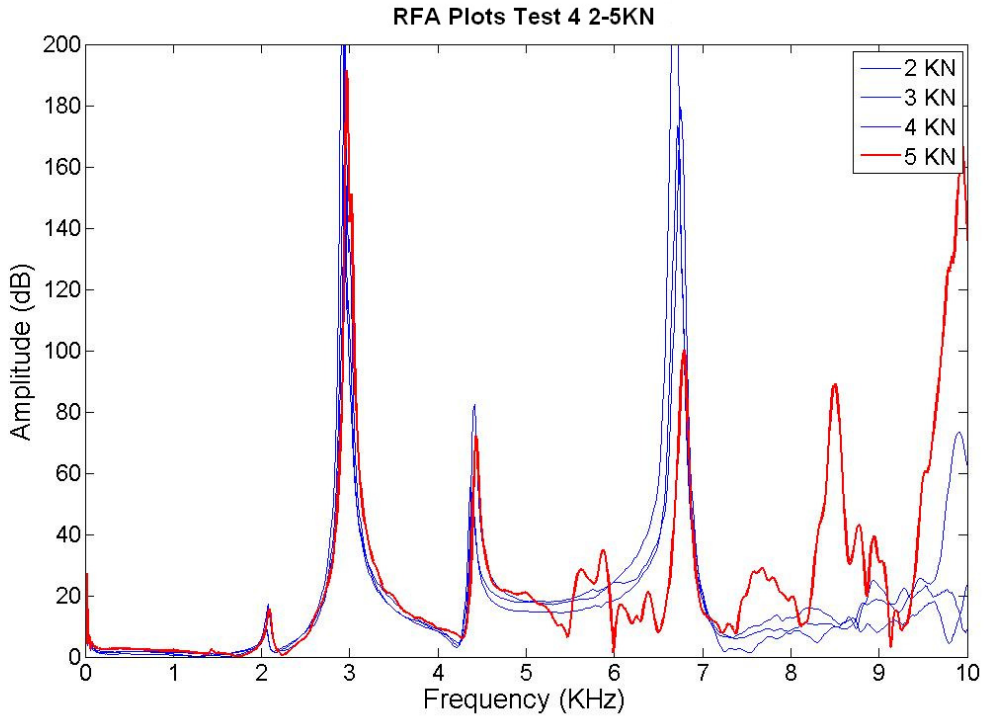

Figure 67 – RFA plots showing distinct shift in frequency response between the 4KN and 5KN load levels

Comparison between embedded and external sensor data

There was a general agreement between internal and external sensor data in terms of acoustic activity, although the detected location of these events was subject to considerable variation (Figure 68). The external sensors had a tendency to detect more distal activity which was not always found from the μ-CT images (Figure 68, Tests 7&8) and it is thought that this may be due to noise from the mounting mechanism of the Tufnol in the Instron machine rather than cement cracking. Furthermore, μ-CT images from Test 6 showed proximal cracking that was not located using the external sensors. The embedded sensors were able to locate cracking with a closer agreement to that observed using the μ-CT images, especially when the events were filtered so that high energy (>100Eu) and short rise time (<20μs) events were highlighted. However, there was an area of activity in Test 6 around 7cm from the distal tip of the stem that was not found on the μ-CT images.

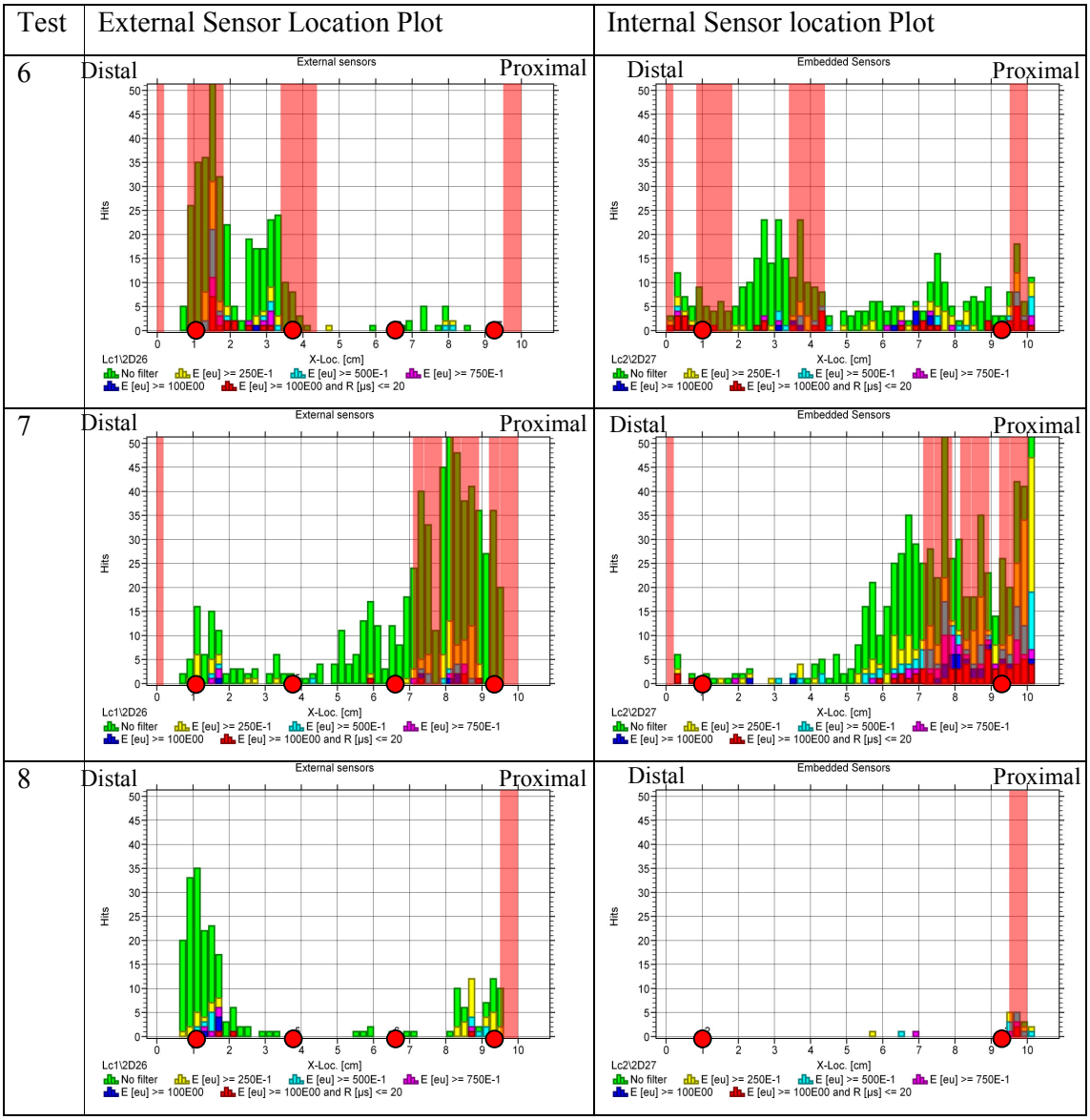

Figure 68 - Comparison plots between embedded and external sensor located activity. Each histogram is graded according to event energies. Events with energy >100Eu and rise-times <20µs are shown in red. Actual locations of loading damage as observed from the µ-CT images are highlighted by the pink bars.

Test 9 was a unique case as there were no externally mounted sensors present on the stem. This test produced a large amount of AE and the sensors detected significant levels of high energy, short rise time events extending most of the way down the cement mantle. It is unknown why this particular construct may have seen extensive cracking as opposed to the other stems; however, this information was verified from the CT images which did indeed report a crack extending most of the way down the length of the mantle (Figure 69).

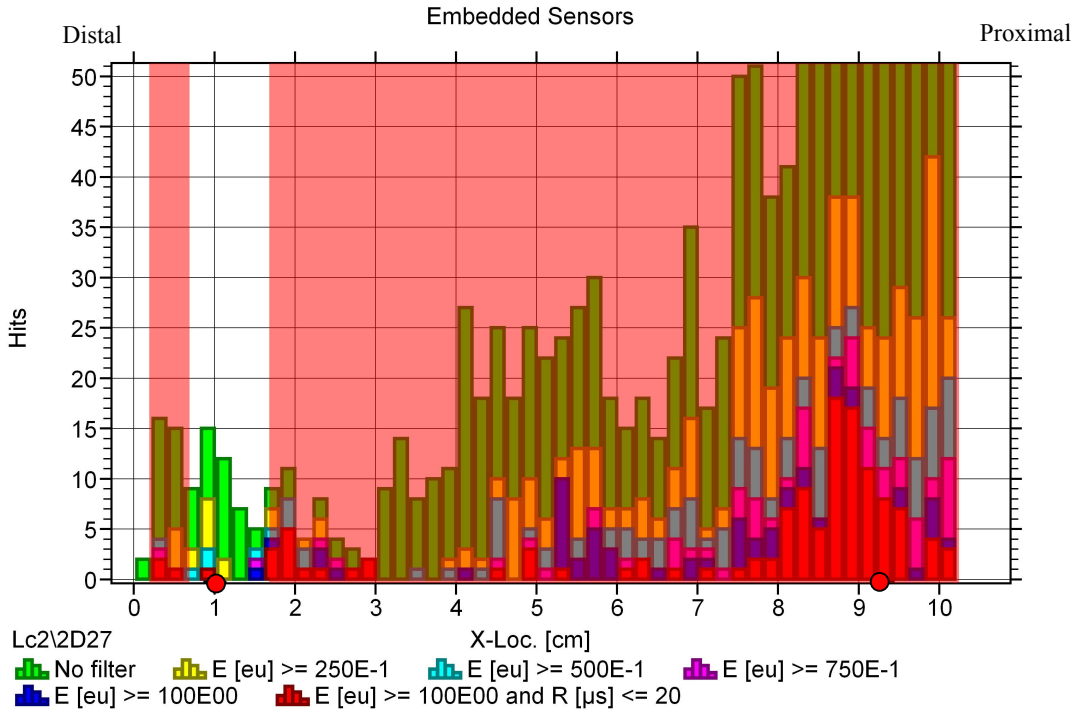

Figure 69 – Plot showing comparison between predicted crack location using embedded sensors and actual crack location as seen on the CT images. Each histogram is graded according to event energies. Events with energy >100Eu and rise-times <20µs are shown in red. Actual locations of loading damage as observed from the µ-CT images are highlighted by the pink bars.

Quantitative measurements of the fracture surface area of the load induced cracks obtained by the extraction and segmentation process described in the methods section are shown below (Figure 70) together with the cumulative energy for each test as detected by the external and embedded sensors (Table 6). However, with only 3 data points for comparison between the embedded and external sensors, it is difficult to draw any meaningful correlation.

Felicity Test Load Induced Cracking			
Test 6	Test 7	Test 8	Test 9
			
Split volume = 4.52mm^3 Split Surface Area = 131.98mm^2	Split volume = 3.92mm^3 Split Surface Area = 61.51mm^2	Split volume = 1.45mm^3 Split Surface Area = 19.48mm^2	Split volume = 52.27mm^3 Split Surface Area = 784.78mm^2

Figure 70 – Images highlighting load induced cracks within the technovit layer together with measurements of their volume and surface area.

Felicity Test	Measured Fracture Surface Area (mm^2)	Cumulative Energy (No filter)		Cumulative Energy (of events >100eu)	
		External	Embedded	External	Embedded
6	131.98	23800	46600	9150	20655
7	61.51	27465	79258	13115	41250
8	19.48	17307	23535	3570	6210
9	784.78		154550		61900

Table 6 – Measured fracture surface areas of load induced cracks from tests 6-9 together with the recorded cumulative energy from external and embedded AE sensors.

Although Figure 68 is able to show all of the information necessary to compare visually observed damage locations to those detected by the AE system, the DVD version of this thesis also contains video correlations between damage detected using AE and load induced cracking observed using μ-CT highlighting where and to what extent damage occurred. These videos are contained within E-Appendix_02. Load induced cracks are highlighted to allow easy identification compared to pre-load cracks which are visible on both the before and after loading scans. There is also a marker that identifies the position of the axial slice in relation to the AE location plot. The located events are categorised into:- all located events = green, events with energy >25Eu = yellow, >50 Eu = light blue, >75Eu = purple, >100Eu = navy blue, and located events with energies > 100eu and rise times < 20μs = red - these higher energy and short rise time type events are believed to be linked to cracking as opposed to rubbing type damage characteristics[148].

6.4 DISCUSSION AND CONCLUSIONS

Although it was difficult to extract any meaningful correlation in terms of locating significant areas of damage between the AE data and the μ-CT reconstructions, a methodology for obtaining quantitative information as to the volume and surface area of load induced cracking has been presented. This technique is, however, subject to subjectivity: The accuracy of any CT segmentation is limited by the voxel size of the image. Furthermore, the X-ray scatter seen around bright objects such as the zinc iodide reduces the clarity of the crack faces and as such are defined by the tolerance by which the seed point growing algorithm uses as well as the grey level of the seed point itself. Since both of these factors may be adjusted by the user, each segmentation may only be considered an approximation of the true crack geometry. Nonetheless, the technique does permit a comparison to be made between the AE data and the visually observed load induced cracks. The embedded sensors seemed to show a closer agreement with the CT images in terms of detecting and locating cement cracks. There may be several factors that could have influenced the results of the external sensors. Firstly, these sensors are exposed to more sources of noise – the sensors themselves are mounted within holes drilled into the Tufnol tube. Mechanical clamps were used to hold these sensors in place and it is possible that the clamps may move against the Tufnol tube during loading. Furthermore, the clamping arrangement used to fix the distal end of the Tufnol tube to the Instron machine may also induce rubbing that could influence the signals detected by the external sensors. Finally, the quality of the acoustic bond between the external sensors and the Technovit may not be as good as the bond between the embedded sensors and the stem. As stated previously, the fixation of the external sensors was designed to be temporary, and therefore the choice of couplant had to be non-adhesive and so rely on sufficient contact from the mechanical clamp which itself may move due to flexion of the construct during loading. In this sense, another hypothesis concerning the advantages of embedded sensors over external sensors is realised.

The use of embedded sensors gave other, unforeseen benefits that proved useful for speed of sound calibrations. By using the PZT crystals as actuators rather than sensors, controlled pulses could be sent into the structure at known locations. Since these pulses originated closer to the bone cement layer than the pencil lead break test performed on the external surface of the Tufnol it is hypothesised that location calibrations based on the embedded pulses would be more accurate. The literature review discussed a study

conducted by Qi et al[150] who attempted to use AE to monitor damage accumulation within the bone cement layer surrounding a femoral stem implanted within an epoxy femur. Their location algorithm was calibrated using pencil lead-break tests on the external surface of the representative femur. Since these events were separated from the material of interest by a layer of foam, this may have accounted for some of the inaccuracies related to their calculated locations of events occurring within the cement mantle, and in this situation the presence of embedded sensors may have aided more accurate location calculations.

A further objective of this experiment was to establish which acoustic parameters were associated with cement cracking. Roques et al[148] proposed that bone-cement cracking could be discriminated from frictional AE generation by the presence of high energy, long duration and short rise-time events based on differences between brittle samples aged in air and more plasticized samples aged in ringers solution and the point at which AE occurred during the loading cycle. They found that longer rise time events occurred during the unloaded phase of the load cycle and hence were more likely to be associated with the rubbing of the crack faces as opposed to crack progression. Similarly, short rise time events were found to occur at peak loads and were therefore associated with crack progression. The location results of this experiment were categorised to identify located events with energies greater than 25, 50, 75 and 100Eu in an attempt to refine the parametric criteria linked to cement cracking. Interrogation of the energy values associated with cracked regions identified using μ-CT suggested that events with an energy of more than 100Eu together with a rise-time of less than 20μs exhibited the closest relationship to observed cracking. These results provide a greater confidence in the discrimination of cement cracking through the use of AE waveform parameters, and the complexity of the experiment may now be built up having defined this cracking criteria, although it should be noted the discriminating values used here may alter according to the material/AE sensors used.

The Felicity ratio effect was not found to be applicable for these polished stems since no reduction in Felicity ratio was observed following bursts of acoustic activity indicative of cracking. Verdonschot and Huiskes[196] identified a stick-slip type behaviour in polished stems and it is believed that the subsequent subsidence and stabilisation of the stem is the reason why no reduction in Felicity ratio was observed despite the presence of permanent damage. It is thought that this behaviour also caused the RFA traces to indicate that the

stem was stable even though the structure had suffered damage. Although the technique was able to show some variances using this test methodology when RFA analysis was performed after every load step, it was concluded that the tendency of the polished stem system to restabilise renders the RFA technique unsuitable for use during fatigue loading since damage may simply not be detected.

In the particular case of distal activity, it was noted that a thin layer of Technovit would form over the lower surface of the stem during polymerisation. This could be observed once the stem had been removed in preparation for initial μ-CT scanning of the construct. Removal of the stem was necessary to achieve sufficient contrast on the subsequently obtained radiographic images. On loading or re-insertion of the stem this thin layer may have been removed, causing distal damage to the Technovit layer as a consequence. Since the stem was re-inserted into the construct following initial scanning but prior to recording of AE activity, this may also explain why some stems showed visible signs of distal disturbance with an unexpectedly low instance of acoustic activity.

There were instances of acoustic activity in locations where no damage was observed using μ-CT. This may indicate the presence of damage that was not visible on the reconstructed CT volumes, or the presence of other acoustic noise sources that were not associated with cement cracking. The AE technique is recognised as being highly sensitive and often acoustic activity is detected in failure zones prior to other techniques such as ultrasound[141]. In the case of the externally mounted sensors, the clamping arrangement used to hold the sensors in place may in itself be a source of unwanted noise as a certain degree of rubbing may occur between the holding clamps and the Tufnol tube.

To summarise, this study set out to assess the ability of embedded AE sensors to monitor progressive failure, and it was hypothesised that the Kaiser and Felicity effects could be used to establish when permanent damage had occurred[156]. The results demonstrated that embedded sensors may be used to monitor the integrity of the cement mantle under static loading conditions and identified certain parameters that are likely to indicate the presence of cement cracks. Although the use of a polished stem prevented the application of the Felicity ratio for determining when permanent damage had occurred, it is hypothesised that this technique would still apply to bonded stems. Nonetheless, the data retrieved from the embedded sensors showed a greater agreement with the visually observed damage and

appear to be less affected by unwanted noise sources due to the lack of temporary fixation techniques needed for external sensors. Having established the functionality of these techniques under simple loading conditions, the next chapter takes the technique to a more representative loading scenario as experienced *in-vivo* by investigating the condition monitoring of the construct under cyclic fatigue loading.

CHAPTER 7 - ACOUSTIC EMISSION MONITORING AND 3-D VISUALISATION OF PROGRESSIVE DAMAGE DURING FATIGUE LOADING OF A SIMPLIFIED TOTAL HIP STEM CONSTRUCT

7.1 INTRODUCTION

According to a study carried out by Goldsmith et al[203], the average hip replacement patient subjects the implant to 1.4-1.7 million load cycles every year. Typical load levels endured by the prosthesis during normal gait have been measured to be between 2.4-2.8 times body weight[44,204] and consequently the performance of hip replacement components and constructs under fatigue loading conditions is one of the most significant factors affecting the survivorship of hip replacement devices. During the 1970's a series of femoral stem fractures occurred due to proximal bone remodelling which resulted in a lack of proximal support and subsequent fatigue failure of slender femoral stems approximately one third of the length of the stem away from the distal tip[205]. Subsequent improvements in standards testing, stem design and fixation have meant that stem fracture is now extremely rare. However, fatigue failure of bone-cement has historically been, and remains, one of the main contributing factors of aseptic loosening within cemented arthroplasites[206] and the majority of developmental work associated with bone cement has been aimed at improving survivorship under fatigue conditions.

Chapters 4-6 have presented evidence that it is possible to embed AE sensors within the femoral stem of a cemented hip replacement construct and detect damage events that occur during polymerisation or Felicity loading regimes. However, fatigue damage is considered to be the main process by which the cement layer degrades[206] ; the aim of this study therefore, is to assess the ability of the embedded AE sensors to monitor the integrity of a cemented stem construct under fatigue loading conditions. This study builds on the work of Qi et al[150] who used AE in an attempt to detect and locate micro-cracking from within a complete stem construct. The authors were able to detect and locate damage occurring within the bone cement layer, although the 3D location accuracy of their results was questioned in view of the fact that some events were located in free space[188]. This inaccuracy was thought to be a result of an inadequate number of sensors used in the

study[207]. The authors used surface mounted AE sensors and the only means available of location calibration was to induce an acoustic source (pencil-lead break) on the external surface of the construct; it is hypothesised that the accuracy of their results could have been improved by using embedded sensors. Results from directly embedded AE sensors located within the femoral stem are compared to surface mount sensors and corroborated using μ-CT imaging analysis.

7.2 METHODS

This experiment used the same simplified constructs as described in Chapter 4. Three femoral stems were manufactured with embedded sensors. In order to minimise the level of porosity present at the stem-cement interface, each stem was heated in accordance with the methodology described in Chapter 4 before being inserted into the Technovit. Each stem was used to make 4 matching constructs such that the same stem could be used for repeat tests. External sensors were attached to the construct using the methodology described in Chapter 4 with the addition of a 1mm layer of rubber placed between the jubilee clip and the Tufnol tube to minimise acoustic activity from the two surfaces rubbing together during testing.

The constructs were mounted in an Instron 8502 hydraulic testing machine using the same methodology as described in Chapter 6.

All data was acquired using a threshold of 40dB and a preamplifier gain of 40dB. In order to determine the speed of sound to be used in location calculations, pulse signals were sent through each sensor in turn. The time taken for the generated signals to reach the other sensors was recorded and the resulting speed of sound as measured in the Tufnol/Technovit and stem for each construct were used for data analysis.

The construct was subjected to a sinusoidal fatigue-loading pattern with a high maximum compressive load of 5kN (~7 times body weight) in order to accelerate the test. The load was increased gradually during the first 3000 cycles to allow the stem to embed itself firmly within the construct in accordance with the loading protocol listed in (Table 7).

Waveform No.	Mean load (kN)	Amplitude (kN)	Frequency (Hz)	No. Cycles
1	-1.25	0.75	1	1000
2	-1.75	1.25	1	1000
3	-2.25	1.75	1	1000
4	-2.75	2.25	1	30,000

Table 7 - Showing how the load settings were varied throughout the initial fatigue testing.

After completing the loading regime, the stem was removed from the construct so that the construct could be re-filled with zinc iodide and scanned again using the methodology described in Chapter 4.

In order to highlight load induced damage within the bone cement layer, video sequences of axial slice images of all constructs were created using Image J[208]. The before and after sequences were then compared side-by-side using windows movie maker. Any areas of damage that were identified on the after loading sequence that were not present on the before loading sequence were highlighted. The position along the femoral stem and length of any load induced cement cracks were recorded such that their locations could be superimposed onto the location results of damage recorded from the AE data.

A quantitative assessment of the extent of load induced cracking was obtained using the same image processing techniques as described in CHAPTER 6 These data were compared to the cumulative energy detected from both the external and embedded sensors for all events and then just for events with an energy greater than 100eu.

7.3 RESULTS

The recorded speed of sound from pulse calibrations within each femoral stem was consistent (Table 8). The average speed of sound was 452cm/ms with a maximum variation of 4.4% for the 3 femoral stems and 182cm/ms with a maximum variation of 14.3% for the 8 Tufnol/Technovit constructs.

Test	Stem	Stem Speed (cm/ms)	Tufnol/Technovit Speed (cm/ms)
1	1	464	199
2		464	169
3	2	432	204
4		432	193
5		432	198
6		432	156
7	3	461	166
8		461	169

Table 8 - Showing variation in measured speed of sound using the pulse calibration method for the stem and for the Tufnol/Technovit construct used in each test.

The corroboration between damage located by the embedded and surface mounted sensors together with damage identified from μ-CT images is shown in Figure 71 & Figure 72. The located AE events are categorised into:- all located events = green, events with energy >25Eu = yellow, >50 Eu = light blue, >75Eu = purple, >100Eu = navy blue, and located events with energies > 100eu and rise times < 20μs = red - these higher energy and short rise time type events are theoretically linked to cracking as opposed to rubbing type damage characteristics[148]. Regions of damage identified from the μ-CT images are overlaid using the translucent pink bars. The DVD version of this thesis also contains video correlations between damage detected using AE and load induced cracking observed using μ-CT highlighting where and to what extent damage occurred. These videos are contained within E-Appendix_03.

3D segmented images of the load induced cracks observed from the CT scans and subsequent image processing are shown in Figure 73 & Figure 74.

Test	Stem	External Sensor Location Plot	Internal Sensor location Plot
1	1	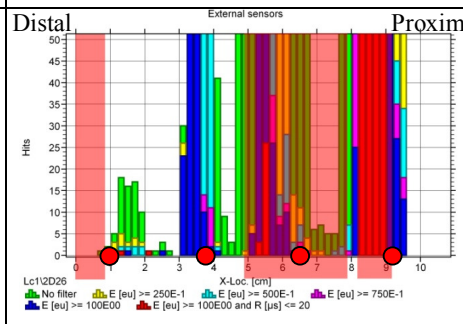	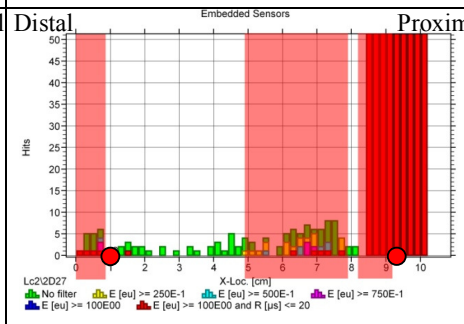
2		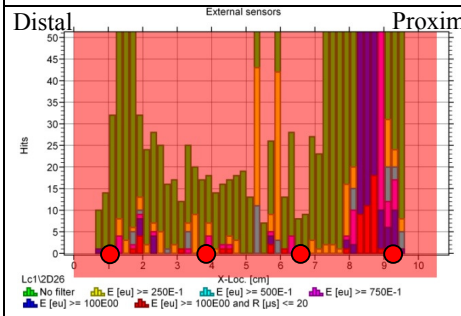	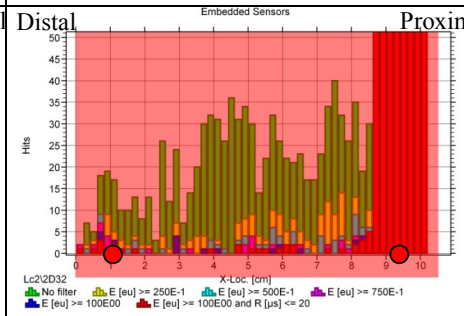
3	2	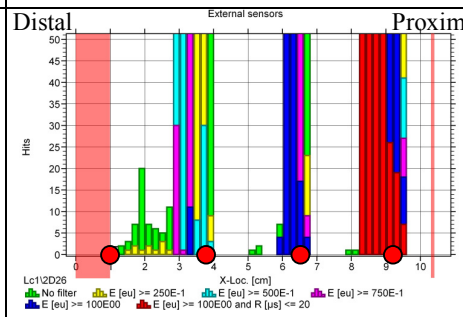	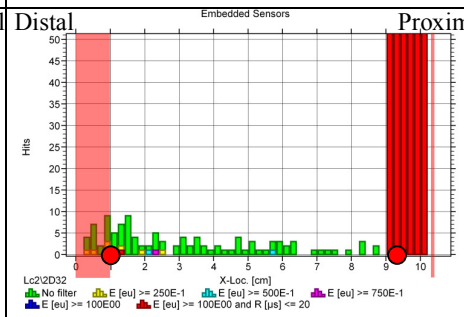
4		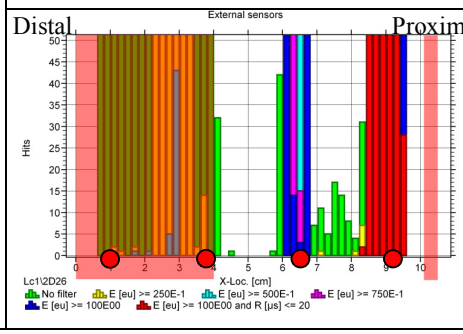	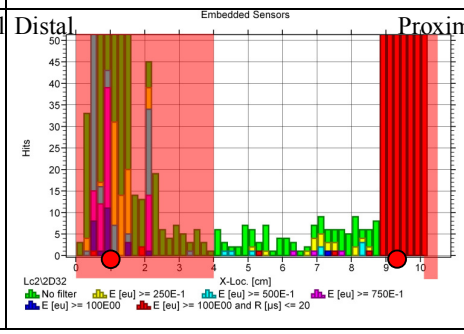

Figure 71 - Plots from tests 1-4 showing located acoustic activity, classified according to event energy. High energy (>100Eu) and short rise time (<20µs) events are highlighted in red. The locations of load induced cement cracks visible from the µ-CT image analysis are highlighted in pink.

Test	Stem	External Sensor Location Plot	Internal Sensor location Plot
5	2	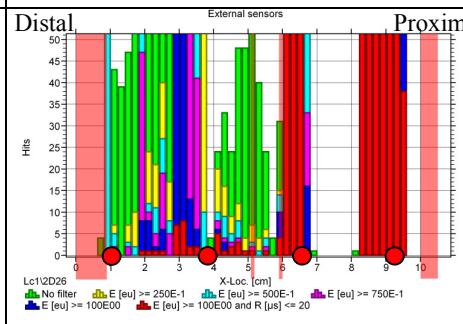	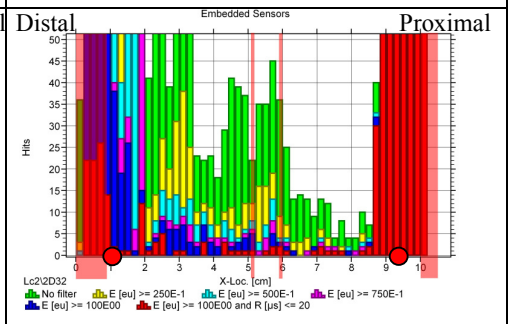
6		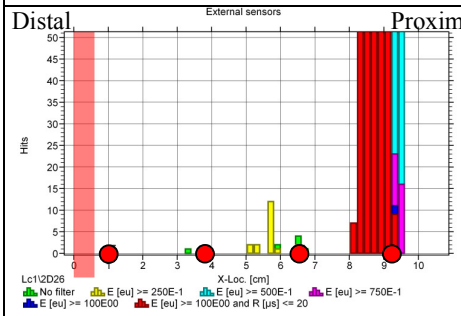	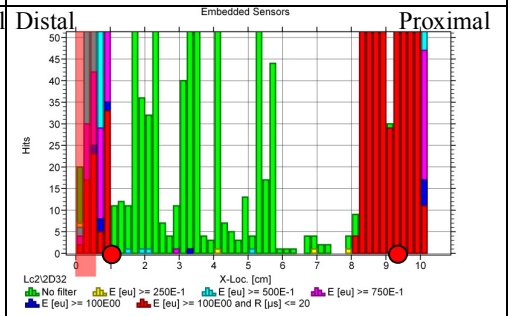
7	3	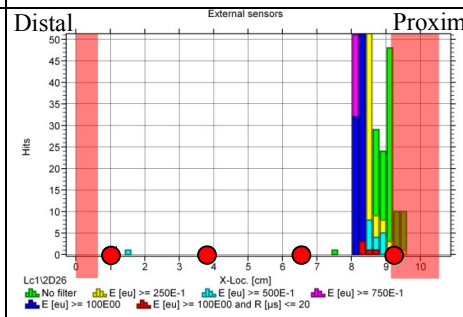	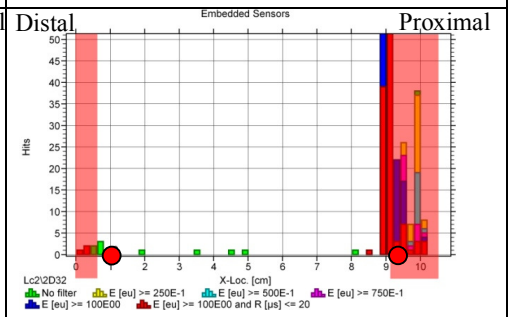
8		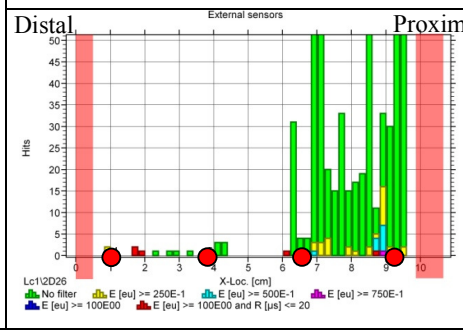	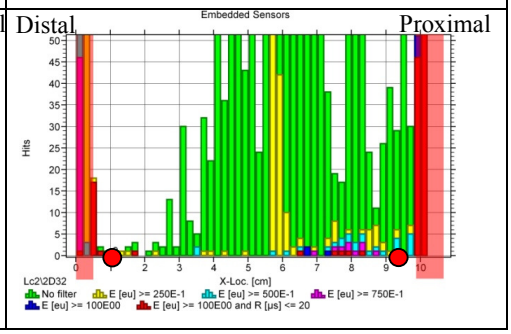

Figure 72 - Plots from tests 5-8 showing located acoustic activity, classified according to event energy. High energy (>100Eu) and short rise time (<20µs) events are highlighted in red. The locations of load induced cement cracks visible from the µ-CT image analysis are highlighted in pink. For orientation, the distal end of the construct is on the left hand side of the plot, and the proximal end is on the right.

Fatigue Test Load Induced Cracking			
Test 1	Test 2	Test 3	Test 4
			
Split volume = 21.46mm^3 Split Surface Area = 361.35mm^2	Split volume = 83.45mm^3 Split Surface Area = 720.98mm^2	Split volume = 0.86mm^3 Split Surface Area = 21.47mm^2	Split volume = 17.95mm^3 Split Surface Area = 302.05mm^2

Figure 73 – Images highlighting load induced cracks within the technovit layer together with measurements of their volume and surface area for fatigue tests 1-4.

Fatigue Test Load Induced Cracking			
Test 5	Test 6	Test 7	Test 8
			
Split volume = 1.85mm^3 Split Surface Area = 34.38mm^2	Split volume = 0.14mm^3 Split Surface Area = 3.24mm^2	Split volume = 4.27mm^3 Split Surface Area = 70.14mm^2	Split volume = 3.55mm^3 Split Surface Area = 42.28mm^2

Figure 74 - Images highlighting load induced cracks within the technovit layer together with measurements of their volume and surface area for fatigue tests 5-8.

Tests conducted using stem #1 reported a large amount of high energy, short rise time acoustic events located towards the proximal end of the construct. These events were particularly notable using the embedded sensors. During test 2, a visible fatigue crack formed in the offset plate originating at the weld joint between the stem and the plate (Figure 75), and it is believed that this is the source of these acoustic events. A similar

pattern of proximal activity was seen in all tests using stem #2. No crack was visible to the naked eye within the weld joint until test 5, and this crack could be seen to migrate from the weld to the bulk plate material during test 6 and the test was stopped automatically after 6,817 cycles when the safety position limits of the Instron machine were tripped.

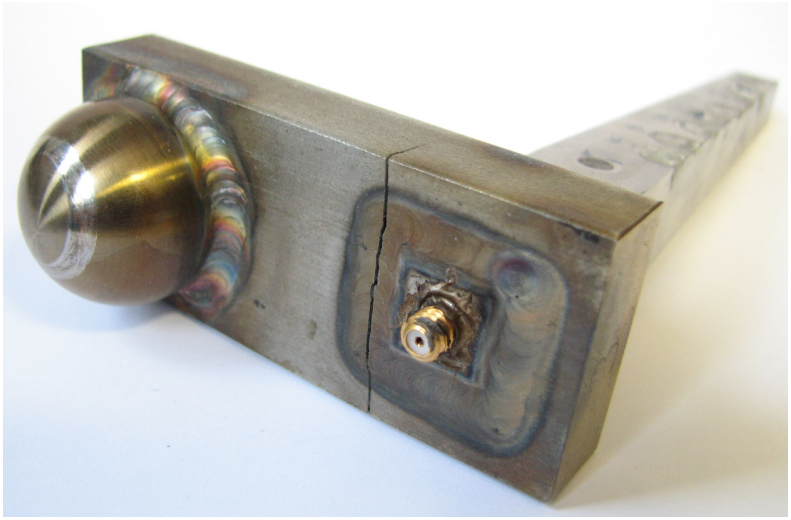

Figure 75 - Photograph showing development of fatigue crack across welded joint during testing - Producing high levels of proximally located events.

The presence of such a feature resulted in the detection of many high energy proximal events. Consequently, the proximal 2cm of load induced cracks were removed from the calculations of segmented crack surface area. Similarly, AE events that were located within this region were removed from the calculation of cumulative energy (Table 9). The correlation between the sensors and the visually observed damage is shown in Figure 76 - Figure 78.

Fatigue Test	Measured Fracture Surface Area (mm^2)	Cumulative Energy (No filter)		Cumulative Energy (of events >100eu)	
		External	Embedded	External	Embedded
1	267.02	785020	4578	253000	2177
2	549.02	52730	25810	9000	12600
3	21.47	431475	1420	109250	228
4	236.45	894200	24400	127500	4045
5	18.73	945600	1594500	345300	1390700
6	0.95	62	2318	0	2181
7	17.43	400	2320	226	2180
8	4.98	6935	102390	2840	10090

Table 9 – Measured fracture surface areas of load induced cracks together with the recorded cumulative energy from external and embedded AE sensors.

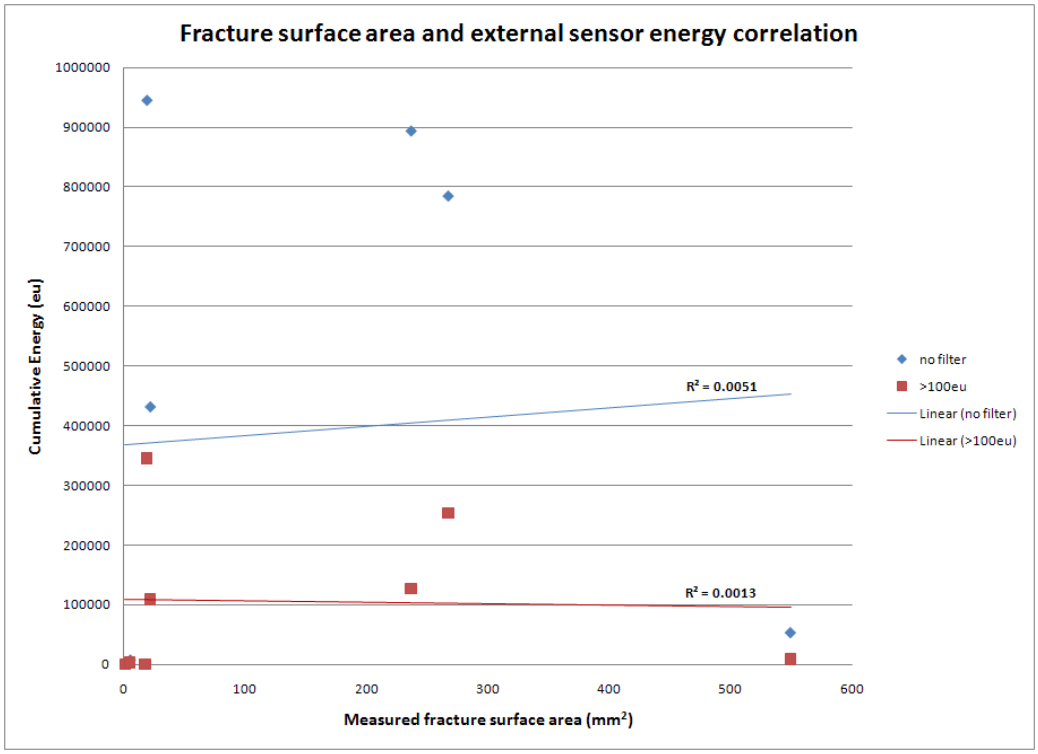

Figure 76 – plot showing cumulative energy detected by the external AE sensors compared to the measured fracture surface area of load induced cracks determined through CT image analysis

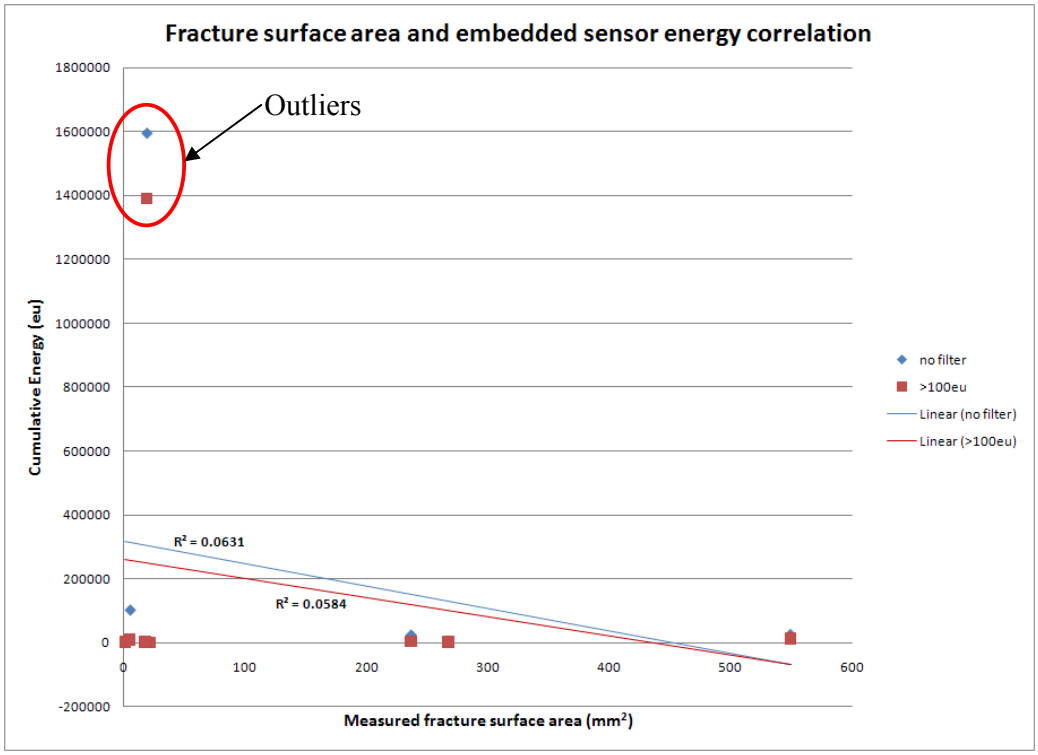

Figure 77 – plot showing cumulative energy detected by the embedded AE sensors compared to the measured fracture surface area of load induced cracks determined through CT image analysis

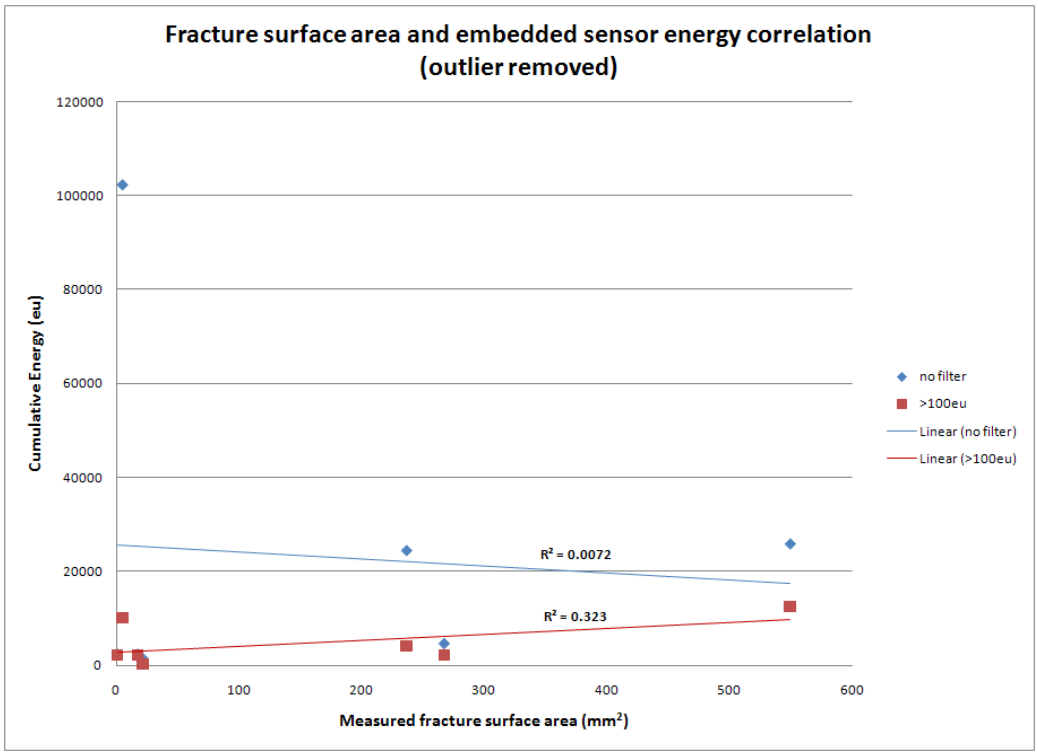

Figure 78 – plot showing cumulative energy detected by the embedded AE sensors compared to the measured fracture surface area of load induced cracks determined through CT image analysis having removed the previously identified outliers (Figure 77).

Again, the low number of data points makes the assessment of an R^2 correlation coefficient very difficult. However, there does seem to be a higher level of scatter associated with the external sensors compared to the embedded sensors and filtering the results such that only events with and energy above 100eu were considered in the analysis also appears to improve the correlation between the CT image analysis and the AE data. The cumulative energy detected during test 5 was far greater than any of the other tests – especially from the embedded sensors. The reason for this is unknown. Figure 74 shows that the amount of load induced cracking within this specimen was not extensive, and for this reason the data point was considered to be an outlier.

The damage occurring around the distal tip would often involve cracking along one or more of the corners and in some cases the very end of the cement layer was observed to have chipped (Figure 80).

Tests that used stem #3 also showed high energy, low rise-time acoustic activity at the proximal tip, however the extent of this activity was far less than that observed in the previous stems and no weld crack was visible during these tests. The 'Hits' axis in Figure 71 & Figure 72 has been scaled in order to prevent these proximal events from completely masking events that occurred further along the stem. As such the build up of proximal events is not fully representative and although proximal cracking was observed using μ-CT, the domination of proximal events from the weld cracks make discrete proximal cement crack identification impossible.

A general agreement was apparent between the levels of acoustic activity detected from the embedded and surface mounted sensors. However, tests 1, 3, 4 & 5 all showed activity detected by external sensors that was not located by the embedded sensors or shown to correspond to any cement cracking that could be identified by μ-CT. These events were located at the positions of the external sensors themselves and it is believed that this activity was the result of the clamping arrangement used to hold the surface mounted sensors in position.

AE was able to identify the load induced cracking observed on the μ-CT image analysis. However, there were instances where cracking was observed on the μ-CT images and not indicated by AE. Distal cracks were observed on the μ-CT images during tests 3 & 4 that were not apparent from data collected from either the embedded or surface mounted sensors. Distal cracks were also observed during tests 5-8 which were not picked up by the surface mounted sensors. Conversely, there were occasions when the AE data indicated evidence of cracking that was not visualized on the μ-CT images. Test 5 produced high energy and short rise time events along the length of the construct, however, the μ-CT images showed little evidence of substantial cracking occurring anywhere other than at the proximal and distal ends of the construct.

7.4 DISCUSSION

The aim of this study was to culminate all of the information gained through previous testing experiences in order to assess the suitability of using embedded AE sensors within the femoral stem to monitor the integrity of a cemented construct during fatigue loading. Poor manufacturing was believed to be responsible for the failure in the weld cracks and subsequent offset plates. The femoral stem and offset plate were designed with a tolerance fit of H7-p6 (an interference fit that can be disassembled). However, due to an inaccuracy during cutting of the square holes in the offset plate, the hole was larger than intended and the femoral stem was only located loosely within the plate. The subsequent increase in stress imposed upon the welded joint is thought to have initiated failure, and the concentration of high energy short rise time events located proximally during testing of stems 1 & 2 are believed to be associated with stem failure rather than cement cracking. The use of guard sensors to eliminate located events originating outside of the cemented region would have simplified analysis, however, the fundamental concept of this research is to investigate the suitability of using embedded sensors to detect and monitor damage of a hip construct. In this respect, the embedded sensors detected a severe region of damage long before any signs of damage could be seen by the naked eye, and certainly long before any damage could have been see using standard radiographic imaging.

The data recorded using embedded sensors showed a closer agreement with observed physical damage than externally mounted sensors. It is believed that the improved bonding accounted for this difference. Li et al[159] discussed a way to improve location accuracy in complex structures using a varying speed of sound algorithm. Decreasing the speed of sound used in location calculations tends to compress located data such that events originating near to the ends of the stem would appear closer to the centre of the stem. To see the effect of using different speeds of sound for location calculations, the data from test 5 was re-run using a speed of sound of just 100cm/ms. The two plots are shown side-by-side in Figure 79, however the plot using the lower speed of sound only shows a marginal increase in the energy associated with distal events, suggesting that the speed of sound was not the reason why these events were not detected.

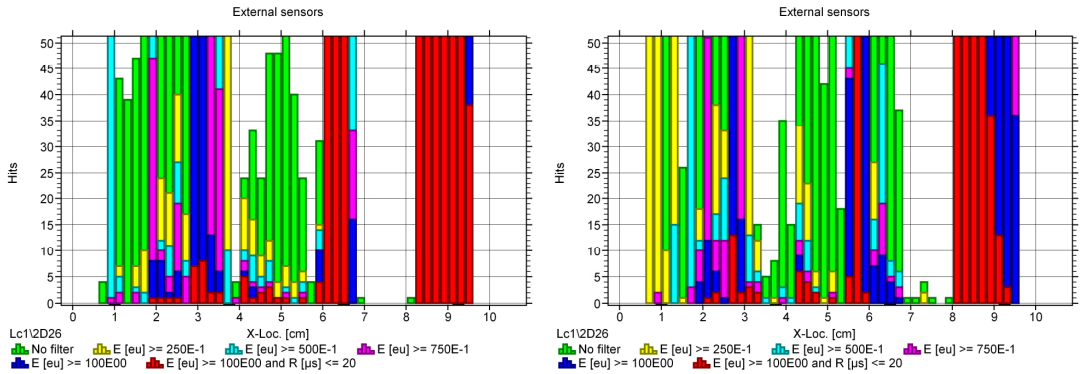

Figure 79 - Plots showing effect of using different speeds of sound for location calculation. The left hand plot shows data recorded during test 5 from the externally mounted sensors using the speed of sound determined from calibration testing of 198cm/ms. The right hand plot shows the same test results located using a speed of sound of 100cm/ms. The different colour bars represent the amount of energy associated with those events. The bars are positioned such that the highest energy events (red) are shown at the front of the plot, and the lowest energy events (green) appear behind all of the higher energy bars.

Inaccuracies around the distal tip will be amplified since the sensors themselves are positioned within the length of the cement layer. Arrival time location analysis fails if the acoustic source is outside of the area between sensors and tends to place all events at the sensor that detects the event first. However, these events should still be detected and one would expect to see a concentration of high energy events around the distal sensor - as shown in the data recorded using embedded sensors, which verifies that distal activity did occur during testing. The surface mounted sensors were positioned 27.5mm apart and since cement cracking produces high-energy events it would be unlikely for such activity not to have been located. A more likely explanation is that there may have been a problem with the sensor fixation causing poor transmission between the cement to the sensing element. The sensors were attached to the bone cement using a petroleum couplant and clamped in position using an adapted jubilee clip in an attempt to provide adequate fixation.

The embedded sensors did not seem to be affected by the same issues with regard to distal event detection. However, test number 3 was an exception and did not show any significant signs of high energy, short rise time events around the distal tip using either the surface mounted or embedded sensors even though cement cracking could be seen using µ-CT. All other tests detected and located distal activity. During polymersation, a thin layer of cement would often form under the base of the distal tip of the femoral stem. This

'flashing' was subsequently removed (Figure 80) - either during preparation of the construct for the initial scan (tests 1, 2, 6, 7 & 8 showed very little signs of flashing on the before loading images, see Figure 81, for example), - or during the initial set up of the stem in the Instron, or during the fatigue test regime itself. Unfortunately, the precise time when the flashing was destroyed for each stem is unknown, but it is hypothesised that the presence or absence of the flashing prior to starting the fatigue test regime and AE recording has a large impact on the level of distal activity picked up by the sensors.

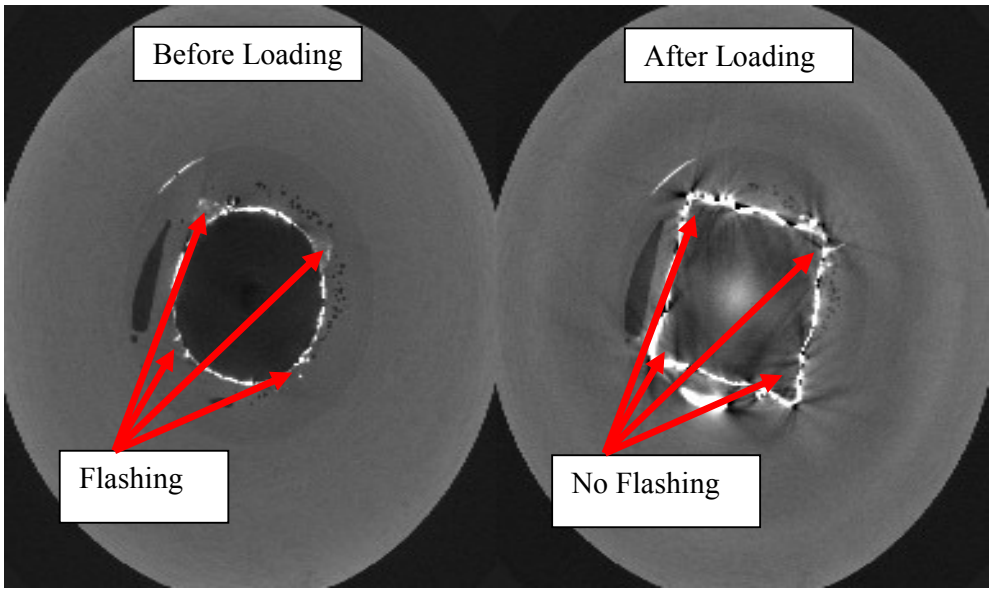

Figure 80- Axial slice images showing distal tip of cement before (Left) and after (Right) loading of test 5. The flashing associated with the polymerisation process has been removed due to the stem subsidence during loading.

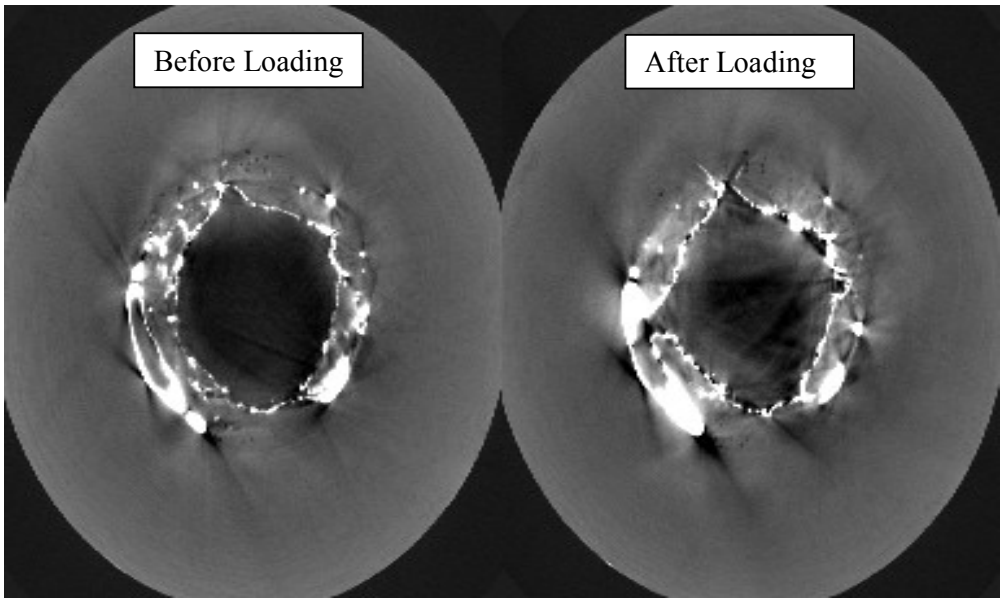

Figure 81 - Axial slice images showing distal tip of cement before (Left) and after (Right) loading of test 7. No flashing is observed on the before or after scan images.

Tests 1,2,3 &7 showed relatively few cracking type events compared to other tests and in order to relate this to the μ-CT images more clearly, the severity of cracking as seen on the images must be taken into consideration since the depth and number of cracks, and any influences of porosity or flashing may also have an effect on the amount of AE recorded and this information cannot be conveyed in Figure 71 & Figure 72. The severity of the distal cement cracking as indicated by the embedded AE sensors was ranked on a scale from 1-8 based on acoustic activity and total energy, effectively sorting the tests by distal activity and enabling a qualitative assessment of how the AE and μ-CT compare generally (Table 10). The variations in crack severity and porosity distribution between specimens is illustrated in Table 11

Test No.	Distal AE ranking (Embedded sensors)	CT crack observations	Porosity observations	Flash removal
1	3	3 corners	2 Large pores	-
2	4	3 corners	2 large pores	-
3	1	1 corner	1 large pore	4 corners removed
4	5	2 corners	Large pore present close to stem	4 corners removed
5	8	2 corners	Large pore present close to stem	4 corners removed
6	7	-	Multiple large pores close to stem	-
7	2	1 corner	-	-
8	6	-	Multiple pores close to stem	-

Table 10 - Qualitative comparison of AE activity and observed cracking, porosity and flashing as observed within the distal 10mm of the cement layer. The amount of AE activity has been ranked on a scale of 1-8 with 1 representing the least activity, and 8 representing the most activity.

Test	Example before/after distal slice images
1	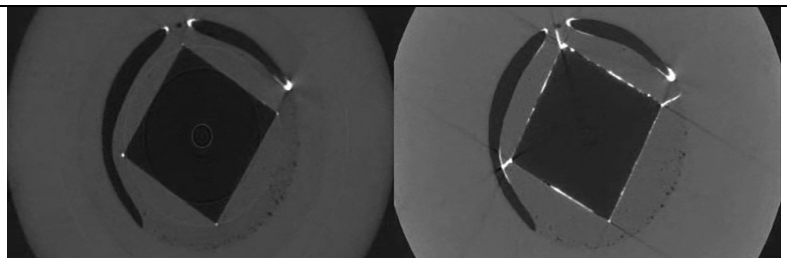
2	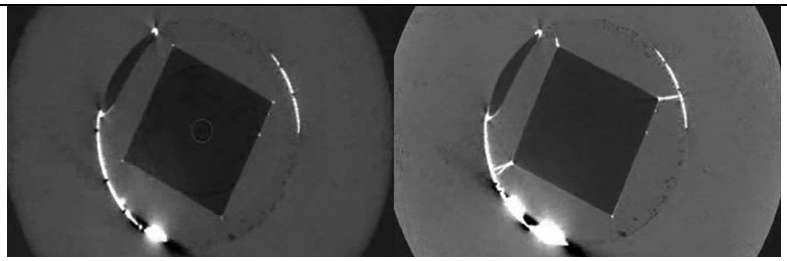
3	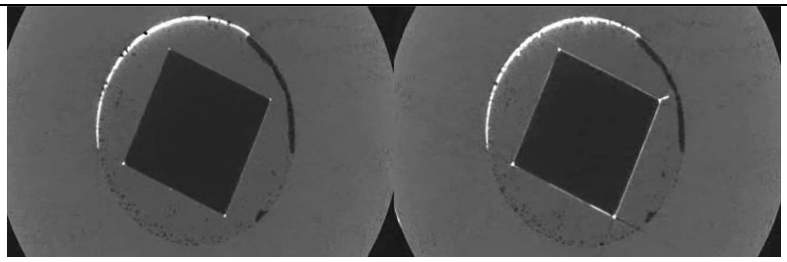
4	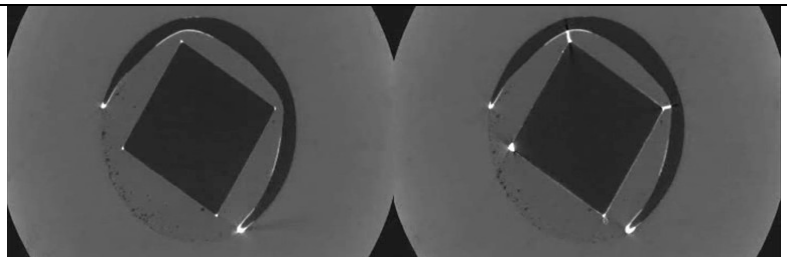
5	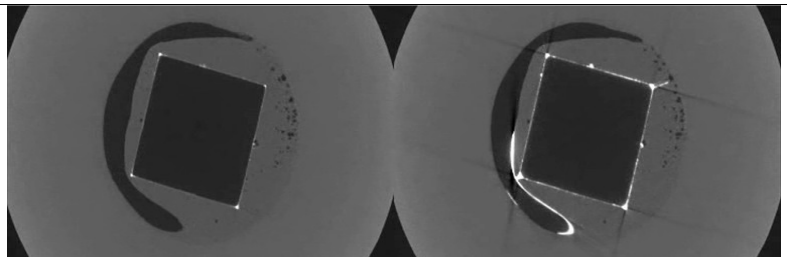
6	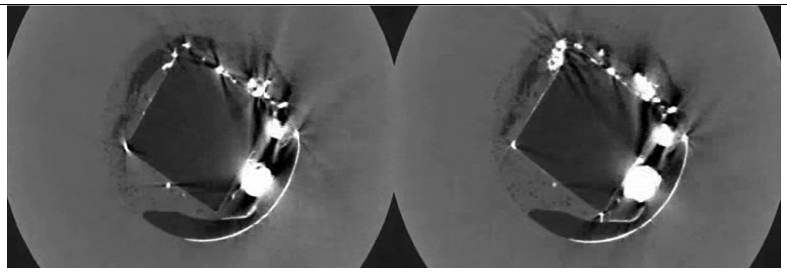

7	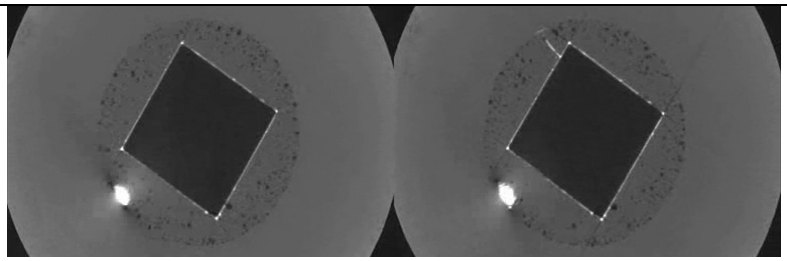
8	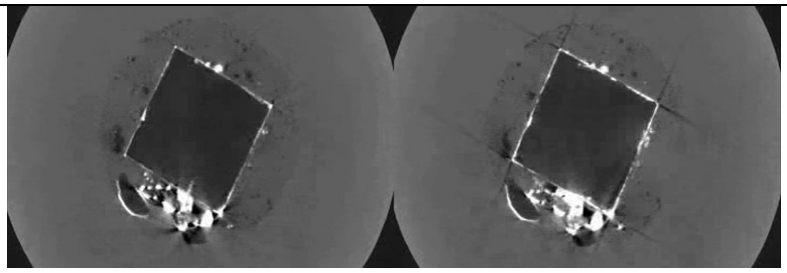

Table 11 - Example distal slice images showing variation in cement cracking and possible interactions with porosity

The correlation between located acoustic activity and the level of either cracking or flash removal is rather complicated as illustrated by the varied interactions possible with porosity and the time when flash removal occurred. The results shown in Table 10 & Table 11 imply that the presence of porosity in close proximity to the stem had a large influence on the level of detected AE. Stems 4, 5, 6 and 8 were shown to have the most significant levels of distal AE and all have porosity located close to the stem. Indeed stem 6 was determined to have the most prevalent distal AE and it can be seen from Table 11 that the distal tip of this particular stem is almost completely surrounded by a void created from the presence of multiple large pores. There are other sources of noise that could have affected the results such as rubbing of the distal clamp arrangement on the Tufnol tube, and possible location inaccuracies if the stem was not embedded sufficiently within the construct (discussed in chapter 4). However, the apparent lack of correlation between the μ-CT cracking alone and AE data, may be explained when the levels of porosity and flash removal are taken into consideration. Hence the AE data does give a good indication as to the state of the cement layer surrounding the distal tip of the stem, and this information was undoubtedly useful when attempting to determine the expected performance of a particular system.

7.5 CONCLUSIONS

The μ-CT imaging technique used in this study enabled clear visualisation of load induced damage whilst taking into consideration any cracking that may have formed prior to loading. Levels of porosity were able to be considered and have been identified as an important factor affecting the level of AE generation when the pores are sufficiently large and in close proximity to the stem to interact with crack formation. This increases the complexity of the system but provides useful information as to the true state of the system.

The embedded sensors seem to offer greater reliability over conventional externally mounted sensors. They are less affected by possible unforeseen mounting artefacts, and it is believed that the closer proximity to the region of interest, permanent fixation and reduction in the number of interfaces between the sensing element and region of interest accounts for this.

The ability to locate damage accurately was inconsistent due to the dominating presence of events caused by failure of the stem. The complicated nature of the structure which consisted of acoustically different materials of varying geometry together with the use of a loading jig and Instron machine which are in themselves sources of acoustic noise were all factors that were also thought to contribute to this. Since damage was shown visually on the μ-CT to be most prevalent around the distal and proximal regions of the femoral stem, noise reduction methods to reduce the impact of external noise should be implemented. Silencing the loading jig and surrounding environment would be impractical. However, the incorporation of guard sensors into the structure would allow specific analysis of events that are known to originate from within the region of interest.

Failure of the femoral stem was unquestionably detected and located by AE. Hence the overall objectives of the monitoring system are maintained despite the resulting difficulty in discriminating between stem and proximal cement failure.

The embedded sensors offered a significant improvement for condition monitoring of a cemented stem construct over surface mounted AE sensors, and this study has added greater confidence to the concept that the AE technique may be used to monitor the integrity of a cemented femoral stem construct.

CHAPTER 8 - OVERALL DISCUSSION

The overall aim of this project was to investigate the feasibility of using acoustic emissions for the condition monitoring of total hip replacements. This non-destructive technique offers many advantages over other potential monitoring methods. To this end a schedule involving sensor development and experimental testing scenarios of increasing complexity was adopted and a methodology developed that demonstrates the viability of self-monitoring prostheses. During the project several key objectives were realised; these are now discussed together with future considerations that need to be addressed to achieve the goal of developing the techniques described herein into a self contained clinical device.

1) In-house manufacture of AE sensors

The first key milestone of the project was reached when the performance of in-house manufactured AE sensors was able to match that of commercially available sensors (Figure 82).

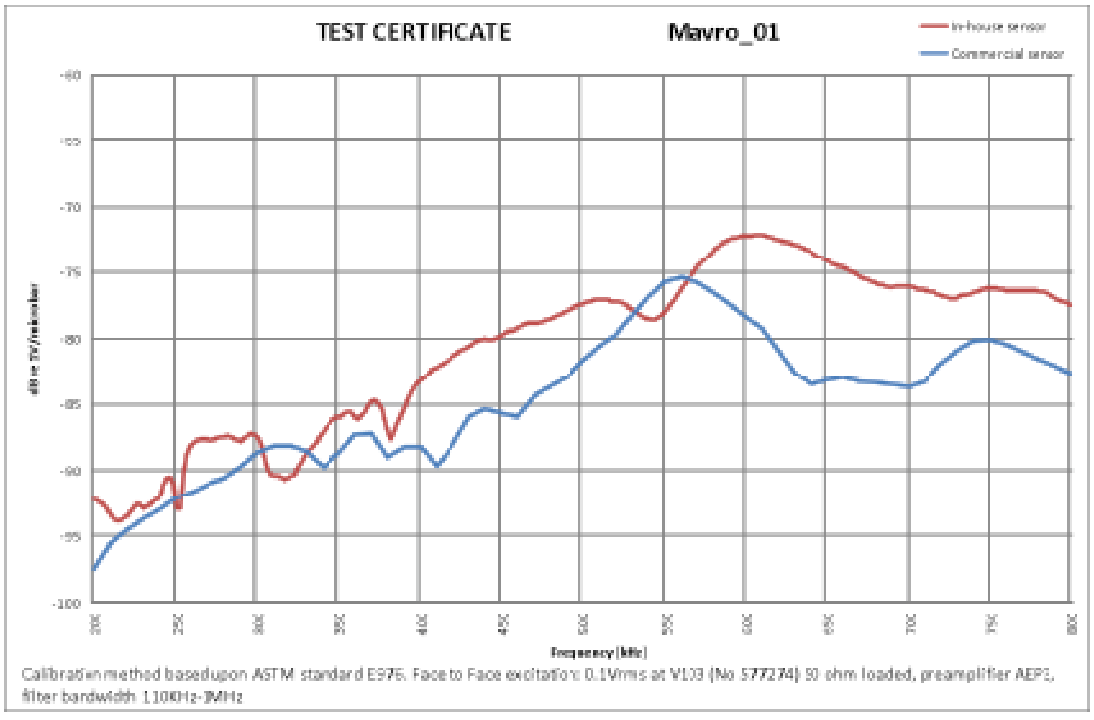

Figure 82 - Calibration response from an in-house sensor (red) compared to the calibration response of a commercial sensor (overlaid in blue).

The final sensor was the result of many attempts at different configurations, case geometries, and connection mechanisms. It is believed that the design of the final sensor is an improvement on its commercial counterpart due to its enhanced mechanical robustness. Commercially available AE sensors come in two general categories; wideband and resonant sensors. Resonant sensors offer high sensitivity at specific frequencies and are useful for detecting specific acoustic events and are most often used where a large area of interest is being monitored. Wideband sensors offer a higher degree of fidelity and are used where more information about the acoustic source event is required; this is why a broadband type sensor was chosen for this study. Another consideration in the selection of AE sensors is their size and very few commercially available sensors meet the size requirements to be embedded within the femoral stem of a THR. Physical Acoustics Corporation (PAC) only produce 2 sensors out of their 90+ range of available sensors that have dimensions less than 5mm in diameter and cover a frequency range of between 200-800kHz. Vallen Systeme GmbH produce over 30 different designs of sensor and again, only 2 of them may be considered broadband sensors less than 5mm in diameter. All of these sensors have an integral cable which cannot be disconnected from the sensor. The in-house sensors developed during this project used a microdot connector which enabled cable replacement, but more importantly, the system allowed the sensors to be incorporated directly into metallic structures, and eliminated the need for clamping systems and the potential noise sources that go along with movement of the clamping system or indeed of the sensor itself. However, attempts to form license agreements with existing sensor manufacturers proved unsuccessful and so the methodology used to manufacture these sensors has been presented explicitly in the hope that future researchers may use similar techniques to manufacture and adapt these AE sensors to their specific needs. The microdot connection was used to allow for a modular separation between the sensing element and the coaxial cable. This configuration permitted easy handling of multiple instrumented femoral stems whilst requiring minimal cable usage, and making it possible to interchange cables if they became damaged.

2) Prototype femoral stem with integrated AE sensors

Having successfully developed a methodology for manufacturing in-house AE sensors the inherent confidence and subsequent design flexibility enabled the second milestone of the project to be reached through the development of the first femoral stem with integrated acoustic emission sensors. The use of bulk PZT as the sensing element for these

embedded sensors was chosen in preference to thick film PZT pastes because of the developmental nature of the project and the relative availability of bulk PZT together with its known sensitivity. It is recognised that thick film processing may offer significant advantages for use in mass produced instrumented prostheses, and that this technology should be considered in preference to bulk PZT elements for the production of a clinical device. The ability to fire the paste directly onto a stainless steel component is surely advantageous and may enable an even more efficient acoustic transfer from the component to the sensing element. Further investigations on the use of thick film PZT devices were not pursued since the focus of the project was to assess the suitability of AE to monitor the condition of total hip replacement devices.

Previous studies that have investigated acoustic emission monitoring of cement failure have tended to use simple bone-cement specimens[141,148,165,166] or complete stem constructs[150,159], with very little work being conducted on a mid-stage experimental platform. The development of the simplified stem construct used in this project provided the intermediate step between simple test specimens and complex stem constructs allowing for a more comprehensive methodology to investigate the processes leading to crack formation within bone cement layers. The simplified geometry and material properties were intended to provide a more controlled means of identification of failure mechanisms. The square cross section was able to eliminate stem rotation and encourage cement failure around the corners of the stem. With such clear initiation sites, the amount of time waiting for damage to initiate was reduced and so the efficiency of the test programme increased. Acoustic emissions were recorded for the first time from within a femoral stem and it was demonstrated that the embedded sensors were able to detect and locate acoustic emissions reliably, through calibration pulse tests and later with corroboration of real damage with μ-CT imaging.

Immediate advantages associated with directly embedding sensors as opposed to mounting them on the external surface were apparent. Previous studies have only considered surface mounted sensors[141,148,150,151,159,165,209], which are sufficient for monitoring simple test specimens. However, where more complicated structures are involved or where the region of interest is buried within other materials, the use of surface mounted sensors makes accurate location calibration difficult and increases the number of interfaces and attenuation between the source signal and the sensor. Qi et al[150] were restricted to surface

mounted sensors in their study on a complete THA construct and the only means available of location calibration was to induce an acoustic source (pencil-lead break) on the external surface of the construct. Since the authors were investigating damage within the bone cement layer, positioning the sensors away from the material of interest and with the presence of multiple interfaces between the bone cement and the AE sensor was not ideal - potentially adding location inaccuracies to their system. All of the studies that have used AE to date in multiple component structures are restricted to surface mounted sensors, reducing flexibility of the test set up and limiting the location calibration options. The permanent fixation and position offered by embedded sensors resulted in repeatable responses during testing; in addition the close proximity of the sensing element to the region of interest reduced attenuation and interface effects on wave propagation; furthermore, the set-up of tests that ran with only embedded sensors offered greater simplicity and a reduction in potential noise sources resulting from external clamping devices used to hold the external sensors in position. In general, the embedded sensors showed a closer corroboration to damage observed using μ-CT imaging and therefore a greater level of confidence over their externally mounted counterparts. This is particularly encouraging for the prospect of an eventual *in-vivo* system. As identified in the literature review, there have been several encouraging studies, despite the signal degradation from source to sensor. Gao et al[153] used the AE technique *in-vivo* to assess the fixation of artificial hip joints and were able to categorise the state of the implant into three main frequency bands indicative of a loose femoral component (main frequency component less than 50Hz), a well fixed implant (main frequency component between 200-350Hz), and a femoral component which had entered cortical bone (main frequency component above 500Hz) . Schwalbe et al[154] looked at the acoustic response from joint friction and were able to link their data to known cartilage defects, and Glaser et al[152] used the technique to investigate hip joint separation and squeaking phenomena. However, all of these studies were limited to low frequency signals due to attenuation through the skin, muscle and fat and therefore lack the sensitivity to categorically provide more information than standard radiographic image analysis. The results of the experiments conducted in this thesis indicate that (*in-vitro*) the embedded sensors provide more reliable information than their external counterparts, and it is hypothesised that the quality of information of embedded sensors *in-vivo* will be even greater than their skin mounted counterparts. Despite this envisaged improvement, there are some disadvantages with embedding sensors directly within a structure. Directly embedding sensors into a structure does mean that those

sensors may only be used on that particular structure, and depending on the method used to seal the sensor within the structure, replacing the sensor in the case of malfunction would be more difficult. It is believed that the ability to directly embed AE sensors extends far beyond the application of total hip replacements and it is hoped that this work may provide the basis for a large range of embedded AE sensor applications. AE is currently used for monitoring many applications such as manufacturing processes[210], bearing performance[211] crack formation in pressure vessels[212], structural integrity of civil structures[213] and engine performance[214]. Many of these applications could be suited to the permanent integration of embedded AE sensors within the structure - allowing the user to simply connect to the structure via the micro-dot connector without needing to reattach sensors for multiple tests. There is a very important caveat to consider though, when embedding any sensor into a structure; the installation process necessitates a certain amount of modification to the structure, and since the areas of interest are likely to be close to failure sites, care must be taken to ensure that the installation of the sensor could not in itself initiate damage.

3) Developing a method for non-destructive data corroboration using μ-CT imaging

One of the problems affecting all forms of AE testing is the ability and confidence to link the AE data to actual damage events as opposed to unwanted noise. Previous authors[141,151] have used a variety of techniques including serial sectioning and dye penetrant techniques, ultrasonic imaging, and radiographic analysis. However, each of these techniques has associated restrictions which are less pronounced through the use of μ-CT imaging combined with a radiopaque dye penetrant. Serial sectioning, as used by Davies et al[151], by definition destroys the test specimen and can only report on the state of the specimen following testing, and temporal information about damage progression may only be obtained from multiple specimens loaded to different points within the test schedule. This is intrinsically inaccurate since there may be large variations between specimens and it can be argued that any corroboration between AE and load induced damage is based on the assumption that the damage was not present prior to testing. However, as various authors[81,84,85] have reported that damage may occur during polymerisation of bone cement and prior to any load bearing activity, one cannot assume that the cement layer was free from damage prior to loading. Therefore, it is inappropriate to link cracks found during serial sectioning to acoustic activity detected during experimental testing unless the state of the cement mantle is known prior to testing. Ultrasonic imaging can provide a progressive picture of damage accumulation, for example Browne et al[141] used the technique to

investigate cement debonding from a high density implant material. However, the technique does rely on accurate positioning of the transducer and the varying geometry associated with a complete stem construct restricts the information available with this technique. Furthermore correct interpretation of ultrasound images requires specific training. Standard X-ray image analysis offers speed and general information relating to the position and overall fixation of a construct. However, the limitation to 2D information restricts corroborating 3D AE information. The use of μ-CT imaging addressed all of the disadvantages associated with the inspection techniques listed above; it enabled before and after information to be collected and thus identify damage that formed during testing as opposed to damage that was present prior to testing. M–CT can image the entire cement layer and is less restricted by geometrical considerations than ultrasound, and provides a 3D representation of the construct at relatively high resolution. Its sensitivity compared to the AE technique may not be ideal and the resolution does suffer as a consequence of imaging the entire length of the cement layer. Nonetheless, the successful corroboration between AE and μ-CT imaging validates this protocol as a useful tool for damage monitoring in constructs of this kind.

4) Identification of waveform parameters linked to cement cracking/interface separation

Parametric analysis of acoustic waveforms is arguably the simplest form of discriminating between different damage mechanisms. Roques et al[148] identified the short rise-time relative to duration associated with bone cement cracking and this project found that events with a rise time of less than 20 microseconds and energies greater than 100Eu gave a good indication that cracking had occurred. The discrimination of lower energy events such as interfacial rubbing/debonding was less pronounced. However, this project identified another potential assessment method using acoustic information from embedded sensors that may be used for this purpose. This potential assessment method of stem fixation resulted from a concern over the location accuracy of embedded sensors due to the apparent inability of embedded sensors to accurately locate pulse calibrations from external sensors mounted towards the ends of the cement layer. However, it was determined that this location accuracy improved with stem subsidence and the consequent interfacial conformity between the stem and the cement. Furthermore, the attenuation of a pulse sent from one embedded sensor to the other increased as the stem achieved greater interfacial conformity. Possible explanations are related to the interface effect on wave propagation or a damping effect of the surrounding material on the stem; however, if this

effect proves reproducible with a demonstrable relationship to interface conformity then this may be very useful as an assessment of stem fixation. The frequency of the signals also was found to change as the stem subsided, in particular the high frequency components (>1MHz) of the signal reduced in amplitude when the stem was well fixed - Figure 83 and Figure 84 are typical responses from poorly fixed and well fixed stems; note the absence of the high frequency component in the well fixed scenario.

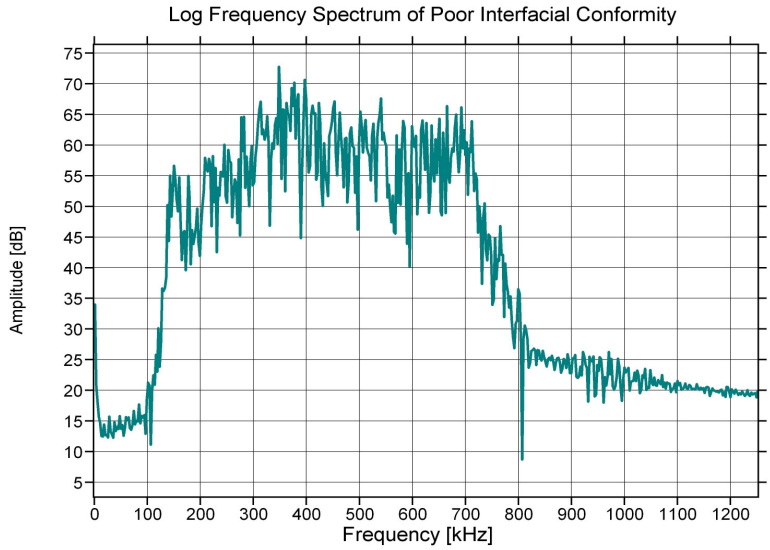

Figure 83 - Log frequency spectrum of receiving embedded sensor response from a calibration pulse sent from another embedded sensor. This pulse was sent when the stem was not embedded properly within the cement and interfacial conformity was low.

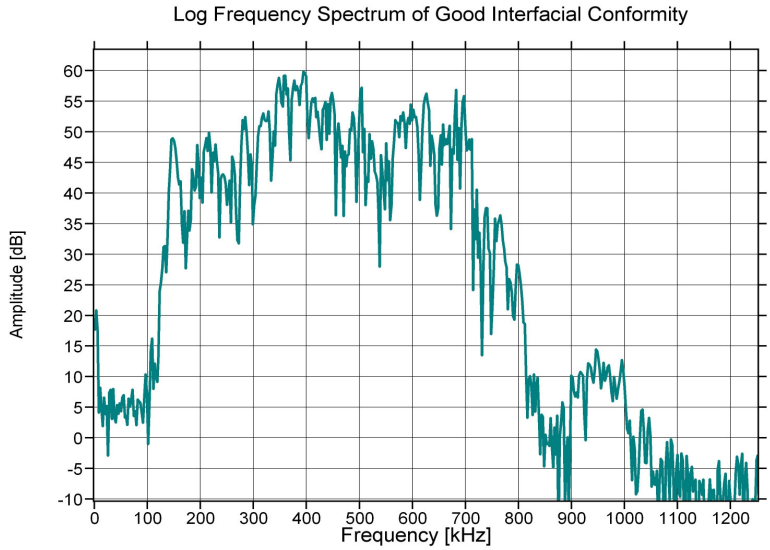

Figure 84 - Log frequency spectrum of receiving embedded sensor response from a calibration pulse sent from another embedded sensor. This pulse was sent when the stem was embedded securely within the cement and interfacial conformity was high.

It is hypothesised that this high frequency component may be lost as a result of the greater attenuation associated with the Technovit as opposed to the stainless steel stem. Initially, when the stem is loose within the construct, the majority of the signal will travel through the stem alone, however, as the stem / Technovit contact increases, more of the signal may be spread into the Technovit. Since higher frequency signals are attenuated more rapidly, this component of the waveform may no longer travel as efficiently through the construct.

The clear shift in location accuracy, signal attenuation and frequency response between a well fixed and poorly fixed stem shown in this study is very encouraging for the development of a simple system to allow condition monitoring of THR devices - especially since aseptic loosening remains the greatest issue regarding survivorship. The question as to whether or not this approach could be used in an *in-vivo* type study would depend on the power requirements and data transmission capabilities of the device.

6) - Information gained from experimental testing during polymerisation, Felicity loading and fatigue loading.

Although much of the information relating to damage progression is specific to the simplified set-up and geometry used throughout this project, it has allowed the type of information that this technique could provide within a clinical device to be ascertained. Unlike most forms of condition monitoring of total hip replacements, the AE technique is able to continuously monitor the structure and report on events as they happen in real time. For example, there is no current method used to monitor the damage induced within the cement layer during polymerisation. A device with integrated AE capabilities would make this possible as demonstrated in Chapter 5. If nothing else, this could be used as a learning tool for the clinicians to improve their individual cementing techniques, but since the development of new cement formulations and techniques is still a strong area of interest, it may also provide an early indication and discrimination of implants and their propensity to fail due to poor initial cement integrity. Using AE to monitor the polymerisation of Technovit, it was possible to determine exactly when in the cure cycle acoustic events occurred. It was demonstrated that polymerisation resulted in several bursts of activity - agreeing with the previous work of Roques et al[85] - and that the majority of this activity occurred after polymerisation was complete and so the effect of thermal contraction was thought to be of greater significance than pure volumetric shrinkage alone. This correlates

well to the findings of Gilbert et al[82] who observed a rapid onset of shrinkage in bone cement between 400–600 seconds and Lennon et al [81] who used an adaptation of Baliga et al [197] and Starke et al's [198] mathematical model incorporated into their finite element model to predict the point of maximum temperature and time to complete polymerisation. They predicted a peak temperature in their samples to occur at 536 seconds and complete polymerisation after 697 seconds. Our results showed the peak temperature to occur at 451 seconds and it would not be unreasonable to assume complete polymerisation to have occurred after 600-700 seconds. The major burst of acoustic activity occurred approximately 3-6 minutes after the maximum temperature reached during exotherm, and it can be assumed that the Technovit had polymerised by this stage, suggesting that the main source of pre-load damage may be attributed to thermal contraction effects rather than pure volumetric shrinkage.

Felicity testing of the structure showed reasonable corroboration between the locations of damage as indicated by the AE to damage visualised using μ-CT imaging. Initially, the Felicity loading regime was proposed since it is an established AE monitoring technique that can be used to assess when permanent structural damage had occurred. However, as became apparent in this study, the stick-slip type behaviour of a polished stem resulted in re-stabilisation of the stem within the cement following cement cracking and as such the Felicity ratio was not an appropriate assessment method in this case. RFA was deemed inappropriate for use on polished stems for the same reason. Despite the apparent stability illustrated by the Felicity ratio and RFA results, the AE data indicated that bursts of activity had occurred and the located regions of this damage were shown to be consistent with areas identified using μ-CT image analysis.

Fatigue testing of the system incorporated a sinusoidal loading pattern that was a simplified representation of that seen *in-vivo* during gait. Despite the presence of fatigue crack formation within the stem construct itself, AE data was able to identify and locate damage within the cement layer and once again the embedded sensors were shown to be less affected by unwanted signals than their external counterparts. The distal tip 'flashing' was recognised as an unwanted artefact and this should be removed prior to testing in future studies.

7) Going beyond a simplified stem construct.

Although all of the reported experiments used a simplified stem construct, the method used to integrate the sensors within a metallic structure would be identical for use in total or resurfacing hip replacement components. Indeed the technique could be integrated into an array of medical devices in which condition monitoring is important such as knees, or external fracture fixation devices. The main thrust of the work contained in this thesis is a proof of concept for the use of embedded AE sensors within a complete femoral stem construct to investigate the behaviour and degradation of the implanted construct, in particular the cement layer. However, to illustrate the concept of transposition between the simplified stem construct and clinical devices, a pilot study was performed using the technique to assess the development of a fluid film lubrication regime during the swing phase of gait in a hip resurfacing model. Since this study was separate from the main thrust of this thesis, it has not been discussed in detail. However, the ability to apply the methodology to directly embed sensors within clinical components and detect events other than cement cracking is important and hence a brief overview of the study is presented below:

Case study 1 – *A feasibility study of using an embedded AE sensor within a resurfacing head*

Throughout the gait cycle, a resurfacing bearing couple may experience different lubrication regimes. The different regimes are defined by the Stribeck (Figure 85) curve where the coefficient of friction is related to the Sommerfeld number (Equation 4)

Sommerfeld number $$z = \frac{\eta u r}{L}$$ **Equation 4**

Where:

z = Sommerfeld number

η = viscosity

r = femoral head radius

μ = velocity

L = load

The proportion of time spent in each regime could have a profound effect on the amount of wear particles released by the implant and influence the life of the artificial joint. Simulator studies have shown that all three types of lubrication regime may exist during the gait cycle[215] and Rowland et al[209] have demonstrated that AE may be used to monitor the different regimes likely to be operating in a hip simulator study.

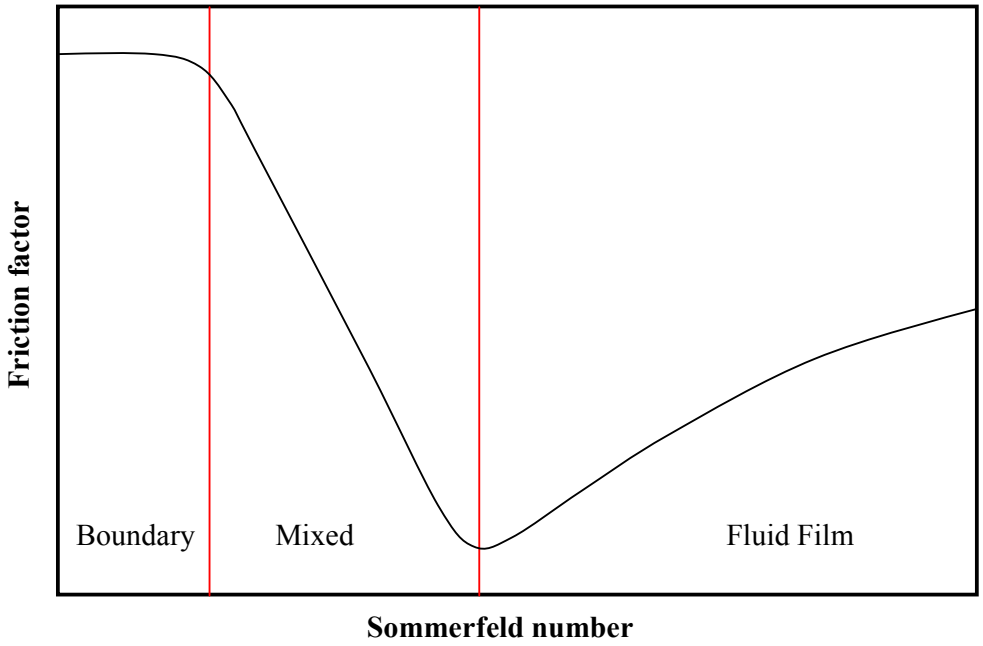

Figure 85 - Ideal representation of the Stribeck curve illustrating changing coefficient of friction with Sommerfeld number

It was hypothesised that an acoustic emission sensor could be integrated into the stem of a metal hip resurfacing femoral component and used to distinguish between different lubrication regimes. An Adept resurfacing 50mm head and matching cup (Finsbury Orthopaedics, Leatherhead, Surrey) were used as the bearing couple for this investigation. The head was prepared with an embedded AE sensor and mounted to a pendulum swing rig (Figure 86) using a custom built press fit mounting adapter (Figure 87).

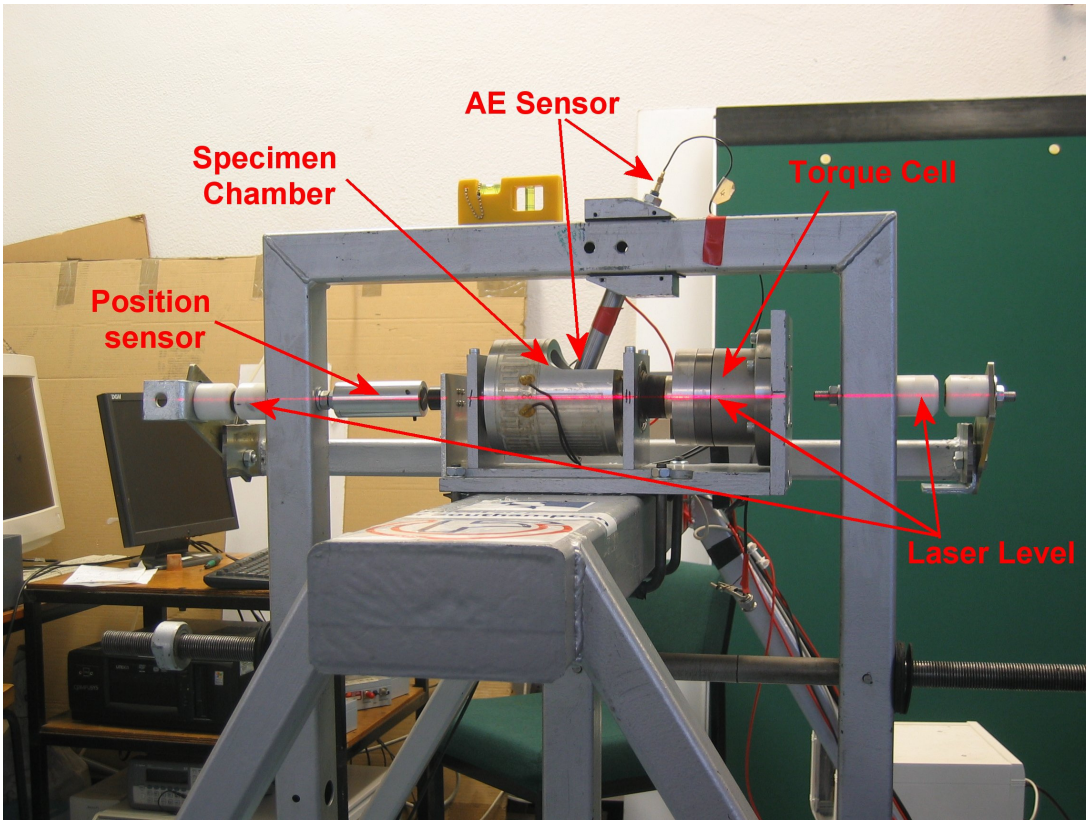

Figure 86 – Photograph showing Pendulum swing rig with laser alignment.

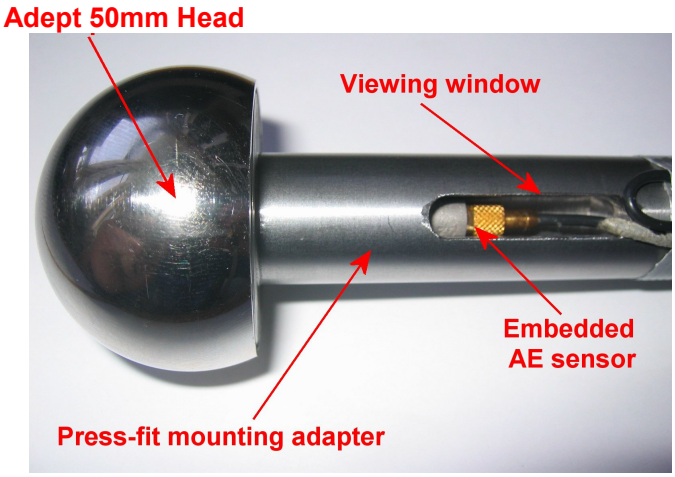

Figure 87 – Photograph showing Adept 50mm resurfacing head mounted onto the custom built press-fit mounting adapter with the embedded AE sensor visible through the viewing window.

The cup was positioned 0.37mm above the surface of the cup holder to ensure that the centre of rotation of the implant was aligned with the axis of the rig's torque cell and alignment magnets. The cup was mounted using Technovit 3040 PMMA resin. A jig was manufactured to ensure that the cup rim stood proud of the resin by 0.37mm and that the cup was held concentrically to the jig during cure (Figure 88).

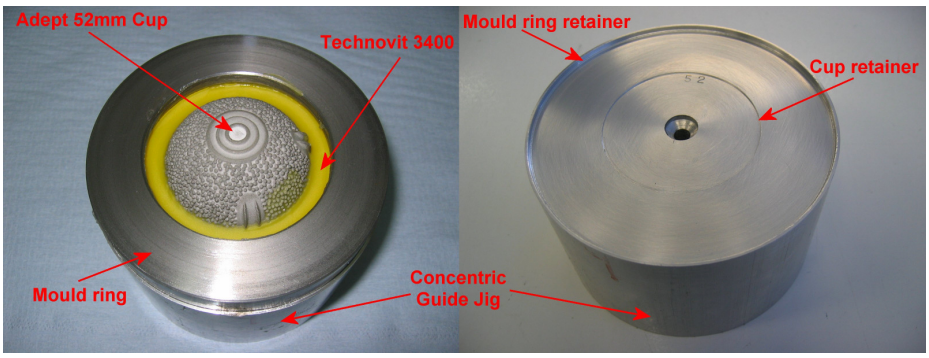

Figure 88 – Photograph showing acetabular cup held concentrically within a holding jig during polymerisation of the Technovit 3040 PMMA potting compound.

Prior to testing the sample chamber and bearing surfaces were thoroughly cleaned with Acetone. During testing, the angle of swing together with the torque transmitted through the bearing couple were recorded simultaneously with the acoustic emission data using a Vallen Systeme AMSY-5 data acquisition package. A further AE sensor was mounted on top of the press fit mounting adapter to enable comparison between the data recorded by the embedded sensor and the external sensor. Alignment of the jig was obtained using a laser level that ensured that all centres of rotation were aligned perfectly along the rig's axis (Figure 86).

The specimen chamber was filled with pure vegetable oil to act as a lubricant and prior to any recorded data the pendulum was displaced through an angle of 25^{o} and held with a length of string. Once recording had commenced, a flame was held against the string until failure and the pendulum was subsequently released. The pendulum was allowed to come to rest without interaction. Very little acoustic activity was recorded during this test until the pendulum was allowed to swing without lubrication. Acoustic activity recorded from the embedded sensor was shown to correlate with the torque magnitude and as the bearing couple "dried out", and three distinct phases were observed (Figure 89), and reflected in the changing peak torque profiles observed during each of the three phases (Figure **90**)

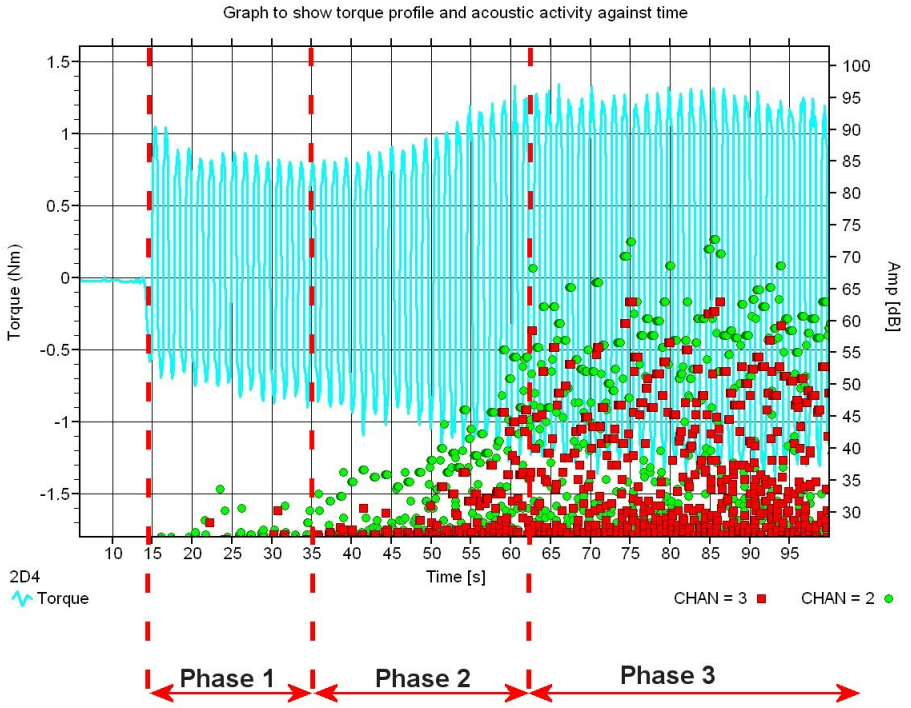

Figure 89 – Plot showing increasing torque and acoustic activity as dry test progresses. Chanel 3 is the external sensor and channel 2 is the embedded sensor.

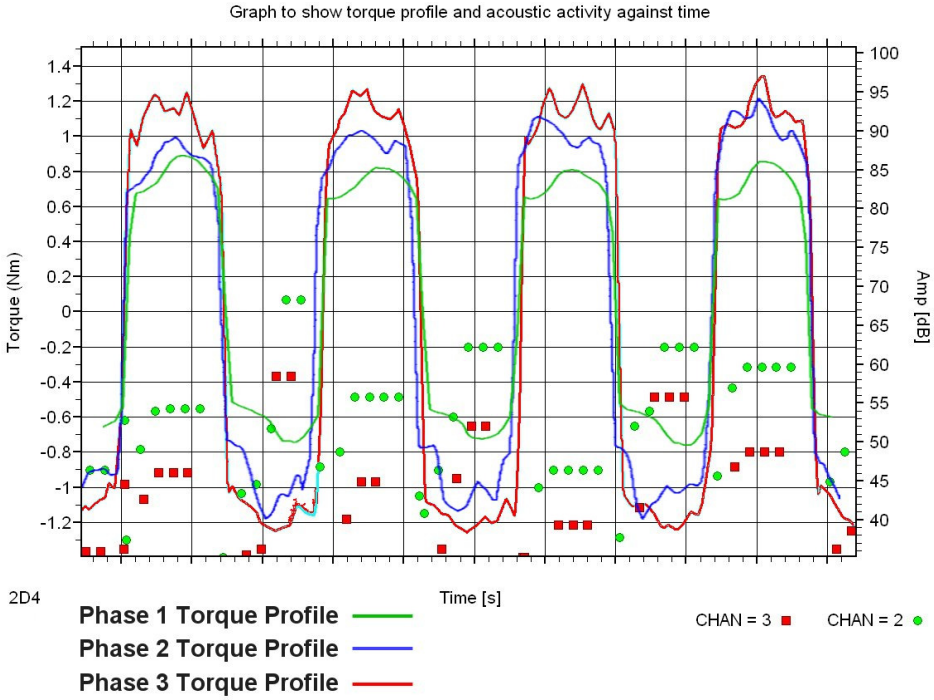

Figure 90 – Plot showing distinct torque profiles for each of the 3 lubrication phases

It is thought that the initial period (Phase 1) of low acoustic activity and low torque values, attributed to residual lubricant, was sufficient to allow fluid film lubrication to occur, and

that the increase in torque and acoustic activity during phases 2 and 3 were indicators that the bearing was going through a transition to the mixed mode and boundary lubrication regimes.

The differences in peak torque profiles for the different phases / lubrication regimes are distinct. The smooth profile associated with phase 1 lubrication is largely in agreement with theoretical models derived from the Stribeck curve although the peak torque occurs slightly later in the cycle than predicted. During mix-mode lubrication, the theoretical model would expect the peak torque profile to peak at the beginning and end of each swing. Although this pattern may be seen to some extent in the experimental torque profiles, the shape of the profile is masked by imperfections within the system – possibly due to uneven surface scratches which caused the torque profile to fluctuate more than expected during each swing. However, what is noticeable is the shift of the peak torque towards the beginning of each swing – suggesting that the bearing is initially subject to a higher resistive force which then decreases as velocity increases, rather than the gradual increase of resistive force with increasing velocity as observed in phase 1. This progressive increase in resistive force during phase 1 is thought to be due to the increase in shear force of the lubricant as velocity increases. Theoretically the torque profile associated with boundary lubrication should see an initial high peak followed by a decrease in torque throughout the rest of the swing. The experimentally obtained profiles show that the torque varies randomly throughout the swing although if one were to average the torque profile it would appear flat over the progression of the swing. Hence it is unknown whether pure boundary lubrication was ever achieved.

Although the torque profiles exhibit at least 2 of the 3 distinct modes of lubrication, it remains to be seen if the acoustic data alone can provide an indication of the lubrication regime in operation. It is clear that the level of acoustic activity changes for each of the different lubrication regimes. Threshold levels of Energy / Amplitude may provide an indication of the type of regime in operation. However, this is likely to vary significantly with different bearings, acoustic sensors, sensor location, and overall situation regarding the surrounding environment housing the bearing under investigation. A more robust approach may be to combine acoustic data with another parameter such as the torque profile or swing angle (Table 12) such that the timing of acoustic activity may be related to the physical position and velocity of the bearing surfaces.

Dry Test	
Phase 1	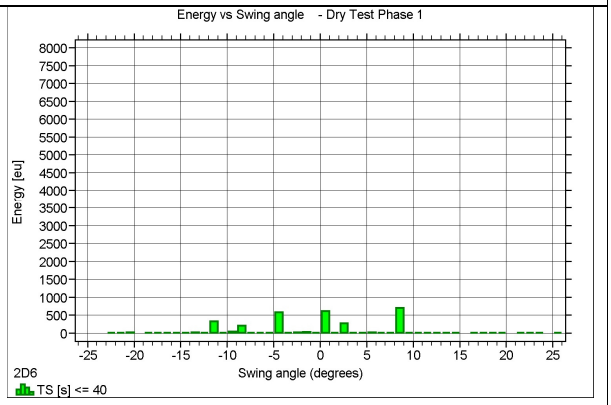
Phase 2	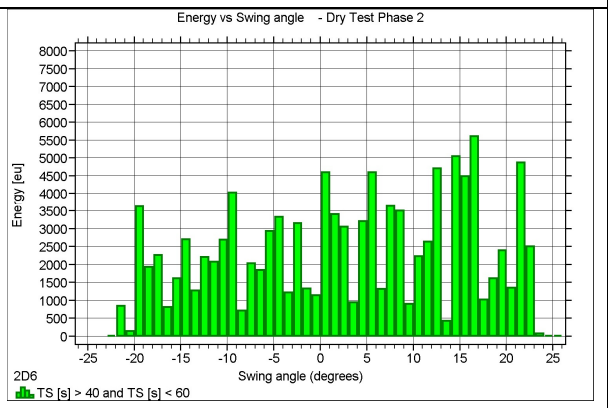
Phase 3	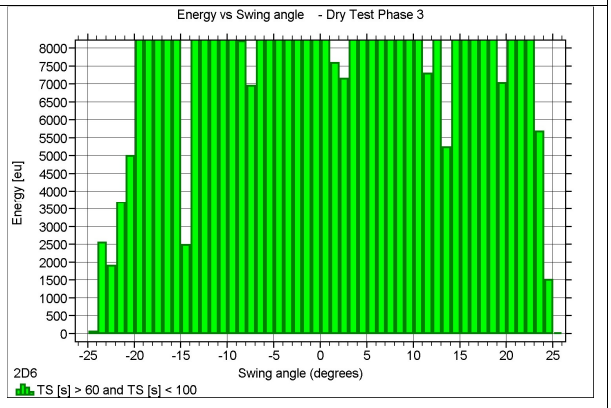

Table 12 - Table showing acoustic energy variation across the swing angle during the different phases of operation as identified from the increasing torque measurements (Figure 89) during swing with no lubricant present in the chamber

Relating this information alone to the type of lubrication regime in operation using theoretical calculation would be difficult since the bearing was running dry, and hence the viscosity of the lubricant is unknown. Two further tests were therefore performed using different lubricants with known viscosities: pure vegetable oil and bovine serum. This allowed the theoretical lubrication regime to be calculated and by varying the load, different lubrication regimes were achieved.

Case study 2 – *Theoretical determination of lubrication regime and effects on acoustic emissions*

Nomenclature:

f	Friction factor
T	Maximum torque
r	femoral head radius
L	Applied load
z	Sommerfeld number
η	viscosity
u_h	Entraining velocity (head)
u_c	Entraining velocity (cup)
u	Entraining velocity $(u_h+ u_c)/2$
h_{min}	minimum film thickness
R_x	Equivalent radius for ball on plane model $R_cR_h/(R_c-R_h)$
E'	Equivalent elastic modulus ($2.3x10^{11}$ Pa for CoCrMo)
R_{qh}	Surface roughness within contact patch of femoral head
R_{qc}	Surface roughness within contact patch of acetabular cup

Equations used in this study:

Friction factor $$f = \frac{T}{rL}$$ **Equation 5**

Sommerfeld number $$z = \frac{\eta u r}{L}$$ **Equation 6**

Minimum film thickness $$\frac{h_{\min}}{R_x} = 2.798\left(\frac{\eta u}{E' R_x}\right)^{0.65}\left(\frac{L}{E' R_x^2}\right)^{-0.21}$$ **Equation 7**

Lambda coefficient $$\lambda = \frac{h_{\min}}{\left(R_{qh}^2 + R_{qc}^2\right)^{0.5}}$$ **Equation 8**

Methodology:

The same head/cup combination was used as in the previous case study. However, the lubricants used were 100% pure vegetable oil for the first run of tests, and then changed to 25% bovine serum + Sodium Azide from batch no. 057K8408 for the second set of tests. The bearing was completely submersed by the lubricant and the specimen chamber was heated and maintained at a steady 37ºC throughout the test. During each test run, the pendulum was forced to swing through an angle of ±25° for several complete swings before being allowed to come to rest. The load acting through the bearing was increased from 150N to a maximum of 1350N in 400N increments. Recordings were taken for the swing angle, velocity and torque acting on the bearing. For calculations, the viscosity of the vegetable oil was measured at 37ºC using a Zeitfuchs cross-arm type viscometer as 0.04576 Pas, and the viscosity of the bovine serum was assumed similar to that of the 100% bovine serum used by Scholes et al[216] measured as 0.007Pas. The head and cup diameters were assumed similar to that of a standard 50mm head coupled with a 56mm cup measured at Finsbury Orthopaedics as having typical values 49.8mm and 50.2mm respectively. Surface roughness values are again assumed similar to those found on a typical head/cup bearing of 260 and 290nm respectively. The friction factor and Sommerfeld number for each test run was calculated and then plotted on a Stribeck curve and the theoretical minimum film thickness and the dimensionless parameter λ were calculated in order to predict the type of lubrication regime that would be expected. A value of λ greater than 3 is assumed to be in fluid film lubrication, less than three and one would expect a mixed or boundary regime to operate[217].

Results:

Bovine serum - Measured Variables:

Load (N)	Head diameter (m)	Cup diameter (m)	Head Surface roughness (m)	Cup Surface roughness (m)	Viscosity (Pas)	Max Torque (Nm)	Max Velocity (Deg/s)
150	4.98E-02	5.02E-02	2.60E-08	2.90E-08	7.00E-03	6.6	124.7
550	4.98E-02	5.02E-02	2.60E-08	2.90E-08	7.00E-03	30.9	139.5
950	4.98E-02	5.02E-02	2.60E-08	2.90E-08	7.00E-03	56.9	167.9
1350	4.98E-02	5.02E-02	2.60E-08	2.90E-08	7.00E-03	82.4	162.1

Table 13 – Table showing measured variables used in calculations for predicting the lubrication regime operating under different loads using a bovine serum lubricant

Bovine serum - Calculated Variables:

Load (N)	Friction Factor	Sommerfeld Number	Predicted Film Thickness (μm)	λ	Predicted lubrication Regime
150	1.78	6.31E-08	0.13	3.36	**Fluid**
550	2.26	1.93E-08	0.11	2.75	**Mixed**
950	2.41	1.34E-08	0.11	2.77	**Mixed**
1350	2.45	9.12E-09	0.10	2.51	**Mixed**

Table 14 - Table showing calculated variables and predicted lubrication regime operating under different loads using a bovine serum lubricant

Vegetable oil - Measured Variables:

Load (N)	Head diameter (m)	Cup diameter (m)	Head Surface roughness (m)	Cup Surface roughness (m)	Viscosity (Pas)	Max Torque (Nm)	Max Velocity (Deg/s)
150	4.98E-02	5.02E-02	2.60E-08	2.90E-08	4.58E-02	0.6	122.7
550	4.98E-02	5.02E-02	2.60E-08	2.90E-08	4.58E-02	1.8	150.3
950	4.98E-02	5.02E-02	2.60E-08	2.90E-08	4.58E-02	2.7	168.0
1350	4.98E-02	5.02E-02	2.60E-08	2.90E-08	4.58E-02	4.0	184.4

Table 15 - Table showing measured variables used in calculations for predicting the lubrication regime operating under different loads using a vegetable oil lubricant

Vegetable oil - Calculated Variables:

Load (N)	Friction Factor	Sommerfeld Number	Predicted film thickness (μm)	λ	Predicted lube regime
150	0.17	4.06E-07	0.44	11.27	**Fluid**
550	0.13	1.36E-07	0.38	9.79	**Fluid**
950	0.11	8.78E-08	0.37	9.38	**Fluid**
1350	0.12	6.78E-08	0.36	9.26	**Fluid**

Table 16 - Table showing calculated variables and predicted lubrication regime operating under different loads using a vegetable oil lubricant

AE observations – Bovine serum

Load (N)	AE response Energy vs Swing Angle	Predicted Lubrication Regime
150	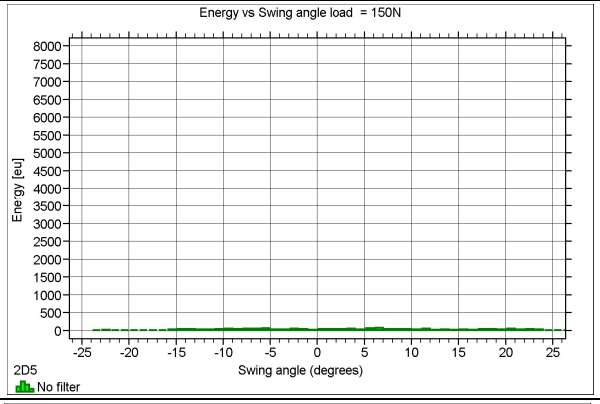	Fluid
550	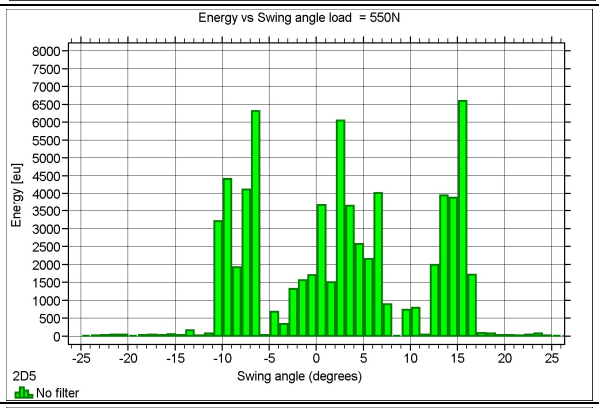	Mixed
950	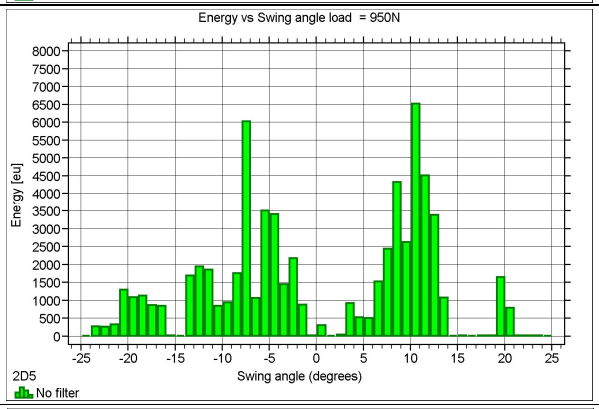	Mixed
1350	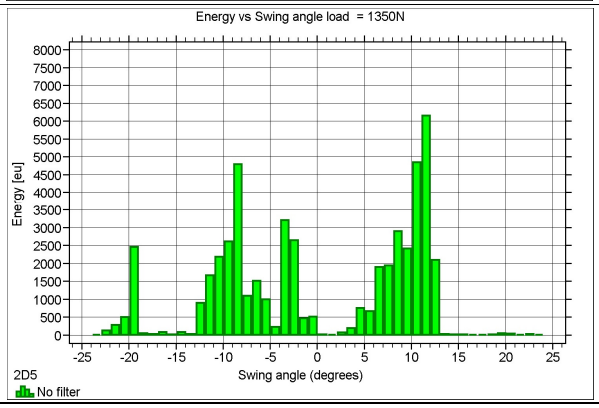	Mixed

Table 17 – Table showing acoustic energy variation across the swing angle at different load levels together with the predicted lubrication regime using bovine serum as the lubricant

AE observations – Vegetable oil

Load (N)	AE response Energy vs Swing Angle	Predicted Lubrication Regime
150	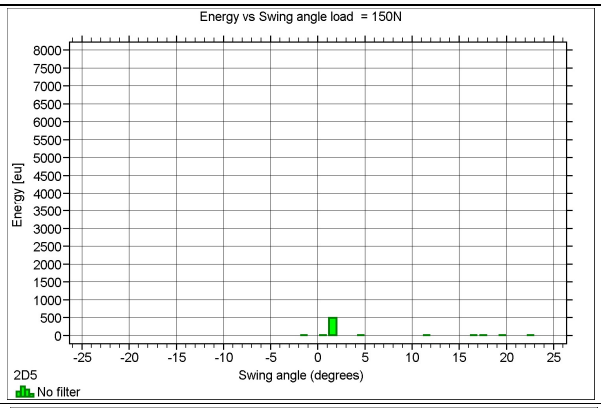	Fluid
550	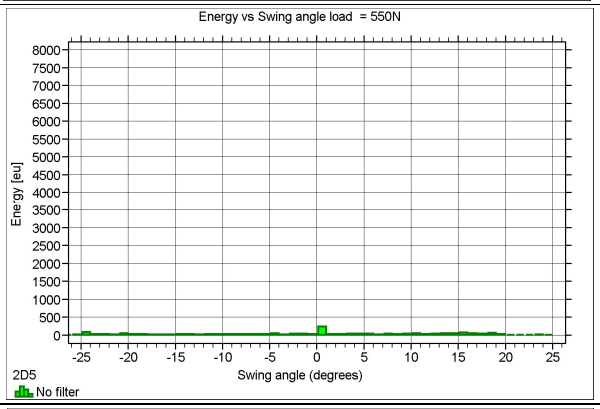	Fluid
950	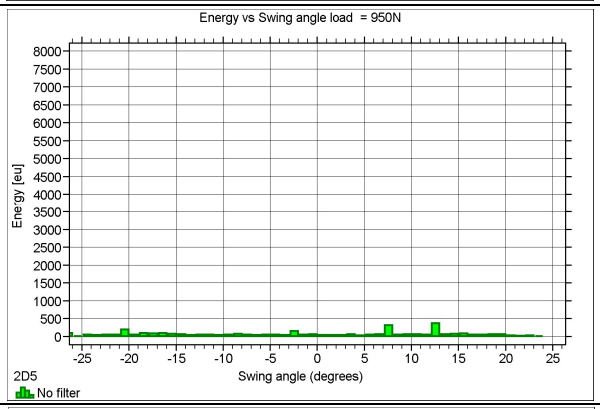	Fluid
1350	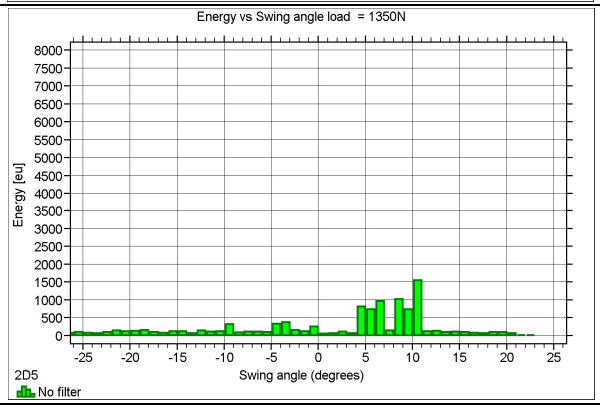	Fluid

Table 18 - Table showing acoustic energy variation across the swing angle at different load levels together with the predicted lubrication regime using vegetable oil as the lubricant

Stribeck plots:

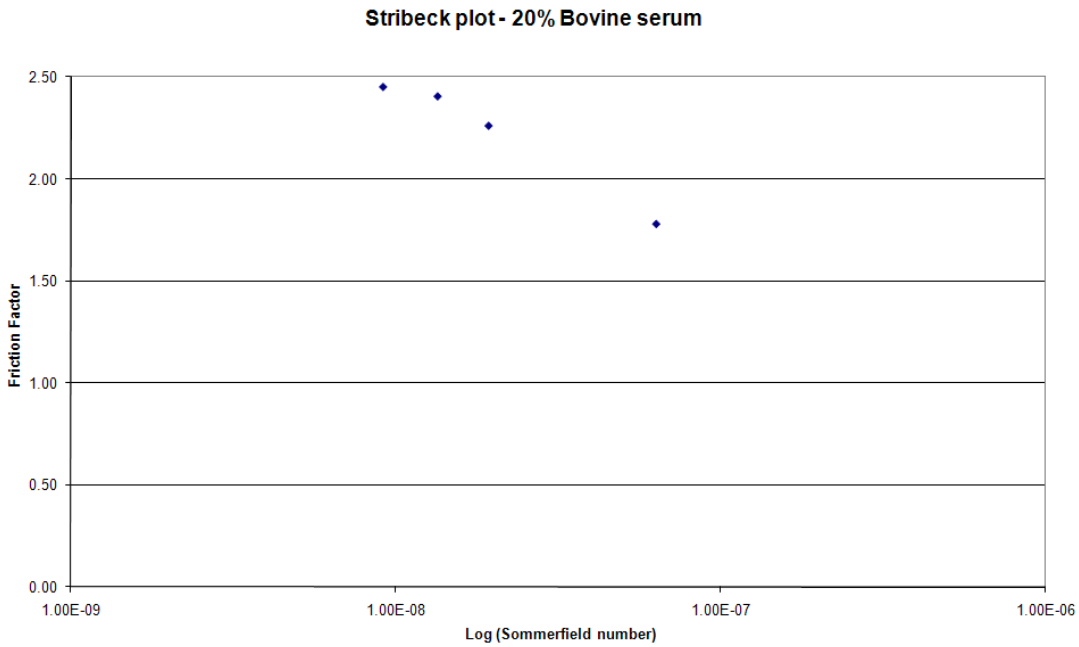

Figure 91 - Stribeck plot for 50mm bearing lubricated using bovine serum.

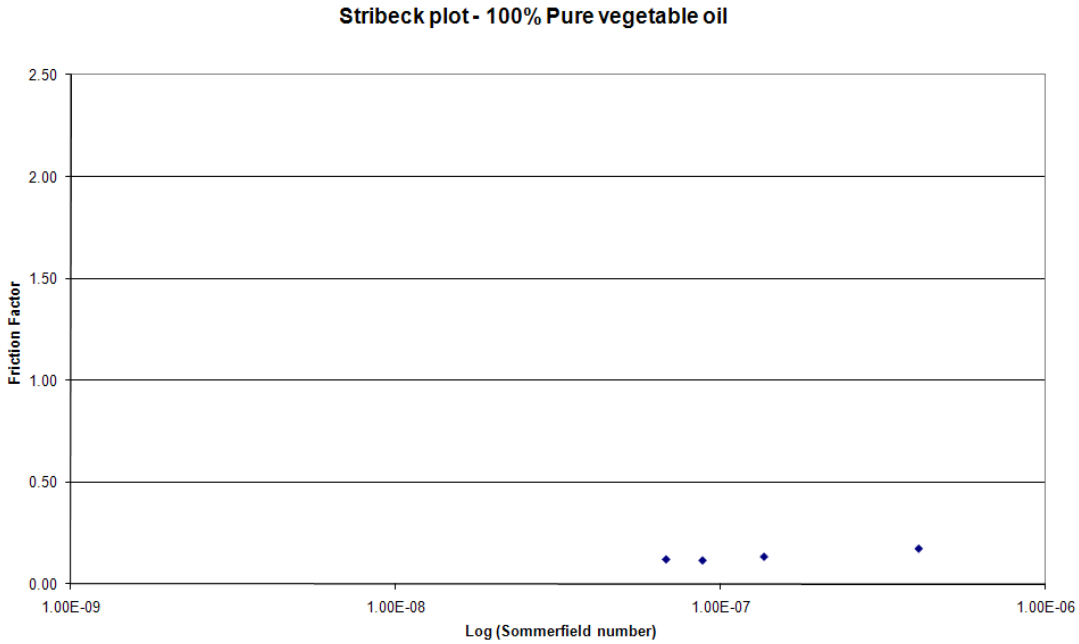

Figure 92 - Stribeck plot for 50mm bearing lubricated using vegetable oil.

Discussion:

The theoretical calculations relate to the maximum entraining velocity achieved during swing – a state that is only achieved briefly at approximately 0º of swing. The load applied is the static load, however, the load experienced by the bearing at 0º of swing will be higher due to the centripetal acceleration acting on the pendulum. Furthermore, the calculations assume a uniform surface roughness across the bearing surface (no scratches). Nonetheless, it the predicted modes of lubrication are corroborated by the associated acoustic energy that was measured during swing.

The bovine lubricated joint was predicted to make the transition from fluid film to mixed mode lubrication as the load was increased from 150N to 550N using λ as the determining factor. The AE energy detected at 150N was very low when compared to all of the other load levels using the same lubricant. When the lubricant was changed to vegetable oil, no significant high energy events were detected during swing at any of the applied load levels - demonstrating that the events detected during the bovine serum lubricated tests were unlikely to have come from any noise of the swing rig itself, but were more likely to be a true measurement of events originating at the bearing surface. Again, the λ prediction calculations showed that the lubrication regime should remain in the fluid film regime for all load levels using such a viscose lubricant. Furthermore, the interpretation of the Stribeck plots for both types of lubricant would tend to agree with this information, suggesting that the vegetable oil tests are in the fluid film region of the curve, and the bovine tests are somewhere in the mixed mode region.

Linking this information back into the dry test, we may be able to draw a comparison between the acoustic energy observed there, and determine what lubrication regime was likely to have been operating. The acoustic energies measured during the dry test, plotted against swing angle can be seen in Table 12 – this uses the same axis scales as the plots presented in Table 17 & Table 18, so a direct comparison may be made. If the conclusions from the lubricated study are correct, then the acoustic emission data alone would imply that the dry bearing was initially operating under fluid film (phase 1) – possibly due to the presence of residual lubricant, but quickly moved into the mixed mode or even boundary modes during phases 2 and 3.

This study has demonstrated that embedded AE sensors may be used within resurfacing components. The study made predictions as to the type of lubrication regime likely to be in operation, and the amount of acoustic energy measured during swing correlated strongly with these predictions. More corroborative evidence to determine the type of lubrication regime in operation would be needed to conclusively state whether or not the acoustic energy could be used as a determinant of lubrication regime without other assessment techniques. However, if this hypothesis is assumed to be positive then it may be concluded that the phases seen during the dry test were related to changes in lubrication regime.

CHAPTER 9 - CONCLUSIONS AND FUTURE WORK

It is believed that the work contained in this thesis represents an initial step towards a viable economic solution to a practical, embedded condition monitoring system. It was hypothesised that: There is a requirement for greater *in-vitro* and *in-vivo* information to be routinely collected. Ultrasound, RFA and AE techniques could all offer great benefits to the field if incorporated into a condition monitoring system and enable earlier detection of loosening without the need for ionising radiation. It was also hypothesised that directly embedding sensors within the femoral stem would:

1) Reduce potential complications of poor sensor fixation and eliminate test-to-test variations in sensor fixation.

2) Reduce attenuation and interface effects due to the proximity of the sensor to the structure of interest.

3) Permit greater experimental flexibility since the sensors do not need to be recovered.

4) Permit a more realistic test environment since the test chamber/bone specimen does not have to be altered in order to accept the sensors.

The research presented in this thesis has concluded that more rigorous *in-vitro* and instrumented *in-vivo* testing is required to prevent the recurrence of unexpected clinical failures[119,218-220], or at least detect these failures earlier such that the numbers of implantations of poor designs may be limited. It was concluded that the ultrasound technique was only applicable for simple geometry specimens used in dry environments. The RFA technique may be useful for stems that form a mechanical interlock with the surrounding cement/bone, however, following the testing conducted in Chapter 6, it was concluded that its use for polished stems was severely limited due to the ability of the stem to restabilise within the cement after damage had occurred. The detection of this damage was therefore too reliant on the timing of the RFA test to coincide with the damage formation. The continuous, passive-monitoring capabilities of the AE technique bypassed this limitation and it was concluded that this was the most appropriate technique for this application.

In chapter 4, AE sensors were incorporated into a simplified femoral stem and the results from the Felicity and fatigue tests described in chapters 6 and 7 indicate that their ability to

accurately assess cement integrity may be superior to their externally mounted counterparts. These initial results offer encouragement for the development of an instrumented *in-vitro* or *in-vivo* system. To date there have only been a few *in-vivo* studies that have considered the acoustic emission technique as a clinical tool for hip implant assessment[154,221]; these typically involve placing AE sensors on the flesh of the patient, losing the majority of information contained within the higher frequency spectrum of the signal. If successful, it is believed that the use of directly embedded sensors would bypass these issues and allow for an acceleration of implant development simply due to the new levels of information available from true *in-vivo* loading and environmental conditions, potentially delay or even prevent failure of implanted systems through lifestyle alterations, and if failure cannot be prevented, then at least the chances of a successful revision operation may be increased by identifying failure before the surrounding bone becomes severely traumatised. *In-vitro* it is believed that the system would allow more authentic information to be acquired than would be possible using externally mounted sensors, together with improvements in test repeatability (no need to detach and reattach sensors after every test), as well as allowing closer proximity of the sensor to the point of interest (the implant/cement/bone interfaces).

It was determined that for this particular experimental set-up and with these particular sensors, that events with a rise time of less than 20μs and energies greater than 100Eu gave a reasonable indication that cracking within the cement layer had occurred. However, increasingly sophisticated analysis techniques are being developed and employed that may enable greater confidence in event discrimination. Modal AE and wavelet analysis are two techniques that move beyond the analysis of fundamental waveform parameters and have been accredited with a greater ability to distinguish between different source mechanisms. Improved location algorithms and techniques are being developed that can be applied to more complicated geometries and material structures, and the ever increasing availability of high performance computer processing and data storage mean that a continuous monitoring system is becoming increasingly realistic in terms of both size and cost. The main outcome of the present study was the incorporation of AE sensors into a femoral stem. Now that this has been achieved and shown to work for simple test scenarios and simple waveform parametric analysis, the potential for further investigations and contributions to the field are substantial. The use of wavelet and modal analysis techniques is just one example of a future direction of this work. Other envisaged avenues

include testing the system under wet environmental conditions, using the system to investigate the ability to detect interfacial debonding of rough stems, analysing the cure characteristics of various commercial cement formulations, integrating the system into a commercial femoral stem, assessing performance within a more realistic construct using either sawbones epoxy femurs or cadaver specimens, re-assessing the possibility of thick film technology, and looking at the development of wireless signal transmission, power generation, links to hand held devices and ultimately the development of a complete stand-alone system suitable for implantation.

Testing under wet environmental conditions

All of the tests conducted throughout this thesis have been run dry, excepting the lubrication study described in chapter 8. However, it is believed that the simplified construct and use of external sensors have served their purpose in terms of verifying the use of embedded sensors and their ability to detect real time damage formation within the bone cement layer. It is known that the fatigue behaviour of bone cement is affected by the environmental conditions[148] and that pre-clinical fatigue testing of total hip replacements is performed in saline solution to represent the *in-vivo* environment. Issues concerning the ability of the embedded sensors to perform in this environment are not envisaged since the sensors are effectively sealed within the stem. Nonetheless this will have to be verified prior to the application of the system in such an environment for widespread pre-clinical tests.

Interfacial debonding of rough stems

Chapter 4 described the influence of polished stem fixation on attenuation and speed of sound characteristics of signals sent from one embedded sensor to the other. This effect in its own right could be a significant contribution to the field. However, it requires further investigation for various surface finishes and fixation techniques. It is hypothesised that the effect could be used as a surgical tool to indicate when sufficient impaction has been achieved in cementless devices, and that periodic assessment of interfacial integrity may also be possible. All of the acoustic information obtained within this thesis was corroborated with μ-CT, and unfortunately it was not possible to scan the construct with the stem in-situ. This eliminated the possibility of using rough stainless steel stems for any of the experiments. However, a separate testing programme may integrate μ-CT corroboration with rough stems if the stem material is changed to aluminium, which has a

similar radiographic absorption to bone-cement and will therefore avoid issues of scatter and contrast variations. Alternatively, other corroborative techniques such as ultrasound could be used to verify the presence of interfacial debonding – effectively building on the previous work of Browne et al[141]. However, this method would require the tests to be run dry since the presence of a fluid may affect the acoustic reflections across the debonded regions and so appear falsely bonded. Overall, if the inter-sensor attenuation and speed of sound effects proved effective for use in rough stem systems then it would add significant weight to the assessment of aseptic loosening as a whole since the system in its own right could be used to verify whether acoustic activity indicative of failure had indeed triggered loosening. Furthermore, it may be possible to establish not only the presence of failure mechanisms, but actually incorporate some form of quantitative assessment of the extent of critical damage.

Analysis of cement formulations and pre-load crack formation

As discussed in Chapter 5, the AE technique was shown to be able to detect, locate and investigate when pre-load cracking occurred within the Technovit layer of the simplified construct. Due to the design of the centralising jig used to hold the stem in position during polymerisation it was not possible to utilise the embedded sensors for this analysis. However, by altering the jig configuration, it would be possible to do this and so assess different cement formulations without inducing inter-experimental variability through the removal and reattachment of external sensors.

Incorporation into commercial stems and representative constructs

The simplified stem used for all of the tests described within this thesis was largely intended to induce damage within the cement mantle. Obviously, this is not the intention of clinical systems; however, it is hypothesised that the same methods used to embed the sensors into the simplified stem could be applied to commercial stems. To a large extent this has already been demonstrated with the incorporation of an embedded sensor into a resurfacing femoral head component as described in chapter 8. To use the system as a widespread pre-clinical testing tool, the sensors would have to be incorporated into a variety of commercially available femoral stems and shown to operate effectively in this environment. The same is true for the use of the system within representative bone simulations. As stated earlier, Tufnol was used in these experiments in order to minimise complications of signal attenuation, location error, and minimise erroneous signals.

However, to build on the work of Qi et al[150] the hypothesis that their location accuracy could have been improved through the use of embedded sensors must be established. It is unlikely that 3D location resolution could ever be achieved using the present system due to the geometry of the femoral stem; however, 2D location accuracy could be assessed.

Progressing towards a self contained system for clinical implantation

Although this thesis has mainly focussed on the development of an instrumented implant for *in-vitro* testing, it has been noted that the idea could be transposed to a clinical device. Bergmann[181] demonstrated that joint contact forces could be measured using an instrumented implant, and an instrumented AE monitoring implant may similarly be developed either as a stand alone system, or perhaps complimentary to Bergmann's system.

The ability to predict failure from the earliest stages of damage initiation and follow the chronological order of damage accumulation are without doubt advantageous. However, the justification for directly embedding these sensor technologies within an endoprosthesis is perhaps less apparent at this stage. It is envisaged that the system could be used to monitor the fixation of both cementless and cemented devices using a personal device interface such as a mobile phone application. This would allow the condition of the prosthesis to be monitored during a range of unrestricted activities. Current monitoring using radiographic imaging, or external vibration/AE analysis restricts the patient to a limited range of activities due to the physical restrictions of the equipment. An instrumented prosthesis may allow more realistic environmental testing *in-vitro*, and the same advantage is envisaged *in-vivo*. The reasons for obtaining such information are multi-factorial:

Firstly, from a research point of view, a great deal of information regarding the dynamic behaviour of THR devices may be obtained from a select group of instrumented prostheses. That is the most likely end-point application for a system of this nature, and several examples of instrumented prostheses that were used for small scale research projects are reported in the literature[45,46,132,168,171-174,204,222-225]. Rydell[172] was the first to successfully incorporate instrumentation within a hip prosthesis using transcutaneous leads to extract information from and supply power to the device. Due to risks related to infection, the leads had to be removed after a short period - greatly limiting the amount of

information that could be collected post operatively. Since the intended use for the device discussed in this thesis is to provide long term condition monitoring, the use of transcutaneous leads is not appropriate, and unnecessary with today's wireless technology. Carlson et al[173] developed a telemetry system for monitoring surface pressures in the hip joint using an inductive loop to power the device, however other authors developing instrumented prostheses around that period shied away from telemetry systems based on financial considerations[222]. English and Kilvinton[174] later used battery powered telemetry system to report joint forces measured *in-vivo* for one patient. Hodge et al[45] used the same telemetry system as developed by Carlson et al[173], and indeed the use of inductive coils to power telemetry systems for monitoring hip joint forces became the system of choice for many of the subsequent devices[46,132,168,171,223-225] barring Davy et al's[204] battery powered system. It would therefore seem logical to build on all of this established work; however, the choice of power source and method for transmitting data should be reviewed. Wireless transmission has seen significant growth in recent years; Bluetooth technology is now enabled on most mobile phone devices and portable computers which may provide a convenient interface for both patients and surgeons. Battery technology has also seen significant improvements, and energy harvesting techniques may also provide an elegant solution on order to provide a long term power source.

Secondly, it has been shown that early revision significantly reduces the risk of complications in surgery and careful monitoring is the only way to identify loosening before too much of the bone stock is destroyed[6]. The predicted performance of *in-vivo* endoprosthetic devices is currently established and optimised using in vitro and in silico methods. However, there are occasions where implants have failed unexpectedly *in-vivo* with expensive consequences: the Capital hip, the Elite plus, the Sulzer Muller prosthesis, the porous coated Exeter hip stem, as well as “improved” bone cements such as Boneloc and “improved” UHMWPE such as Hylamer; all suggestive that the pre-clinical testing of devices and *in-vivo* monitoring need to see improvements. Registry information has been shown to be essential information that can feed into implant designs/materials/implantation techniques. Unfortunately, this information can only highlight poor performing implants/bone cement formulation/implantation techniques after multiple failures have been detected through the current monitoring techniques i.e. patient pain scores and standard radiographic imaging; methods that detect failure late or even after failure has occurred. This results in a delayed feedback situation during which time there may be

many poor implant designs implanted in to patients that will subsequently require revision. Therefore a system that can detect early signs of loosening without necessitating ionising radiation or periodic review via hospital appointments would represent a step change in the information available to design engineers, clinicians, and patients alike. However, the use of embedded AE sensors in an attempt to address the clinical monitoring aspect of this problem would involve instrumentation on a massive scale. It is unlikely, that the present costs associated with instrumentation, and implementation would allow such a development. However, ongoing advances in miniaturised low cost electronics may result in this becoming feasible in the future.

The use of thick film technology

As discussed in Chapter 3, thick film devices have the potential for significant cost benefits for large-scale device manufacture. The use of bulk PZT was used throughout this thesis due to the ease of incorporation into the stem, and because it is an established material that is used in commercial AE sensors. In this respect, the use of bulk PZT in embedded sensors remains useful for prototype development and small-scale *in-vitro* test procedures. However, for the progression to an *in-vivo* system then thick film technology may be able to provide a cost efficient and space saving alternative. Having said that, there are substantial obstacles that must be overcome in order to successfully integrate a thick film sensor into a femoral stem - namely the ability to fire the paste directly onto the stem. An alternative would be to fire the paste onto separate substrates and then fix these inside the stem separately, however, this would negate one of the main envisaged advantages of the thick film process which is the quality of fixation between the paste and the stem and avoidance of the sensor-stem interface altogether.

REFERENCES

1. Huiskes R. Failed Innovation in Total Hip Replacement. Acta Orthopaedica Scandinavica 1993;64(6):699-716.
2. Sarmiento A. Staying the Course. Journal of Bone and Joint Surgery 1991;73-A(4):479-483.
3. Gheduzzi S, Miles AW. A Review of Pre-Clinical Testing of Femoral Stem Subsidence and Comparison with Clinical Data. Proceedings of the Institution of Mechanical Engineers, Part H: Journal of Engineering in Medicine 2007;221(1):39-46.
4. Faro LMC, Huiskes R. Quality Assurance of Joint Replacement Legal Regulation and Medical Judgement. Acta Orthopaedica Scandinavica 1992;63(s250):1-33.
5. Ling R. The Use of a Collar and Precoating on Cemented Femoral Stems Is Unnecessary and Detrimental. Clinical Orthopaedics and Related Research 1992;285:73-83.
6. Müller M. Lessons of 30 Years of Total Hip Arthroplasty. Clinical Orthopaedics and Related Research 1992;274:12-21.
7. Barnett CH, Cobbold AF. Lubrication within Living Joints. Journal of Bone and Joint Surgery 1962;44-B(3):662-674.
8. National Joint Registry for England and Wales 5th Annual Report; 2008.
9. Gluck T. Autoplastik-Transplantation-Implantation Von Fremdkörpern. Berlin klinische Wochenschrift 1894;27:421-427.
10. Riska EB. Ceramic Endoprosthesis in Total Hip Arthroplasty. Clinical Orthopaedics and Related Research 1993;297:87-94.
11. Bergmann G, Graichen F, Rohlmann A. Hip Joint Contact Forces During Stumbling. Langenbeck's Archives of Surgery 2004;389(1):53-59.
12. Joshi MG, Advani SG, Miller F, Santare M. Analysis of a Femoral Hip Prosthesis Designed to Reduce Stress Shielding. Journal of Biomechanics 2000;33:1655-1662.
13. Silva MJ, Sandell LJ. What's New in Orthopaedic Research. Journal of Bone and Joint Surgery 2002;84-A(8):1490-6.
14. Mann KA, Ayers DC, Damron LA. Effects of Stem Length on Mechanics of the Femoral Hip Component after Cemented Revision. Journal of Orthopaedic Research 2005;15(1):62-68.
15. Stone MH, Wilkinson R, Stother IG. Some Factors Affecting the Strength of the Cement-Metal Interface. Journal of Bone and Joint Surgery 1989;71-B:217-21.
16. Fowler JL, Gie GA, Lee AJC, Ling RSM. Experience with the Exeter Total Hip Replacement since 1970. The Orthopaedic clinics of North America 1988;19(3):477-89.
17. Rockborn P, Olsson SS. Loosening and Bone Resorption in Exeter Hip Arthroplasties. Journal of Bone and Joint Surgery 1993;75-B:865-868.
18. Maguire JK, Coscia MF, Lynch MH. Foreign Body Reaction to Polymeric Debris Following Total Hip Arthroplasty. Clinical Orthopaedics and Related Research 1987;216:213-223.
19. Kärrholm J, Garellick G, Rogmark C, Herberts P. Swedish Hip Arthroplasty Register Annual Report 2007: Sahlgrenska University Hospital; 2008.
20. Kärrholm J, Anderber C, Snorrason F, Thanner J, Langeland N, Malchau H, Herberts P. Evaluation of a Femoral Stem with Reduced Stiffness : A Randomized Study with Use of Radiostereometry and Bone Densitometry. Journal of Bone and Joint Surgery 2002;84-A:1651-1658.
21. Huiskes R, Weinans H, Harrie MS, Rietbergen BV. The Relationship between Stress Sheilding and Bone Resorption around Total Hip Stems and the Effects of Flexible Materials. Clinical Orthopaedics and Related Research 1992;274:124-134.
22. Weinans H, Sumner DR. Finite Element Analyses to Study Periprosthetic Bone Adaptation. In: Lowet G, Ruegsegger P, Weinans H, Meunier A, (eds). Bone Research in Biomechanics. Amsterdam: ISO Press; 1997. p 3-16.
23. Evans SL, Gregson PJ. Composite Technology in Load-Bearing Orthopaedic Implants. Biomaterials 1998;19(15):1329-1342.
24. Gravius S, Wirtz DC, Siebert CH, Andereya ST, Muller-Rath R, Maus U, Mumme T. In Vitro Interface and Cement Mantle Analysis of Different Femur Stem Designs. Journal of Biomechanics 2008;41:2021-2028.
25. Weightman B, Freeman MAR, Revell PA, Braden M, Alberktsson BEJ, Carlson LV. The Mechanical Properties of Cement and Loosening of the Femoral Component of Hip Replacements. The Journal of Bone and Joint Surgery 1987;69-B(4):558-564.
26. Charnley J, Kamangar A, Longfield MD. The Optimum Size of Prosthetic Heads in Relation to the Wear of Plastic Sockets in Total Replacement of the Hip. Medical and Biological Engineering and Computing 1968;7(1):31-39.

27. Dumbleton JH, Manley MT. Metal-on-Metal Total Hip Replacement What Does the Literature Say? The Journal of Arthroplasty 2005;20(2):174-188.
28. Burroughs BR, Hallstrom B, Golladay GJ, Hoeffel D, Harris WH. Range of Motion and Stability in Total Hip Arthroplasty with 28-, 32-, 38-, and 44-mm Femoral Head Sizes. The Journal of Arthroplasty 2005;20(1):11-19.
29. Smith SL, Dowson D, Goldsmith AAJ. The Effect of Femoral Head Diameter Upon Lubrication and Wear of Metal-on-Metal Total Hip Replacements. Proceedings of the Institution of Mechanical Engineers, Part H: Journal of Engineering in Medicine 2001;215(2):161-170.
30. Eastaugh-Waring SJ, Seenath S, Learmonth DS, Learmonth ID. The Practical Limitations of Resurfacing Hip Arthroplasty. The Journal of Arthroplasty 2006;21(1):18-22.
31. Naal F-D, Maffiuletti NA, Munzinger U, Hersche O. Sports after Hip Resurfacing. The American Journal of Sports Medicine 2007;35(5):705-711.
32. Charnley J. The Bonding of Prostheses to Bone by Cement. The Journal of Bone and Joint Surgery 1964;46-B(3):518-529.
33. Jones LC. Cement Disease. Clinical Orthopaedics and Related Research 1987;255:192-206.
34. Huiskes R. The Various Stress Patterns of Press-Fit, Ingrown, and Cemented Femoral Stems. Clinical Orthopaedics and Related Research 1990;261:27-38.
35. Burke DW, O'Connor DO, Zalenski EB, Jasty M, Harris WH. Micromotion of Cemented and Uncemented Femoral Components. Journal of Bone and Joint Surgery 1991;73-B(1):33-37.
36. Pilliar RM, Lee JM, Maniatopoulos C. Observations on the Effect of Movement on Hone Ingrowth into Porous-Surfaced Implants. Clinical Orthopaedics and Related Research 1986;208:108-113.
37. Callaghan JJ. The Clinical Results and Basic Science of Total Hip Arthroplasty with Porous-Coated Prostheses. The Journal of Bone and Joint Surgery 1993;75-A(2):299-310.
38. Berger RA, Kull LR, Rosenberg AG, Galante JO. Hybrid Total Hip Arthroplasty. Clinical Orthopaedics and Related Research 1996;333:134-146.
39. McLaughlin JR, Lee KR. The Outcome of Total Hip Replacement in Obese and Non-Obese Patients at 10- to 18-Years. Journal of Bone and Joint Surgery 2006;88-B(10):1286-1292.
40. Paterno SA, Lachiewicz PF, Kelly SS. The Influence of Patient-Related Factors and the Position of the Acetabular Component on the Rate of Dislocation after Total Hip Replacement. Journal of Bone and Joint Surgery 1997;79:1202-1210.
41. Sundfelt M, Carlsson LV, Johansson CB, Thomsen P, Gretzer C. Aseptic Loosening, Not Only a Question of Wear - a Review of Different Theories. Acta Orthopaedica 2006;77(2):177-197.
42. DiPisa JA, Sih GS, Berman AT. The Temperature Problem at the Bone-Acrylic Cement Interface of the Total Hip Replacement. Clinical Orthopaedics and Related Research 1976;121:95-98.
43. Gruen TA, MvNeice GM, Amstutz HC. "Modes of Failure" Of Cemented Stem-Type Femoral Components. Clinical Orthopaedics and Related Research 1979;141:17-27.
44. Bergmann G, Deuretzbacher G, Heller M, Graichen F, Rohlmann A, Strauss J, Duda GN. Hip Contact Forces and Gait Patterns from Routine Activities. Journal of Biomechanics 2001;34(7):859.
45. Hodge WA, Fijan RS, Carlson KL, Burgess RG, Harris WH, Mann RW. Contact Pressures in the Human Hip Measured in Vivo. Proceedings of the National Academy of Scinces of the United States of America 1986;83:2879-2883.
46. Graichen F, Bergmann G, Rohlmann A. Hip Endoprosthesis for in Vivo Measurement of Joint Force and Temperature. Journal of Biomechanics 1999;32:1113-1117.
47. Agarwal S. Osteolysis - Basic Science, Incidence and Diagnosis. Current Orthopaedics 2004;18:220-231.
48. Manolagas SC. Birth and Death of Bone Cells: Basic Regulatory Mechanisms and Implications for the Pathogenesis and Treatment of Osteoporosis. Endocrine Reviews 2000;21(2):115-137.
49. Dimitriou R, Tsiridis E, Giannoudis PV. Current Concepts of Molecular Aspects of Bone Healing. Injury 2005;36(12):1392-1404.
50. Aspenberg P, van der Vis H. Fluid Pressure May Cause Periprosthetic Osteolysis: Particles Are Not the Only Thing. Acta Orthopaedica Scandinavica 1998;69(1):1-4.
51. Haboush EJ. A New Operation for Arthroplasty of the Hip. Buletin of the Hospital for Joint Diseases 1953;14:242.
52. Charnley J. Anchorage of the Femoral Head Prosthesis to the Shaft of the Femur. The Journal of Bone and Joint Surgery 1960;42-B(1):28-30.
53. Roques A. Novel Approaches to the Structural Integrity Assessment of Acrylic Bone Cement as Part of the Bone/Cement/Stem Construct, Phd: University of Southampton; 2003.
54. Bloch B. Bonding of Fractures by Plastic Adhesives. The Journal of Bone and Joint Surgery 1958;40-B(4):804-812.
55. Heiss C, Kraus R, Schluckledier D, Stiller A-C, Wenisch S, Schnettler R. Bone Adhesives in Trauma and Orthopedic Surgery. European Journal of Trauma 2006;32:141-148.

56. Herberts P, Ahnfelt L, Malchau H, Strömberg C, Anderson GBJ. Multicenter Clinical Trials and Their Value in Assessing Total Joint Arthroplasty. Clinical Orthopaedics and Related Research 1989;249:48-55.
57. Wroblewski BM, Siney PD. Charnley Low-Friction Arthroplasty of the Hip: Long-Term Results. Clinical Orthopaedics and Related Research 1993;292.
58. Judet J, Judet R. The Use of an Artificial Femoral Head for Arthroplasty of the Hip Joint. The Journal of Bone and Joint Surgery 1950;32-B(2):166-173.
59. Harris WH. Osteolysis and Particle Disease in Hip Replacement a Review. Acta Orthopaedica Scandinavica 1994;65(1):113-123.
60. Willert HG, Ludwig J, Semlitsch M. Reaction of Bone to Methacrylate after Hip Arthroplasty: A Long-Term Gross, Light Microscopic, and Scanning Electron Microscopic Study. The Journal of Bone and Joint Surgery 1974;56-A:1368-1382.
61. Mjöberg B, Pettersson H, Rosenqvist R, Rydholm A. Bone Cement, Thermal Injury and the Radiolucent Zone. Acta Orthopaedica Scandinavica 1984;55:597-600.
62. Lidgren L, Bodelind B, Möller J. Bone Cement Improved by Vacuum Mixing and Chiiiing. Acta Orthopaedica Scandinavica 1987;57:27-32.
63. Li C, Schmid S, Mason J. Effects of Pre-Cooling and Pre-Heating Procedures on Cement Polymerization and Thermal Osteonecrosis in Cemented Hip Replacements. Medical Engineering and Physics 2003;25:559-564.
64. Dahl OE, Garvik LJ, Lyberg T. Toxic Effects of Methylmethacrylate Monomer on Leukocytes and Endothelial Cells in Vitro. Acta Orthopaedica Scandinavica 1994;65(2):147-153.
65. Meyer PR, Lautenschlager EP, Moore BK. On the Setting Properties of Acrylic Bone Cement. The Journal of Bone and Joint Surgery 1973;55:149-156.
66. Reckling FW, Dillon WL. The Bone-Cement Interface Temperature During Total Joint Replacement. The Journal of Bone and Joint Surgery 1977;59:80-82.
67. Pitto RP, Koessler M, Kuehle JW. Comparison of Fixation of the Femoral Component without Cement and Fixation with Use of a Bone-Vacuum Cementing Technique for the Prevention of Fat Embolism During Total Hip Arthroplasty. The Journal of Bone and Joint Surgery 1999;81-A(6):831-843.
68. Donaldson AJ, Thompson HE, Harper NJ, Kenny NW. Bone Cement Implantation Syndrome. British Journal of Anaesthesia 2009;102(1):12-22.
69. Parvizi J, Holiday AD, Ereth MH, Lewallen DG. Sudden Death During Primary Hip Arthroplasty. Clinical Orthopaedics and Related Research 1999;369:39-48.
70. Orsini EC, Byrick RJ, Mullen JBM, Kay JC, Waddell JP. Cardiopulmonary Function and Pulmonary Microemboli During Arthroplasty Using Cemented or Non-Cemented Components the Role of Intramedullary Pressure. Journal of Bone and Joint Surgery 1987;69:822-832.
71. Byrick RJ, Bell RS, Kay JC, Waddell JP, Mullen JB. High-Volume High-Pressure Pulsatile Lavage During Cemented Arthroplasty. Journal of Bone and Joint Surgery 1989;71-A:1331-1336.
72. Petterson B, Healey J, Cornell C, Sharrock N. Cardiac Arrest During Hip Arthroplasty with a Cemented Long-Stem Component. A Report of Seven Cases. Journal of Bone and Joint Surgery 1991;73:271-277.
73. Dunne NJ, Orr JF. Influence of Mixing Techniques on the Physical Properties of Acrylic Bone Cement. Biomaterials 2001;22:1819-1826.
74. James SP, Schmalzried TP, McGarry FJ, Harris WH. Extensive Porosity at the Cement-Femoral Prosthesis Interface: A Preliminary Study. Journal of Biomedical Materials Research 2004;27(1):71-78.
75. Wixson RL, Lautenschlager EP, Novak MA. Vacuum Mixing of Acrylic Bone Cement. Journal of Arthroplasty 1987;2(2):141-149.
76. Messick KJ, Miller MA, Damron LA, Race A, Clarke MT, K.T M. Vacuum-Mixing Cement Does Not Decrease Overall Porosity in Cemented Femoral Stems an in Vitro Laboratory Investigation. Journal of Bone Joint Surgery 2007;89-B(8):1115-1121.
77. Muller SD, Green SM, McCaskie AW. The Dynamic Volume Changes of Polymerising Polymethyl Methacrylate Bone Cement. Acta Orthopaedica Scandinavica 2002;73(6):684-687.
78. Malefijt JdeWaal, Sloof TJJH, Huiskes R. The Actual Staus of Acrylic Bone Cement in Total Hip Replacement - a Review. Acta Orthopaedica Belgica 1987;53:52-58.
79. Kwong FCNK, Power RA. Comparison of Bone Cement Shrinkage between Different Polymethylmethacrylate Commercial Preparations in Use. Journal of Bone and Joint Surgery 2006;88-B(s2):237.
80. Li C, Wang Y, Mason J. The Effects of Curing History on Residual Stresses in Bone Cement During Hip Arthroplasty. Journal of Biomedical Materials Research 2004;70B:30-36.

81. Lennon AB, Prendergast PJ. Residual Stress Due to Curing Can Initiate Damage in Porous Bone Cement: Experimental and Theoretical Evidence. Journal of Biomechanics 2002;35:311-321.
82. Gilbert JL, Hasenwinkel JM, Wixson RL, Lautenschlager EP. A Theoretical and Experimental Analysis of Polymerization Shrinkage of Bone Cement: A Potential Major Source of Porosity. Journal of Biomedical Materials Research 2000;52:210-218.
83. Orr JF, Dunne NJ, Quinn JC. Shrinkage Stresses in Bone Cement. Biomaterials 2003;24:2933-2940.
84. Race A, Miller MA, Ayers DC, Mann KA. Early Cement Damage around a Femoral Stem Is Concentrated at the Cement/Bone Interface. Journal of Biomechanics 2003;36:489-496.
85. Roques A, Browne M, Taylor A, New A, Baker D. Quantitative Measurement of the Stresses Induced During Polymerisation of Bone Cement. Biomaterials 2004;25(18):4415-4424.
86. Topoleski LDT, Ducheyne P, Cuckler JM. A Fractographic Analysis of in Vivo Poly(Methylmethacrylate) Bone Cement Failure Mechanisms. Journal of Biomedical Materials Research 1990;24:135-154.
87. Culleton TP, Prendergast PJ, Taylor D. Fatigue Failure in the Cement Mantle of an Artificial Hip Joint. Clinical Materials 1993;12:95-102.
88. Jasty M, Maloney WJ, Bragdon CR, O'Connor DO, Haire T, Harris WH. The Initiation of Failure in Cemented Femoral Components of Hip Arthroplasties. The Journal of Bone and Joint Surgery 1991;73-B(4):551-558.
89. Lewis G. Fatigue Testing and Performance of Acrylic Bone-Cement Materials: State-of-the-Art Review. Journal of Biomedical Materials Research 2002;66-B(1):457-486.
90. Davies JP, O'Connor DO, Burke DW, Harris WH. Influence of Antibiotic Impregnation on the Fatigue Life of Simplex P and Palacos R Acrylic Bone Cements, with and without Centrifugation. Journal of Biomedical Materials Research 1988;23(4):379-397.
91. Murray WR. Use of Antibiotic-Containing Bone Cement. Clinical Orthopaedics and Related Research 1984;190:89-95.
92. Koole LH, Kruft MB, Colnot JM, Kuijer R, Bulstra SK. Studies on a New, All-Polymeric Radiopaque Orthopaedic Bone Cement; Transactions of the 25th Annual Meeting of Society Biomaterials; 1999; Rhode Island. p 316.
93. Molino LN, Topoleski LDT. Effect of BaSO4 on the Fatigue Crack Propagation Rate of PMMA Bone Cement. Journal of Biomedical Materials Research 1996;31:131-137.
94. Baleani M, Cristofolini L, Minari C, Toni A. Fatigue Strength of PMMA Bone Cement Mixed with Gentamicin and Barium Sulphate Vs Pure PMMA. Proceedings of the Institution of Mechanical Engineers, Part H: Journal of Engineering in Medicine 2003;217:9-12.
95. Bhambri SK, Gilbertson LN. Micromechanisms of Fatigue Crack Initiation and Propagation in Bone Cements. Journal of Biomedical Materials Research 1995;29:233-237.
96. Ishihara S, McEvily AJ, Goshima T, Kanekasu K, Nara T. On Fatigue Lifetimes and Fatigue Crack Growth Behaviour of Bone Cement. Journal of Materials Science: Materials in Medicine 2000;11:661-666.
97. Ling RSM, Lee AJC. Porosity Reduction in Acrylic Cement Is Clinically Irrelevant. Clinical Orthopaedics and Related Research 1998;355:249-253.
98. Geiger MH, Keating EM, Ritter MA, Ginther JA, Faris PM. The Clinical Significance of Vacuum Mixing Bone Cement. Clinical Orthopaedics and Related Research 2001;382:258-266.
99. Malchau H, Herberts P, Söderman P, Odén A. Prognosis of Total Hip Replacement: Update and Validation of Results from the Swedish National Hip Arthroplasty Registry. 2000. Web Page. www.jru.orthop.gu.se
100. Hoey D, Taylor D. Fatigue in Porous PMMA: The Effect of Stress Concentrations. International Journal of Fatigue 2008;30:989-995.
101. Mavrogordato M.N, Taylor M, Taylor A, M. B. Acoustic Emission Monitoring and 3D Visualization of Polymerization-Induced Damage of Acrylic Polymer Materials. Journal of Biomedical Materials Research 2008;90-B(1):223-228.
102. Topoleski LDT, Ducheyne P, Cuckler JM. Microstructural Pathway of Fracture in Poly(Methyl Methacrylate) Bone Cement. Biomaterials 1993;14:1165-72.
103. Sinnett-Jones PE, Browne M, Moffat AJ, Jeffers JRT, Saffari N, J.Y B, Sinclair I. Crack Initiation Processes in Acrylic Bone Cement. Journal of Biomedical Materials Research 2008;89A(4):1088-1097.
104. Evans SL. Fatigue Crack Propagation under Variable Amplitude Loading in PMMA and Bone Cement. Journal of Materials Science: Materials in Medicine 2007;18:1711-1717.
105. Döll W, Könczöl L. Micromechanics of Fracture under Static and Fatigue Loading: Optical Interferometry of Crack Tip Craze Zones Crazing in Polymers Vol. 2: Springer Berlin / Heidelberg; 1990. p 137-214.

106. Pulos GC, Knauss WG. Nonsteady Crack and Craze Behavior in PMMA under Cyclical Loading: Ii. Effect of Load History on Growth Rate and Fracture Morphology. International Journal of Fracture 1998;93:161-185.
107. Pulos GC, Knauss WG. Nonsteady Crack and Craze Behavior in PMMA under Cyclical Loading: I. Experimental Preliminaries. International Journal of Fracture 1998;93:145-159.
108. Pulos GC, Knauss WG. Nonsteady Crack and Craze Behavior in PMMA under Cyclical Loading: Iii. Effect of Load History on Cohesive Force Distribution on the Craze. International Journal of Fracture 1998;93:187-207.
109. Koenczoel L, Hiltner A, Baer E. Crazing and Fracture in Polystyrene Studied by Acoustic Emission. Journal of Applied Physics 1986;60(8):2651-2654.
110. Johnson JA, Provan JW, Krygler JJ, Chan KH, Miller J. Fatigue of Acrylic Bone Cement - Effect of Frequency and Environment. Journal of Biomedical Materials Research 2004;23(8):819-831.
111. Cristofolini L, Erani P, Savigni P, Bordini B, Viceconti M. Preclinical Assessment of the Long-Term Endurance of Cemented Hip Stems. Part 2: In-vitro and Ex-Vivo Fatigue Damage of the Cement Mantle. Proceedings of the Institution of Mechanical Engineers, Part H: Journal of Engineering in Medicine 2007;221(6):585-599.
112. Murphy BP, Predergast PJ. On the Magnitude and Variability of the Fatigue Strength of Acrylic Bone Cement. International Journal of Fatigue 2000;22:855-864.
113. Total Hip Replacement: A Guide to Best Practice: British Orthopaedic Association; 1999. 1-12.
114. Bankes MJ, Coull R, Ferris BD. How Long Should Patients Be Followed-up after Total Hip Replacement? Current Practice in the Uk. Annals of the Royal Collage of Surgeons of England 1999;81(5):348-351.
115. Bhatia M, Obadare Z. An Audit of the out-Patient Follow-up of Hip and Knee Replacements. Annals of the Royal Collage of Surgeons of England 2003;85:32-35.
116. Browne M, Roques A, Taylor A. The Acoustic Emission Technique in Orthopaedics - a Review. Journal of Strain Analysis 2004;40(1):59-79.
117. Selvik G. Roentgen Stereophotogrrammetry: A Method for the Study of the Kinematics of the Skeletal System. Acta Orthopaedica Scandinavica 1989;s232:1-51.
118. Kärrholm J, Borssén B, Löwenhielm G, Snorrason F. Does Early Micromotion of Femoral Stem Prostheses Matter? Journal of Bone and Joint Surgery 1994;76-B:912-917.
119. Hauptfleisch J, Glyn-Jones S, Beard DJ, Gill HS, Murray DW. The Premature Failure of the Charnley Elite-Plus Stem a Confirmation of Rsa Predictions. Journal of Bone and Joint Surgery 2006;88-B(2):179-83.
120. Walker PS, Mai SF, Cobb AG, Bently G, Hua J. Prediction of Clinical Outcome of Thr from Migration Measurements on Standard Radiographs. Journal of Bone and Joint Surgery 1995;77-B:705-714.
121. Wilkinson MJ, Stockley I, Peel NFA, Hamer AJ, Elson RA, Barrington AN, Eastell R. Effect of Pamidronate in Preventing Local Bone Loss after Total Hip Arthroplasty: A Randomised, Double-Blind, Controlled Trial. Journal of Bone and Mineral Research 2001;16(3):556-564.
122. Wilkinson MJ, Hamer AJ, Rogers A, Stockley I, Eastell R. Bone Mineral Density and Biolchemical Markers of Bone Turnover in Aseptic Loosening after Total Hip Arthroplasty. Journal of Orthopaedic Research 2003;21:691-696.
123. Kwong LM, Jasty M, Mulroy RD, Maloney WJ, Bragdon C, Harris WH. The Histology of the Radiolucent Line. Journal of Bone and Joint Surgery 1992;74-B:67-73.
124. Mjöberg B, Brismar J, Hansson LI, et al. Definition of Endoprosthetic Loosening: Comparison of Arthrography, Scintigraphy and Roentgen Stereophotogrammettry in Prosthetic Hips Acta Orthopaedica Scandinavica 1985;56:469-473.
125. Murray DW, Carr AJ, Bulstrode CJ. Which Primary Total Hip Replacement? Journal of Bone and Joint Surgery 1995;77-B:520-527.
126. Kaneko T, Nagai Y, Ogino M, Futami T, Ichimura T. Acoustoelectric Technique for Assesing the Mechanical State of the Dental Implant-Bone Interface. Journal of Biomedical Materials Research 1986;20(2):169-176.
127. Kaneko T. Pulsed Oscillation Technique for Assessing the Mechanical State of the Dental Implant-Bone Interface. Biomaterials 1991;12:555-560.
128. Meredith N, Alleyne D, Crawley P. Quantitive Determination of the Stability of the Implant-Tissue Interface Using Resonance Frequency Analysis. Clinical Oral Implant Research 1996(7):261-267.
129. Glauser R, Sennerby L, Meredith N, Ree A, Lundgren AK, Gottlow J, Hammerle CHF. Resonance Frequency Analysis of Implants Subject to Immediate or Early Functional Occlusal Loading. Clinical Oral Implant Research 2004(15):428-434.
130. Rosenstein AD, McCoy GF, Bulstrode CJ, McLardy-Smith PD, Cunningham JL, Turner-Smith AR. The Differentiation of Loose and Secure Femoral Implants in Total Hip Replacement Using a

Vibrational Technique: An Anatomical and Pilot Clinical Study. Proceedings of the Institution of Mechanical Engineers, Part H: Journal of Engineering in Medicine 1989:77-81.
131. Collier RJ, Donarski RJ, Worley AJ, Lay A. The Use of Externally Applied Mechanical Vibrations to Assess Both Fractures and Hip Prostheses. Oxford Medical Engineering Series: Micromovement in Orthopaedics 1993:151-163.
132. Puers R, Catrysse M, Vandevoorde G, Collier RJ, Louridas E, Burny F, Donkerwolcke M, Moulart F. A Telemetry System for the Detection of Hip Prosthesis Loosening by Vibration Analysis. Sensors and Actuators 2000;85:42-47.
133. Georgiou AP, Cunningham JL. Accurate Diagnosis of Hip Prosthesis Loosening Using a Vibrational Technique. Clinical Biomechanics 2001;16:315-323.
134. Pastrav CL, Jaecques SVN, Mulier M, Van der Perre G. Determination of Total Hip Replacement Stem Insertion Endpoint and Stability Assessment by Vibration Analysis: First Experiences with Per-Operative Measurements; ISMA; 2006; Leuven p897-908.
135. Szabo TL. Diagnostic Ultrasound Imaging: Inside Out. Boston: Elsevier Academic Press; 2004. ISBN: 0-12-680145-2.
136. Cheeke JD. Fundamentals and Applications of Ultrasonic Waves: CRC Press; 2002. ISBN: 0-8493-0130-0.
137. Davies JP, Tse MK, Harris WH. In Vitro Evaluation of Bonding of the Cement-Metal Interface of a Total Hip Femoral Component Using Ultrasound. Journal of Orthopaedic Research 1995;13:335-338.
138. Gibbon WW, Long G, Barron DA, O'Connor PJ. Complications of Orthopaedic Implants: Sonographic Evaluation. Journal of Clinical Ultrasound 2001;30:288-299.
139. Carbó S, Rosón N, Vizcaya S, Escribano F, Zarcero M, Medrano S. Can Ultrasound Help to Define Orthopaedic Surgical Complications? Current Problems in Diagnostic Radiology 2006;35:75-89.
140. Ostlere S, Soin S. Imaging of Prosthetic Joints. Imaging 2003;15:270-285.
141. Browne M, Jeffers JRT, Saffari N. Non-Destructive Evaluation of Bone Cement and Bone Cement/Metal Interface Failure. Journal of Biomedical Materials Research 2009;92-B(2):420-429.
142. Beattie AG. Acoustic Emission, Principles and Instrumentation. Journal of Acoustic Emission 1983;2:95-128.
143. Holroyd T. Acoustic Emissions and Ultrasonics: Coxmoor; 2000 p 1-147. ISBN.
144. Vellekoop MJ. Acoustic Wave Sensors and Their Technology. Ultrasonics 1998;36(7):1-5.
145. Viktorov IA. Rayleigh and Lamb Waves: Plenum Press; 1967. ISBN.
146. Drafts B. Acoustic Wave Technology Sensors. 2000. Web Page. www.sensormag.com
147. Ng ET, Qi G. Material Fatigue Behaviour Characterization Using the Wavelet-Based Ae Technique - a Case Study of Acrylic Bone Cement. Engineering Fracture Mechanics 2001;68(13):1477-1492.
148. Roques A, Browne M, Thompson J, Rowland C, Taylor A. Investigation of Fatigue Crack Growth in Acrylic Bone Cement Using the Acoustic Emission Technique. Biomaterials 2004;25(5):769-778.
149. Sundaresan MJ, Henneke EG, Reifsnider KL. Prediction of Fatigue Life of Composite Femoral Prostheses Using Acoustic-Emission Technique. Journal of Composites Technology Research 1994;16(2):127-131.
150. Qi G, Mann KA, Mouchon WP, Hamstad MA, Salehi A, Whitten SA. 3D Real Time Methodology Monitoring Cement Failures in Tha. Journal of Biomedical Materials Research 2004;71-A(3):391-402.
151. Davies JP, Tse MK, Harris WH. Monitoring the Integrity of the Cement-Metal Interface of Total Joint Components in Vitro Using Acoustic Emission and Ultrasound. Journal of Arthroplasty 1996;11(5):594-601.
152. Kohn DH. Acoustic Emission and Non Destructive Evaluation of Biomaterials and Tissues. Critical Reviews in Biomedical Engineering 1995;23(3/4):221-306.
153. Gao XJ, Murota K, Tomita Y, MOno, Higo Y, Nunomura S. Evaluation of the Fixation of Artificial Hip-Joint by Acoustic-Emission. Japanese Journal of Applied Physics 1990;29(1):215-217.
154. Schwalbe-J H, Bamfaste G, Franke-J R. Non-Destructive and Non-Invasive Observation of Friction and Wear of Human Joints and of Fracture Initiation by Acoustic Emission. Proceedings of the Institute of Mechanical Engineers 1999;213(H):41-48.
155. Funk JR, Bass CR, Rudd R, Crandall JR, Tourret L, McMahon C. Dynamic Crack Detection in the Human Tibia Using Acoustic Emission; Biomechanics Research: Experimental and Computational, Proceedings of the Twenty Seventh International Workshop; 2000.
156. Tensi HM. The Kaiser-Effect and Its Scientific Background; 26th European Conference on Acoustic Emission Testing; 2004; Berlin. p 31-42.
157. Beall FC. Monitoring Cumulative Damage in Shear Wall Testing with Acoustic Emission; 14th International Symposium on Nondestructive Testing of Wood 2005. Shaker Verlag.

158. Holford KM, Davies AW, Pullin R, Carter DC. Damage Location in Steel Bridges by Acoustic Emission. Journal of Intelligent Material Systems and Structures 2001;12:567-576.
159. Li J, Qi G. Improving Source Location Accuracy of Acoustic Emission in Complicated Structures. Journal of Nondestructive Evaluation 2009;28:1-8.
160. Baxter MG, Pullin R, Holford KM, Evans SL. Delta T Source Location for Acoustic Emission. Mechanical systems and signal processing 2007;21(3):1512-1520.
161. Matsushige K, Sakurada Y, Takahashi K. X-Ray Microanalysis and Acoustic Emissionstudies on the Formation Mechanism of Secondary Cracks in PMMA. Journal of Materials Science 1984;19:1548-1555.
162. Boudet JF, Ciliberto S. Interaction of Sound with Fast Crack Propagation. Physical Review Letters 1998;80(2):341-344.
163. Qi G. Attenuation of Acoustic Emission Body Waves in Acrylic Bone Cement and Synthetic Bone Using Wavelet Time-Scale Analysis. Journal of Biomedical Materials Research 2000;52:148-156.
164. Coultrup O, Browne M, Hunt C, Taylor M. Accounting for Inclusions and Voids Allows the Prediction of Tensile Fatigue Life of Bone Cement. Journal of Biomechanical Engineering 2009;131(5):51007-51015.
165. Jeffers JRT, Browne M, Taylor M. Damage Accumulation, Fatigue and Creep Behaviour of Vacuum Mixed Bone Cement. Biomaterials 2005;26:5532-5541.
166. Qi G, Pujol J, Fan ZF. 3-D Ae Visualization of Bone-Cement Fatigue Locations Journal of Biomedical Materials Research 2000;52(2):256-260.
167. Ong A, Wong KL, Lai M, Garino JP, Steinberg ME. Early Failure of Precoated Femoral Components in Primary Total Hip Arthroplasty. Journal of Bone and Joint Surgery 2002;84-A:786-792.
168. Bergmann G, Graichen F, Rohlmann A. Hip Joint Loading During Walking and Running, Measured in Two Patients. Journal of Biomechanics 1993;26(8):969.
169. Bergmann G, Graichen F, Rohlmann A. Is Staircase Walking a Risk for the Fixation of Hip Implants? Journal of Biomechanics 1995;28(5):535.
170. Stansfield BW, Nicol AC, Paul JP, Kelly IG, Graichen F, Bergmann G. Direct Comparison of Calculated Hip Joint Contact Forces with Those Measured Using Instrumented Implants. An Evaluation of a Three-Dimensional Mathematical Model of the Lower Limb. Journal of Biomechanics 2003;36(7):929.
171. D'Lima DD, Townsend CP, Arms SW, Morris BA, Jr CWC. An Implantable Telemetry Device to Measure Intra-Articular Tibial Forces. Journal of Biomechanics 2005;38:299-304.
172. Rydell NW. Forces Acting on the Femoral Head Prosthesis. Acta Orthopaedica Scandinavica 1966;s86-93.
173. Carlson CE, Mann RW, Harris WH. A Look at the Prosthesis-Cartilage Interface: Design of a Hip Prosthesis Containing Pressure Transducers. Journal of Biomedical Materials Research 1974;8:261-269.
174. English TA, Kilvington M. In Vivo Records of Hip Loads Using a Femoral Implant with Telemetric Output. Journal Biomedical Engineering 1979;1:111-115.
175. Bergmann G, Kolbel R, Siraky J, Rohlmann A. Direct Measurement of Hip Joint Forces in Sheep. Journal of Biomechanics 1980;13(9):805.
176. Heller MO, Bergmann G, Deuretzbacher G, Durselen L, Pohl M, Claes L, Haas NP, Duda GN. Musculo-Skeletal Loading Conditions at the Hip During Walking and Stair Climbing. Journal of Biomechanics 2001;34(7):883.
177. Heller MO, Bergmann G, Kassi JP, Claes L, Haas NP, Duda GN. Determination of Muscle Loading at the Hip Joint for Use in Pre-Clinical Testing. Journal of Biomechanics 2005;38(5):1155.
178. Bergmann G, Graichen F, Rohlmann A, Verdonschot N, van Lenthe GH. Frictional Heating of Total Hip Implants, Part 1: Measurements in Patients. Journal of Biomechanics 2001;34(4):421.
179. Puers R, Catrysse M, Vandevoorde G, Collier RJ, Louridas E, Bunny F, Donkerwolcke M, Moulart F. A Telemetry System for the Detection of Prosthesis Loosening by Vibration Analysis Sensors and Actuators 1999;85:42-47.
180. Bergmann G, Kniggendorf H, Graichen F, Rohlmann A. Influence of Shoes and Heel Strike on the Loading of the Hip Joint. Journal of Biomechanics 1995;28(7):817.
181. Bergmann G, Graichen F, Rohlmann A. Five Month in Vivo Measurement of Hip Joint Forces. Journal of Biomechanics 1989;22(10):986.
182. Jefferiss CD, Lee AJC, Ling RSM. Thermal Aspects of Self-Curing Polymethylmethacrylate. Journal of Bone and Joint Surgery 1975;57-B(4):511-518.
183. Larry JR, Rosenberg RM, Uhler RO. Thick-Film Technology: An Introduction to the Materials. IEEE Transactions on Components, Hybrids, and Manufacturing Technology 1980;3(2):211-225.

184. Torah R, Beeby SP, White NM. An Improved Thick-Film Piezoelectric Material by Powder Blending and Enhanced Processing Parameters. IEEE Transactions on Ultrasonics, Ferroelectrics, and Frequency Control 2005;52(1):10-16.
185. Morgan_Matroc_Limited. Piezoelectric Ceramics Data Book for Designers. ISBN.
186. Visual Ae Help File. Vallen Systeme Gmbh, Germany.
187. Harris NR, Hill M, White NM, Beeby SP. Acoustic Power Output Measurements for Thick-Film Pzt Transducers. Electronics Letters 2004;40(10):636-637.
188. Akkus O. Comments on Acoustic Emission Visualization of Bone Cement Fatigue Locations. Journal of Biomedical Materials Research 2002;59:398-401.
189. Reilly DT, Burstein AH. The Mechanical Properties of Cortical Bone. Journal of Bone and Joint Surgery 1974;56-A:1001-1022.
190. Hodgskinson R, Currey JD. Young's Modulus, Density and Material Properties in Cancellous Bone over a Large Density Range. Journal of Materials Science 1992;3:377-381.
191. Liu C, Green SM, Wakins ND, Gregg PJ, McCaskie AW. Some Failure Modes of Four Clinical Bone Cements. Proceedings of the Institution of Mechanical Engineers, Part H: Journal of Engineering in Medicine 2001;215:359-366.
192. kulzer-technik.de. Web Page. kulzer-technik.de
193. Wang JS, Franzén H, Toksvig-Larsen S, Lidgren L. Does Vacuum Mixing of Bone Cement Affect Heat Generation? Analysis of Four Cement Brands. Journal of Applied Biomaterials 2004;6(2):105-108.
194. Mann KA, Gupta S, Race A, Miller MA, Cleary RJ, Ayers DC. Cement Microcracks in Thin-Mantle Regions after in Vitro Testing. The Journal of Arthroplasty 2004;19(5):605-612.
195. Kortschot MT, Zhang CJ. Characterization of Composite Mesostructures and Damage by De-Ply Radiography. Composites Science and Technology 1995;53:175-181.
196. Verdonschot N, Huiskes R. Subsidence of Tha Stems Due to Acrylic Cement Creep Is Extremely Sensitive to Interface Friction. Journal of Biomechanics 1996;29(12):1569-1575.
197. Baliga BR, Rose PL, Ahmed AM. Thermal Modelling of Polymerizing Polymethylmethacrylate, Considering Temperature Dependent Heat Generation. Journal of Biomechanical Engineering 1992;114:251-259.
198. Starke GR, Birnie C, van den Blink PA. Numerical Modelling of Cement Polymerisation and Thermal Bone Necrosis.; In: Middleton J, Jones MN, Pande GN, (eds); Third International Symposium on Computer Methods in Biomechanics and Biomedical Engineering; 1997; London. Gordon and Breach. p 163-172.
199. Bishop NE, Ferguson S, Tepic S. Porosity Reduction in Bone Cement at the Cement-Stem Interface. Journal of Bone Joint Surgery 1996;78-B(3):349-356.
200. Iesaka K, Jaffe WL, Kummer FJ. Effects of Preheating of Hip Prostheses on the Stem-Cement Interface. Journal of Bone Joint Surgery 2003;85-A:421-427.
201. Yan J, Zili Q, Mian C, Guangqing Z, Guangqiang X. Time-Sensitivity of the Kaiser Effect of Acoustic Emission in Limestone and Its Application to Measurements of in-Situ Stress. Petroleum Science 2009;6(2):176-180.
202. Crocker MJ. Handbook of Acoustics: Wiley-Interscience; 1998. ISBN: 0-471-25293-X.
203. Goldsmith AAJ, Dowson D, Wroblewski BM, Siney PD, Flemming PA, Lane JM, Stone MH, Walker R. Comparative Study of the Activity of Total Hip Arthroplasty Patients and Normal Subjects. The Journal of Arthroplasty 2001;16(5):613-619.
204. Davy DT, Kotzar GM, Brown RH, Heiple KG, Goldberg VM, Heiple KGJr, Berilla J, Burstein AH. Telemetric Force Measurements across the Hip after Total Arthroplasty. The Journal of Bone and Joint Surgery 1988;70-A(1):45-50.
205. Paul JP. Development of Standards for Orthopaedic Implants. Proceedings of the Institution of Mechanical Engineers, Part H: Journal of Engineering in Medicine 1997;211:119-126.
206. Cristofolini L, Minari C, Viceconti M. A Methodlogy and Criterion for Acrylic Bone Cement Fatigue Tests. Fatigue & Fracture of Engineering Materials & Structures 2000;23:953-957.
207. Pujol J, Qi G. Letter to the Editor - Reply to Dr. Akkus's Comments Journal of Biomedical Materials Research 2001;59-A(2):399-401.
208. Abramoff MD, Magelhaes PJ, Ram SJ. Image Processing with Imagej. Biophotonics International 2004;11(7):36-42.
209. Rowland C, Browne M, Taylor A. Dynamic Health Monitoring of Metal on Metal Hip Prostheses Using Acoustic Emission; European Working Group for Acoustic Emissions; 2004.
210. Lee DE, Hwang I, Valente CMO, Oliveira JFG, Dornfeld DA. Precision Manufacturing Process Monitoring with Acoustic Emission. International Journal of Machine Tools and Manufacture 2006;46(2):176-188.

211. Al-Ghamd A, Mba D. A Comparative Experimental Study on the Use of Acoustic Emission and Vibration Analysis for Bearing Defect Identification and Estimation of Defect Size. Mechanical systems and signal processing 2006;20(7):1537-1571.
212. Ennaceur C, Laksimi A, Hervé C, Cherfaoui M. Monitoring Crack Growth in Pressure Vessel Steels by the Acoustic Emission Technique and the Method of Potential Difference. International Journal of Pressure Vessels and Piping 2006;83(3):197-204.
213. Carpinteri A, Lacidogna G, Pugno N. Structural Damage Diagnosis and Life-Time Assessment by Acoustic Emission Monitoring. Engineering Fracture Mechanics 2007;74(1-2):273-289.
214. Steel JA, Reuben RL. Recent Developments in Monitoring of Engines Using Acoustic Emission. The Journal of Strain Analysis for Engineering Design 2005;40(1):45-57.
215. Smith SL, Dowson D, Goldsmith AAJ. The Lubrication of Metal-on-Metal Total Hip Joints: A Slide Down the Stribeck Curve. Proceedings of the Institution of Mechanical Engineers, Part J: Journal of Engineering Tribology 2001;215(5):483-493.
216. Scholes SC, Unsworth A, Goldsmith AAJ. A Frictional Study of Total Hip Joint Replacements. Physics in Medicine and Biology 2000;45:3721-3735.
217. Johnson KL, Greenwood JA, Poon SY. A Simple Theory of Asperity Contact in Elastohydrodynamic Lubrication. Wear 1972;19(91-108).
218. Norton MR, Yarlagadda R, Anderson GH. Catastrophic Failure of the Elite Plus Total Hip Replacement, with a Hylamer Acetabulum and Zirconia Ceramic Femoral Head. Journal of Bone and Joint Surgery 2002;84-B:631-635.
219. von Schewelov T, Sanzén L, Önsten I, Carlsson A, Besjakov J. Total Hip Replacement with a Zirconium Oxide Ceramic Femoral Head. Journal of Bone and Joint Surgery 2005;87-B:1631-1635.
220. Hummer III CD, Rothman RH, Hozack WJ. Catastophic Failure of Modular Zirconia-Ceramic Femoral Head Components after Total Hip Arthroplasty. The Journal of Arthroplasty 1995;10(6):848-850.
221. Glaser D, Komistek RD, Cates HE, Mahfouz MR. Clicking and Squeaking: In Vivo Correlation of Sound and Separation for Different Bearing Surfaces. Journal of Bone and Joint Surgery 2008;90-A(s4):112-120.
222. Häggström R. A Transducer for the Measurement of Forces and Moments in the Hip Joint of the Living Human Body. VDI-Berichte 1974;212:93-100.
223. Taylor SJG. A Telemetry System for Measurement of Forces in Massive Orthopeadic Implants in Vivo 18th Annual International Conference of the IEEE Engineering in Medicine and Biology 1996; Amsterdam.
224. Burny F, Donkerwolcke M, Moulart F, Bourgois R, Puers R, Van Schuylenbergh K, Barbosa M, Paiva O, Rodes F, Bégueret JB and others. Concept, Design and Fabrication of Smart Orthopaedic Implants. Medical Engineering & Physics 2000;22:469-479.
225. Morris BA, D'Lima DD, Slamin J, Kovacevic N, Arms S, Townsend CP, Colwell C. E-Knee: Evolution of the Electronic Knee Prosthesis. Journal of Bone and Joint Surgery 2001;83-A:62-66.

APPENDIX A – V103 CALIBRATION TRANSDUCER RESPONSE

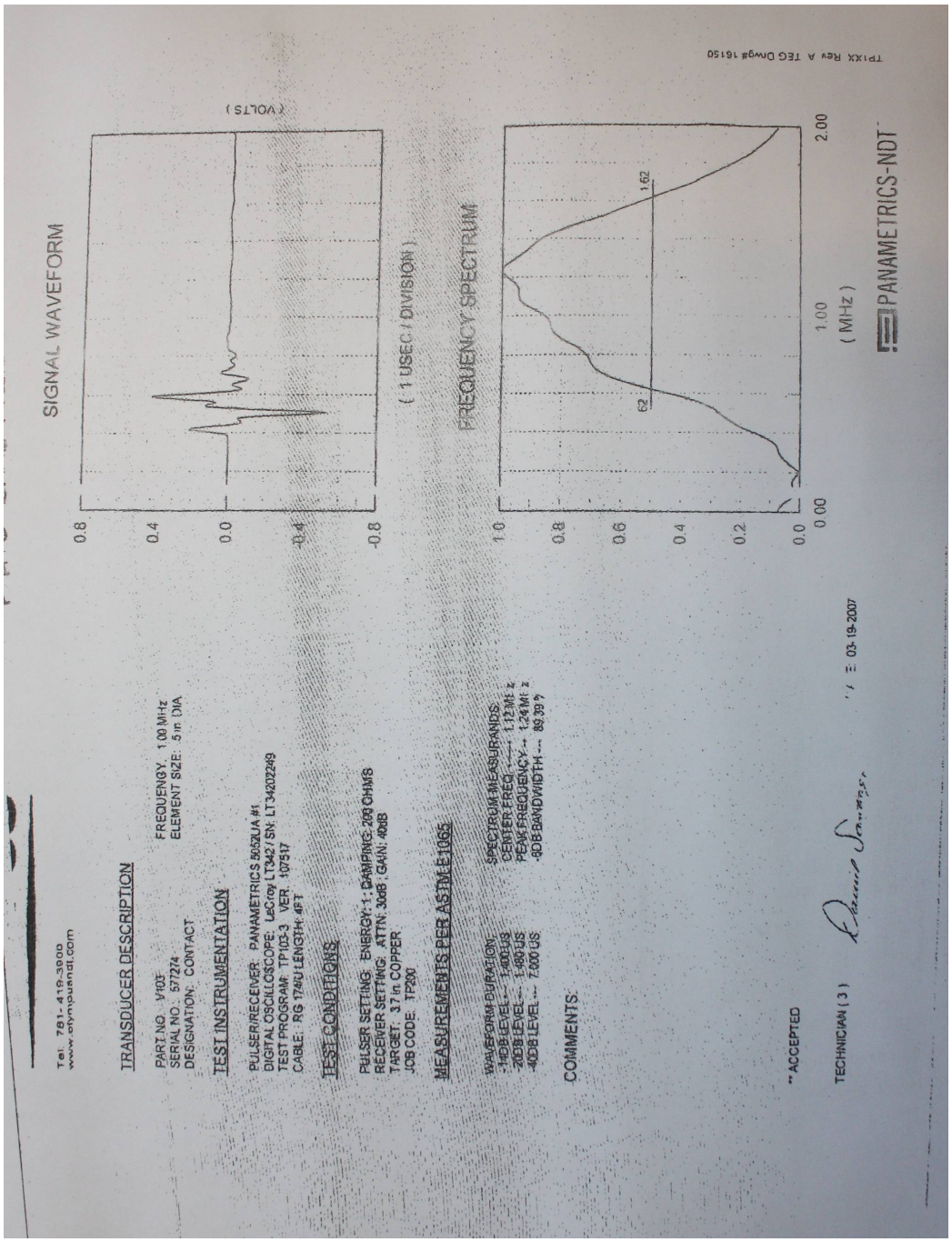

APPENDIX B – IN-HOUSE SENSOR CALIBRATION CERTIFICATES

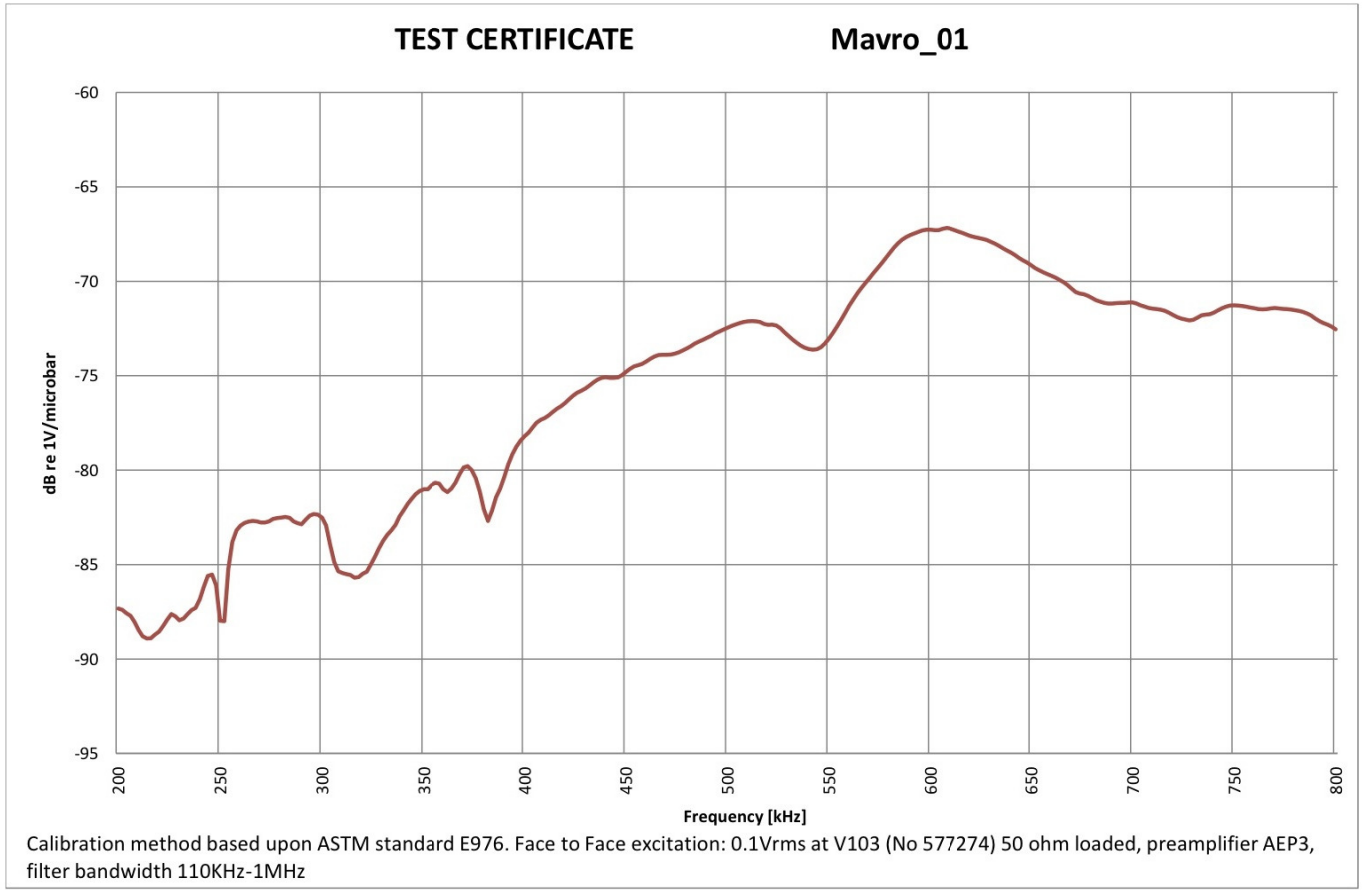

Calibration method based upon ASTM standard E976. Face to Face excitation: 0.1Vrms at V103 (No 577274) 50 ohm loaded, preamplifier AEP3, filter bandwidth 110KHz-1MHz

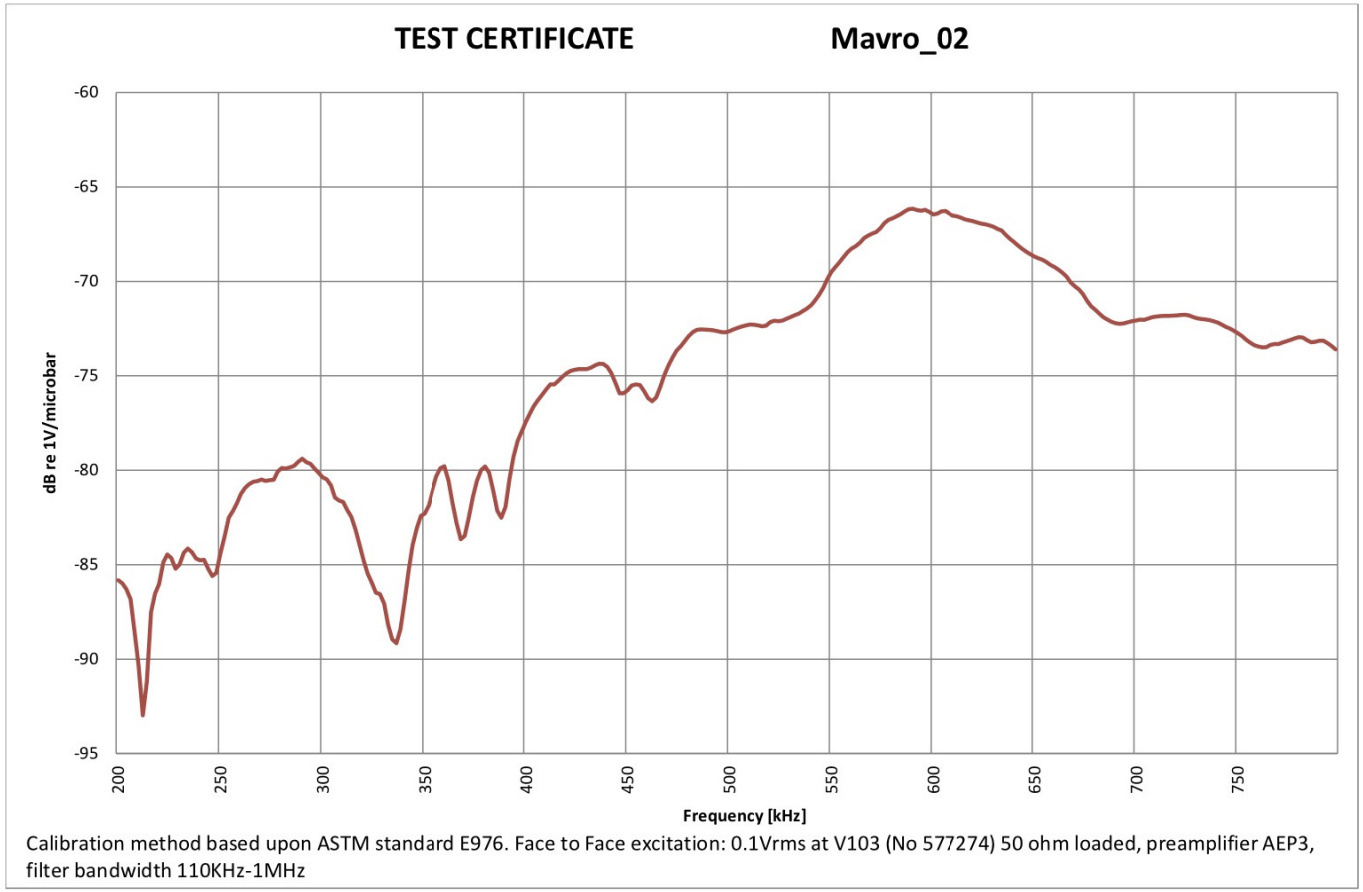

Calibration method based upon ASTM standard E976. Face to Face excitation: 0.1Vrms at V103 (No 577274) 50 ohm loaded, preamplifier AEP3, filter bandwidth 110KHz-1MHz

TEST CERTIFICATE Mavro_03

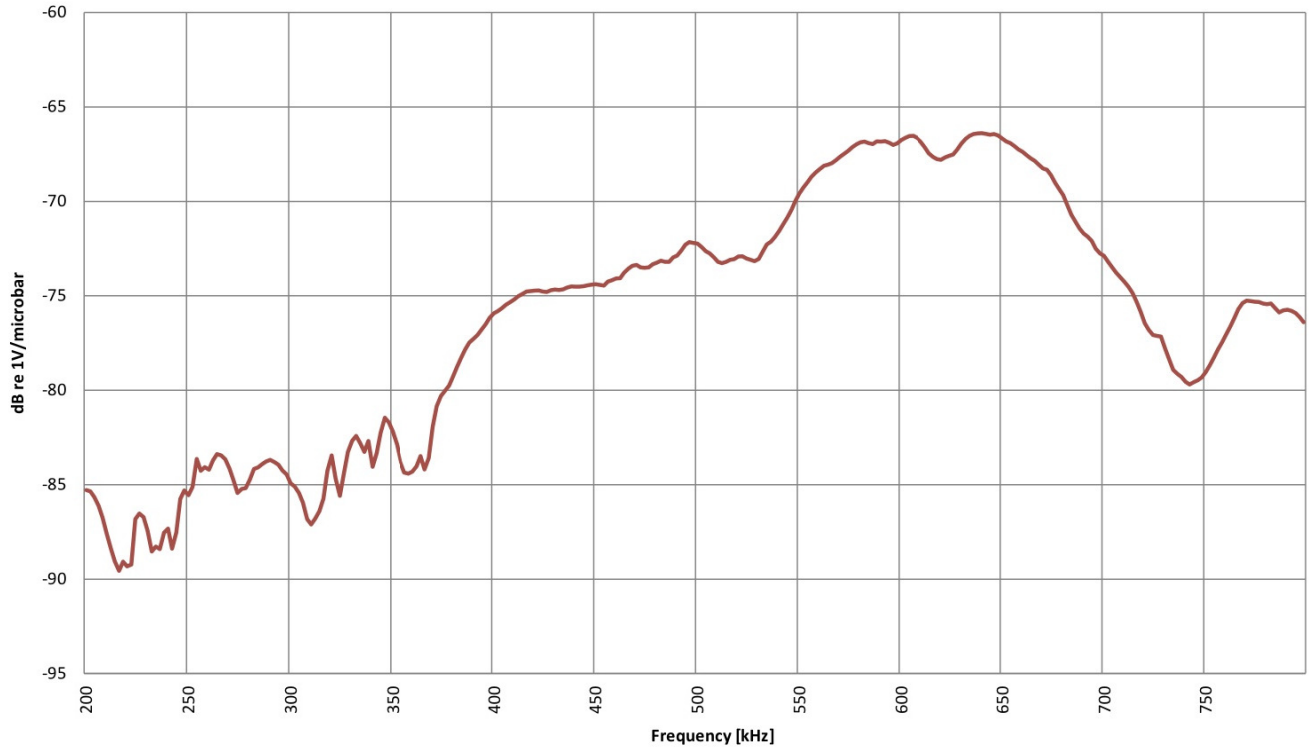

Calibration method based upon ASTM standard E976. Face to Face excitation: 0.1Vrms at V103 (No 577274) 50 ohm loaded, preamplifier AEP3, filter bandwidth 110KHz-1MHz

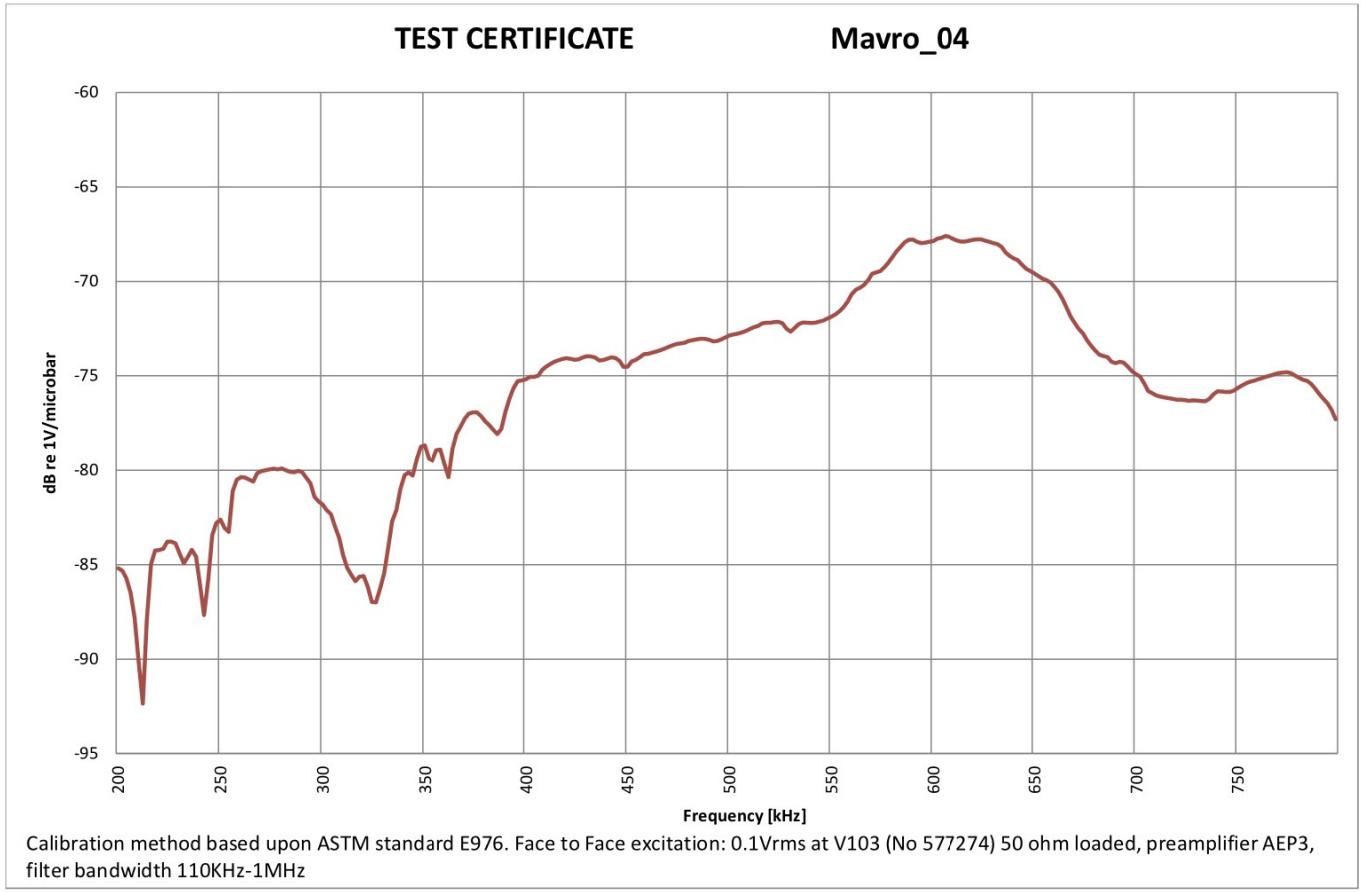

Calibration method based upon ASTM standard E976. Face to Face excitation: 0.1Vrms at V103 (No 577274) 50 ohm loaded, preamplifier AEP3, filter bandwidth 110KHz-1MHz

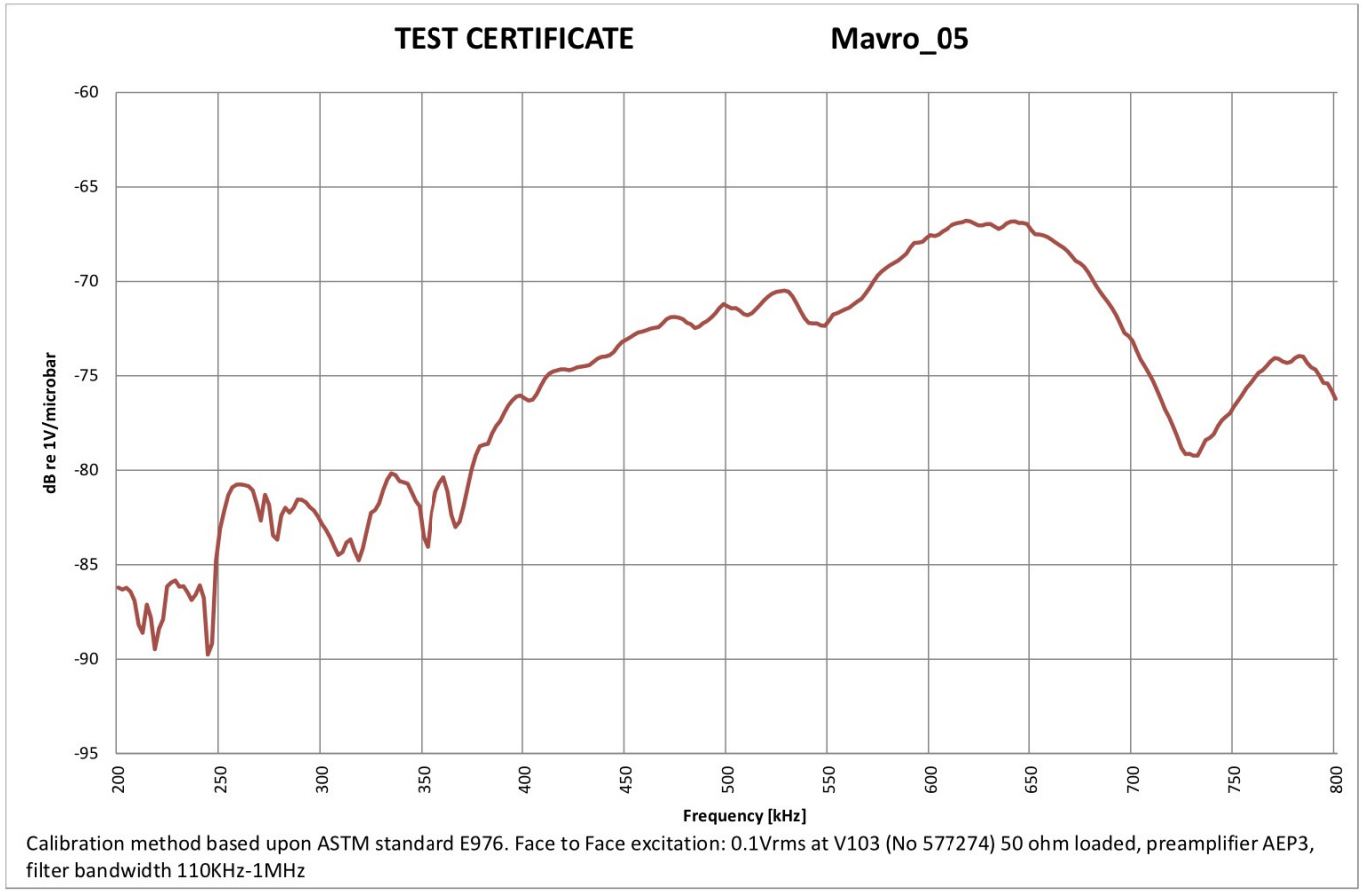

Calibration method based upon ASTM standard E976. Face to Face excitation: 0.1Vrms at V103 (No 577274) 50 ohm loaded, preamplifier AEP3, filter bandwidth 110KHz-1MHz

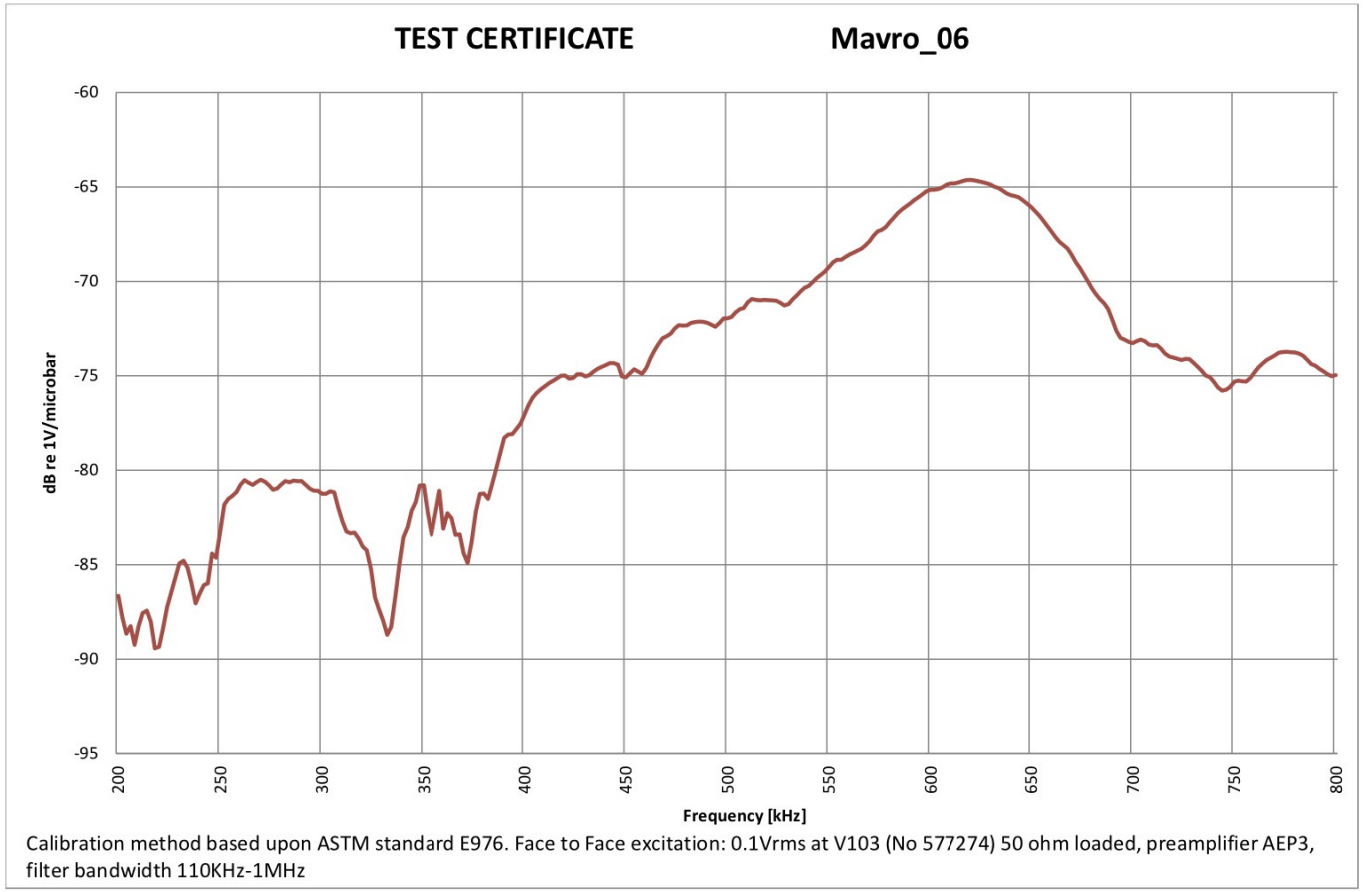

Calibration method based upon ASTM standard E976. Face to Face excitation: 0.1Vrms at V103 (No 577274) 50 ohm loaded, preamplifier AEP3, filter bandwidth 110KHz-1MHz

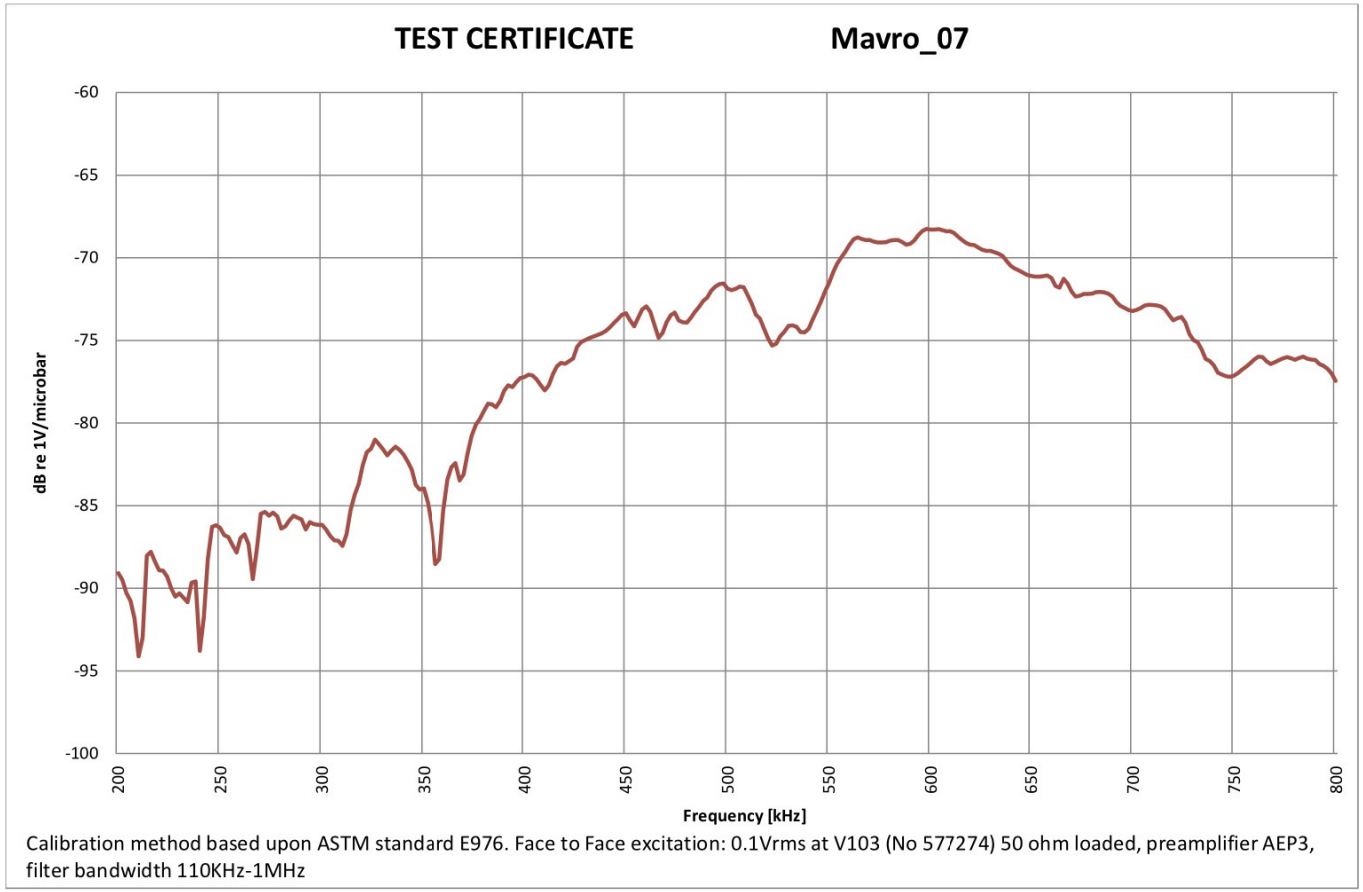

Calibration method based upon ASTM standard E976. Face to Face excitation: 0.1Vrms at V103 (No 577274) 50 ohm loaded, preamplifier AEP3, filter bandwidth 110KHz-1MHz

X

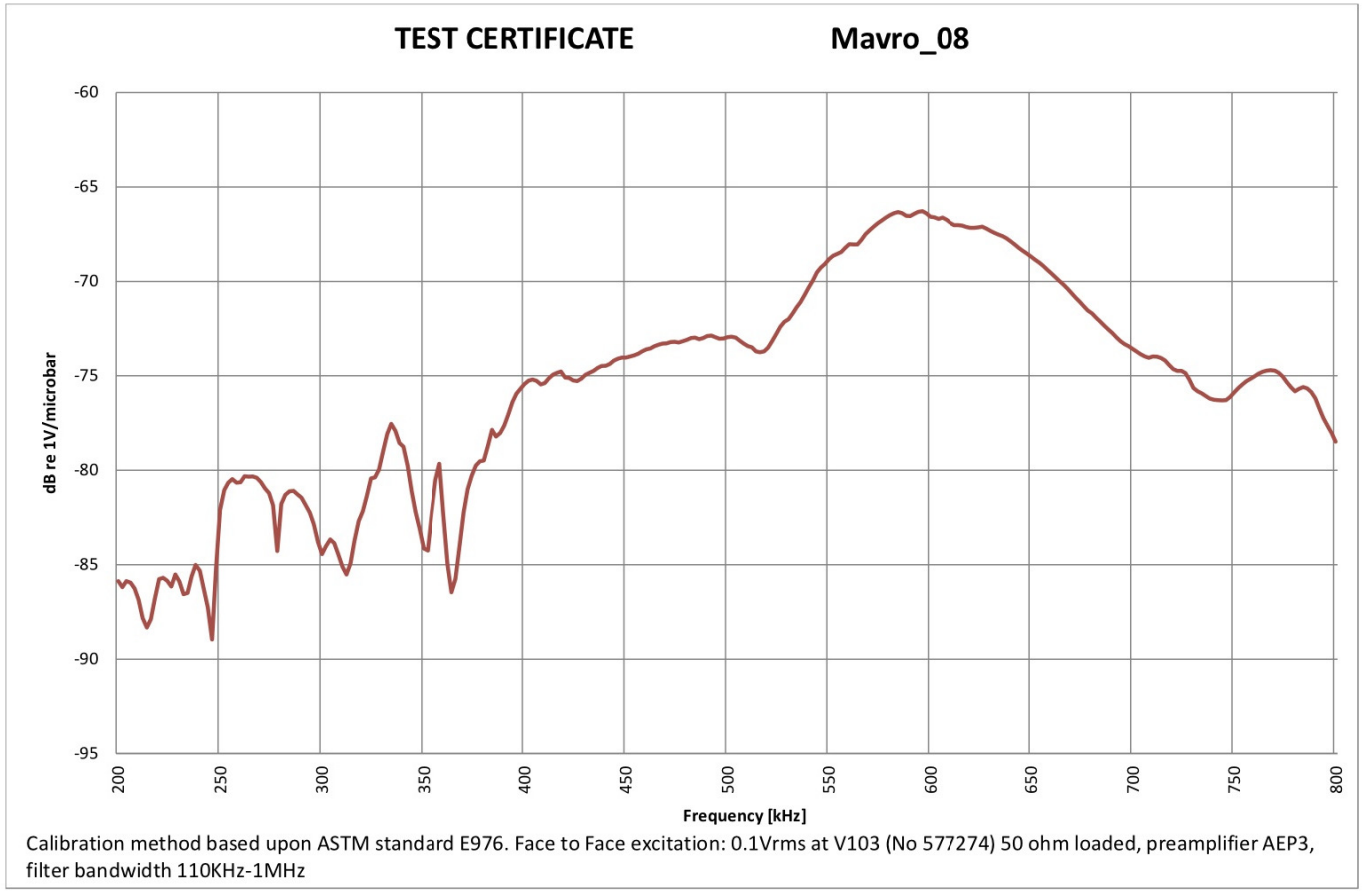

Calibration method based upon ASTM standard E976. Face to Face excitation: 0.1Vrms at V103 (No 577274) 50 ohm loaded, preamplifier AEP3, filter bandwidth 110KHz-1MHz

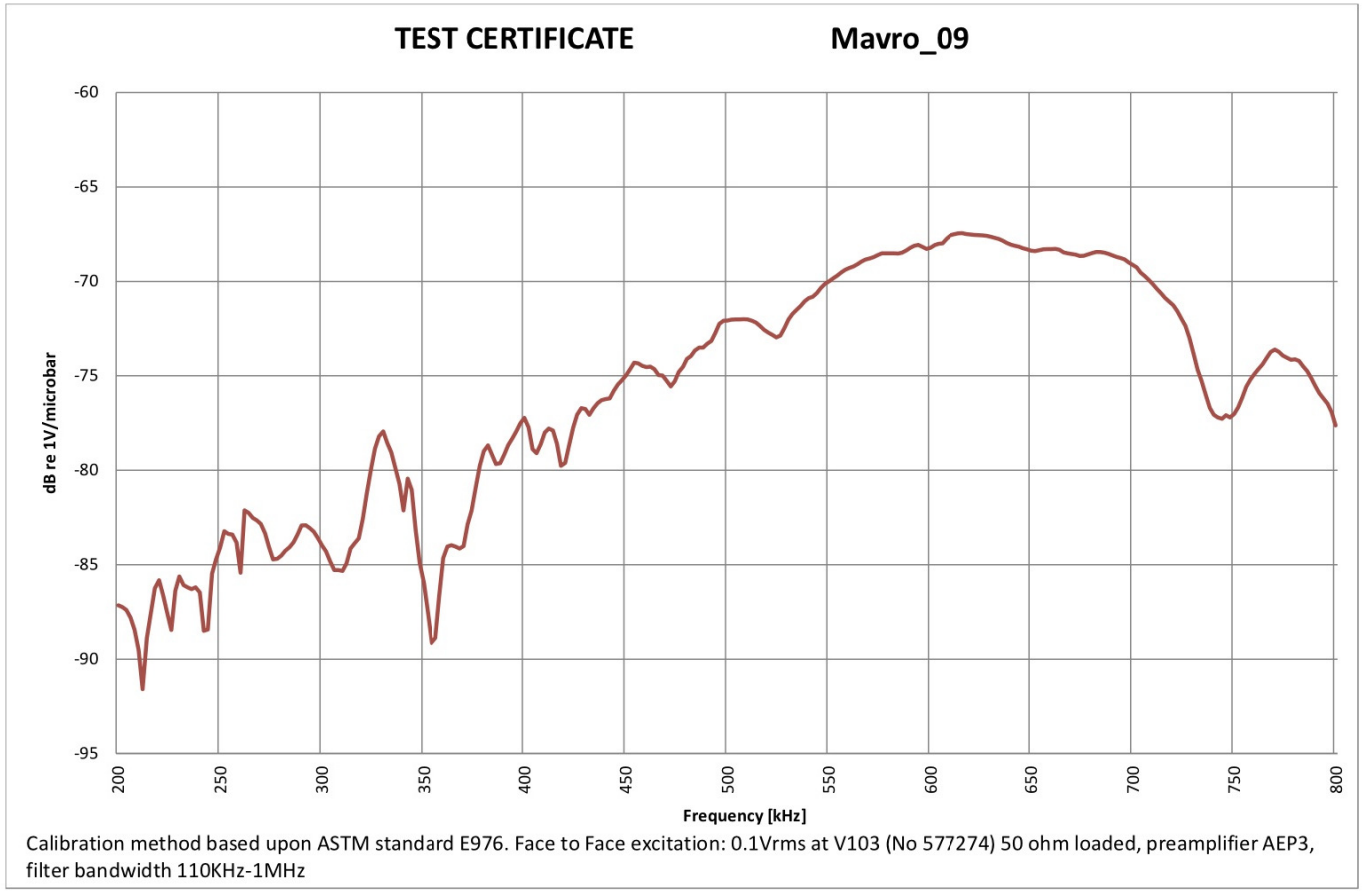

Calibration method based upon ASTM standard E976. Face to Face excitation: 0.1Vrms at V103 (No 577274) 50 ohm loaded, preamplifier AEP3, filter bandwidth 110KHz-1MHz

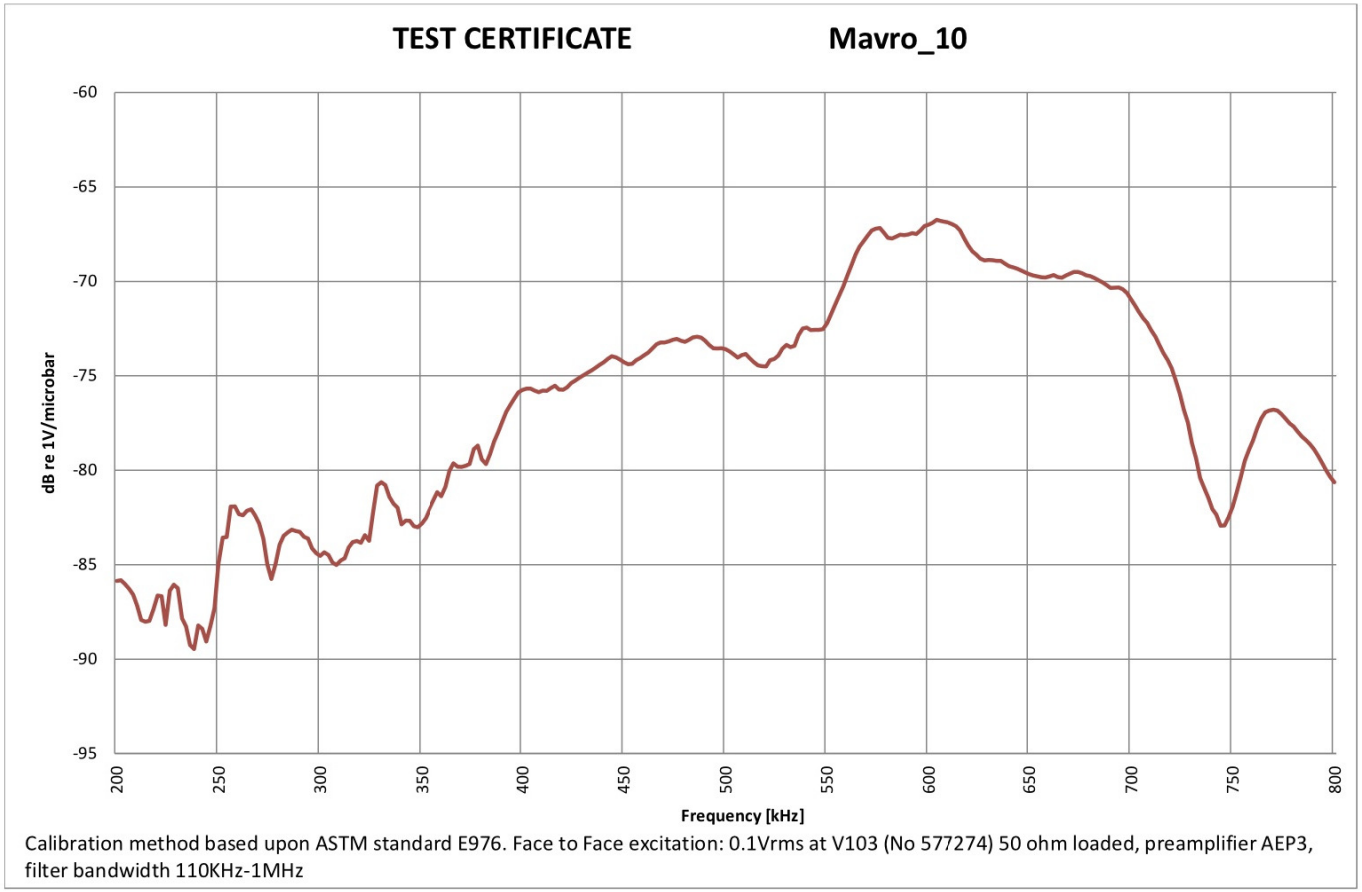

Calibration method based upon ASTM standard E976. Face to Face excitation: 0.1Vrms at V103 (No 577274) 50 ohm loaded, preamplifier AEP3, filter bandwidth 110KHz-1MHz

APPENDIX C – BREAKDOWN OF IN-HOUSE SENSOR COST

Part	Cost (£)
PZT (Morgan Electro Ceramics PZT5H1 Disc Dia 3mm x Th 1mm)	17.22
Case material	2.00
BNC Connector (RS ref 546-3793)	1.47
Microdot connector & extension (Bruel & Kjaer refs JJ0032 & JP0012)	9.80
1m coaxial cable (RS ref 235-5419)	1.00
Other (solder, rubber discs, silver-loaded epoxy, heat shrink)	10.00
Total	**41.49**

This total cost is reduced if the side-mounted versions of the sensors are used as no microdot connector or extension is required and as such the cost of these is £31.69. It should be noted that these figures do not include any labour charges or overhead adjustments - they are intended as a guide for research projects only.

APPENDIX D – DESIGN DRAWINGS

SIMPLE STEM CONSTRUCT

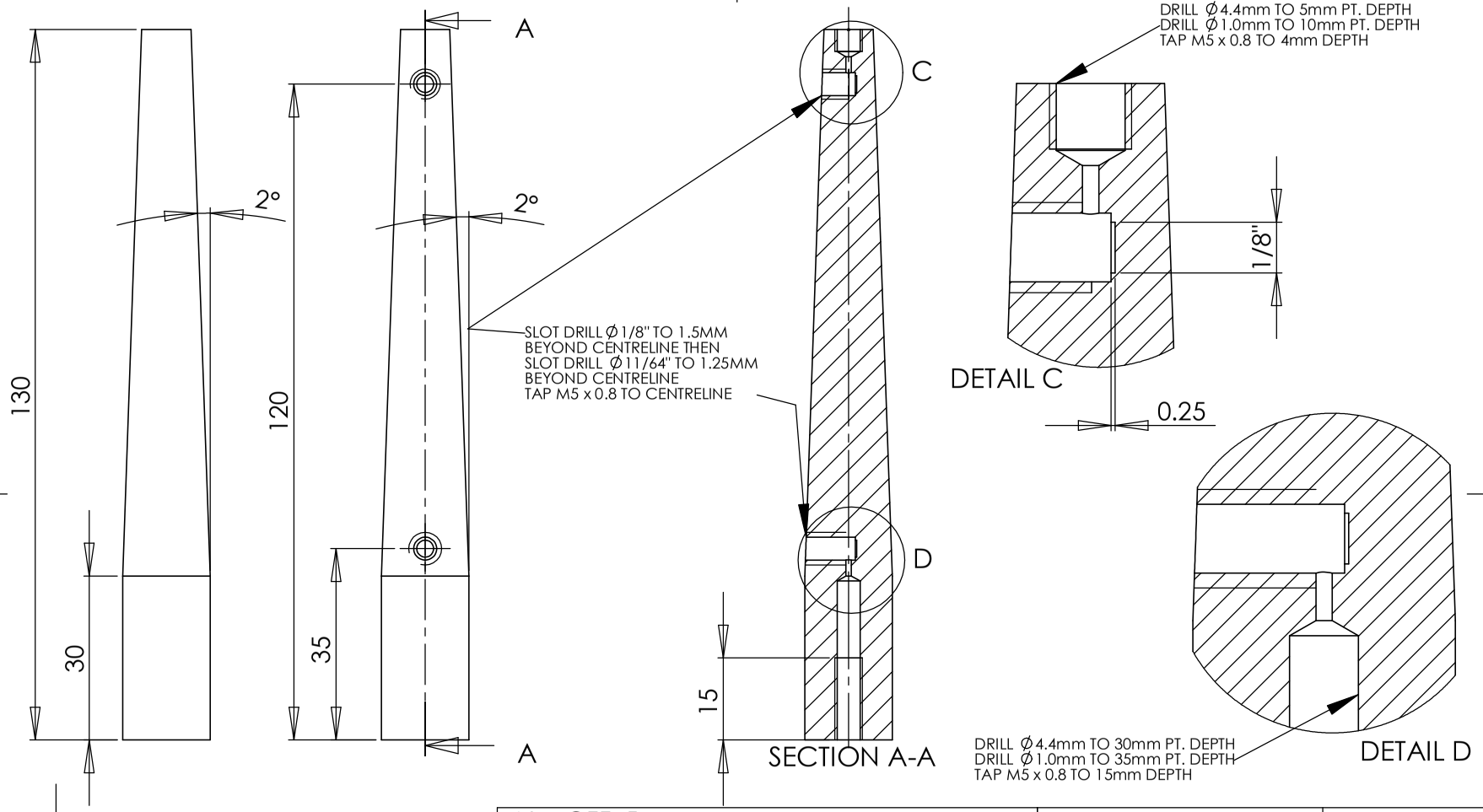

No. OFF: 5				DO NOT SCALE DRAWING	REVISION
UNLESS OTHERWISE SPECIFIED: DIMENSIONS ARE IN MILLIMETERS SURFACE FINISH: TOLERANCES: LINEAR: 0.2mm ANGULAR: 0.2°	FINISH: Machined		DEBUR AND BREAK SHARP EDGES	TITLE: **Square Stem**	
	NAME	SIGNATURE	DATE	MATERIAL:	DWG NO. **EngD Square STEM 001**
DRAWN	MN Mavrogordato		20-2-08	Stainless Steel 316	
CHK'D					SCALE: Do Not Scale Drawing / SHEET 1 OF 1
DEADLINE FOR COMPLETION: 24-3-2008				**CONTACT: mnm100@soton.ac.uk Ext: 27665**	

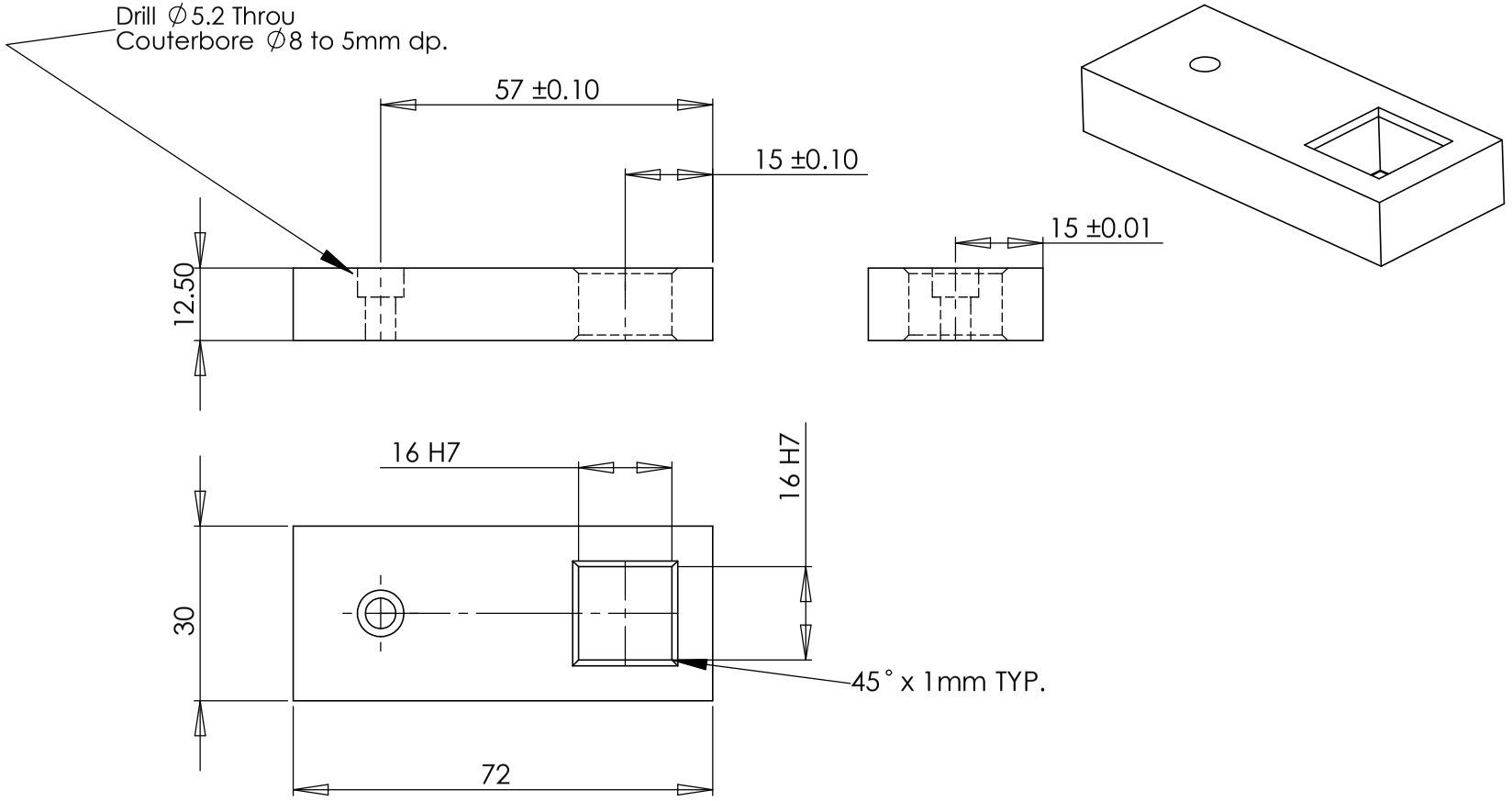

No. OFF: 5				DO NOT SCALE DRAWING	REVISION
UNLESS OTHERWISE SPECIFIED: DIMENSIONS ARE IN MILLIMETERS SURFACE FINISH: TOLERANCES: LINEAR: 0.2mm ANGULAR: 0.2°	FINISH: Machined	DEBUR AND BREAK SHARP EDGES		TITLE: **Offset Plate**	
	NAME	SIGNATURE	DATE	MATERIAL:	DWG NO. **EngD Offset Plate 001**
DRAWN	MN Mavrogordato		20-2-08	Stainless Steel 316	
CHK'D					SCALE: Do Not Scale Drawing / SHEET 1 OF 1
DEADLINE FOR COMPLETION: 24-3-2008				**CONTACT: mnm100@soton.ac.uk**	**Ext: 27665**

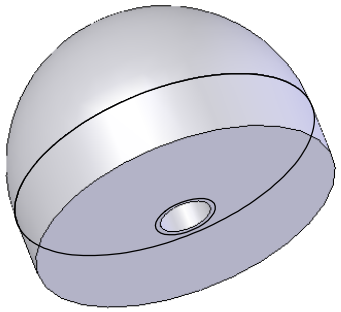

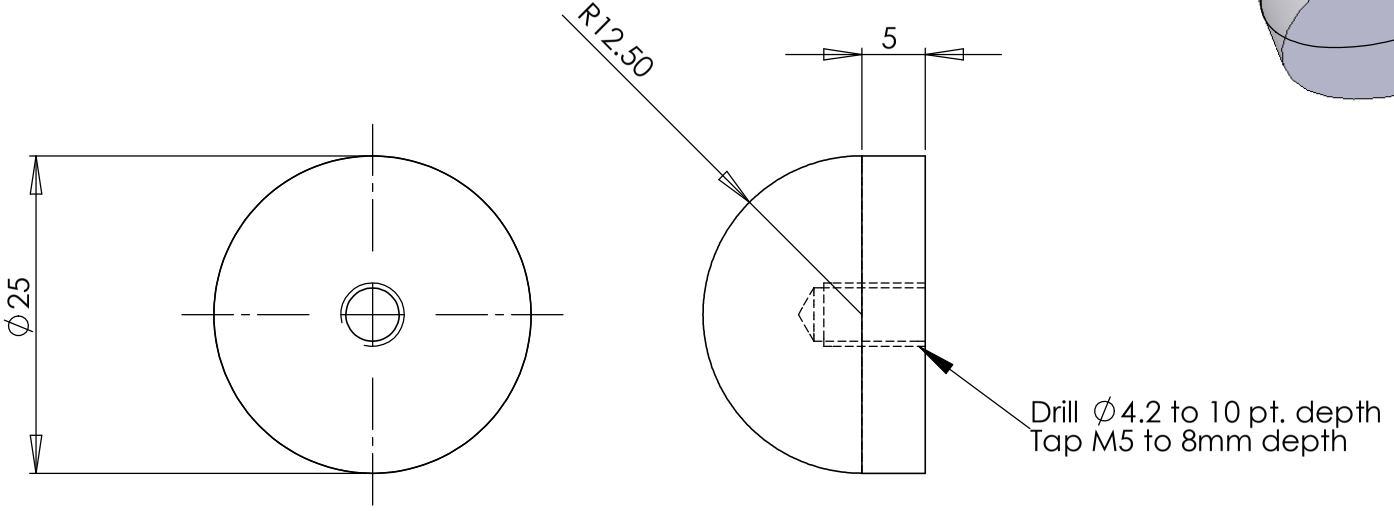

No. OFF: 10				DO NOT SCALE DRAWING	REVISION
UNLESS OTHERWISE SPECIFIED: DIMENSIONS ARE IN MILLIMETERS SURFACE FINISH: TOLERANCES: LINEAR: 0.2mm ANGULAR: 0.2°	FINISH: Highly Polished	DEBUR AND BREAK SHARP EDGES		TITLE: **Ball**	
	NAME	SIGNATURE	DATE	MATERIAL:	DWG NO. **EngD ROUND Ball 001**	A4
DRAWN	MN Mavrogordato		19-2-08	Stainless Steel 316		
CHK'D					SCALE:2:1	SHEET 1 OF 1
DEADLINE FOR COMPLETION: 24-3-2008				**CONTACT: mnm100@soton.ac.uk**		**Ext: 27665**

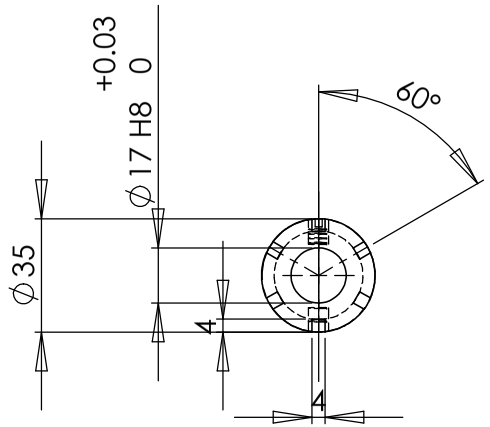

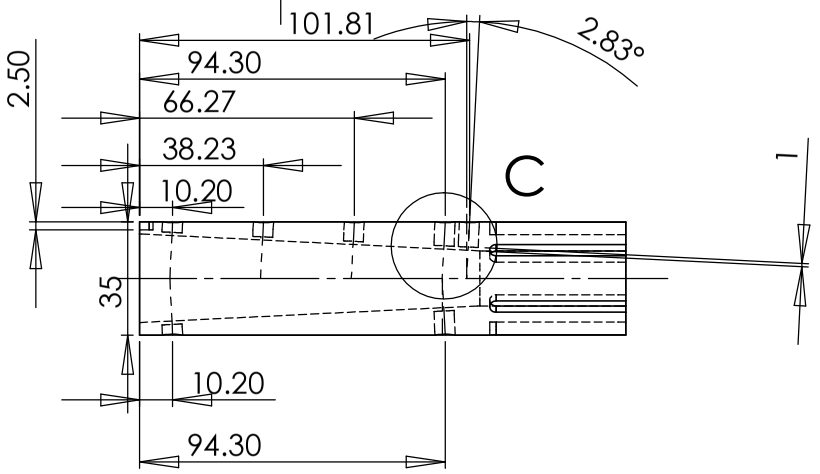

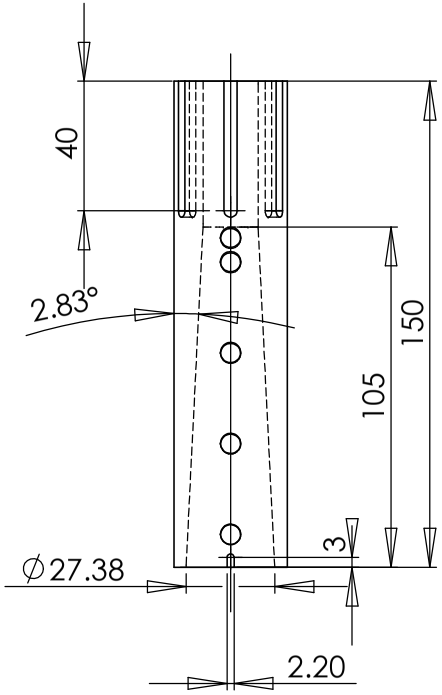

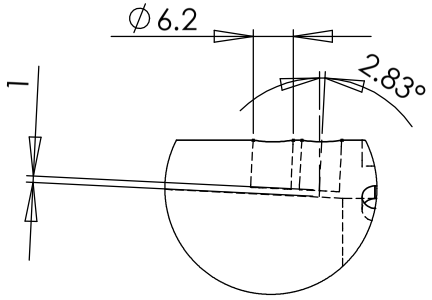

DETAIL C
SCALE 1 : 1

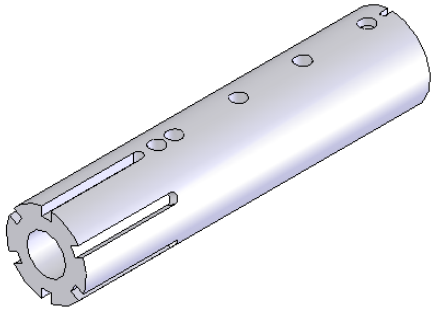

No. OFF: 20				DO NOT SCALE DRAWING	REVISION
UNLESS OTHERWISE SPECIFIED: DIMENSIONS ARE IN MILLIMETERS SURFACE FINISH: TOLERANCES: LINEAR: 0.2mm ANGULAR: 0.2°	FINISH: Machined	DEBUR AND BREAK SHARP EDGES		TITLE: **Tufnol Tube**	
	NAME	SIGNATURE	DATE	MATERIAL:	DWG NO. **EngD Tufnol 001**
DRAWN	MN Mavrogordato		20-2-07	Tufnol Carp	A4
CHK'D					SCALE:1:2 SHEET 1 OF 1
DEADLINE FOR COMPLETION: 24-3-2008				**CONTACT: mnm100@soton.ac.uk Ext: 27665**	

CENTRALISING JIG

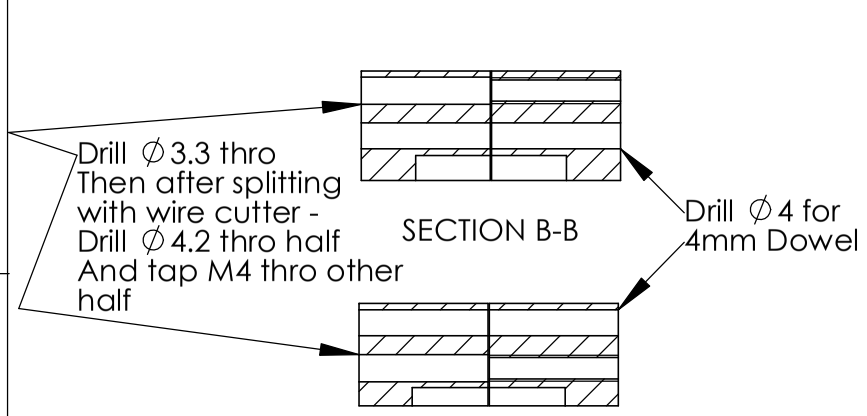

SECTION B-B

SECTION C-C

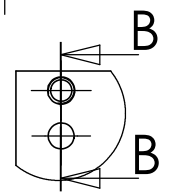

DETAIL A

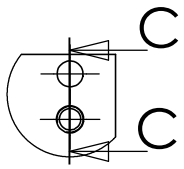

DETAIL B

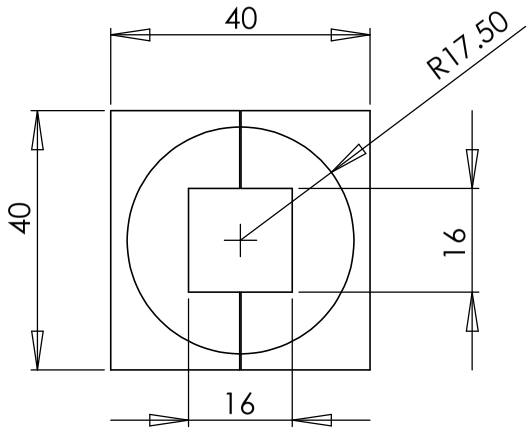

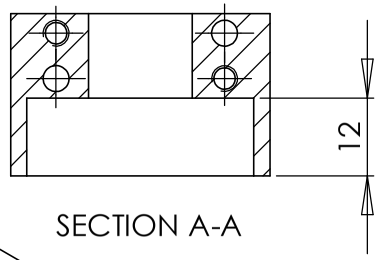

SECTION A-A

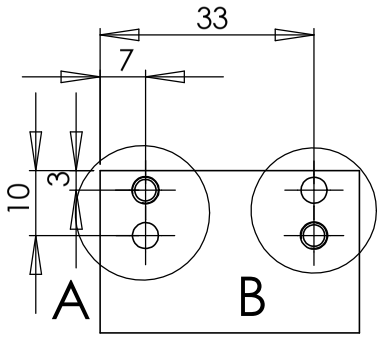

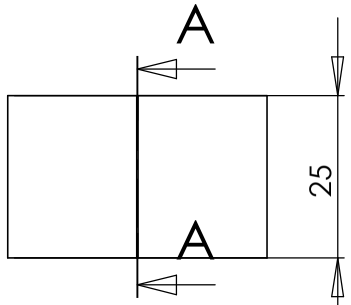

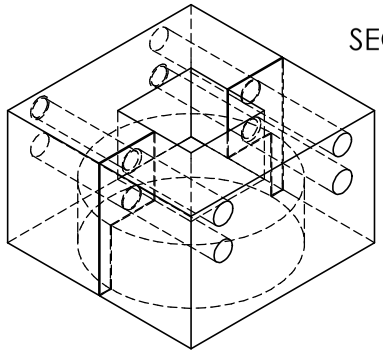

No. OFF: 1				DO NOT SCALE DRAWING	REVISION
UNLESS OTHERWISE SPECIFIED: DIMENSIONS ARE IN MILLIMETERS SURFACE FINISH: TOLERANCES: LINEAR: 0.2mm ANGULAR: 0.2°	FINISH: Machined	DEBUR AND BREAK SHARP EDGES		TITLE: **Proximal Center Jig**	
	NAME	SIGNATURE	DATE	MATERIAL:	DWG NO. **EngD Prox jig 001** A4
DRAWN	MN Mavrogordato		14-4-07		
CHK'D					SCALE:1:1 SHEET 1 OF 1
DEADLINE FOR COMPLETION: 18-4-2007				**CONTACT: mnm100@soton.ac.uk Ext: 27665**	

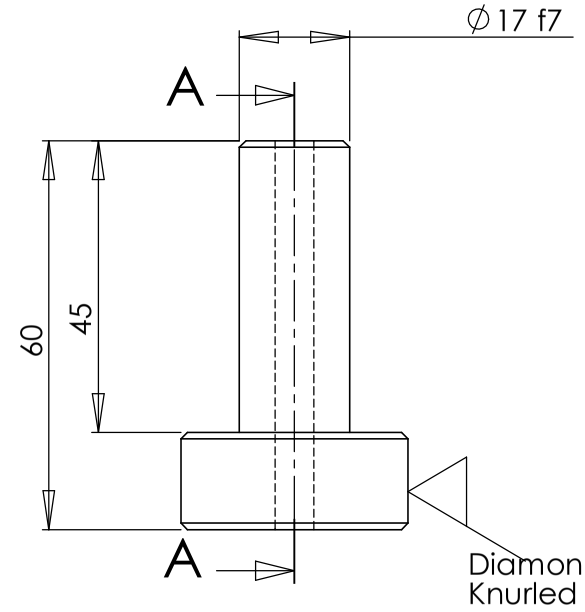

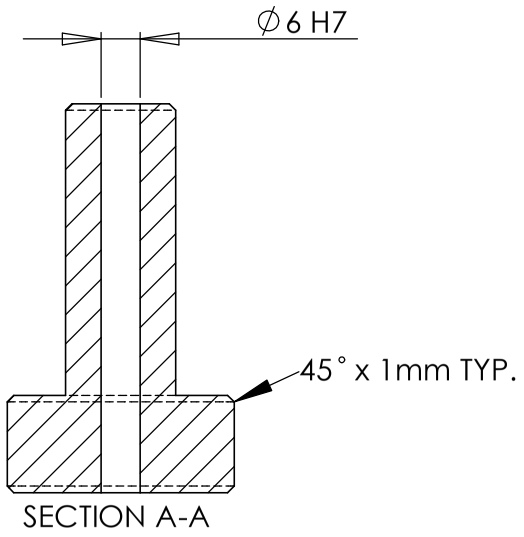

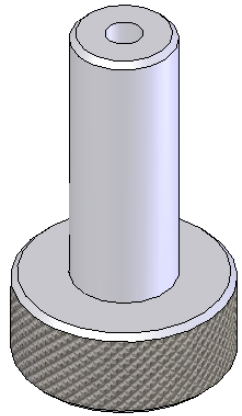

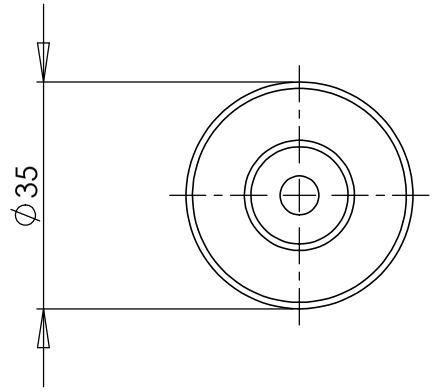

No. OFF: 1				DO NOT SCALE DRAWING	REVISION
UNLESS OTHERWISE SPECIFIED: DIMENSIONS ARE IN MILLIMETERS SURFACE FINISH: TOLERANCES: LINEAR: 0.2mm ANGULAR: 0.2°	FINISH: MACHINED	DEBUR AND BREAK SHARP EDGES		TITLE: **DISTAL CENTER JIG**	
	NAME	SIGNATURE	DATE	MATERIAL:	DWG NO. **EngD DIST JIG 001**
DRAWN	MN Mavrogordato		20-2-08	Stainless Steel 316	
CHK'D					SCALE: Do Not Scale Drawing / SHEET 1 OF 1
DEADLINE FOR COMPLETION: 24-3-2008				**CONTACT: mnm100@soton.ac.uk Ext: 27665**	

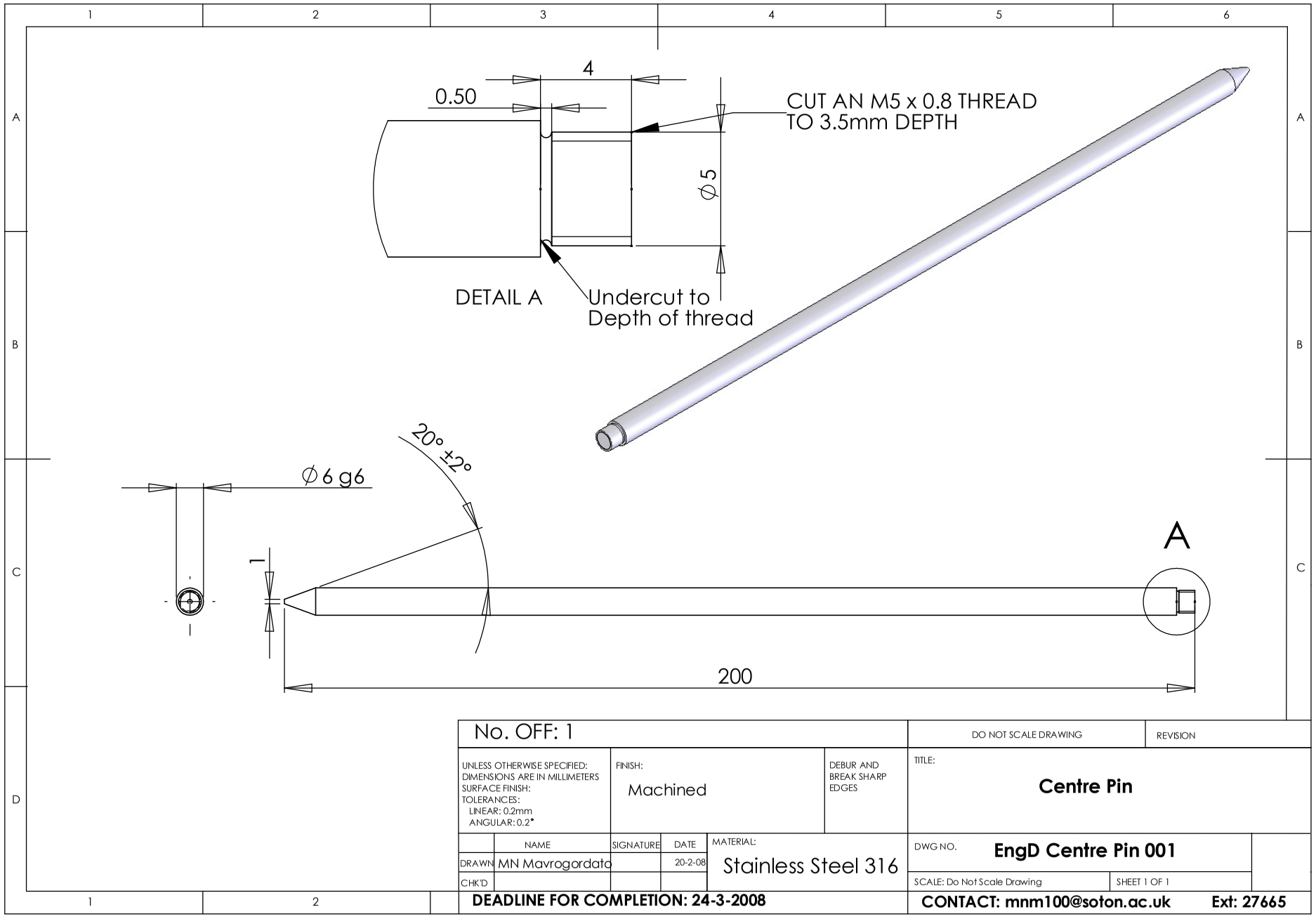

No. OFF: 1				DO NOT SCALE DRAWING	REVISION
UNLESS OTHERWISE SPECIFIED: DIMENSIONS ARE IN MILLIMETERS SURFACE FINISH: TOLERANCES: LINEAR: 0.2mm ANGULAR: 0.2°	FINISH: Machined	DEBUR AND BREAK SHARP EDGES	TITLE: **Centre Pin**		
	NAME	SIGNATURE	DATE	MATERIAL:	DWG NO. **EngD Centre Pin 001**
DRAWN	MN Mavrogordato		20-2-08	Stainless Steel 316	
CHK'D					SCALE: Do Not Scale Drawing SHEET 1 OF 1
DEADLINE FOR COMPLETION: 24-3-2008				**CONTACT: mnm100@soton.ac.uk Ext: 27665**	

SIDE MOUNT AE SENSOR

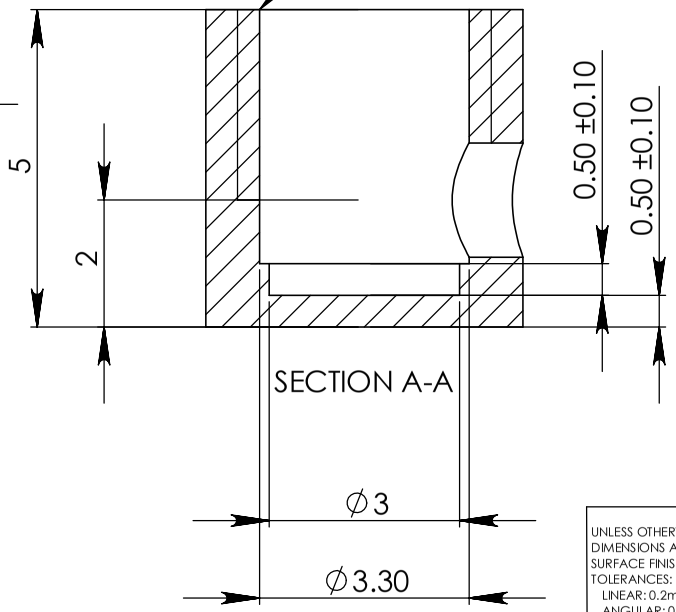

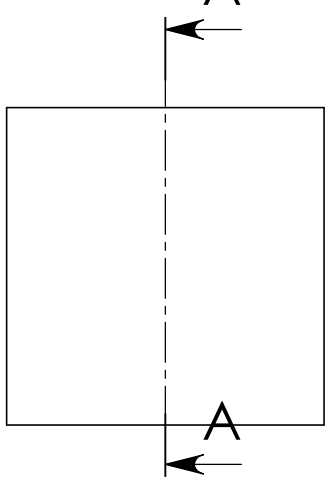

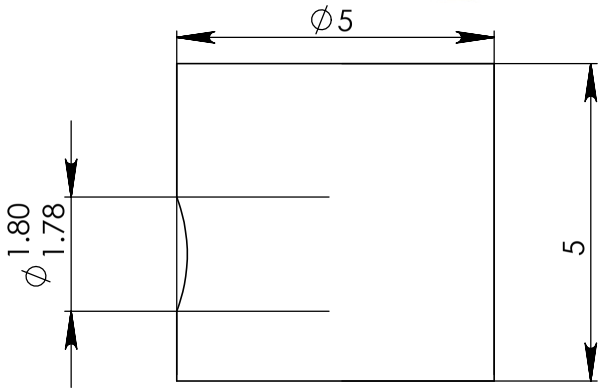

UNLESS OTHERWISE SPECIFIED: DIMENSIONS ARE IN MILLIMETERS SURFACE FINISH: TOLERANCES: LINEAR: 0.2mm ANGULAR: 0.2°	FINISH:	DEBUR AND BREAK SHARP EDGES	DO NOT SCALE DRAWING	REVISION	
			TITLE: **Sensor case**		
NAME / SIGNATURE / DATE	MATERIAL:		DWG NO. **EngD 001**		A4
DRAWN: MN Mavrogordato	Stainless Steel 316		SCALE:10:1	SHEET 1 OF 1	
CHK'D					
DEADLINE FOR COMPLETION: 18-8-2006			**CONTACT: mnm100@soton.ac.uk**		**Ext: 27665**

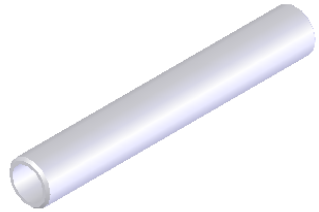

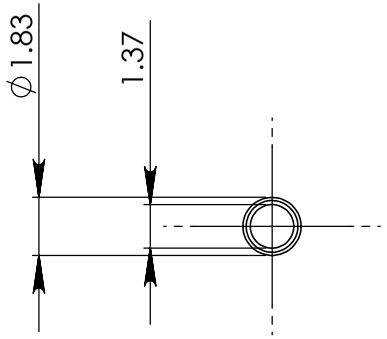

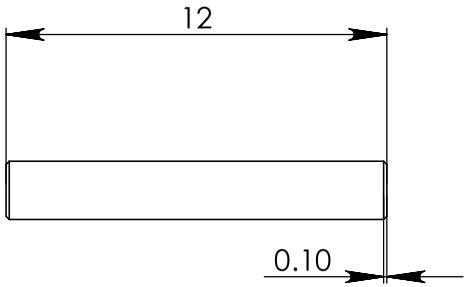

DO NOT SCALE DRAWING				REVISION	
UNLESS OTHERWISE SPECIFIED: DIMENSIONS ARE IN MILLIMETERS SURFACE FINISH: TOLERANCES: LINEAR: 0.2mm ANGULAR: 0.2°	FINISH:		DEBUR AND BREAK SHARP EDGES	TITLE: **Case small tube**	
	NAME	SIGNATURE	DATE	MATERIAL:	DWG NO. **EngD 002**
DRAWN	MN Mavrogordato			Stainless Steel 316	A4
CHK'D					SCALE:5:1 SHEET 1 OF 1
DEADLINE FOR COMPLETION: 18-8-2006				**CONTACT: mnm100@soton.ac.uk**	**Ext: 27665**

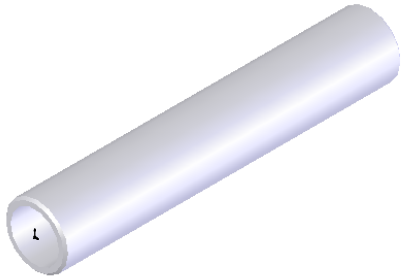

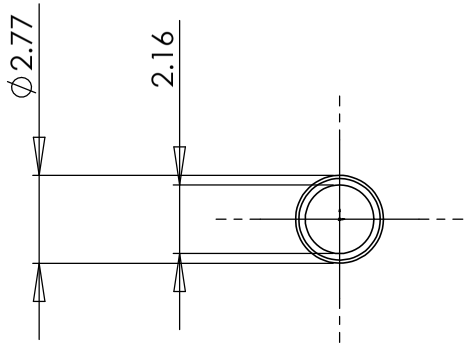

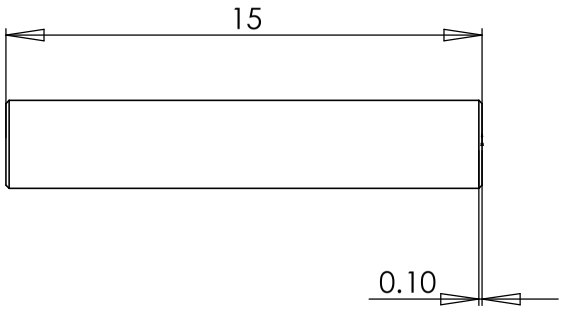

DO NOT SCALE DRAWING			REVISION
UNLESS OTHERWISE SPECIFIED: DIMENSIONS ARE IN MILLIMETERS SURFACE FINISH: TOLERANCES: LINEAR: 0.2mm ANGULAR: 0.2°	FINISH:	DEBUR AND BREAK SHARP EDGES	TITLE: **Case large tube**
	NAME	SIGNATURE / DATE	MATERIAL: Stainless Steel 316
DRAWN	MN Mavrogordato		DWG NO. **EngD 003** — A4
CHK'D			SCALE:5:1 — SHEET 1 OF 1
DEADLINE FOR COMPLETION: 18-8-2006			**CONTACT: mnm100@soton.ac.uk Ext: 27665**

ITEM NO.	PART NUMBER	DESCRIPTION	QTY.
1	case	Sensor case	1
2	case tubes	Small Hyperdermic tubing	1
3	case tubes	Large Hyperdermic tubing	1

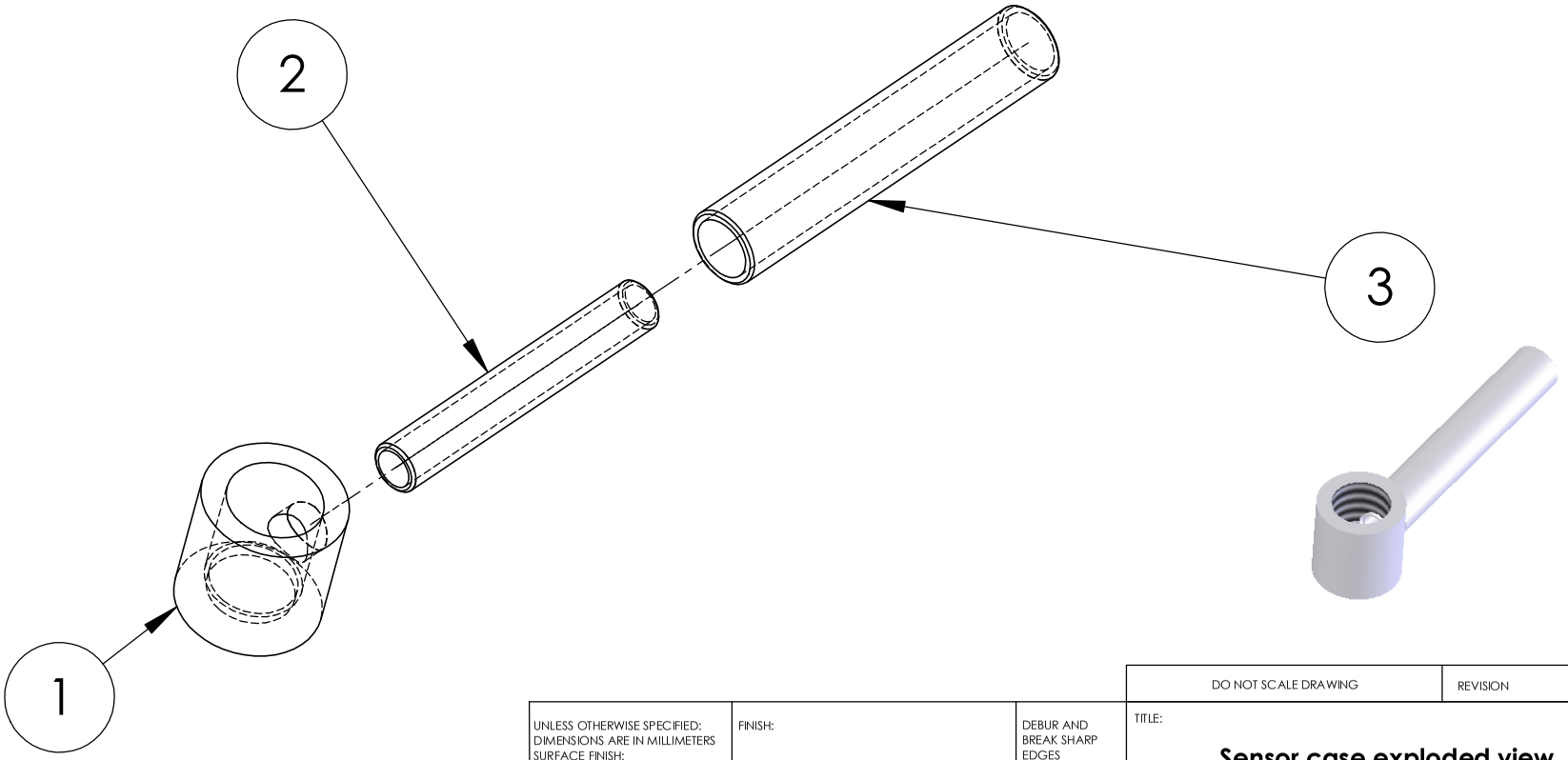

DO NOT SCALE DRAWING | REVISION

UNLESS OTHERWISE SPECIFIED:
DIMENSIONS ARE IN MILLIMETERS
SURFACE FINISH:
TOLERANCES:
LINEAR: 0.2mm
ANGULAR: 0.2°

FINISH:

DEBUR AND BREAK SHARP EDGES

TITLE:

Sensor case exploded view

	NAME	SIGNATURE	DATE
DRAWN	MN Mavrogordato		
CHK'D			

MATERIAL: Stainless Steel 316

DWG NO. **EngD 004**

A4

SCALE:2:1 | SHEET 1 OF 1

DEADLINE FOR COMPLETION: 18-8-2006

CONTACT: mnm100@soton.ac.uk Ext: 27665

TOP MOUNT AE SENSOR

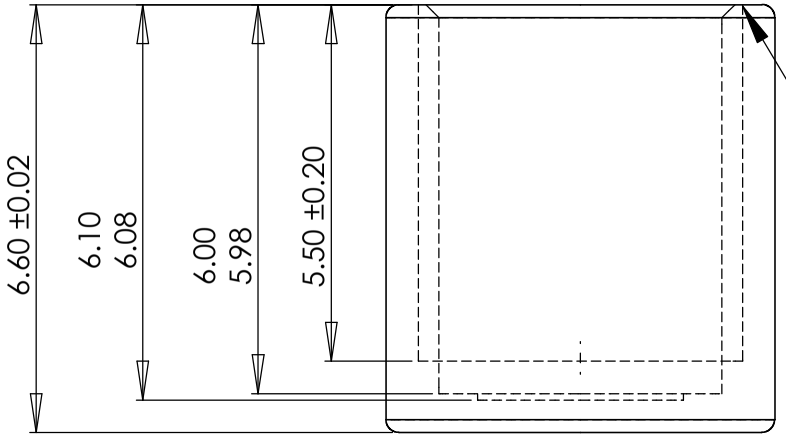

Slot Drill ∅4.37 to 6mm pt.
Depth then Tap M5 to
5.5mm Pt. Depth

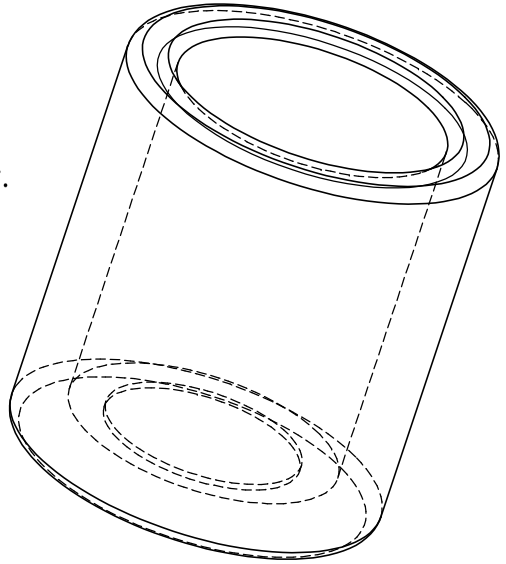

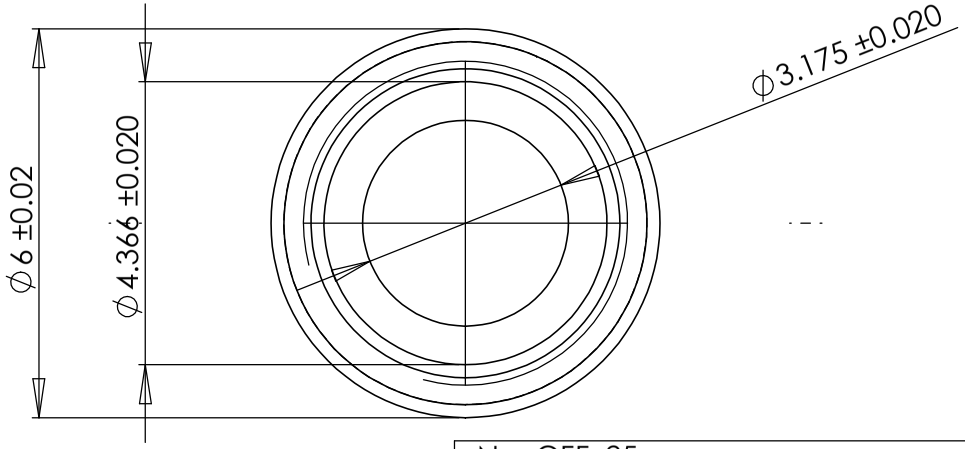

No. OFF: 25				DO NOT SCALE DRAWING	REVISION
UNLESS OTHERWISE SPECIFIED: DIMENSIONS ARE IN MILLIMETERS SURFACE FINISH: TOLERANCES: LINEAR: 0.2mm ANGULAR: 0.2°	FINISH: Machined	DEBUR AND BREAK SHARP EDGES		TITLE: **Sensor case**	
	NAME	SIGNATURE	DATE	MATERIAL:	DWG NO. **EngD sens case 001** A4
DRAWN	MN Mavrogordato		13-11-07	Brass	
CHK'D					SCALE:5:1 SHEET 1 OF 1
DEADLINE FOR COMPLETION: 20-11-2007				**CONTACT: mnm100@soton.ac.uk Ext: 27665**	

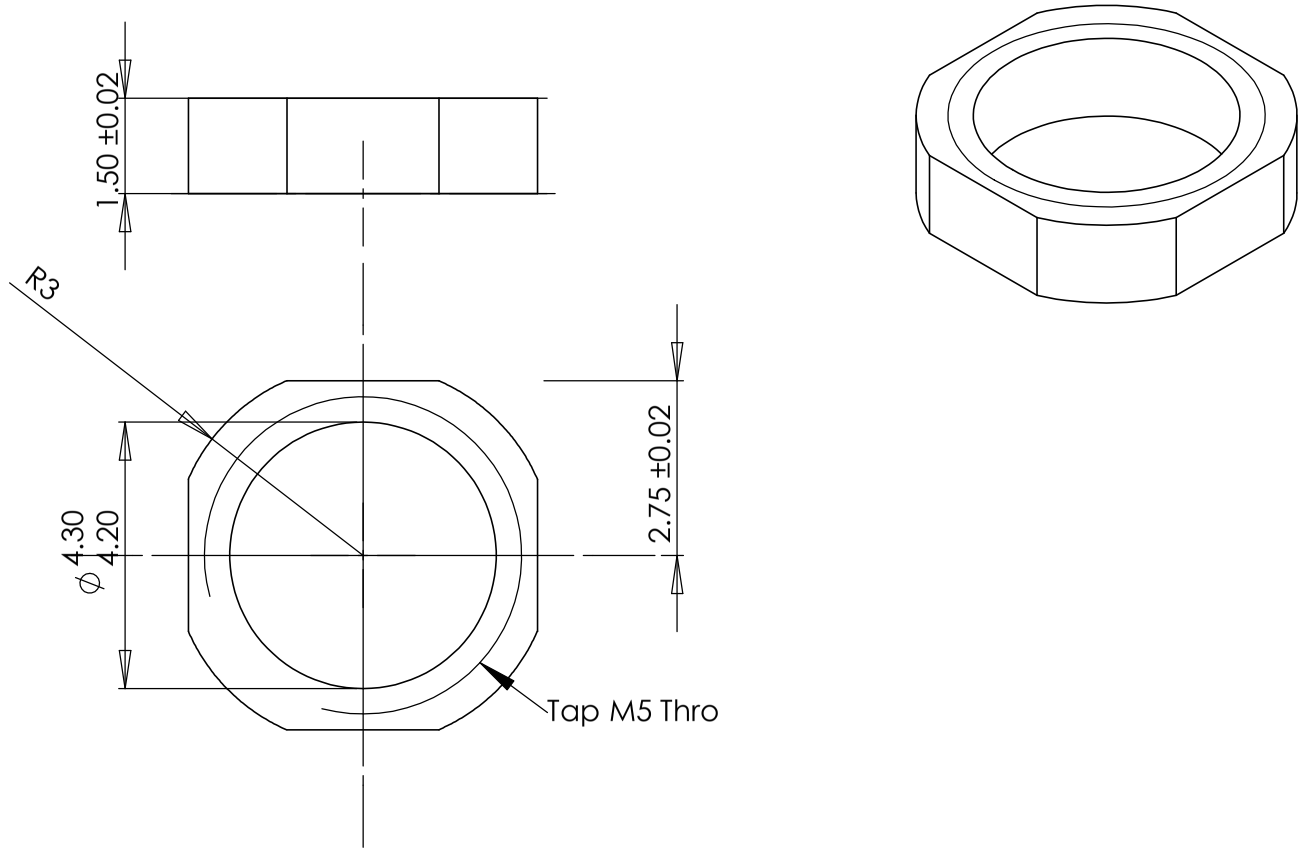

No. OFF: 25

DO NOT SCALE DRAWING | REVISION

UNLESS OTHERWISE SPECIFIED:
DIMENSIONS ARE IN MILLIMETERS
SURFACE FINISH:
TOLERANCES:
LINEAR: 0.2mm
ANGULAR: 0.2°

FINISH: Machined

DEBUR AND BREAK SHARP EDGES

TITLE: **Sensor Lock nut**

	NAME	SIGNATURE	DATE
DRAWN	MN Mavrogordato		13-11-07
CHK'D			

MATERIAL: Brass

DWG NO. **EngD Locknut 001**

A4

SCALE:10:1 | SHEET 1 OF 1

DEADLINE FOR COMPLETION: 20-11-2007

CONTACT: mnm100@soton.ac.uk Ext: 27665

APPENDIX E – 3D CT IMAGES OF LOAD INDUCED DAMAGE

FELICITY TESTED SPECIMENS

Felicity Test 6		
Before Load	After Load	Load Induced Cracks
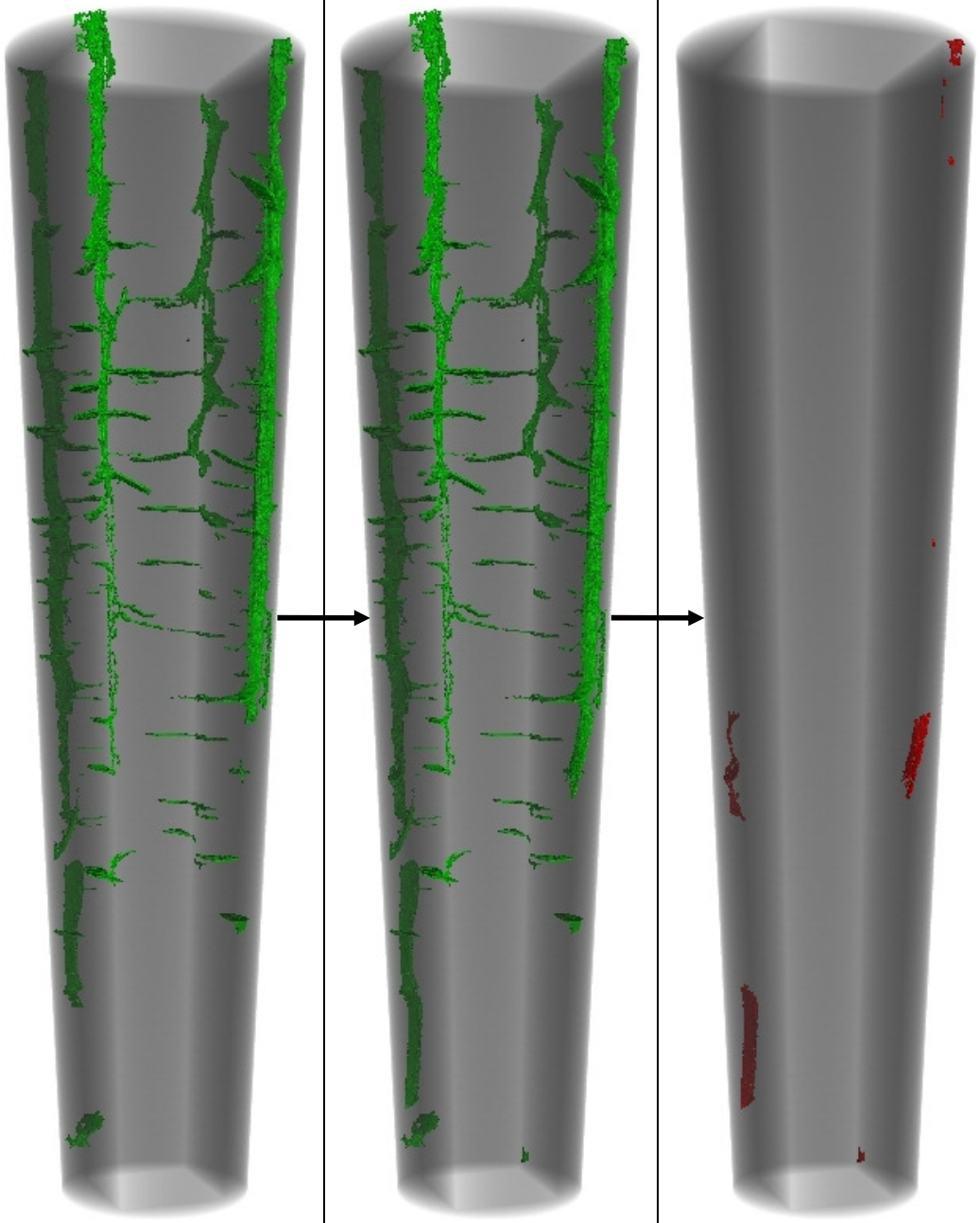		
		Split volume = 4.52mm^3 Split Surface Area = 131.98mm^2

Felicity Test 7		
Before Load	After Load	Load Induced Cracks
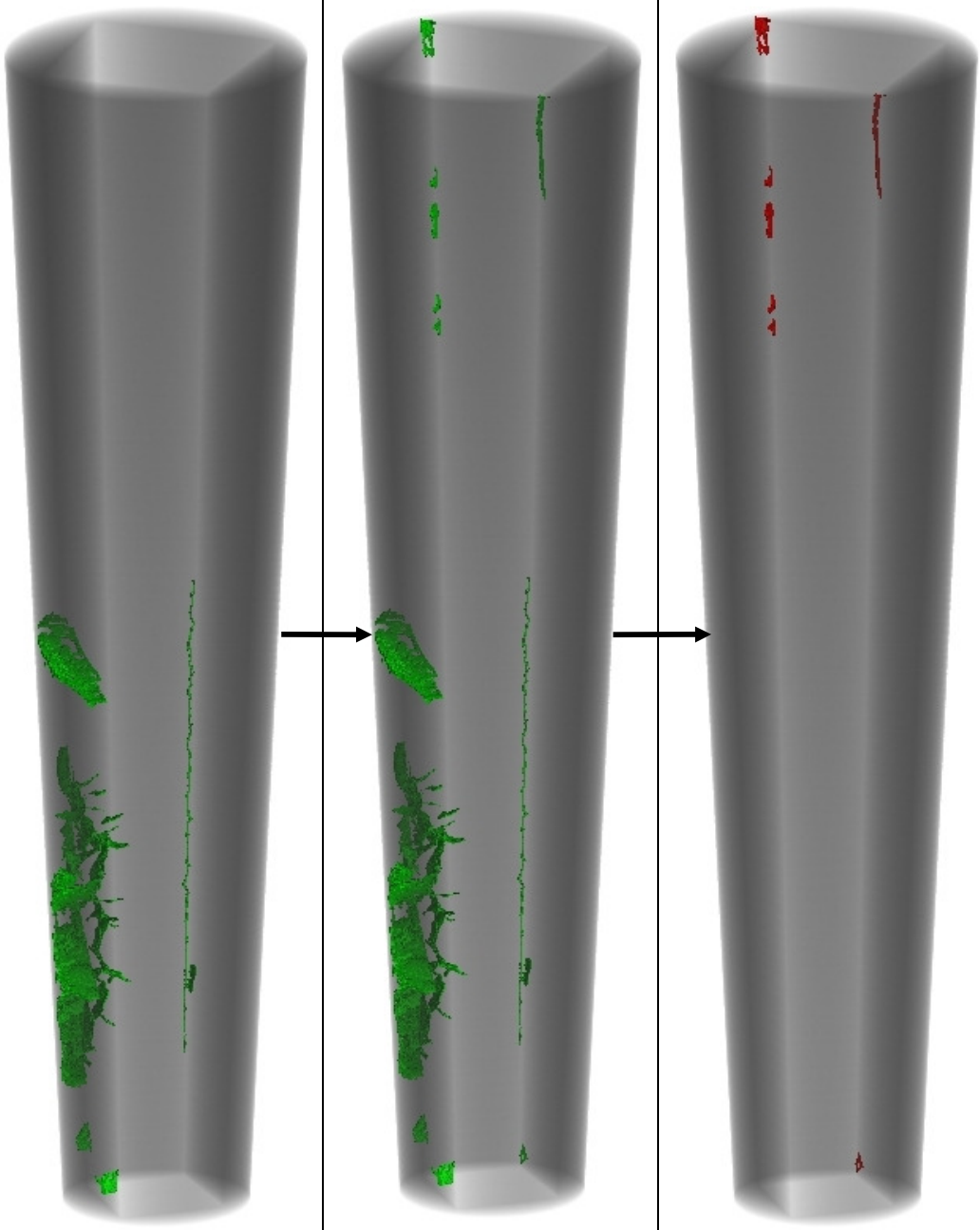		
		Split volume = 3.92mm^3 Split Surface Area = 61.51mm^2

Felicity Test 8		
Before Load	After Load	Load Induced Cracks
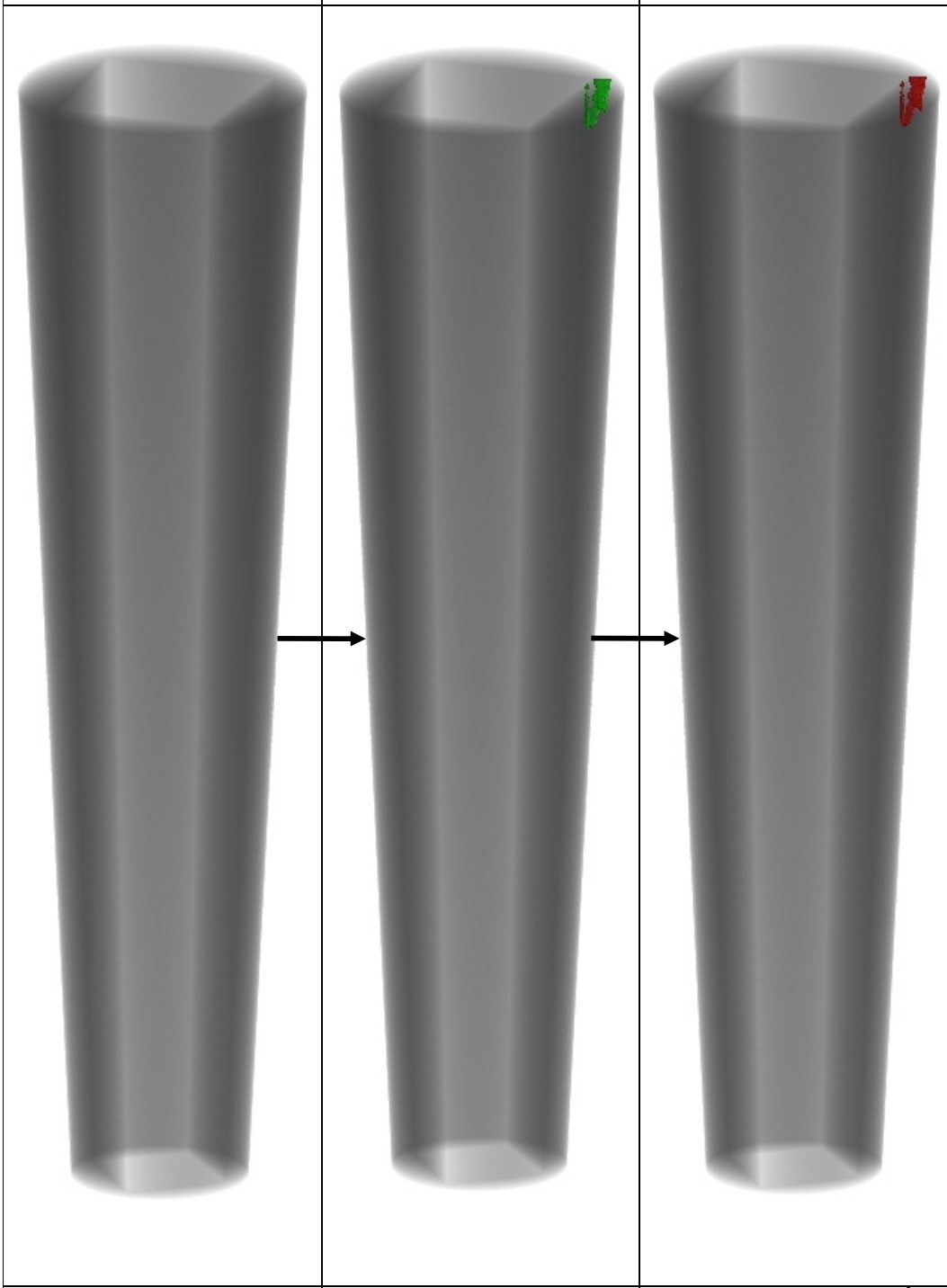		
		Split volume = 1.45mm^3 Split Surface Area = 19.48mm^2

Felicity Test 9		
Before Load	After Load	Load Induced Cracks
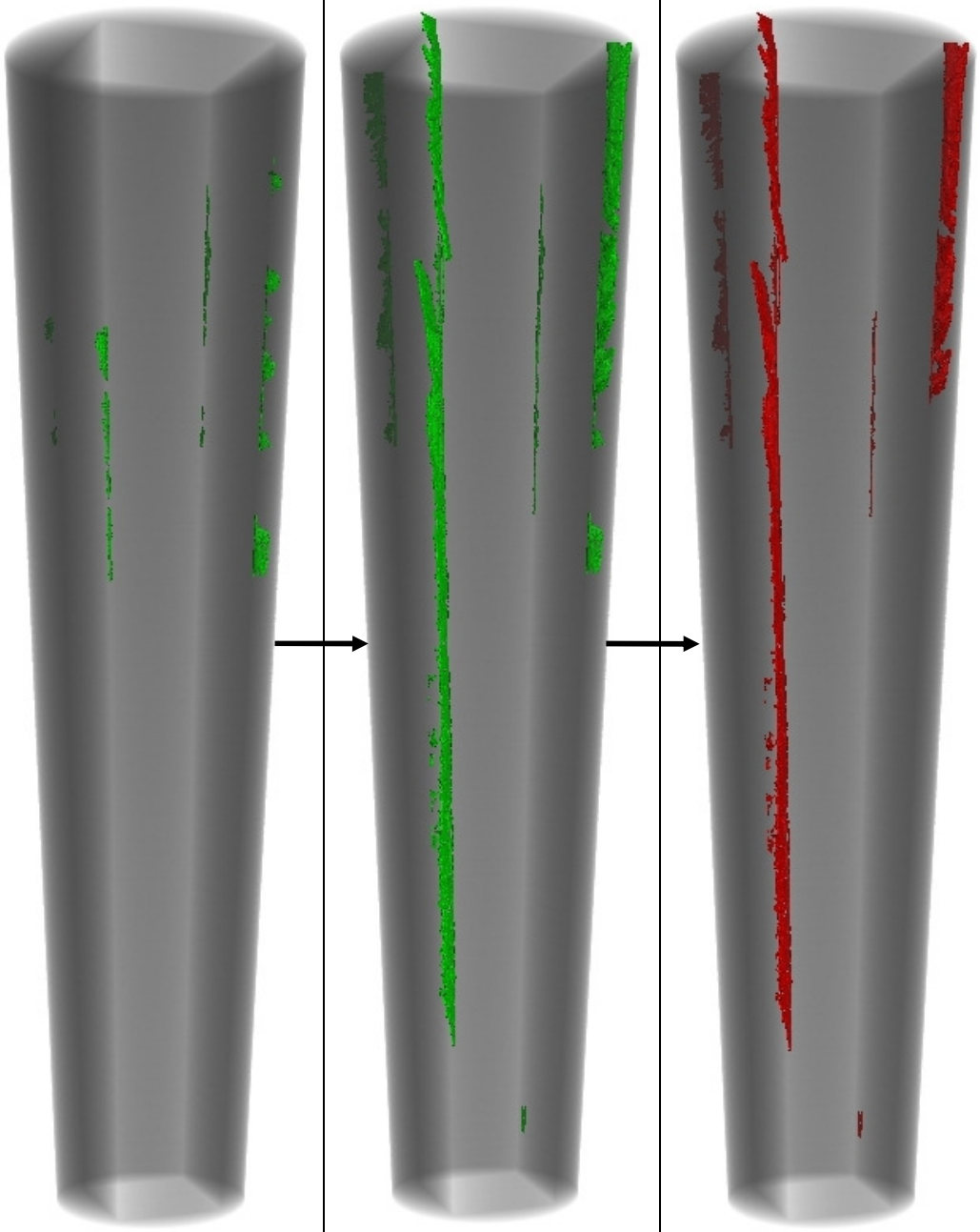		
		Split volume = 52.27mm^3 Split Surface Area = 784.78mm^2

Felicity Test Load Induced Cracking			
Test 6	Test 7	Test 8	Test 9
			
Split volume = 4.52mm^3 Split Surface Area = 131.98mm^2	Split volume = 3.92mm^3 Split Surface Area = 61.51mm^2	Split volume = 1.45mm^3 Split Surface Area = 19.48mm^2	Split volume = 52.27mm^3 Split Surface Area = 784.78mm^2

FATIGUE TESTED SPECIMENS

Fatigue Test 1			
Before Load	After Load	Load Induced Cracking	Load Induced Cracks (Distal 8cm)
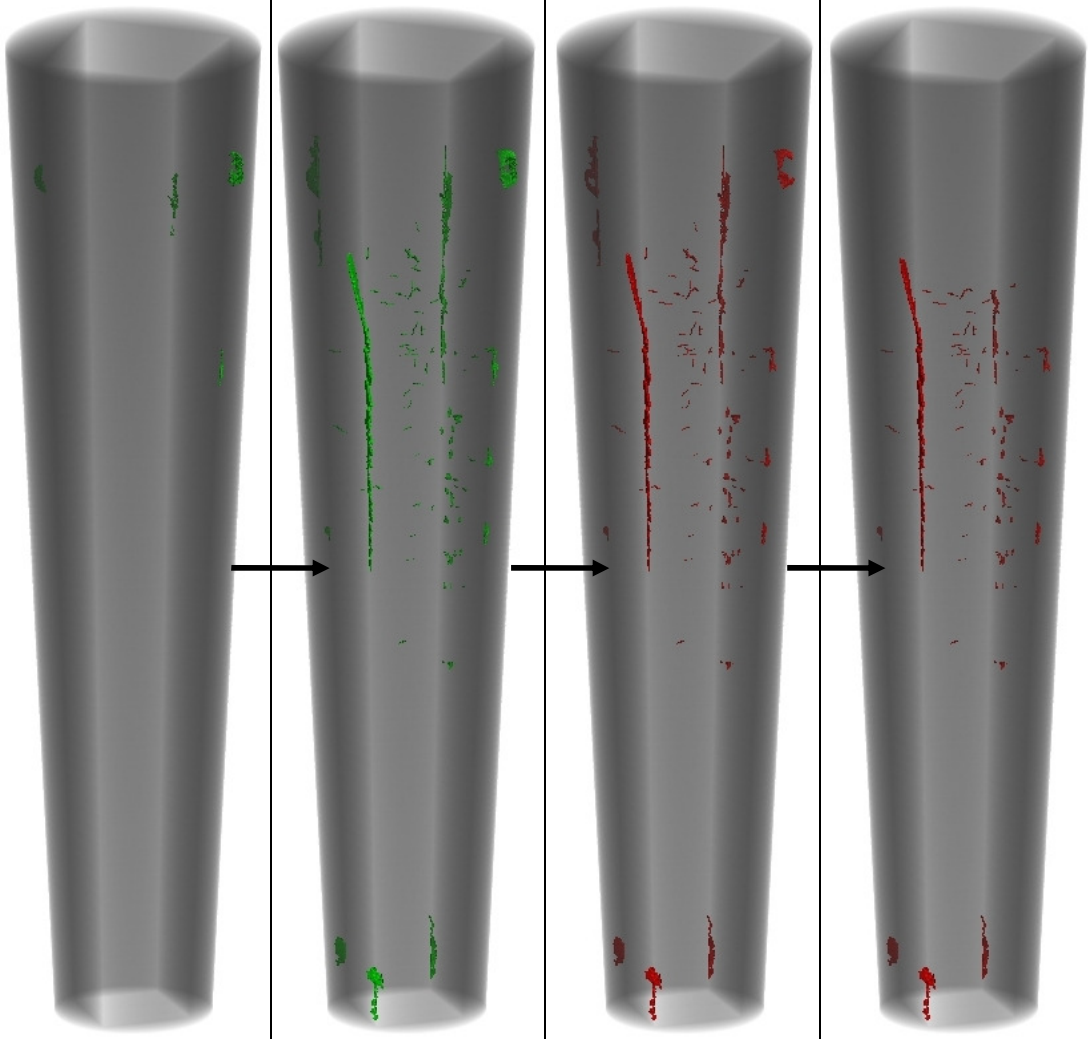			
		Split volume = 21.46mm^3 Split Surface Area = 361.35mm^2	Split volume = 16.49mm^3 Split Surface Area = 267.02mm^2

Fatigue Test 2			
Before Load	After Load	Load Induced Cracking	Load Induced Cracks (Distal 8cm)
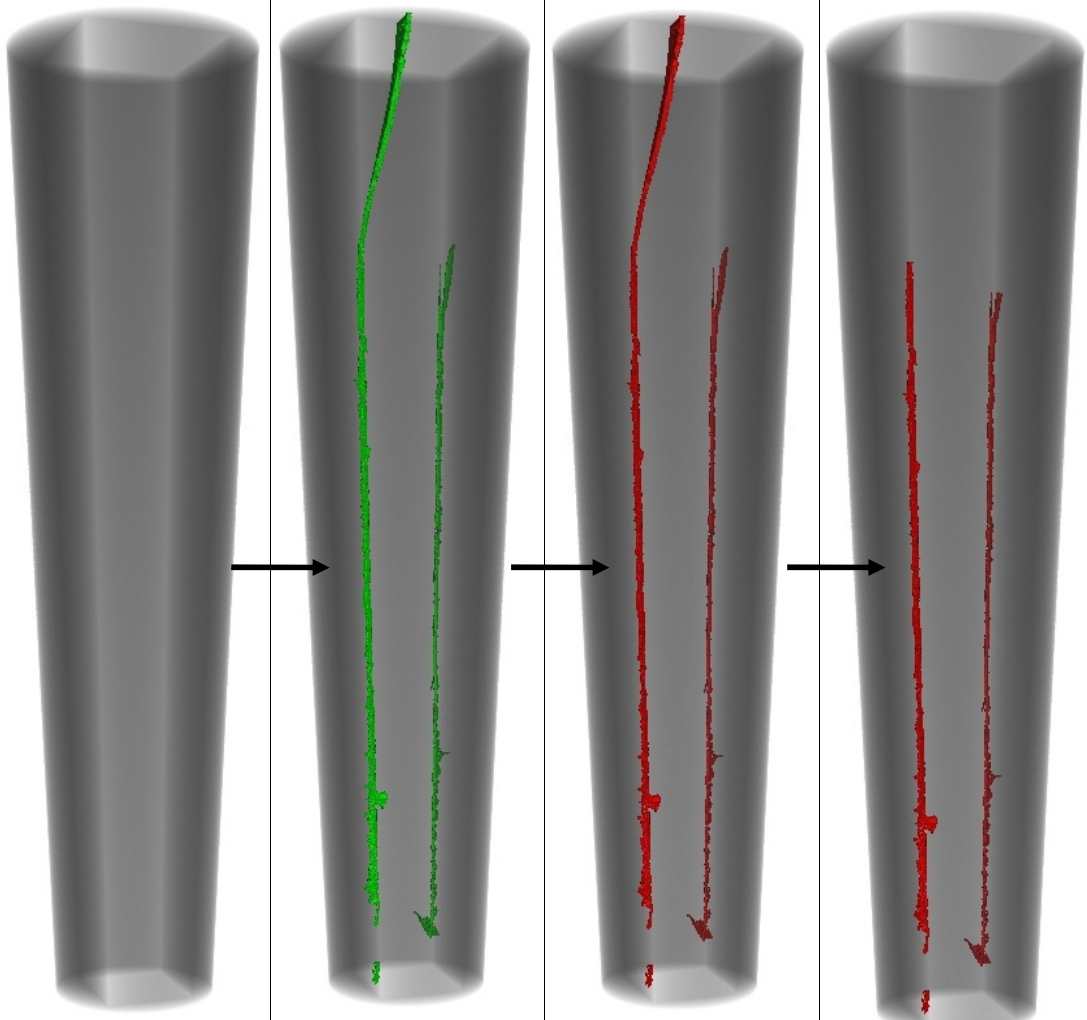			
		Split volume = 83.45mm^3 Split Surface Area = 720.98mm^2	Split volume = 54.33mm^3 Split Surface Area = 549.02mm^2

Fatigue Test 3			
Before Load	After Load	Load Induced Cracking	Load Induced Cracks (Distal 8cm)
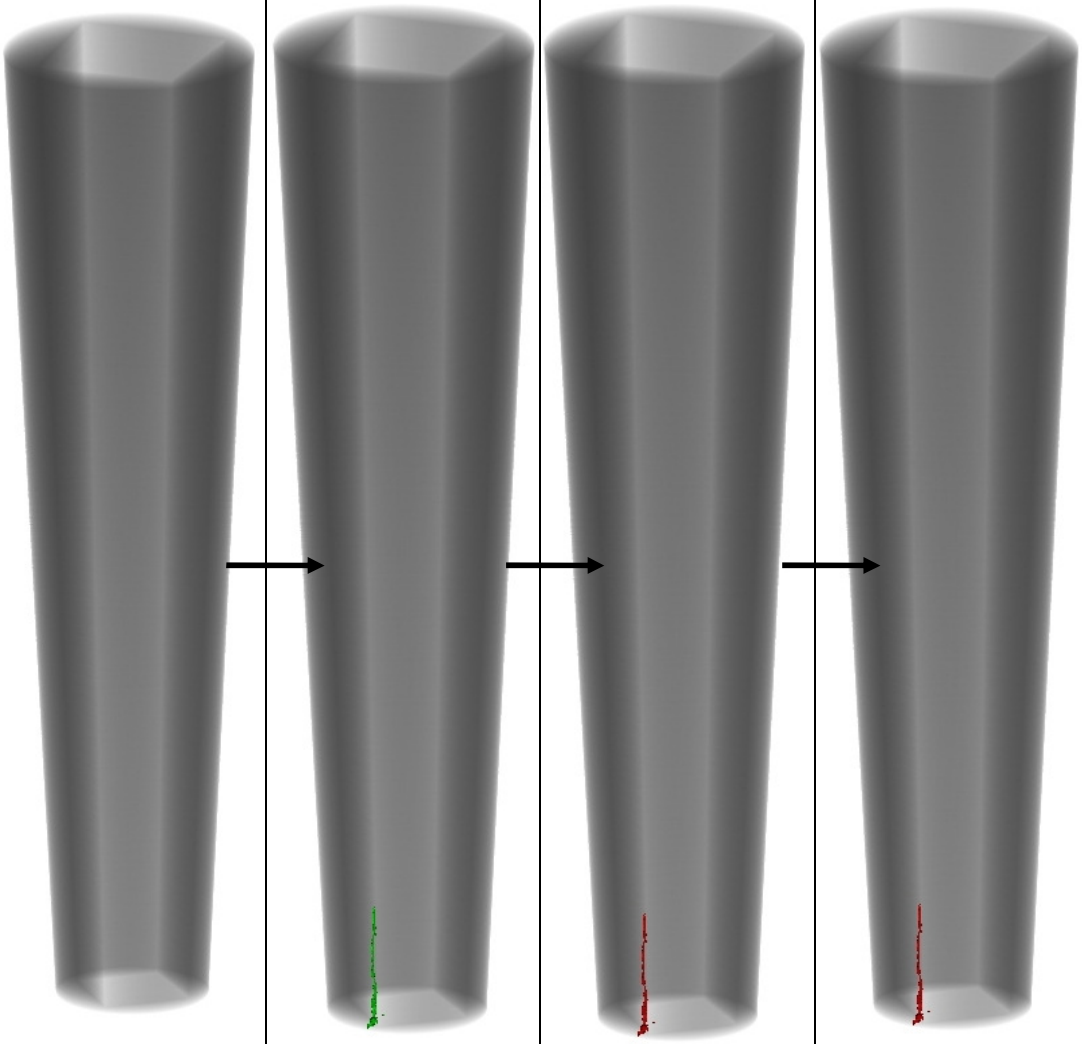			
		Split volume = 0.86mm^3 Split Surface Area = 21.47mm^2	Split volume = 0.86mm^3 Split Surface Area = 21.47mm^2

Fatigue Test 4			
Before Load	After Load	Load Induced Cracking	Load Induced Cracks (Distal 8cm)
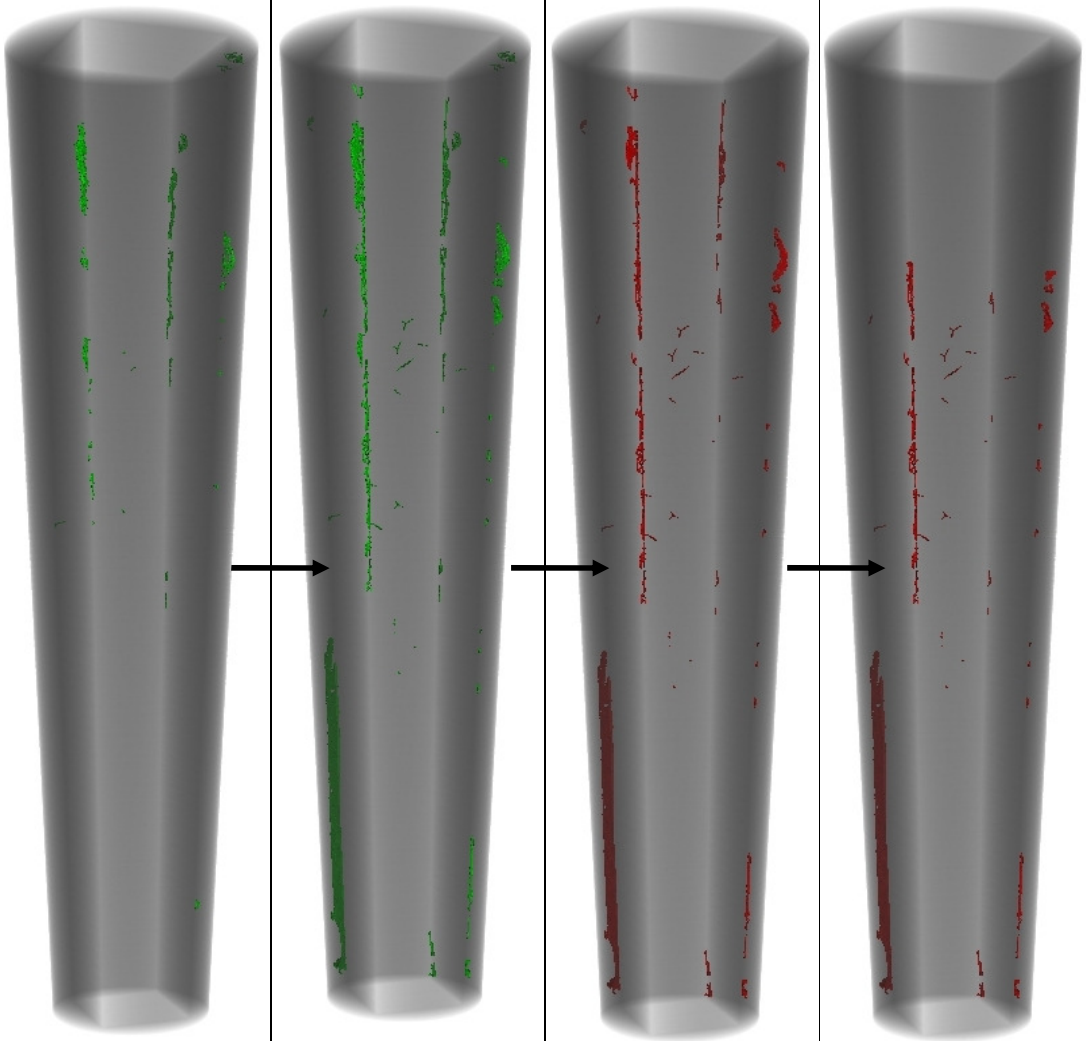			
		Split volume = 17.95mm^3 Split Surface Area = 302.05mm^2	Split volume = 15.31mm^3 Split Surface Area = 236.45mm^2

Fatigue Test 5			
Before Load	After Load	Load Induced Cracking	Load Induced Cracks (Distal 8cm)
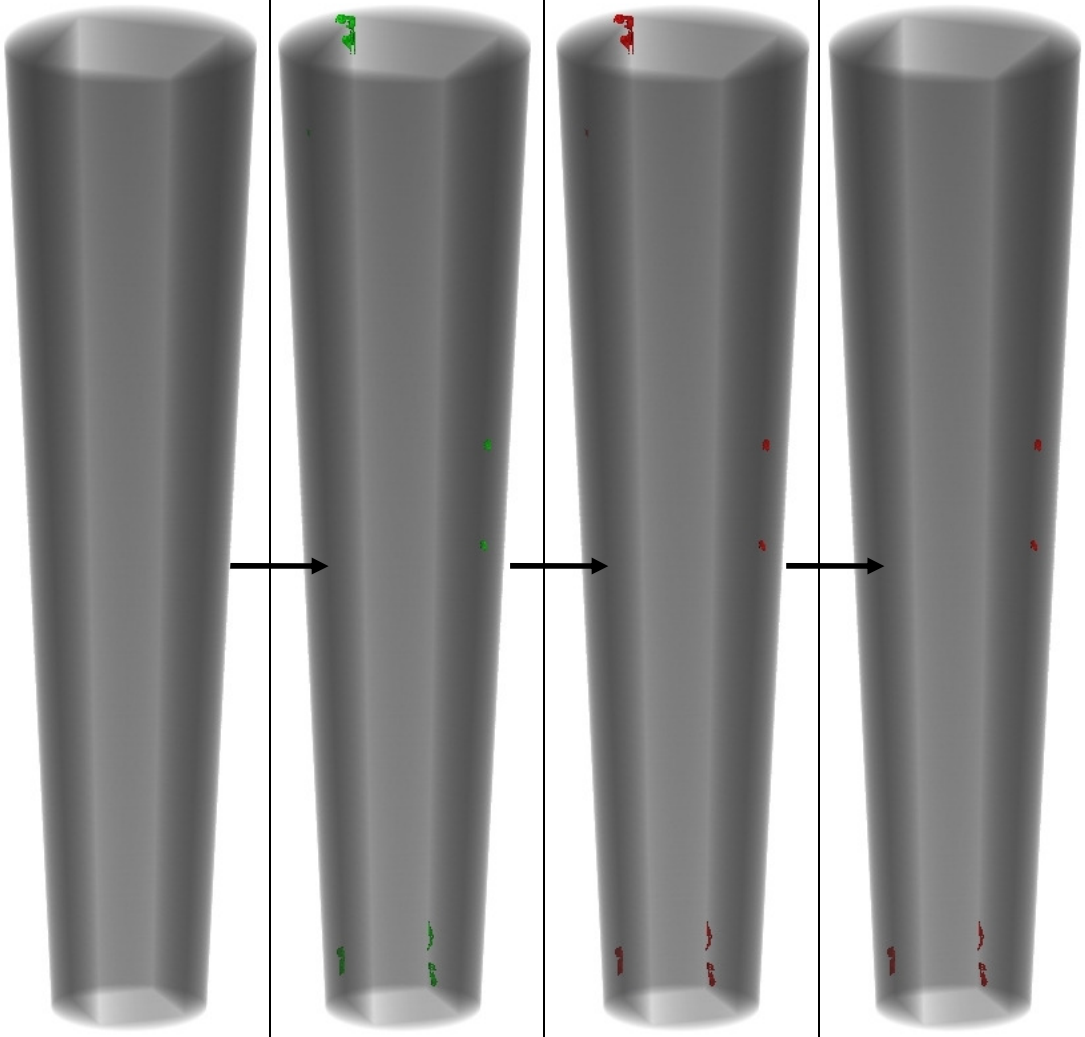			
		Split volume = 1.85mm^3 Split Surface Area = 34.38mm^2	Split volume = 0.88mm^3 Split Surface Area = 18.73mm^2

Fatigue Test 6			
Before Load	After Load	Load Induced Cracking	Load Induced Cracks (Distal 8cm)
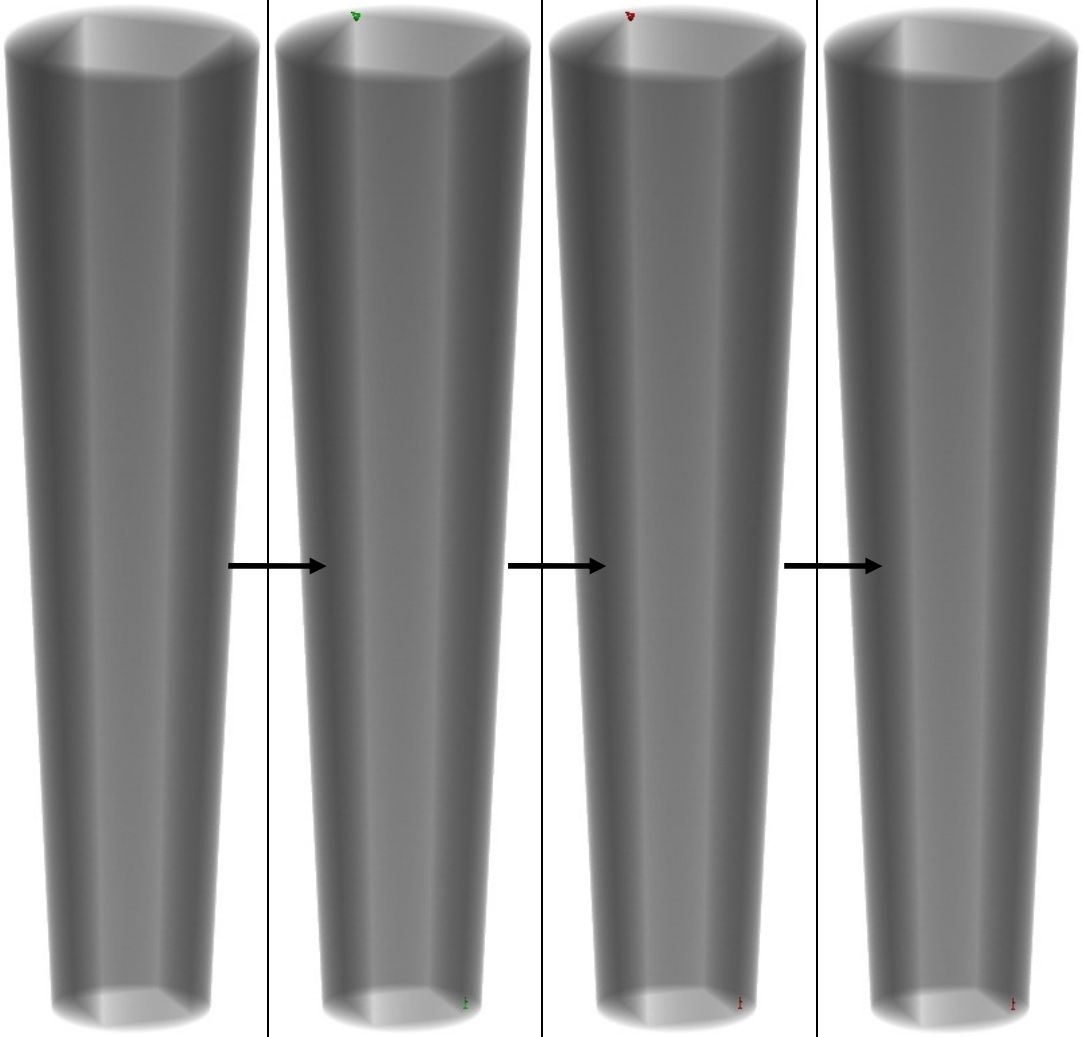			
		Split volume = 0.14mm^3 Split Surface Area = 3.24mm^2	Split volume = 0.04mm^3 Split Surface Area = 0.95mm^2

Fatigue Test 7			
Before Load	After Load	Load Induced Cracking	Load Induced Cracks (Distal 8cm)
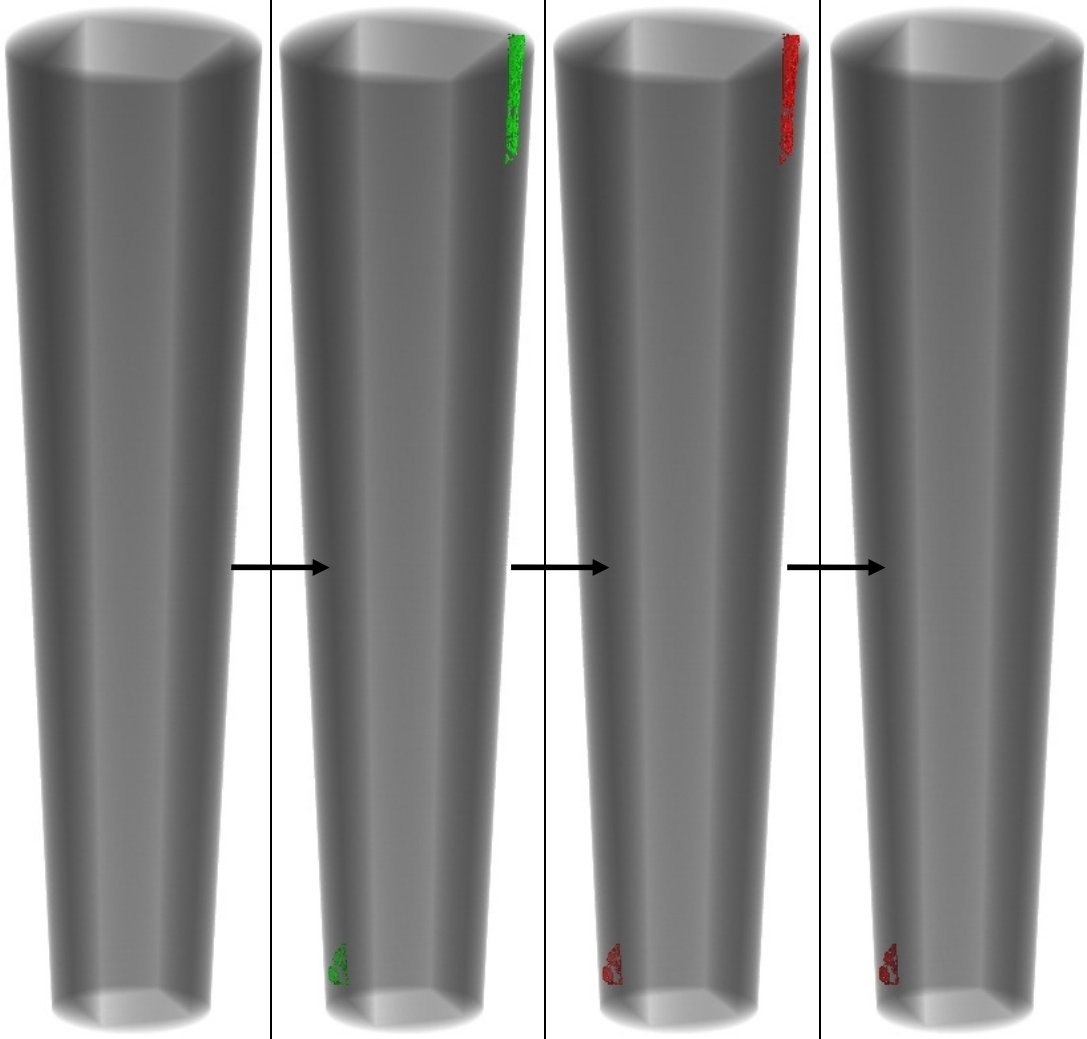			
		Split volume = 4.27mm^3 Split Surface Area = 70.14mm^2	Split volume = 0.59mm^3 Split Surface Area = 17.43mm^2

Fatigue Test 8			
Before Load	After Load	Load Induced Cracking	Load Induced Cracks (Distal 8cm)
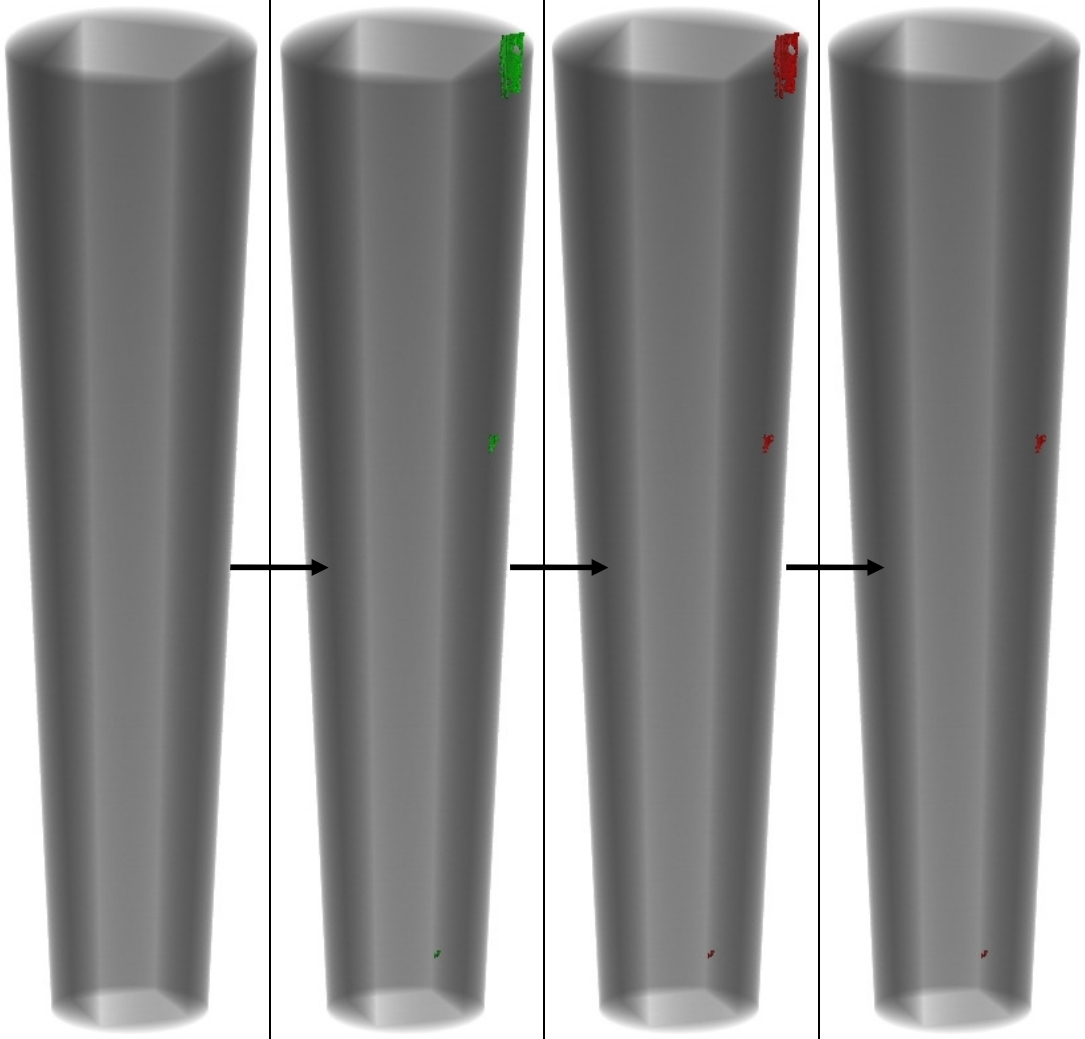			
		Split volume = 3.55mm^3 Split Surface Area = 42.28mm^2	Split volume = 0.2mm^3 Split Surface Area = 4.98mm^2

Fatigue Test Load Induced Cracking			
Test 1	Test 2	Test 3	Test 4
			
Split volume = 21.46mm^3 Split Surface Area = 361.35mm^2	Split volume = 83.45mm^3 Split Surface Area = 720.98mm^2	Split volume = 0.86mm^3 Split Surface Area = 21.47mm^2	Split volume = 17.95mm^3 Split Surface Area = 302.05mm^2

Fatigue Test Load Induced Cracking			
Test 5	Test 6	Test 7	Test 8
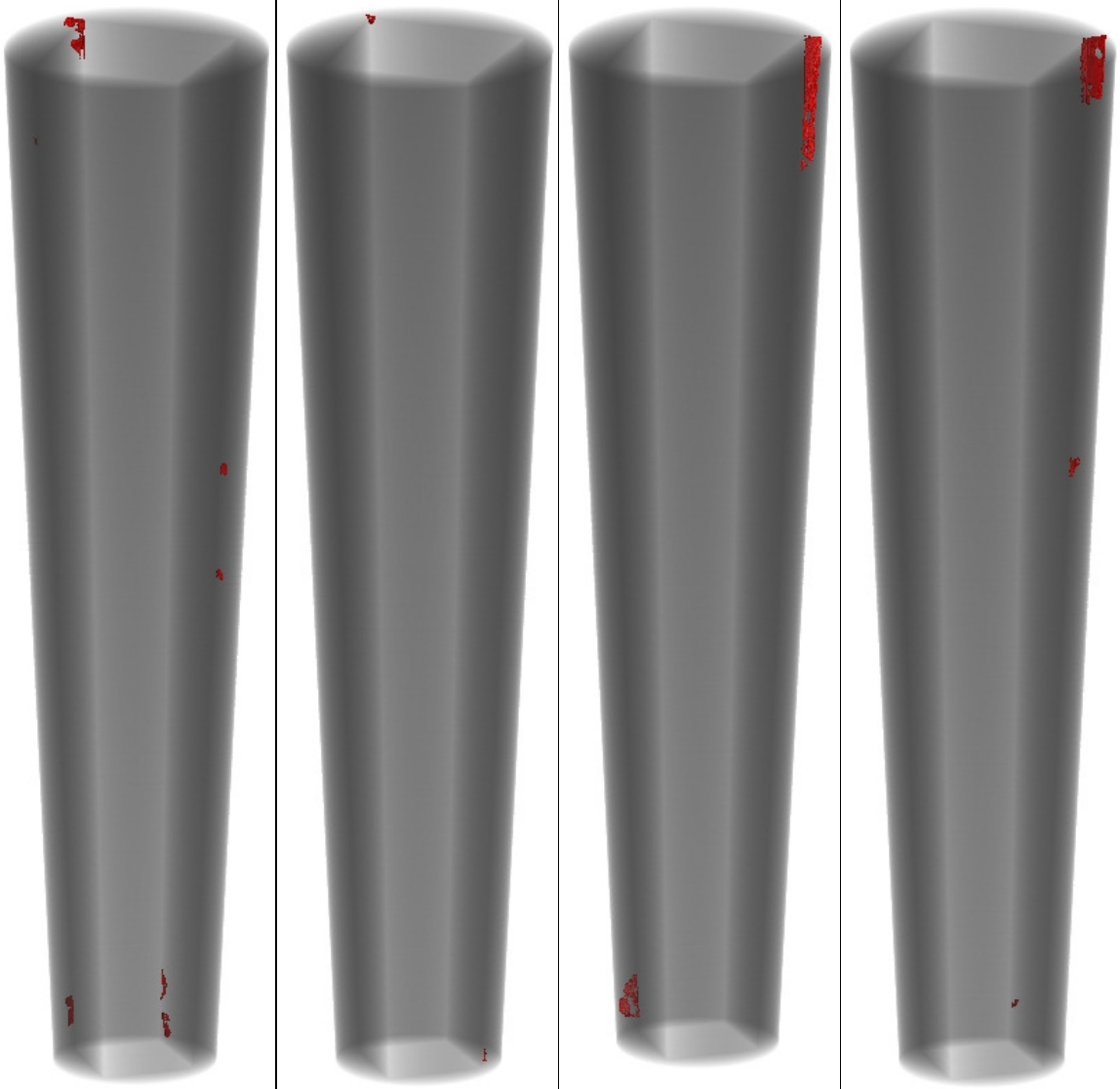			
Split volume = $1.85mm^3$ Split Surface Area = $34.38mm^2$	Split volume = $0.14mm^3$ Split Surface Area = $3.24mm^2$	Split volume = $4.27mm^3$ Split Surface Area = $70.14mm^2$	Split volume = $3.55mm^3$ Split Surface Area = $42.28mm^2$

APPENDIX F – MACRO CODE TO REMOVE RESIDUAL ZINC IODIDE FROM THE TECHNOVIT SURFACE OF RECONSTRUCTED CT VOLUME IMAGES

```
//This macro is used to extract the Technovit layer only from the Fatigure scan subtracted volumes.
//Written by M.N. Mavrogordato 2/6/2010
//The user is asked to draw a rectangle around the top and bottom of the stem interface, and a circle around the top and bottom of the technovit.
//The macro calculates the stem taper and position, before selecting an adjusted region for each slice in turn through the volume.
//The macro fills the area inside the rectangle, and outside the circle black, leaving just the technovit as visible.
//But the user will have to save the processed volume after processing has completed!
//open the scan volume to be processed and run the macro script. All user inputs are obtained from the dimensions of the bounding shapes drawn on the images.
//Define the top and bottom dimensions of the stem:
	setSlice (1);
	waitForUser("Draw a rectangle at the proximal end that just includes the inside edge of the technovit, then click OK");
	getSelectionBounds(rx_top, ry_top, rw_top, rh_top);
	setSlice (nSlices-100);
	waitForUser("Adjust the rectangle at the distal end that just includes the inside edge of the technovit, then click OK");
	getSelectionBounds(rx_bottom, ry_bottom, rw_bottom, rh_bottom);
	bottom_slice_r = getSliceNumber();
//Calculate factor to reduce rectangle by for each slice
	top_slice = 1;
	reduction_rx = (rx_bottom - rx_top)/(bottom_slice_r - top_slice);
	reduction_ry = (ry_bottom - ry_top)/(bottom_slice_r - top_slice);
	reduction_rw = (rw_bottom - rw_top)/(bottom_slice_r - top_slice);
	reduction_rh = (rh_bottom - rh_top)/(bottom_slice_r - top_slice);
//Define the top and bottom dimensions of the technovit:
	setSlice (1);
	waitForUser("Draw a circle at the proximal end that just includes the outside edge of the technovit, then click OK");
	getSelectionBounds(cx_top, cy_top, cw_top, ch_top);
	setSlice (nSlices-100);
	waitForUser("Adjust the circle at the distal end that just includes the outside edge of the technovit, then click OK");
	getSelectionBounds(cx_bottom, cy_bottom, cw_bottom, ch_bottom);
	bottom_slice_c = getSliceNumber();
//Calculate factor to reduce circle by for each slice
	top_slice = 1;
	reduction_cx = (cx_bottom - cx_top)/(bottom_slice_c - top_slice);
	reduction_cy = (cy_bottom - cy_top)/(bottom_slice_c - top_slice);
	reduction_cw = (cw_bottom - cw_top)/(bottom_slice_c - top_slice);
	reduction_ch = (ch_bottom - ch_top)/(bottom_slice_c - top_slice);
//Define start of circle loop conditions:
	cx = cx_top;
	cy = cy_top;
	cw = cw_top;
	ch = ch_top;
	setForegroundColor(0, 0, 0);
	for (i=1; i<=nSlices; i++) {
		setSlice (i);
		makeOval(cx, cy, cw, ch);
		run("Make Inverse");
		run("Fill", "slice");
		cx = cx+reduction_cx;
		cy = cy+reduction_cy;
		cw = cw+reduction_cw;
		ch = ch+reduction_ch;		}
//Define start of rectangle loop conditions:
	rx = rx_top;
	ry = ry_top;
	rw = rw_top;
	rh = rh_top;
	setForegroundColor(0, 0, 0);
	for (i=1; i<=nSlices; i++) {
		setSlice (i);
		makeRectangle(rx, ry, rw, rh);
		run("Fill", "slice");
		rx = rx+reduction_rx;
		ry = ry+reduction_ry;
		rw = rw+reduction_rw;
		rh = rh+reduction_rh;		}
//End
```